# Rapid assessment tool for turbulence in backward facing step flow

Jasper Benjamin Hoeve
22nd of September 2015

UNIVERSITY OF TWENTE.

ARCADIS

# Rapid assessment tool for turbulence in backward facing step flow

## Thesis

**J. B. Hoeve**

9/22/2015

Graduation committee:

| | |
|---|---|
| Dr. ir. J. S. Ribberink | Univeristy of Twente |
| Prof. dr. ir. W. S. J. Uijttewaal | TU Delft |
| Dr. ir. H. G. Voortman | Arcadis |
| Dr. J. J. Warmink | Univeristy of Twente |

UNIVERSITY OF TWENTE.  ARCADIS

# Preface

This report is the result of my master thesis research at Arcadis in Amersfoort. By successfully finishing this research, I have obtained my Master's degree in Civil Engineering. Researching the topic of turbulence for half a year has been very educational. During my time at Arcadis, I also got a good impression what working at a civil engineering consultancy firm encompasses. I will use my experiences there when considering a field of work in the coming year.

I would like to express my sincere gratitude towards my commission for their help. Thank you Hessel Voortman, for your time, patience, enthusiasm, knowledge, humor, sympathy, and for explaining it to me One. Last. Time. Thank you Jan Ribberink, for your constructive feedback, flexibility, experience, and for filling in as the daily supervisor from the University of Twente. Thank you Wim Uijttewaal for helping me understand the complex monstrosity of turbulence mathematics and for giving feedback on my own monstrous math and on my report. And finally thank you Jord Warmink, for helping me create a good research proposal (the fundament of this thesis), for helping me successfully start my graduation assignment, for providing me with good suggestions and relevant papers and for helping me dotting the i's and crossing the t's of this final report.

I would also like to thank my colleagues at Arcadis, who helped me with a lot of ad hoc questions, and who made me feel part of Arcadis.

Finally, I would like to thank my sister, for providing me with someone to look up to, and my parents, who motivated me to do my best since primary school, who offered a loving home to grow up in, and who facilitated and encouraged all my study and extracurricular activities.

*Jasper Hoeve*

*Amersfoort, September 2015*

# Summary

An estimation of the turbulent intensity in a flow is needed when designing hydraulic structures. Not taking the turbulent intensity of a flow into account can result in the destruction of otherwise correctly designed hydraulic structures. During the preliminary design of loose rock bed protection, rules of thumb (e.g. found in the Rock Manual, 2007) are used to take into account the turbulent load on the bed protection. However, these rules of thumb only provide very rough estimates. Only a low, medium or high value for the effect of turbulence on the bed protection is given. The difference between low and high levels of turbulence can result in 8 times heavier rocks. Dissipation of turbulence downstream of the hydraulic structure is not incorporated at all in these rules of thumb, resulting in one value of turbulence for the whole length of the bed protection. This thesis discusses a rapid assessment tool (the 'ATM') to estimate turbulent energy in a flow. The rapid assessment tool should be able to estimate turbulence in a quick way, more accurately than rules of thumb, and more easy to apply than complicated numerical turbulence models. It is the objective of this study to test the theoretical and empirical validity of the rapid assessment tool for the flow conditions of a channel with a backward facing step (BFS) and to show that the rapid assessment tool can be a viable alternative to applying rules of thumb for these flow conditions.

The ATM assumes that 100% of the mean flow energy loss is converted into turbulent energy. Multiple scientific sources state that the reduction of mean flow energy is related to the increase of turbulent energy. The literature analysis did not make clear if it is valid to assume that 100% of the mean flow energy loss is converted into turbulent energy. Using the turbulent kinetic energy equation, it was shown that the production of turbulence is exactly proportional to the reduction of mean flow energy under a set of assumptions. However, some of the assumptions made seem questionable. The empirical validation elaborates further on the applicability of these assumptions.

The ATM models turbulence dissipation as a relaxation function. No instances in literature were found of modelling turbulence dissipation similar to the ATM. The theoretical validation concludes that some principles on which the ATM is build might not represent reality accurately. However, the empirical validation shows that despite these assumptions, the ATM is still able to approximate the turbulence in a flow.

The empirical validation showed that the ATM was able to approximate the order of magnitude of the turbulence. However, calibrating the ATM made it clear that the ATM has issues modelling the correct turbulent energy downstream of the reattachment point. The ATM was able to approximate the turbulent energy levels up until the reattachment point reasonably accurate after calibration.

The empirical validation also showed that turbulence can be produced due to non-uniform flow velocity profiles (on top of the turbulence production due to bottom friction). Flow velocity differences that still exist downstream of the reattachment point result in internal viscous stresses in the flow; internal viscous stresses cause turbulence. Non-uniformity of the flow velocity profile is therefore an important factor to take into account when considering mean and turbulent energy in a flow.

The ATM is already usable to estimate the upper limit of turbulence at the reattachment point during the preliminary design phase (for subcritical backward facing step flow). Using the ATM

output results in up to 3 times heavier stones compared to the stone weight design based on the experimentally measured turbulence. This is significantly more accurate then applying rules of thumb, which results in stone weights up to 80 times heavier. Thus the ATM can be a more accurate alternative to using rules of thumb when calculating the effect of turbulence on loose rock bed protection.

The ATM was introduced as a rapid assessment tool that would potentially combine the ease of rules of thumb with the more accurate measures of turbulence found using complex turbulence models. The results of this thesis indicate that the ATM is not there yet. The ATM has difficulty modelling the turbulent energy levels downstream of the reattachment point. The ATM is able to more accurately estimate the turbulent energy levels at the reattachment point compared to applying rules of thumb. This thesis shows the potential of the ATM to become a rapid assessment tool for turbulence in a flow during the preliminary design phase. The ATM does need to be improved in order to accurately model turbulence after the reattachment point.

# Contents

# List of figures

## List of tables

# List of symbols

| | | |
|---|---|---|
| $\alpha$ | ATM dissipation coefficient | (-) |
| $\alpha_{Bern}$ | Non-uniformity coefficient used in equation of Bernoulli | (-) |
| $B$ | Width of the flume | (m) |
| $\beta$ | Non-uniformity coefficient used in the momentum equation | (-) |
| $c_0$ | Constant of Hoffmans (1993) | (-) |
| $C$ | Chezy coefficient | ($m^{1/2}$/s) |
| $D_{50}$ | Characteristic sieve size of the stones | (m) |
| $\Delta x$ | Forward Euler step size | (m) |
| $\delta$ | Kronecker delta | (-) |
| $err$ | the error in the experimental measurement due to the extraction process | (m/s) |
| $E$ | Mean flow energy | ($J/m^3$) |
| $\epsilon$ | Dissipation term following the theory of large scale to smaller scale eddy dissipation | ($m^2/s^3$) |
| $f$ | Source or sink term for kinetic energy | ($m^2/s^3$) |
| $f_{step}$ | Force of BFS acting on the water | (N) |
| $F$ | Froude number | (-) |
| $g$ | Gravitational constant | ($m/s^2$) |
| $h$ | Water depth | (m) |
| $h_{step}$ | Step height of the BFS | (m) |
| $H$ | Hydraulic head | (m) |
| $\hat{H}$ | ATM head level that takes into account turbulent energy in the mean flow | (m) |
| $i,j$ (*subscript*) | Free index which can take on the values $x, y,$ and $z$ corresponding to the three dimensions | |
| $k$ | Kinetic turbulent energy | ($m^2/s^2$) |
| $\bar{k}$ | Depth averaged kinetic turbulent energy | ($m^2/s^2$) |
| $\bar{k}_0$ | Depth averaged upstream incoming kinetic turbulent energy | ($m^2/s^2$) |
| $\bar{k}_e$ | Depth averaged equilibrium turbulence energy | ($m^2/s^2$) |
| $K$ | Kinetic energy of the mean flow | ($m^2/s^2$) |
| $l$ | Characteristic length scale | (m) |
| $mom$ (*subscript*) | Variable found using the conservation of momentum | |
| $M$ | Depth and time averaged momentum | (N/s) |
| $n$ | Manning's roughness coefficient | ($s/m^{1/3}$) |
| $n$ (*subscript*) | Variable at $n \times \Delta x$ steps downstream of the upstream study area edge | |
| $\bar{p}$ | The root mean squared pressure fluctuations | ($N/m^2$) |
| $\bar{P}$ | The time averaged pressure | ($N/m^2$) |
| $q$ | Specific discharge | ($m^2/s$) |
| $r$ | Turbulence intensity | (-) |
| $r_0$ | Depth and width averaged equilibrium turbulence intensity | (-) |
| $R$ | Hydraulic radius | (m) |
| $R_e$ | Reynolds number | (-) |
| $\rho_w$ | Density of water | ($kg/m^3$) |
| $t$ | Time | (s) |
| $\tilde{u}$ | Instantaneous flow velocity | (m/s) |
| $\bar{u}$ | Time averaged flow velocity | (m/s) |
| $\acute{u}$ | Instantaneous deviation from the time averaged flow velocity | (m/s) |
| $u'$ | Root mean squared velocity fluctuation | (m/s) |

| | | |
|---|---|---|
| $\bar{u}'$ | Depth averaged root mean squared velocity fluctuation | (m/s) |
| $\bar{\bar{u}}$ | Depth and time averaged flow velocity | (m/s) |
| $v$ | Kinematic viscosity of water | (m²/s) |
| $x, y, z$ | Cartesian coordinates | (m) |
| $z$ | Bottom elevation above reference plane | (m) |

# 1 Introduction

## 1.1 Background

A hydraulic structure is a submerged or partially submerged structure that can be used to divert, restrict, stop, or otherwise manage the natural flow of water (Yang & Wang, 2014). A famous example of a hydraulic structure (which will be used to introduce the research topic) is the Oosterschelde. The Oosterschelde storm surge barrier is a sealable hydraulic structure located in the Oosterschelde estuary in the Netherlands. The storm surge barrier functions as a protection against flooding of the Zeeland hinterlands. It closes when water heights larger than 3 m +NAP are expected. The Oosterschelde storm surge barrier is a prominent hydraulic structure that connects the Schouwen-Duiveland and Noord-Beveland isles in Zeeland (Rijkswaterstaat, 2015).



Figure 1 Aerial view of the Oosterschelde Storm Surge barrier (Rijkswaterstaat, 2015)

Hydraulic structures can lead to scour downstream of the structure (Chen & Liew, 2012). Bed protection helps to prevent scour from occurring at undesired locations (Schiereck, 2004). The Oosterschelde storm surge barrier is an example of a large hydraulic structure that influences the hydraulic load on its surrounding bed. When the barrier is partly opened, water is flowing in or out of the Oosterschelde. Due to the restricted flow area through the Oosterschelde barrier the water velocity through and near the Oosterschelde barrier is increased relative to the depth and width averaged flow velocity in the Oosterschelde and North Sea. An increase in flow velocity leads to an increase in the hydraulic load on the surrounding bed. When the hydraulic load is too large, bed particles are mobilized and scour holes appear near the structure. To prevent scour holes from damaging the hydraulic structure, 500 meter of bottom protection up and downstream of the Oosterschelde storm surge barrier was constructed.
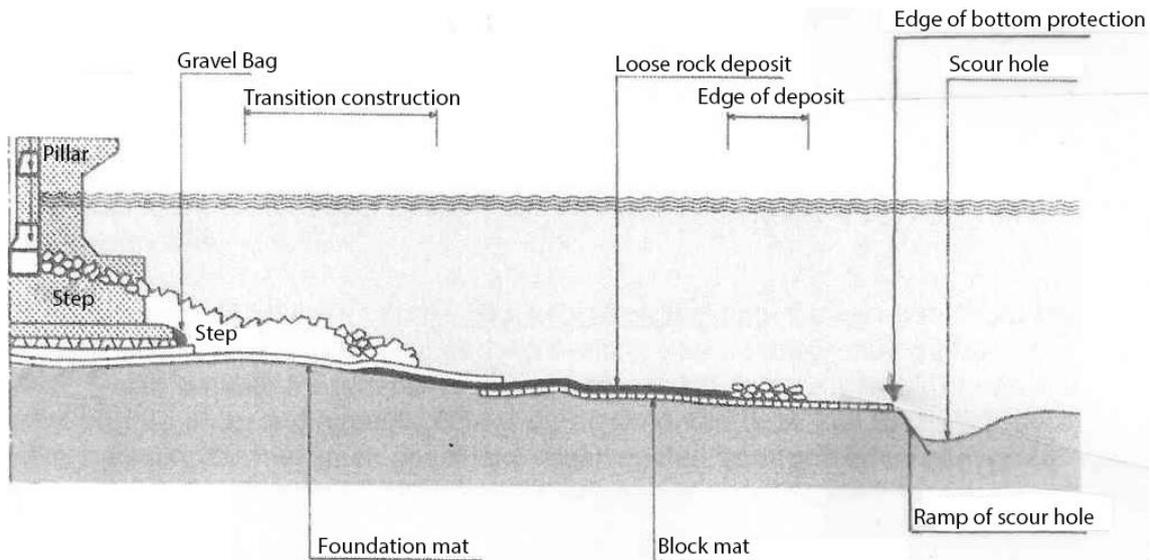
Figure 2 Bottom protection at the Oosterschelde storm surge barrier (Stoutjesdijk et al., 2012)

Figure 2 shows the bottom protection of the barrier. Behind the hydraulic structure, large concrete blocks (transition construction) and foundation mats are placed to protect the bed from the large hydraulic loads. Further downstream the hydraulic load is reduced and smaller protection works (loose rock deposits and block mats) suffice in protecting the bed. Prevention of scour behind hydraulic structures by constructing bed protection is an integral part when designing any hydraulic engineering solution. Accurate design of bed protection can prevent problems later in the hydraulic structure's lifecycle. As can be seen in figure 2, multiple options exist for protecting the bottom against unwanted scour. All bottom protection methods have advantages and disadvantages when applied. A number of bottom protection methods are discussed in appendix A.

### Forces mobilizing the bottom

The instantaneous velocity over the bed determines the force acting on the bed, and thus the stability of the bed. The instantaneous velocity can be decomposed in several parts. A mean flow velocity with a constant size and direction acts on the bed. Waves, when present, result in a to-and-fro fluctuation of the flow velocity, acting along or against the mean flow velocity. Turbulence can be classified as chaotic variations in the flow velocity that result in temporary increases or decreases of the instantaneous flow velocity. The average flow velocity results in a drag force that can wash away bed protection elements (e.g. loose rocks, asphalt, or placed rocks). The presence of waves (e.g. as a result of tides) and turbulence can mobilize the bed protection due to a temporarily increase in flow velocity, resulting in a temporarily increased drag force on any protruding bed protection elements. A sloping bed will results in a horizontal gravity component that also works as a mobilizing force. (The Rock Manual, 2007). Combining above features results in the hydraulic load on the bed protection. For accurate design of stable bed protection, the hydraulic load need to be quantified. Appendix B gives an overview of how the mentioned forces mobilize a grain.
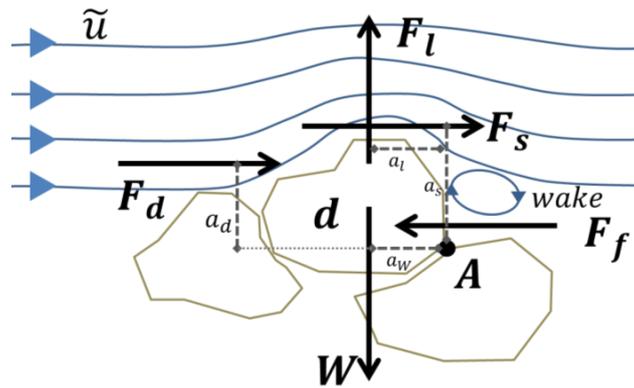
**Figure 3** Forces acting on a grain on the bed. For an explanation of the forces, see appendix B

Because of its easy application, the most applied method for bed protection is using loose rock (Cheng et al., 2014). Because loose rock, by definition, is not fixated on the bed, it can easily be mobilized when the hydraulic load acting on the bed is larger than the design load of the bed protection. In appendix C a design formula is described that can be used to calculate the required stone size for loose rock bed protection under certain hydraulic loads. Among other phenomena, the stability of loose rock bed protection is affected by the mean flow velocity, presence of waves, and turbulence. This study will focus on the turbulence part of the decomposed instantaneous flow velocity affecting bottom stability.

Turbulence affects all river processes of interest to engineers (Nikora & Smart, 1997). More turbulent flows will mobilize larger loose rock bed protection than more laminar flows if all other conditions are similar (Pilarczyk, 1995; Hofland, 2005; The Rock Manual, 2007). For steady uniform flow conditions experiencing equilibrium turbulence intensities, turbulence is implicitly accounted for in the standard design parameters (Pilarczyk, 1995). However, for flows with increased turbulence intensities, for example as a result of sharp bends or due to the presence of hydraulic structures, the required bed protection is significantly altered. When similar flow conditions are considered with the exception of the turbulence intensities, then flows experiencing larger turbulence intensities need loose rock bed protection many times heavier than of flows without increased turbulence intensities (The Rock Manual, 2007, appendix C). Not taking turbulence intensities into account can result in the destruction of the designed bed protection. Therefore an accurate estimation of the turbulence intensities in a flow are paramount in designing stable loose rock bed protection.

## 1.2 Research motivation
During the preliminary design phase of loose rock bed protection, initial designs (multiple alternatives) as well as a construction schedule and cost estimates are made for the project. Bed protection is usually designed in different compartments for different hydraulic loads. The number of compartments, its contents (stone size, winnowing reduction method etc.), and the length of the compartment needs to be determined for each design alternative. A quick estimation of the turbulence intensities is therefore needed to achieve an accurate preliminary design of the bed protection in each compartment.

The effect of turbulence on bed protection can be estimated using two different methods: using rules of thumb in design manuals as a rough estimation or calculating turbulence intensities using complex turbulence models. Using a rule of thumb is a quick method for estimating the effect of turbulence. However, design guides (e.g. Pilarczyk, 1990; The Rock Manual, 2007 or Bezuijen and Vastenburg, 2012) only provide very rough estimates, stating, for example, a low,

medium and high value for the effect of turbulence on the bed protection, where the difference between low and high levels of turbulence can result in 8 times (or more) heavier rocks (appendix C). Dissipation of turbulence over time is not incorporated at all in these rules of thumb, resulting in one value of turbulence for the whole length of the bed protection. Figure 4 graphically depicts the problem with rules of thumb not incorporating production and dissipation of turbulence. The rule of thumb possibly correctly represents the maximum occurring turbulence. However, even if the rule of thumb correctly represents the maximum occurring turbulence, it still overestimates the turbulent energy in the flow for most of the downstream area. It is also possible that the rule of thumb locally underestimates turbulence (because the maximum occurring turbulent energy is larger than the rule of thumb turbulence estimation). This could result in unexpected damages to bed protection due to an underestimation of the turbulence. Vice versa an overestimation of turbulent energy level can result in an oversized bed protection design, which is undesirable from a cost and time perspective.
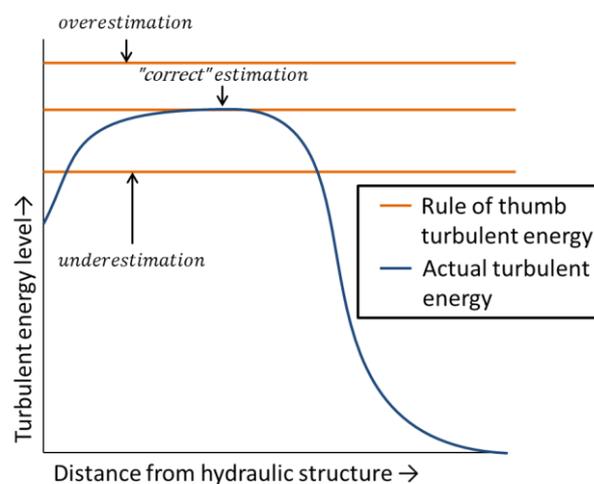


**Figure 4 Turbulent energy downstream of a hydraulic structure according to the rule of thumb versus hypothetical occurring turbulent energy levels[1]**

Alternatively, numerical turbulence models like the $k - \epsilon$ model can be used to calculate the turbulence intensities. According to Mohammadi and Pironneau (1993) these models are more generally applicable and use little assumptions but require more time and expert knowledge to apply due to model setup, runtime and complexity. Ideally, a rapid assessment tool would exist that combines the ease of use of the rules of thumb with the more accurate measures of turbulence found using complex turbulence models. Voortman (2013) designed the Arcadis Turbulence Model (ATM) as an alternative model to estimate turbulent energy in a quick way, more accurately than the rules of thumb and more easy to apply than complex $k - \epsilon$ models. However, the theoretical foundation of the ATM has not been elaborated. The ATM has also not been compared with experimental data to test its empirical validity. The ATM models turbulence generation and dissipation. A dissipation coefficient in the ATM needs to be determined before the ATM can be applied. If the ATM is to be used with confidence as a rapid assessment tool in preliminary design practices, the theoretical and empirical validity of the model should be determined and guidelines should be made about setting the dissipation coefficient. If the ATM is able to estimate turbulence with reasonable accuracy, then a description should also be given how the ATM can be used in the preliminary design phase. During the preliminary design phase

---

[1] The exact shape of the actual turbulent energy in a flow depends on the exact flow circumstances and does not necessarily have to be similar to the hypothetical shape as depicted in figure 4.

only limited data is available. Thus a method should be developed in order to apply the ATM using only the data available during the preliminary design phase.

## 1.3 Research objectives and questions

Different flow scenarios are encountered around hydraulic structures. Water flowing out of a reservoir through a weir can be schematised as backward facing step flow (figure 6) or weir flow (figure 7), depending on the placement of the weir opening (at the bed level or near the surface). When water is flowing towards a weir, the toe of the weir can be schematised as a forward facing step. Downstream of a sluice, an expansion of the channel is often found. This expansion can be schematised as sudden widening of the channel. All above flow scenarios result in a change in flow velocity and turbulence. Because this study did not perform any flume experiments of its own, obtaining data from other studies was necessary. Therefore, for this study backward facing step flow (BFS) is used as the normative flow condition because scientific studies often perform flume experiment with a backward facing step (Nakagawa & Nezu, 1987; Xingkui & Fontijn, 1993; Kasagi & Matsunaga, 1995; De Gunst, 1999; Hofland, 2005). If the ATM is able to accurately approximate the turbulent energy levels in BFS flow, then its field of application could be extended to other flow scenarios (e.g. as depicted in the figures below). For each new flow scenario, the ATM should first be validated before it is used in practice.
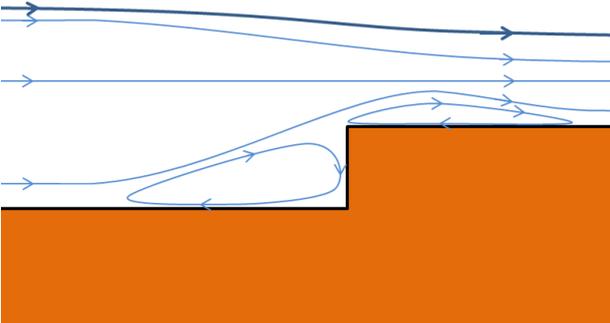
Figure 5 Schematisation of a forward facing step (longitudinal section)
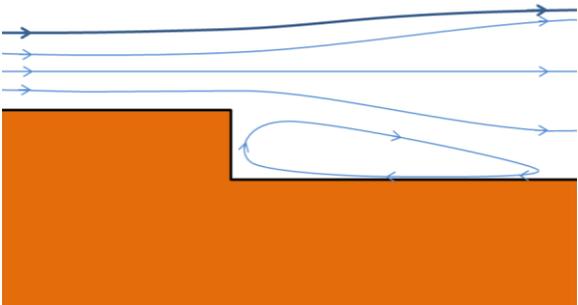
Figure 6 Schematisation of a backward facing step (longitudinal section)
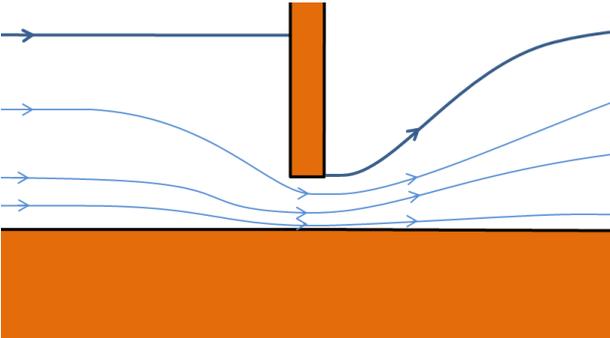
Figure 7 Schematisation of a culvert (flow contraction; longitudinal section)
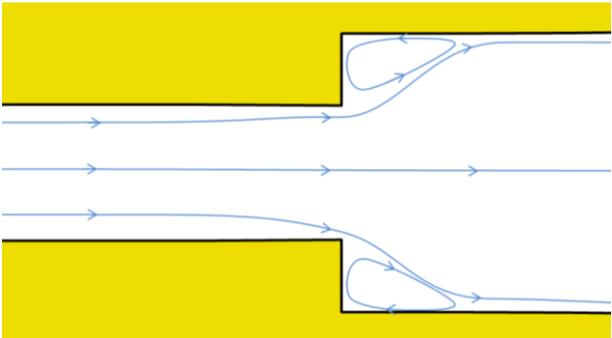
Figure 8 Schematisation of a widening channel (flow widening; top view)

It is the objective of this study to test the theoretical and empirical validity of the ATM as a rapid assessment tool for the flow conditions of a wide channel with a backward facing step. Its application in the preliminary design phase is also discussed due to the limited data available during this phase.

To reach the research objective, the following research questions are answered:

1. What is the theoretical validity of the ATM?
2. What is the accuracy of the ATM turbulence estimations compare to experimental measurements of BFS turbulence?
3. How can the ATM be applied in the preliminary design phase?

## 1.4 Methodology

### Theoretical validation

The theoretical validity of the ATM is assessed in a number of ways. The principles on which the ATM is based are compared to existing literature to show that these principles are partly founded in science. The model is also compared to the turbulent kinetic energy (TKE) equation (derived from the Navier-Stokes equation). The turbulent kinetic energy (TKE) equation is the equation that is used for almost every turbulence model in one form or another. Relating the ATM to the TKE equation will make clear in what ways the ATM simplifies reality. The dissipation coefficient of the ATM is compared to the present knowledge about the rate of dissipation in turbulent flows to check if the dissipation term of the ATM does not conflict with this knowledge.

### Empirical validation

The empirical validity of the ATM is assessed by comparing the turbulent energy levels that follow from the ATM to turbulent energy levels that were measured in experiments. Experimental data was collected from literature to validate the ATM output. The experimental data used to run and validate the ATM is first analysed. Because the experimental data cannot be put into the ATM straight away, a number of methods are discussed to convert the experimental data into ATM input data. The empirical validation of the ATM is then performed by comparing the ATM output against the measured turbulent energy levels for every input data alternative. This will result in a thorough understanding whether the ATM is able to estimate the turbulent energy levels using the selected input data.

### Applying the ATM in the preliminary design phase

Using the results of the theoretical and empirical validation, an assessment is made about the applicability of the ATM in the preliminary design of loose rock bed protection. An example calculation is made to show how the ATM can be used in the preliminary design phase when little information about the BFS flow is available. The benefit of using the ATM instead of rules of thumb during the design of loose rock bed protection is then discussed.

## 1.5 Report outline
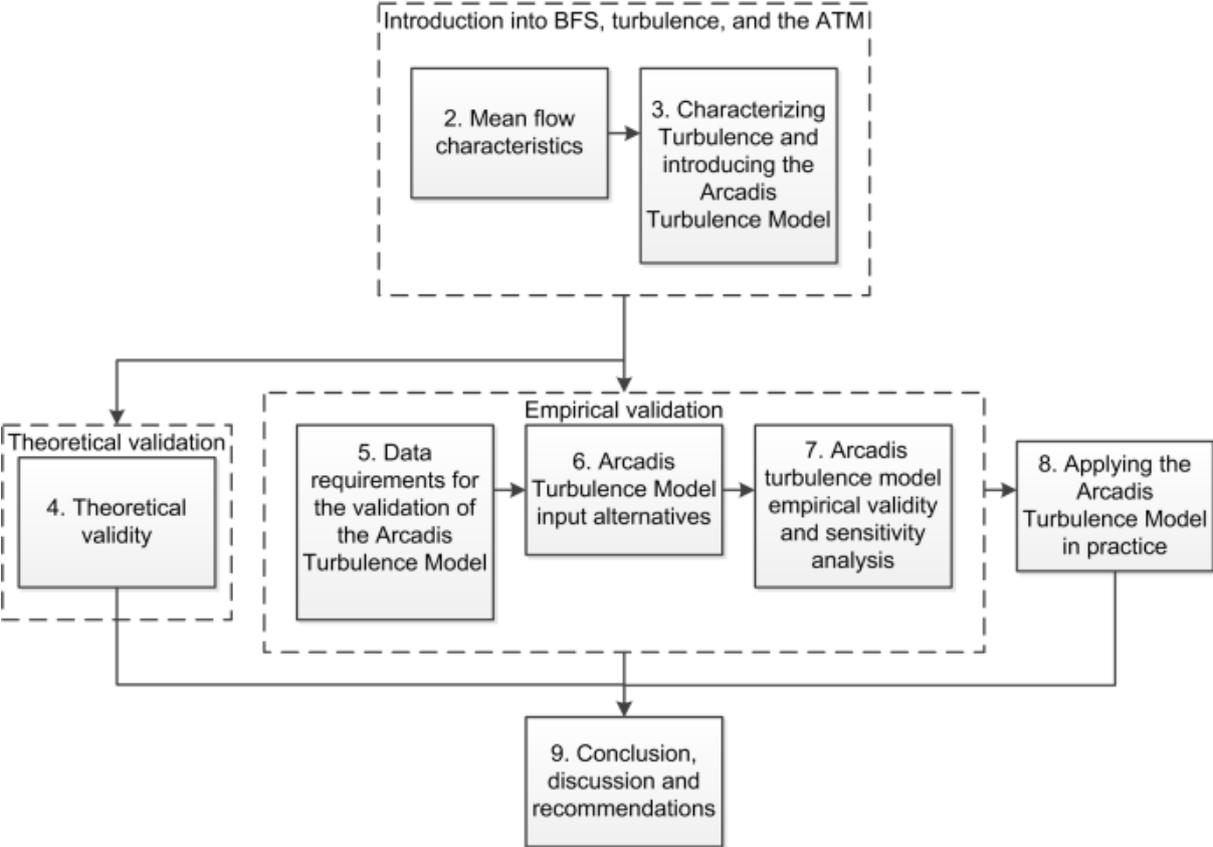


Figure 9 Schematization of report outline

Chapter 2 of this report discusses the properties of the mean flow over a BFS. This information is then used in chapter 3 to describe the turbulence in a flow over a BFS. Chapter 3 will also describe the Arcadis Turbulence Model. The theoretical validation is given in chapter 4. Chapter 5 introduces the data required for the empirical validation, chapter 6 discussed how this data is used to run the ATM and chapter 7 then discusses the results of the empirical validation of the ATM. Based on the results of the empirical validation of the ATM, a method is shown how the ATM can be used in the preliminary design phase in chapter 8. This thesis is concluded in chapter 9 where the theoretical and empirical validity are compared and discussed.

# 2 Mean flow characteristics

## 2.1 Introduction

Turbulence is a function of the mean flow conditions (Tennekes & Lumley, 1972). Therefore, in order to understand turbulence in a flow, first, the mean flow conditions of a flow should be clear. Mean flow characteristics of simple stationary flow are discussed in section 2.2. The more complex backward facing step flow is discussed after that. However first two general remarks about the flow scenarios in this chapter are given:

- The flow scenarios discussed in this chapter are schematizations of reality. This means that although the flow schematizations approximate the water behaviour as observed in reality, they do not represent the water behaviour exactly due to some assumptions made in the schematization of the flow.
- In this chapter, flow patterns are discussed neglecting flow variations in the flume width. In fact for this whole study, the world is schematized in 2DV dimensional space because flow is expected to behave reasonably uniform in the transverse plane ($z$ direction). In chapter 9 this assumption is discussed.

## 2.2 Stationary flow over a flat bottom

Uniform stationary flow over a horizontal plane, without bottom friction
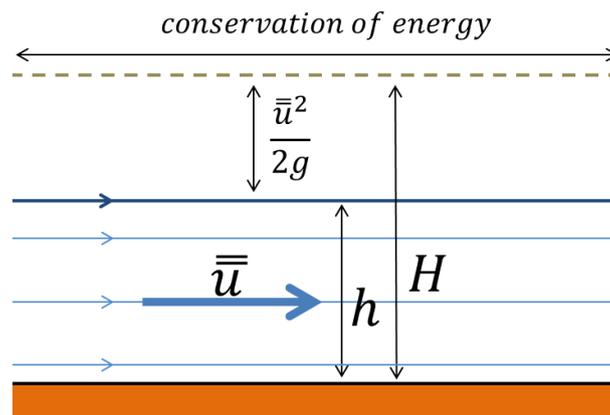


Figure 10 Uniform stationary flow without slope or bottom friction

Figure 10 shows a schematization of uniform stationary flow over a horizontal plane, without bottom friction. The term $\bar{\bar{u}}$ equals the depth and time averaged flow velocity (m/s) where the flow velocity is time averaged to average out any turbulent fluctuations in the flow. The term $h$ equals the water depth (m). Water is flowing in and out of the domain with a certain speed $\bar{\bar{u}}$ and water height $h$. All water flowing into the domain is also flowing out of it because the water level is assumed (modelled) to be stationary. Assuming the width $B$ (m) of the schematized channel does not change then the mass of the flow in the domain is preserved following:

$$q = \bar{\bar{u}} \times h = constant \qquad (2.1)$$

Where $q$ equals the specific discharge (m²/s). Because bottom friction is ignored, the mean flow energy in the domain is preserved. Flow energy can be defined using the formula of Bernoulli. Given in energy head levels this formula equals:

$$H = z + h + \frac{1}{2}\frac{\bar{\bar{u}}^2}{g} \qquad (2.2)$$

Where $H$ equals the energy of a fluid (m), $z$ the elevation above a reference plane (m), $h$ the water height (m), $\bar{\bar{u}}$ the depth and time average flow velocity (m/s), and $g$ the gravitational constant (m/s[2]). When it is assumed that no energy is lost[2], then the head levels won't change. In figure 10 it can be seen that the head level $H$ remains constant for the whole domain. Because of the horizontal bed and no external forces, the water depth and flow velocity also do not change.

## Stationary flow over a slope, without bottom friction
When water is flowing over a slope, the flow conditions of the schematization change (figure 11):
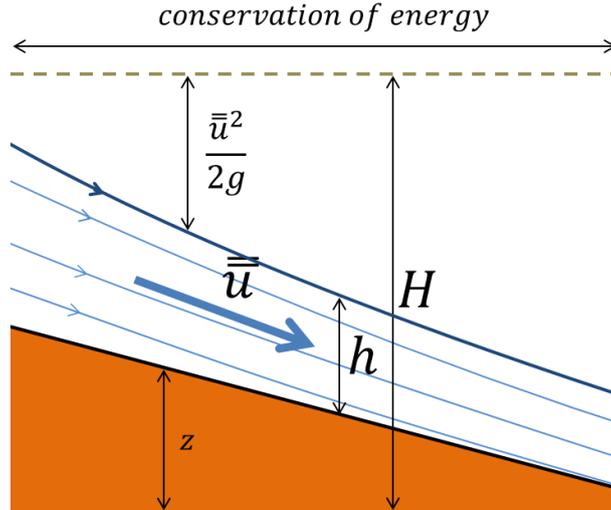


Figure 11 Stationary flow over a sloped surface without bottom friction

Formula 2.2 still applies to this flow situation. However, due to the slope, gravity is transforming potential energy into kinetic energy. In equation 2.2 this means a reduction of $z$ and an increase of $\frac{\bar{\bar{u}}^2}{2g}$. The change in head level can now be calculated by taking the derivative of the Bernoulli equation (derivation given in appendix D):

$$\frac{dH}{dx} = \frac{dz}{dx} + \frac{dh}{dx} + \bar{\bar{u}}\frac{d\bar{\bar{u}}}{dx}\frac{1}{g} \qquad (2.3)$$

Because an equal amount of water is flowing in and out of the domain of figure 11 mass is preserved following equation 2.1. Using the conservation of mass, conservation of energy $\left(\frac{dH}{dx} = 0\right)$, and equation 2.3 the change in water height due to the slope can be calculated. Rewriting equation 2.3 into an expression of $\frac{dh}{dx}$ is not part of the scope of this study. For further information refer to Tuin et al. (2014) who derived this formula in their paper. For the flow situation described in figure 11 the water depth $h$ asymptotically reaches zero when the slope is extended indefinitely. Because of conservation of mass, the flow velocity $\bar{\bar{u}}$ is then increase until it reaches infinity (for $h = 0$). This peculiar behaviour is the result of neglecting bottom friction. The above flow situation cannot occur in reality because in reality, bottom friction always affects the flow.

---

[2] In this thesis, it is sometimes stated that energy is preserved or not. When it is stated in this thesis that energy is not preserved, it is meant that the mean flow energy is not preserved. Per definition, energy is preserved in the universe, so when mean flow energy is lost, this energy is transferred out of the mean flow, and into another energy carrier (e.g. into turbulence).

### Uniform stationary flow over a slope, with bottom friction

When bottom friction is considered, the flow conditions reach an equilibrium at $h > 0$ and for the flow schematisation, flow conditions are found that better represent reality:
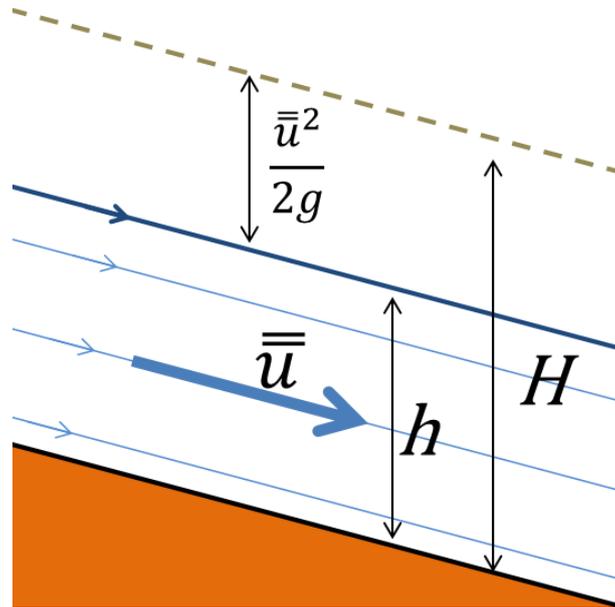


Figure 12 Uniform stationary flow over a sloped surface with bottom friction

When bottom friction is considered, the water level reaches an equilibrium where the conversion of potential into kinetic energy due to the sloped bed is cancelled by the loss of (kinetic) energy due to bottom friction. Note that the head level is now running parallel with the sloped bed level thus energy is not preserved in the flow anymore. For equilibrium stationary flow conditions, the slope of the head level now follows $\frac{dH}{dx} = -\frac{\bar{\bar{u}}^2}{C^2 R}$ better known as the law of Chezy. Conservation of energy and conservation of mass cannot be used anymore to calculate the water depth in figure 12. However, equation 2.4 can be used to calculate the water depths when bottom friction following the law of Chezy is affecting the flow.

$$\frac{dH}{dx} = -\frac{\bar{\bar{u}}^2}{C^2 R} = \frac{dz}{dx} + \frac{dh}{dx} + \bar{\bar{u}}\frac{d\bar{\bar{u}}}{dx}\frac{1}{g} \tag{2.4}$$

Where $\frac{dH}{dx}$ equals the head loss due to bottom friction (-), $\bar{\bar{u}}$ equals the depth and time averaged flow velocity (m/s), $C$ the Chezy coefficient (m$^{1/2}$/s), and $R$ the hydraulic radius (m)[3]. A method to calculate the water height from equation 2.4 is discussed in the paper of Tuin et al. (2014).

### Flow assumptions required to apply the formula of Bernoulli

Formula 2.2 (and to a lesser extent 2.3 and 2.4) can only be applied when certain assumptions are valid. The formula of Bernoulli assumes a steady flow, and can therefore not be applied to flow conditions that change in time. The Bernoulli equation also does not take into account energy loss (equation 2.4 is an adjusted Bernoulli formula that does take into account energy loss due to wall friction). The Bernoulli equation also assumes parallel stream lines. When streamlines are not parallel, the hydrostatic pressure distribution might not be correctly represented by the water depth $h$ which will result in an incorrect representation of the mean flow energy (by applying

---

[3] Note that for uniform flow conditions, the terms $\frac{dh}{dx} = \bar{\bar{u}}\frac{d\bar{\bar{u}}}{dx}\frac{1}{g} = 0$ in equation equation 2.4. Resulting in $\frac{dH}{dx} = -\frac{\bar{\bar{u}}^2}{C^2 R} = \frac{dz}{dx}$ (Chezy's law).

the Bernoulli equation). The Bernoulli equation also assumes an uniform velocity profile as a function of the depth (water velocity at the water surface equals water velocity at the bottom with no change in between). A correction parameter $\alpha_{Bern}$ exists when the velocity profile is not uniform for the water depth $\left(H = z + h + \alpha_{Bern}\frac{1}{2}\frac{\bar{\bar{u}}^2}{g}\right)$. However, the Bernoulli equation is most often applied to log-law velocity profiles, which have a water depth velocity profile resulting in a $\alpha_{Bern} \approx 1$, thus $\alpha_{Bern}$ is generally left out of the Bernoulli equation. The Bernoulli equation is also not valid when external forces act on the flow like centrifugal forces or propeller machines. The above stated limitations of the Bernoulli equation are also discussed in Cruise, et al. (2007). Before applying the Bernoulli equation, it is important to check whether the assumptions on which it is based are valid.

## 2.3 Backward facing step flow

### Flow pattern over a backward facing step

Figure 13 depicts the channel schematization of a backward facing step for this study. Upstream of the step, water is flowing with a certain velocity and depth. For the above schematisation, it is assumed that energy loss due to bottom friction is negligible (smooth channel and short flow distance from beginning to end of the domain). The smooth slope of the step at the upstream location eliminates the energy loss due to flow separation (no wakes) (Greenblatt & Wygnanski, 2000). Without bottom friction or wakes, energy is preserved up until the end of the step. The Bernoulli law can then be used to calculate the flow velocities and water depths up until the end of the step using equation 2.3. This study, however, focusses on the area above and downstream of the step (study area shown in figure 13) because the flow is decelerated in that region (and no experimental data was available for the location upstream of the step).
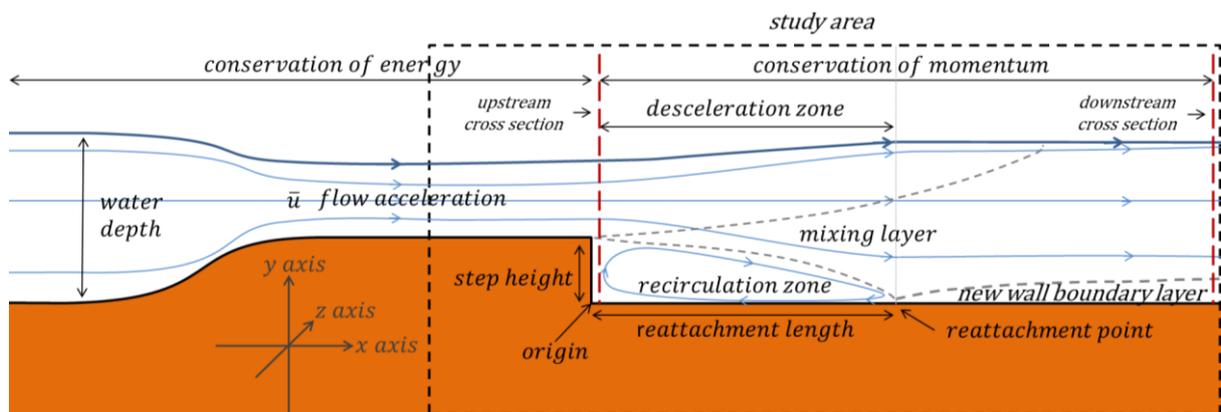


Figure 13 Schematization of BFS flow

Downstream of the step, the flow is decelerated and a recirculation zone is formed (Nakagawa & Nezu, 1987; Xingkui & Fontijn, 1993; Hofland, 2005). The water flow in the recirculation zone has a lower speed than the water arriving from the step (Nakagawa & Nezu, 1987; Xingkui & Fontijn, 1993; Kasagi & Matsunaga, 1995; De Gunst, 1999; Hofland, 2005). Whenever two bodies of fluid move along each other with different velocities, a mixing layer will grow between them (Schiereck, 2004). This mixing layer continues to grow until the water cross-section is fully mixed. After the mixing layer reaches the bed at the reattachment point, the flow starts to develop into a new equilibrium flow condition downstream of the reattachment point. However, it can take more than 52 step heights before the flow velocity profile (as a function of the water depth) reverts fully back to a log-law profile (Nakagawa & Nezu, 1987).

**Using the conservation of momentum to define the backward facing step flow characteristics**

Figure 14 shows the head levels, as it is assumed to occur for a BFS flow. Due to viscous friction in the water, decelerating flow causes a decrease in flow energy (Song & Chiew, 2001). Because flow energy is lost downstream of the backward facing step, the Bernoulli law can no longer be used to calculate the water depths and flow velocities without knowing exactly how much flow energy is lost $\left(H_{downstream} = H_{upstream} - H_{deceleration}\right)$. The law of Chezy can be used to find the mean flow energy loss due to wall friction. However, energy loss due to internal viscous frictions is then wrongfully omitted. In order to find the total mean flow energy loss (wall and viscous friction), the conservation of momentum is considered instead of conservation of energy.
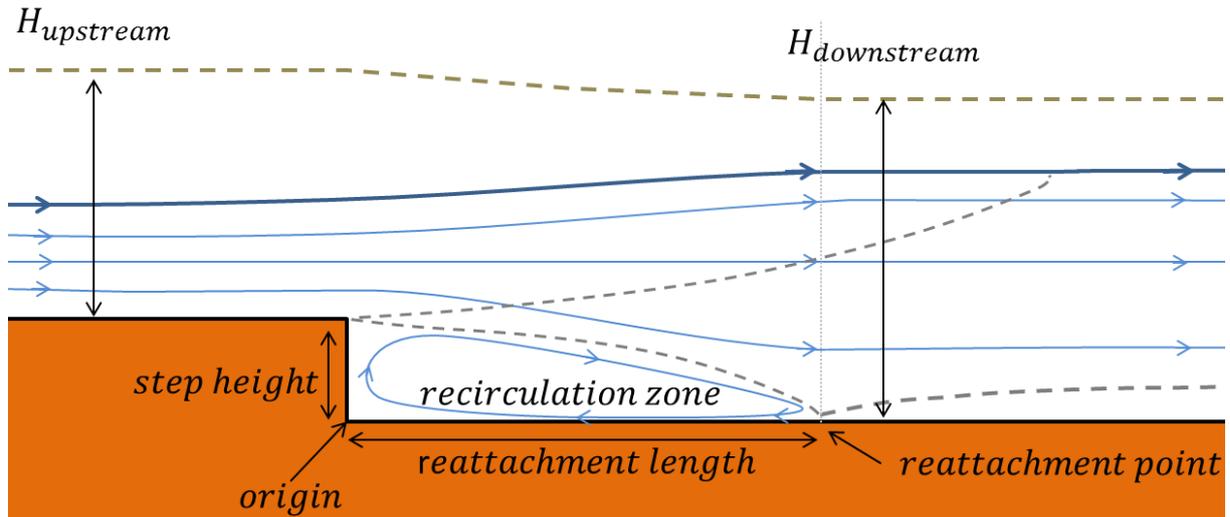


Figure 14 Schematization of BFS flow showing mean flow energy levels

Conservation of momentum is defined as follows: For a depth and width averaged flow, the sum of forces acting on two cross sections cancel each other out, assuming no external force is acting on or in between the cross sections. The formula for momentum in a flow including the hydrostatic pressure term is given by (Battjes, 1990):

$$M = \frac{1}{2}\rho_w gh^2 + \rho_w \beta h\bar{\bar{u}}^2 \qquad (2.5)$$

Where $M$ equals the momentum (N/m), $\rho_w$ equals the density of water (kg/m³), $g$ the gravitational constant (m/s²), $\bar{\bar{u}}$ equals the depth and time averaged flow velocity (m/s) and $\beta$ (-) a term that corrects the momentum for non-uniformity of the flow profile $\bar{u}$ similar to $\alpha_{Bern}$ in the Bernoulli equation.
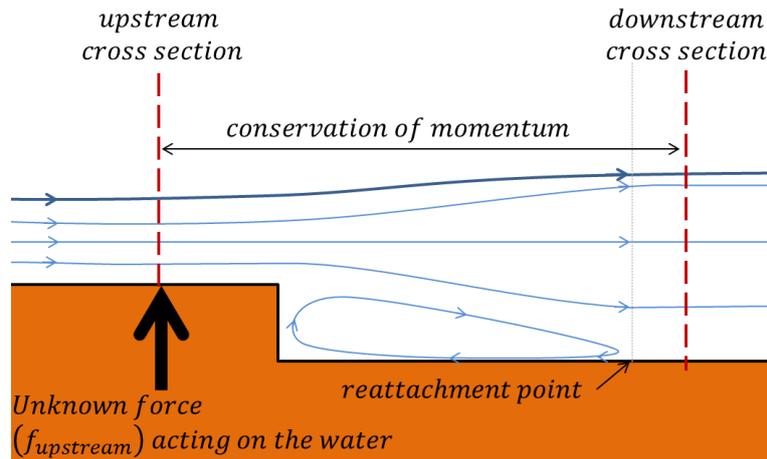
Figure 15 Cross sections with unknown force $f_{step}$ acting on the water

Initially, one would expect that using the cross sections as depicted in figure 15 is the most convenient (to calculate the water depth downstream of the reattachment point using the preservation of momentum). However, using the conservation of momentum at the cross sections shown in figure 15 in combination with formula 2.5 will be hard. An unknown force $f_{upstream}$ acts on the upstream cross section. The force $f_{upstream}$ is the result of the elevated bottom of the step. The cross sections shown in figure 13 (red lines) are proposed in order to circumvent estimating this unknown force.

Let's assume the upstream cross section located at an infinitely small distance downstream of the step, as shown in figure 16 (and figure 13).
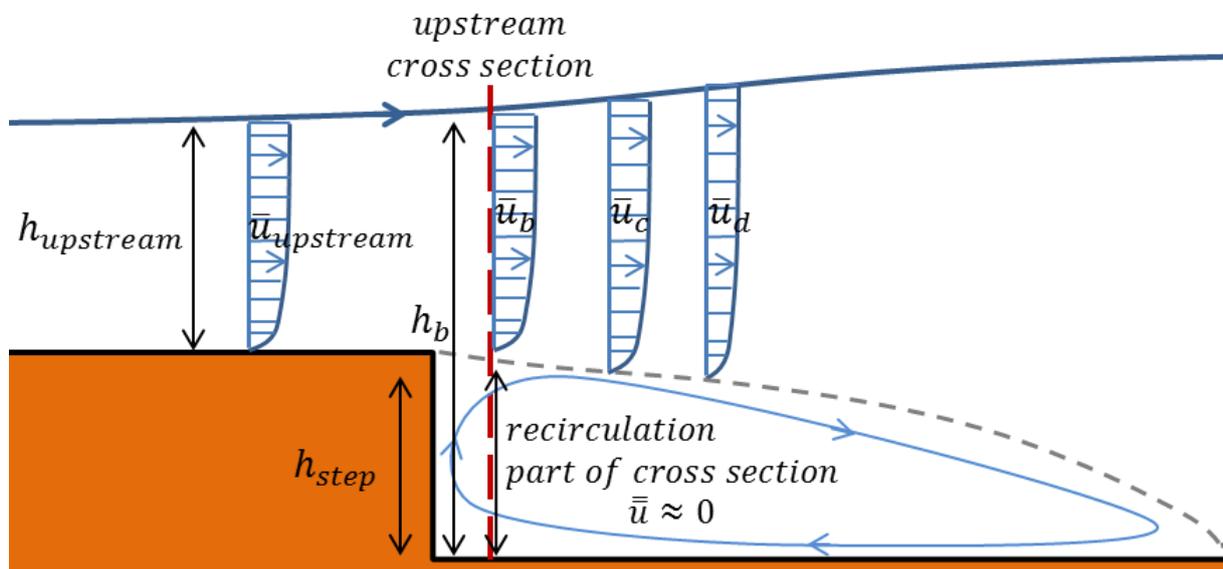


Figure 16 Velocity profile at an infinitely small distance downstream of the step

At the cross section depicted in figure 16, the momentum[4] can be defined using the following formula:

$$M_{upstream} = \frac{1}{2}\rho_w\left(h_{upstream} + h_{step}\right)^2 + \rho_w h_{upstream}\bar{\bar{u}}_{upstream}{}^2 \qquad (2.6)$$

---

[4] Including the hydrostatic pressure term

This formula follows from equation 2.5, the assumption that the flow velocity profile and water depth just downstream of the step has not changed much $\left(\bar{\bar{u}}_{upstream} = \bar{\bar{u}}_b \;\& \; h_b = h_{upstream} + h_{step}\right)$, and the assumption that the flow velocity in the recirculation zone is negligible small just downstream of the step. Because of these assumptions, $\beta = 1$ in equation 2.6. Formula 2.6 is derived in appendix E.

Between the cross section as shown in figure 16, and the cross section located downstream of the reattachment point (see figure 13) the momentum in the flow is preserved. If the flow velocity $\bar{\bar{u}}_{upstream}$, the water depth $h_{upstream}$ and the step height $h_{step}$ are known, then the momentum can be calculated using equation 2.6. If it is assumed that at the downstream cross section (figure 13) the flow velocity profile approximates an uniform profile, then $\beta \approx 1$ and:

$$M_{downstream} = \frac{1}{2}\rho_w g(h_{downstream})^2 + \rho_w h_{downstream}\bar{\bar{u}}_{downstream}^{\;2}$$

$$q = \bar{\bar{u}}_{upstream} \times h_{upstream} = \bar{\bar{u}}_{downstream} \times h_{downstream}$$

$$M_{upstream} = M_{downstream}$$

Gives:

$$h_{downstream} = \frac{M_{upstream} - \frac{1}{2}\rho_w g(h_{downstream})^2}{\rho_w \dfrac{q^2}{h_{downstream}^2}} \qquad (2.7)$$

Where $q$ equals the specific discharge (m2/s). Equation 2.7 is derived in appendix F. Equation 2.7 can be solved analytically or using a computer programme like MathCad. The analytical solution of equation 2.7 is not depicted in this thesis because of its complexity (analytical solution is one page long).

### Flow assumptions required to apply the conservation of momentum

Following the method described above, the water height and flow velocity at the reattachment point can be calculated using the conservation of momentum. However, there are some limitations to applying the conservation of momentum like this. Conservation of momentum using equation 2.5 is only applicable when the flow streamlines are parallel and straight (Battjes, 1990). Figure 13 shows that just downstream of the end of the step and at the reattachment point, this is (by approximation) the case. However, the area in between these cross sections show diffusive sloped stream lines. In this area, equation 2.5 is not applicable anymore. Thus the preservation of momentum can only be used to calculate the water depth at the downstream cross section. Because bed friction acts as a force on the flow, momentum is lost in between the cross sections as the result of bed friction. For smooth beds or small flow distances, it can be assumed that this loss of momentum is negligible (and thus momentum is preserved). A depth profile with large variations in the flow velocity is not represented accurately by the depth and time averaged flow velocity $\bar{\bar{u}}$ when calculating the momentum (Battjes, 1990). By applying the $\beta$ coefficient (equation 2.5) correctly, the non-uniformity of the velocity profile can be taken into account. The validity of calculating the water depth and flow velocity using the conservation of momentum is discussed in section 6.5 in more detail by comparing the results to experimentally measured data.

## 2.4 Concluding remarks

This chapter introduced how the flow patterns over a simple sloping bed and a more complex backward facing step beds can be schematized. Water levels and flow velocities under uniform stationary or BFS flow conditions can be approximated by using flow schematizations and the laws of conservation of mass, energy and momentum. Although there are some assumptions required when applying the conservation of energy or momentum, we can estimate the downstream water depth using the upstream flow variables (water depth, flow velocity profile).

# 3 Characterizing turbulence and introducing the Arcadis Turbulence Model

## 3.1 introduction

Turbulent energy contained within a flow can be measured or approximated. In this chapter, first, an introduction is given into turbulence. The generation and dissipation of turbulence for the flow scenarios given in chapter 2 are then discussed to introduce the reader in the phenomena affecting turbulent energy in a flow. After that, the ATM is introduced as a rapid assessment tool for estimating turbulent energy. Finally, it is shown that the Arcadis Turbulence Model can confirm with the formula of Hoffmans (1993) for equilibrium turbulence.

## 3.2 Quantifying turbulence

The Reynolds decomposition (e.g. as discussed by Adrian, et al., 2000) defines turbulence as a function of the fluctuating velocity component superimposed on the mean velocity of a flow. The mean flow velocity is found by time averaging the instantaneous flow velocity, the fluctuating velocity component is the difference between the time averaged and instantaneous velocity component:

$$\tilde{u}_i = \bar{u}_i + \acute{u}_i \tag{3.1}$$

Where $\tilde{u}_i$ equals the instantaneous flow velocity (m/s), and $\bar{u}_i$ equals the time averaged flow velocity (m/s). The time averaged flow velocity $\bar{u}_i$ is averaged over the characteristic turbulence duration, so no turbulent eddies are present in the time averaged flow velocity measures anymore. The term $\acute{u}_i$ equals the instantaneous deviation from the time averaged flow velocity (m/s). The subscript $i$ is a free index which can take on the values $x, y,$ and $z$ corresponding to the three dimensions[5].

For a certain location, $\bar{u}_i$ now gives a single time averaged value, whereas $\acute{u}_i$ gives the deviation from this time averaged value for each measurement in time and $\sum \acute{u}_i = 0$. To get the non-zero time averaged value for the velocity fluctuations, the root mean square (RMS) of the turbulent fluctuations $\acute{u}_i$ is taken:

$$u_i' = \sqrt{\frac{1}{t} \sum_{t=1}^{t} (\acute{u}_i)^2} \tag{3.2}$$

Where $u_i'$ equals the root mean squared velocity fluctuation[6] (m/s), $\acute{u}_i$ equals the instantaneous velocity fluctuations (m/s) and $t$ the number of realisations of $\acute{u}_i$ (-) (or in other words, the number of times $\acute{u}_i$ is measured in time at a certain location).

---

[5] The Einstein summation convention is used in this thesis when an index variable appears twice in a single term (e.g. equation 3.2) (Einstein, 1916)

[6] In the thesis, a variable with a bar on top (e.g. $\bar{u}$) indicates a variable that is averaged over a dimension (length, time etc.). Therefore, the correct notation of the RMS flow velocity fluctuations would be $\bar{\acute{u}}_i$. However, in order to improve the readability of the presented formulae, $\bar{\acute{u}}_i$ is written as $u_i'$ instead. The notation $\bar{u}_i'$ is used for the RMS depth averaged velocity fluctuations. Also keep in mind that all variables are considered to be uniform over the width of the study domain, thus no width averaging bar is shown anywhere.

Turbulent energy in a flow is defined as:

$$k = \frac{1}{2}(u_i')^2 \qquad\qquad (3.3)$$

Where $k$ equals the turbulent kinetic energy[7] (m²/s²), and $u_i'$ the RMS velocity fluctuation (m/s).

The turbulent intensity is defined as:

$$r = \frac{\sqrt{k}}{\bar{u}} \qquad\qquad (3.4)$$

Where $r$ equals the turbulence intensity (-), $\bar{u}$ equals the time averaged flow velocity and $k$ equals the turbulent energy. The turbulence intensity (instead of the turbulent energy) is often used in the design of bed protection (The Rock Manual, 2007).

## 3.3 Turbulence under different flow scenarios

### Generation of turbulence due to shear stresses

The generation and dissipation of turbulence depends on the mean flow conditions (Tennekes & Lumley, 1972). Whenever two bodies of fluid move along each other with different velocities, a mixing layer will grow between them (Schiereck, 2004). Due to shear stresses the velocity differences around the mixing layer lead to generation of turbulence (Schiereck, 2004). When water is flowing over a bottom or a wall, the shear stresses acting on the water (due to the presence of the bottom/wall) also generates turbulence. Turbulence is dissipated due to internal viscous friction of the turbulent eddies (Schiereck, 2004).
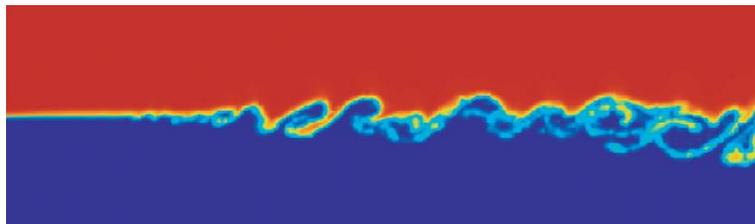


Figure 17 Example of mixing of two gasses flowing side by side at different velocities (Uchiyama, 2006)

Figure 17 shows a numerical simulation of two gasses flowing side by side at different speeds. No walls are present in the above figure. Due to the difference in flow velocity, shear friction acts on both gasses. The shear friction results in an unstable flow condition, and as a result the gasses start to mix. The generation of a mixing layer goes hand in hand with generation of turbulent energy (Schiereck, 2004). In the above figure gasses mix and turbulence is generated, the mixing of fluids shows similar behaviour.

### Turbulence in uniform stationary flow over a slope experiencing bottom friction

For uniform stationary flow over a slope experiencing bottom friction (figure 12) the water level and flow velocity are in equilibrium. Due to the water flowing over a rough bed (shear stresses), turbulence is constantly generated. Without turbulence dissipation, this would mean turbulence grows indefinitely for a slope that continues indefinitely. However, according to Hoffmans (1993), under stationary uniform equilibrium flow conditions, turbulent energy is also in equilibrium. This means that turbulence needs to be dissipated and generated at an equal rate to reach an

---

[7] The units of turbulent energy as defined in equation 3.3 do not correspond with the units of energy ($J$ or $kg\, m^2/s^2$). The convention is to leave out the density of water $\rho_w$ when calculating the turbulent energy because the density is often assumed to be constant. When the density of water is added to equation 3.3, the units of turbulent energy equal $J/m^3$, or in words: energy per volume of water.

equilibrium (and not grow indefinitely). For uniform stationary flow and depth average turbulence Hoffmans (1993) formulated a formula describing the equilibrium turbulence intensity:

$$r_0 = 1.21 \frac{\sqrt{g}}{C}$$

(3.5)

Where $r_0$ equals the depth and width averaged equilibrium turbulence intensity (-), $g$ the gravitational constant (m/s2) and $C$ the Chezy coefficient (m1/2/s). This formula describes the equilibrium turbulence level found as the result of undisturbed flow experiencing bottom friction. After a flow disturbance (e.g. a BFS), a distance downstream of the disturbance the turbulence levels revert to equilibrium turbulence levels as defined by equation 3.5.

### Turbulence in backward facing step flow

For BFS flow, the flow depth is suddenly increased downstream of the step and a recirculation zone is formed (figure 13). The water arriving from the step has a larger velocity than the water flow in the recirculation zone. As a result a mixing layer is formed that mixes the slow and fast flowing water. Due to the interaction between the low velocity and high velocity flows, internal viscous stresses act on the flow, and turbulence is generated. At the reattachment point, it is assumed that the flow is fully mixed and turbulence is only generated due to the bottom roughness. The turbulent energy downstream of the reattachment point is expected to slowly revert back to an equilibrium level.

## 3.4 The Arcadis Turbulence Model

### Introduction in the Arcadis turbulence model

"Turbulence (...) can be interpreted as the process that allows the kinetic energy of the main flow to dissipate, leaving the system as heat due to viscous friction"(Schiereck, 2004, p. 44). This is one of the premises on which the ATM is build.

The ATM is based on the assumption that depth averaged turbulent energy $\bar{k}$ can be added to the Bernoulli equation. To add the depth averaged turbulent energy to the Bernoulli equation (2.2) it is first divided by the gravitational constant $g$ to express the kinetic turbulent energy in the right units, this results in:

$$\hat{H} = z + h + \frac{1}{2}\frac{\bar{\bar{u}}^2}{g} + \frac{\bar{k}}{g}$$

(3.6)

Notice that the notation $\hat{H}$ is used because equation 3.6 no longer represents the head levels as defined by the Bernoulli principle, but now represents a new head level that takes into account the turbulent energy in the flow. This new head level will be called the ATM head level. The ATM head level takes into account the turbulent energy in a flow. The mean flow energy as defined by the formula of Bernoulli assumes stationary flow velocities. The mean flow energy as defined by the ATM head levels, also assumes stationary flow velocities, but adds the turbulent kinetic energy which disappeared in the Bernoulli equation due to time averaging of the flow velocity profile.

### Turbulent energy production

Shear stresses result in production of turbulent energy and dissipation of mean flow energy. The energy cascade states that mean flow energy loss is first transformed into turbulent energy before being dissipated (Schiereck, 2004). Thus when the mean flow energy is decreased, the turbulent energy is increased. The ATM assumes that this conversion is 100% efficient. Taking the derivative of equation 3.6 (similar to the derivative performed in appendix D) and rewriting the

equation gives an expression how the turbulent energy changes when the mean flow energy changes, assuming 100% conversion efficiency:

$$\left(\frac{d\bar{k}}{dx}\right)_{production} = -g\left(\frac{dz}{dx} + \frac{dh}{dx} + \frac{1}{2g}\left(2\bar{\bar{u}}\frac{d\bar{\bar{u}}}{dx}\right)\right) = -g\frac{dH}{dx} \quad (3.7)$$

Equation 3.7 states that the production of turbulent energy is proportional to the energy loss of the mean flow. Testing the validity of this equation is one of the research goals of this study. Note that equation 3.7 does not elaborate on the cause of the mean flow energy loss. This means that, in theory, the term $\frac{dH}{dx}$ incorporates every mean flow energy loss term (e.g. bottom friction, flow deceleration, other causes of viscous stress). The exact sources of mean flow energy loss incorporated in equation 3.7 depends on the application of the formula.

Equation 3.7 does not contain a dissipation term but only describes the production of turbulent energy. Turbulence dissipation needs to be added to correctly model the energy cascade. If turbulent energy dissipation is left out, the turbulent energy will increase up to infinity when the mean flow continuously loses energy (e.g. for uniform stationary flow experience bottom friction).

**Turbulent energy dissipation**
It was already discussed that flow looses energy due to bottom friction following the formula of Chezy:

$$\frac{dH}{dx} = -\frac{\bar{\bar{u}}^2}{C^2 R} \quad (2.4)$$

Rewriting equation 2.3 using flow energy (J/m³) instead of head levels (m) gives:

$$\frac{dE}{dx} = -\frac{g}{C^2}\frac{\rho_w \bar{\bar{u}}^2}{R} \quad (3.8)$$

Where $\frac{dE}{dx}$ equals the energy loss due to bottom friction per unit of distance (J/m⁴). The term $\frac{g}{C^2}$ in equation 3.8 is a dimensionless constant that defines the kinetic energy loss per unit of distance due to friction. The energy cascade states that energy loss is first transformed into turbulent energy before being dissipated (Schiereck, 2004). The ATM assumes that there exists a constant that determines the turbulent energy dissipation per unit of distance, similar to the dissipation of flow energy due to bottom friction:

Dissipation of flow energy:

$$\frac{dE}{dx} = -constant \times \frac{\rho_w \bar{\bar{u}}^2}{R} \quad (3.9)$$

Dissipation of turbulent energy:

$$\left(\rho_w \frac{d\bar{k}}{dx}\right)_{dissipation} = -constant \times \frac{\rho_w \bar{k}}{R} \quad (3.10)$$

In equation 3.9, following Chezy, the constant equals $\frac{g}{C^2}$. In equation 3.10, the constant is unknown. The turbulent energy dissipation constant in equation 3.10 will be called $\alpha$. The dissipation of turbulent energy according to the ATM is thus given by:

$$\left(\frac{d\bar{k}}{dx}\right)_{dissipation} = -\alpha\frac{\bar{k}}{R} \tag{3.10}$$

Combining the production and dissipation terms gives the final expression of the ATM for turbulence in a flow that will be tested for its validity:

$$\frac{d\bar{k}}{dx} = \underset{(production)}{-g\frac{dH}{dx}} \quad \underset{(dissipation)}{-\alpha\frac{\bar{k}}{R}} \tag{3.11}$$

This differential equation models the change in depth averaged turbulent energy as a function of the change in head levels, and the turbulent energy itself. Using some assumptions, the ATM can be solved analytically. However, the analytical solution for the ATM model is only as valid as the assumptions on which it is based. In appendix G the analytical solution for the ATM is given, assuming a constant production term $\frac{dH}{dx} = D$.

## 3.5 The Arcadis Turbulence Model for equilibrium turbulence

As a rapid assessment tool, the ATM should be applicable to a large number of flow scenarios. For BFS flow, the ATM will be validated using empirical data. For stationary uniform flow experiencing a rough bottom, it can already be shown the ATM is consistent with the existing formula for equilibrium turbulence.

Hoffmans (1993) formulated an equation describing the turbulence intensity under stationary uniform flow conditions (equation 3.5). Under stationary uniform flow conditions turbulent energy does not change in the flow direction (Hoffmans, 1993), thus $\frac{d\bar{k}}{dx} = 0$. To satisfy no change in turbulent energy the production of turbulence should then equal the dissipation[8]. Applied to the ATM, this results in the following equation:

$$\frac{d\bar{k}}{dx} = 0 \rightarrow -g\frac{dH}{dx} = \alpha\frac{\bar{k}}{R} \tag{3.12}$$

---

[8] Note that $\frac{d\bar{k}}{dx} = 0$ is also valid by assuming laminar flow $\left(\bar{k} \approx 0\right)$. However, it is assumed that the incoming flow is turbulent.
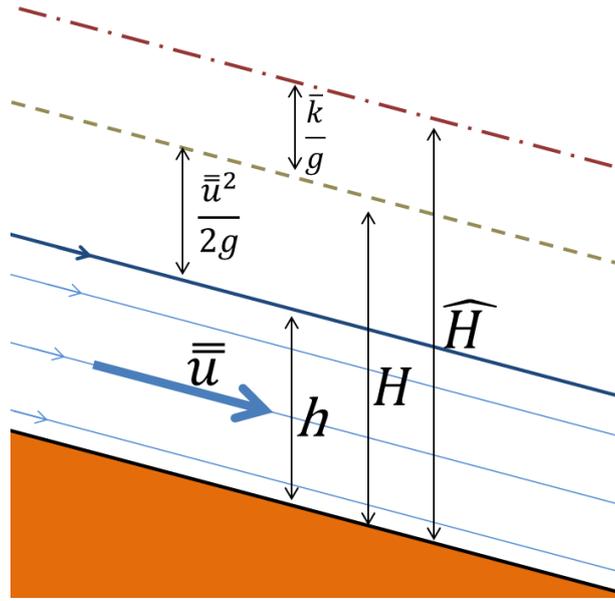
**Figure 18 Uniform stationary flow over a rough bottom with head levels $H$ and ATM head $\widehat{H}$**

Under steady uniform flow conditions the flow velocity and water depth do not change. Due to the sloping bottom, potential energy is transferred into kinetic energy. Because there is no change in flow velocity, the increased kinetic energy is immediately dissipated again due to bottom friction. Bottom friction can be described by the Chezy law. The loss in mean flow energy (and thus the increase in turbulent energy) due to bottom friction $\frac{dH}{dx} = -\frac{\bar{\bar{u}}^2}{C^2 R}$ can be substituted into the ATM (equation 3.12) which gives:

$$g \frac{\bar{\bar{u}}^2}{C^2} = \alpha \bar{k} \qquad (3.13)$$

In equation 3.13 the hydraulic radius $R$ appears at both the left and right side of the equation, and is thus left out. A known value for the turbulent energy $\bar{k}$ can be filled in equation 3.13 to find a value for $\alpha$. Equilibrium turbulent energy under uniform stationary flow conditions can be calculated using the formula for equilibrium turbulent intensity 3.6 of Hoffmans (1993). This formula can be rewritten into turbulent energy using equation 3.5 for turbulence intensity (see appendix H for the derivation):

$$\bar{k}_e = \bar{\bar{u}}^2 c_0^2 \frac{g}{C^2} \qquad (3.14)$$

Where $\bar{k}_e$ equals the equilibrium turbulent energy (m²/s²) under the flow conditions specified above and $c_0 = 1.21$.

Substituting equation 3.14 into 3.13 gives $\alpha = \frac{1}{c_0^2}$ (appendix H). This means the ATM can confirm with the formula for equilibrium turbulence as described by Hoffmans (1993), when the dissipation coefficient is set at $\alpha = \frac{1}{c_0^2}$. For stationary uniform (in all directions) flow conditions, the value for $c_0$ was determined empirically, so $\frac{1}{c_0^2}$ is therefore also empirically determined. This gives some initial confidence in the ATM because the formula for equilibrium turbulence of Hoffmans (1993) has been used for some time to find equilibrium turbulent energy levels (Hoffmans, 2012).

## 3.6 Concluding remarks

This chapter introduced how turbulence follows from properties of the flow. It was shown how the turbulent energy can be calculated using the velocity fluctuations in a flow. Turbulence is generated as the result of shear stresses affecting the flow. For uniform stationary flow, the flow is only affected by the shear stress between the walls and the flow. For backward facing step flow, flow deceleration results in internal viscous stresses on top of the shear stresses due to wall friction. To quantify the turbulent energy levels as the result of flow over a BFS, the ATM is introduced. The ATM is based on the energy cascade principle. The energy cascade states that mean flow energy loss is first transformed into turbulent energy before being dissipated (Schiereck, 2004). The ATM assumes that 100% of the mean flow energy loss is first transformed into turbulence. For the dissipation of turbulence, the ATM assumes that turbulence is dissipated similar to the dissipation of flow energy due to bottom friction. Whether these assumptions approximate reality for BFS flow will be studied in the coming chapters. For uniform stationary flow over a slope, it was shown that the ATM is at least consistent with the formula of Hoffmans (1993) for equilibrium turbulence levels. This gives some initial confidence in the validity of the ATM.

# 4 Theoretical validity

## 4.1 Introduction

Now that the ATM is defined, its theoretical validity is examined. First the assumptions made by the ATM about turbulence in a flow are discussed by looking at what terms are included and excluded in the ATM. The principles on which the ATM is based are compared to existing literature to show that these principles are partly founded in science. The ATM is compared to the turbulent kinetic energy (TKE) equation to show that the turbulence production term in the ATM follows from the turbulent kinetic energy equation when certain assumptions are made. The validity of these assumptions are discussed in the empirical validation. The dissipation term of the ATM is then compared to the present knowledge about the rate of dissipation in turbulent flows to show that the dissipation term of the ATM does not necessarily conflict with this knowledge.

Table 1 Theoretical validation techniques used and the location where they are discussed

| Validation technique used: | Discussed in: | What is discussed? |
|---|---|---|
| Analysing the ATM formula | Section 4.2 | The implicit assumptions of the ATM |
| Comparison of ATM principles to literature | Section 4.3 | The validity of the principles on which the ATM is build |
| Comparing the production term of the ATM to the turbulent kinetic energy equation | Section 4.4 | Validity of the production term of the ATM |
| Comparing the dissipation term of the ATM to the theory of large scale to smaller scale eddy dissipation | Section 4.5 | Validity of the dissipation term of the ATM |

## 4.2 Implicit assumptions of the Arcadis Turbulence Model

Some of the assumptions implicitly made about turbulence by the ATM can be identified by simply looking at the formula of the ATM.

$$\frac{d\bar{k}}{dx} = -g\frac{dH}{dx} - \alpha\frac{\bar{k}}{R} \qquad (3.11)$$

Four assumptions about turbulence made by the ATM are identified:

1. Turbulent energy can be approximated as a depth and width averaged value
2. Turbulence is stationary
3. No advective or diffusive transport of turbulence
4. Turbulence production is equal to mean flow energy loss and turbulence dissipation is a relaxation function

These assumptions are discussed in more detail below.

1. The turbulence levels in the ATM can only vary in the $x$ direction (no $\frac{d}{dy}$ or $\frac{d}{dz}$ terms) so the model assumes that turbulent energy can be approximated as a depth and width averaged value, or in other words, the ATM is a one dimensional model.

2. The ATM does not contain a time varying term (e.g. $\frac{d\bar{k}}{dt}$). Therefore, stationarity of the turbulence levels is assumed. Because turbulence is a function of the main flow (Tennekes & Lumley, 1972), stationary mean flow needs to be assumed for stationarity of the turbulence to be valid. Thus the ATM is only valid for stationary flow.

3. The ATM defined turbulence production and dissipation as a convective process. No additional turbulent transport parameters (e.g. diffusion) are present. It is assumed that turbulent energy is generated and/or dissipated for each step in space in the flow direction. The ATM does not permit for turbulence to be transported in the flow (either advective or diffusive) without a change in the turbulence levels. Thus, transport of turbulence in the opposite direction of the flow is also not possible.

4. The ATM states that production of turbulent energy is equal to the loss of mean flow energy and dissipation of turbulence is a function of the turbulent energy itself (a relaxation function). The validity of these assumptions are discussed more in depth in the coming sections.

## 4.3 Comparison to literature

Although the ATM is a new model, the principles it is based on are mentioned in scientific literature. In this section, the ATM production and dissipation term is compared to literature to test its validity.

### Turbulence production originating from mean flow energy loss discussed in literature

Laufer (1954) states that the energy (pressure) loss in pipe flow due to wall friction is partly converted into turbulent energy and partly dissipated. No explanation is given for the partial conversion of pressure energy into turbulent energy by Laufer (1954). However, a possible explanation can be hypothesised. Due to the speed difference between the wall and the flow, shear stresses induce turbulence in the flow (similar to figure 17). At the same time, the flow also loses flow energy due to the wall friction heating up the pipe. A different study from Klingmann & Alfredsson (1989-1993) performed experiments under laminar flow conditions with artificial introduced turbulence spots. They hypothesize in their study that the laminar fluid entering the turbulent region from upstream is slowed down and its excess mean flow energy is converted into turbulent energy. Townsend (1970, p. 13) states that "most free turbulent flows depend for their energy supply on converting mean flow energy into turbulent energy by entrainment of non-turbulent ambient fluid". Nakagawa and Nezu (1987, p. 86) found for BFS flow that "the decay of mean flow energy is balanced with an increase of potential energy and a production or generation of turbulent energy". These results corresponds with the assumption of the ATM that the decrease of mean flow energy is inversely proportional to the increase in turbulent energy. Schiereck (2004) defined turbulence as the process that allows mean flow energy to be dissipated. Mean flow energy is first transformed into turbulence which, due to viscous stresses in the Kolmogorov microscales, is then dissipated into heat. George (2013) (among others) showed that turbulent energy can only originate from the mean flow energy using the Navier-Stokes equation. So the assumption that the decrease in mean flow energy is inversely proportional to the increase in turbulent energy is supported by literature. However, the theoretical validation did not reveal whether it can be reasonably assumed that all mean flow energy loss is 100% converted in turbulent energy. The empirical validation will give more insight whether assuming all mean flow energy loss is 100% converted in turbulent energy approximates reality sufficiently.

### Turbulence dissipation discussed in literature

The ATM states that turbulence dissipation is a function of turbulence itself. The dissipation coefficient $\alpha$ determines the rate of dissipation of the present turbulent energy, according to the ATM. Multiple ways for measuring and/or estimating turbulence dissipation exists in literature. By measuring the relevant velocity fluctuations, the turbulence dissipation rate, as given by the turbulent kinetic energy equation (TKE) (equation 4.2 discussed in the following section) can be

calculated following: $\epsilon = \nu \frac{du_i'}{dx_j}\frac{du_i'}{dx_j}$ where $\epsilon$ equals the dissipation rate (m²/s³) and $\nu$ equals the kinematic viscosity (m²/s). This term can be physically interpreted as the dissipation of turbulent energy due to internal viscous friction (George, 2013). Measuring this term was done by Andreopoulos and Honkan (1996). Attempts made during this study to relate the dissipation term of the ATM $\left(\alpha\frac{k}{R}\right)$ to the dissipation term of the turbulent kinetic energy equation $\left(\nu\frac{du_i'}{dx_j}\frac{du_i'}{dx_j}\right)$ were unsuccessful. It is therefore concluded that the dissipation of turbulence, as modelled by the ATM, does not follow from the TKE equation.

A second method for estimating turbulence dissipation is based on the separation of scales producing turbulence and scales dissipating turbulence. The dissipation rate of turbulence is primarily determined by the large scale turbulent eddies transferring their energy to smaller scale turbulent eddies (George, 2013) (figure 19). The very small turbulent eddies lose their energy quickly due to viscosity (transforming kinetic energy into heat). The overall rate of dissipation is therefore controlled by the rate of energy transfer from the larger scales to the smaller scales (George, 2013). The amount of kinetic energy (per unit mass) in large scale turbulent eddies is proportional to $u_j'^2$ (m²/s²). The rate that large eddies transfer energy to smaller eddies is assumed to equal $\frac{u_j'}{l}$ (s⁻¹) where $l$ represents the size of the largest eddies (m) (or another characteristic length scale) (Tennekes & Lumley, 1972). Because the dissipation rate is limited by the supply of energy from the large scale turbulent eddies to the smaller scales, the dissipation rate can be estimated as:

$$\epsilon \sim \frac{u_j'}{l}u_j'^2 = \frac{u_j'^3}{l} \qquad\qquad (4.1)$$

This definition of turbulent dissipation is only an approximation. However, it is supported by literature as a good approximation ( see for example Tennekes & Lumley, 1972 or George, 2013).
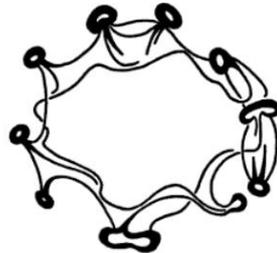


Figure 19 Visualisation of large scale turbulent eddy transferring energy into smaller scale eddies (sketch of ink droplet falling into glass of water, Tennekes and Lumley, 1972, p.21)

Dissipation of turbulence is described in numerous other ways, the $k-\epsilon$ model describes the dissipative capacity as something that is produced, convected and dissipated similar to the turbulence itself (Mohammadi & Pironneau, 1993). A summary of some of the methods to describe turbulence dissipation is given by Sheng, Meng, and Fox (2000). One thing that all above described turbulence dissipation approximations have in common is that none of them seem to closely resemble the turbulence dissipation term as described by the ATM (in section 4.5, it will be shown that the turbulence dissipation term in the ATM can confirm to the turbulence dissipation as described by equation 4.1).

## 4.4 Comparing the production term of the Arcadis Turbulence Model to the turbulent kinetic energy equation

### Introduction

The ATM assumes that the production of turbulent energy is exactly proportional to the energy loss of the mean flow. In this section it is shown what assumptions are needed to let the production term of the turbulent kinetic energy equation (TKE) confirm with the ATM production term. Because the production of turbulence is related to the mean flow energy loss, the mean flow kinetic energy (MKE) equation is introduced alongside the turbulent kinetic energy equation (TKE).

### Introducing the turbulent kinetic energy equation

The Navier-Stokes equation describes the motion of fluids by applying Newton's second law of motion. "It is believed that the solution of time-dependent 3-D Navier-Stokes equations can describe turbulent flows completely" (Nallasamy, 1987, p. 152). However, no general solution of the Navier-Stokes equation is currently known (a solution is continuously searched for by the scientific community) (Moskvitch, 2014). By time averaging the Navier-Stokes equation, the Reynolds averaged Navier-Stokes equation is found (George, 2013). The velocity fluctuations that describe turbulence can be found by subtracting the Reynolds averaged Navier-Stokes equation from the regular Navier-Stokes equation, taking the scalar product with the fluctuating velocity itself and then ensemble averaging in time (George, 2013). The resulting turbulent kinetic energy equation (TKE) cannot currently be solved as it requires information on the turbulence properties that can only come from a direct numerical simulation. The computational cost of solving the TKE equation via direct numerical simulations for practical purposes is currently too large (Lermusiaux, 2011). The TKE equation is useful for theoretically describing the different phenomena affecting turbulence or to calculate turbulence after applying simplification to the equation. A step by step guide how to deduce the TKE equation is given by George (2013).

The ATM is compared to the TKE equation because it is believed that the Navier-Stokes equation can describe turbulent flows completely (Nallasamy, 1987) and the TKE equation is needed to approximate the turbulence terms in the Navier-Stokes equation (approximate because the Navier-Stokes equation has currently not been solved). The TKE equation equals:

$$\frac{dk}{dt} + \bar{u}_j \frac{dk}{dx_j} = \frac{d}{dx_j}\left(-\frac{1}{\rho_w}\bar{p}u_i'\delta_{ij} - \frac{1}{2}u_i'u_i'u_j' + v\frac{dk}{dx_j}\right)$$
$$- u_i'u_j'\frac{d\bar{u}_i}{dx_j} - v\frac{du_i'}{dx_j}\frac{du_i'}{dx_j} \tag{4.2}$$

$$\delta_{ij}\begin{cases}0 \ if \ i \neq j \\ 1 \ if \ i = j\end{cases}$$

Where $k$ equals the turbulent energy in the flow (m²/s²), $t$ equals the time (s), $\bar{u}_i$ equals the time averaged flow velocity (m/s), $\rho_w$ equals the density of the fluid (kg/m³), $\bar{p}$ equals the root mean squared (RMS) pressure fluctuations (N/m²), $\delta_{ij}$ equals Kronecker delta (-), $u_i'$ equals the RMS velocity fluctuations (as discussed in section 3.2) (m/s), and $v$ equals the kinematic viscosity (m²/s). The subscripts $i$ and $j$ are free indices that can take on the values $x$, $y$, and $z$ corresponding to the three dimensions.

The term $\frac{dk}{dt}$ in equation 4.2 represents the change in turbulent energy over time. This term equals zero under stationary conditions. The term $\bar{u}_j\frac{dk}{dx_j}$ represents the rate of change of turbulent energy due to advection of turbulent energy in the mean flow direction. The term

$\frac{d}{dx_j}\left(-\frac{1}{\rho_w}\bar{p}u_i'\delta_{ij}\right)$ represents the transport of turbulent energy due to pressure fluctuation in the three dimensions. The term $\frac{d}{dx_j}\left(-\frac{1}{2}u_i'u_i'u_j'\right)$ represents the transport (diffusion) of turbulent energy due to turbulence itself. The term $\frac{d}{dx_j}\left(v\frac{dk}{dx_j}\right)$ represents the transport of turbulent energy due to viscous stresses. The term $-u_i'u_j'\frac{d\bar{u}_i}{dx_j}$ represents the production rate of turbulent energy due to a mean flow velocity gradient and the term $-v\frac{du_i'}{dx_j}\frac{du_i'}{dx_j}$ represents the dissipation of turbulent energy due to internal viscous stresses. Above is also discussed in George (2013). Note that in equation 4.2 turbulence can only be generated by the production term $-u_i'u_j'\frac{d\bar{u}_i}{dx_j}$.

### Introducing the mean flow kinetic energy (MKE) equation

The production term $-u_i'u_j'\frac{d\bar{u}_i}{dx_j}$ of the TKE equation is related to the change in the mean flow kinetic energy. To better understand the production of turbulent kinetic energy, first the origin of the production term $-u_i'u_j'\frac{d\bar{u}_i}{dx_j}$ is discussed.

Equation 4.2 depicts the kinetic energy of the velocity fluctuations in a flow. Similarly, the kinetic energy of the mean flow (MKE) can be found by taking the scalar product of the Reynolds averaged Navier-Stokes equation with the mean flow velocity (George, 2013). This results in:

$$\frac{dK}{dt} + \bar{u}_j\frac{dK}{dx_j} = \frac{d}{dx_j}\left(-\frac{1}{\rho_w}\bar{P}\bar{u}_i\delta_{ij} - \frac{1}{2}u_i'u_i'\bar{u}_i + v\frac{dK}{dx_j}\right)$$
$$+ u_i'u_j'\frac{d\bar{u}_i}{dx_j} - v\frac{d\bar{u}_i}{dx_j}\frac{d\bar{u}_i}{dx_j} + f \qquad (4.3)$$
$$\delta_{ij}\begin{cases} 0 \ if \ i \neq j \\ 1 \ if \ i = j \end{cases}$$

Where $K$ equals the kinetic energy of the mean flow $\left(K = \frac{1}{2}\bar{u}_i\bar{u}_i\right)$ (m²/s²), $t$ equals the time (s), $\bar{u}_i$ equals the time averaged flow velocity (m/s), $\rho$ equals the density of the fluid (kg/m³), $\bar{P}$ equals the time averaged pressure (N/m²), $\delta_{ij}$ equals Kronecker delta (-), $u_i'$ equals the time averaged velocity fluctuations (m/s), $v$ equals the kinematic viscosity (m²/s), and $f$ equals a source or sink term for kinetic energy (m²/s³) e.g. gravity adding energy to the flow by transforming potential into kinetic energy. The subscripts $i$ and $j$ are free indices that can take on the values $x, y,$ and $z$ corresponding to the three dimensions.

Equation 4.3 is very similar to equation 4.2 (e.g. similar transport and diffusion terms). One important difference between the two equations is the change in sign in front of the production term $u_i'u_j'\frac{d\bar{u}_i}{dx_j}$. This means that when the mean flow loses energy following $u_i'u_j'\frac{d\bar{u}_i}{dx_j}$, the turbulent energy increases by an equal amount. This corresponds with the assumption of the ATM that turbulence gains its energy as a result of the decrease of mean flow energy. The mean flow can also loose energy due to internal viscous stress, which can be seen in the term $v\frac{d\bar{u}_i}{dx_j}\frac{d\bar{u}_i}{dx_j}$. This conflicts with the assumption of the ATM that 100% of the mean flow energy loss is converted into turbulent energy.

**Steps taken to relate the TKE production term to the ATM production term**
Four steps are taken in order to relate the TKE production term to the ATM production term:

1. The TKE and MKE are simplified by assuming stationarity, no additional transport of turbulence beside advection and negligible mean flow energy dissipation due to water viscosity
2. The MKE is rewritten using the incompressibility of water and assuming uniformity of flow and turbulence in the $y$ and $z$ directions
3. The Bernoulli equation is differentiated in the $x$ direction and it is shown that the resulting formula equals the MKE equation as defined in step 2 (excluding the turbulence production term)
4. Because the Bernoulli equation can be found in the MKE equation (under certain assumptions), and the MKE loss equals the TKE gain (under certain assumptions), it is shown that the Bernoulli equation can be used to calculate the production of the turbulent energy in the TKE equation.

The ATM models the production of turbulent energy as a function of the mean flow energy loss according to Bernoulli. Following the above steps, it is shown that the TKE equation can confirm with the production term of the ATM. The derivation described in these four steps is complex. Therefore, only the assumptions required to make the TKE production term confirm with the production term of the ATM are presented in this chapter. The mathematical derivation as described in these four steps is depicted in appendix I.

**Assumptions required to make the TKE production term confirm with the ATM production term**
The production term of turbulence found in the ATM can be derived from the TKE equation when it is assumed that:

1. Turbulence transport due to pressure fluctuations, turbulence itself, and viscous stresses can be neglected
2. Mean flow energy transportation due to mean flow energy itself and viscous stresses can be neglected
3. Mean flow energy dissipation due to water viscosity can be neglected
4. The flow is defined by incompressible fluid
5. Stationarity
6. The flow is perfectly uniform in the $y$ and $z$ directions.

A great number of assumptions are needed before the ATM turbulence production term follows from the TKE equation. The empirical validation performed in chapter 7 will show whether the ATM assumptions approximate reality sufficiently to accurately model turbulence.

The third assumption as stated above is discussed here in more detail because this assumption is closely related to the assumption of 100% conversion of mean flow energy into turbulent energy. In appendix I it is assumed that the mean flow energy dissipation due to water viscosity can be neglected at high (local) Reynolds numbers (Burden, 2008). This is true for most of the flow, but not for the flow in the boundary layer (flow near the wall) (George, 2013). Very close to the boundary, viscous stresses even at high Reynolds numbers result in a drag force of the flow on the boundary (and vice versa). The work performed by the flow on the boundary results in a mean flow energy loss (energy dissipation due to water viscosity) that is not 100% converted into turbulence (according to the TKE and MKE). This means that the assumption of the ATM that 100% of the mean flow energy loss is converted into turbulence is not strictly valid. However, if

the error due to this assumption is small enough, the approximation can still be useful. Whether all above stated assumptions about the production of turbulence approximates reality sufficiently will be clarified further in the empirical validation.

## 4.5 Comparing the dissipation term of the ATM to the turbulent energy transfer to smaller scales

As discussed, in section 4.3, the dissipation of turbulent energy can also be considered to be controlled by the rate of energy transfer from the larger scales to the smaller scales. This rate is approximated by $\epsilon = \frac{u_j'^3}{l}$. The dissipation term of the ATM equals $\alpha \frac{k}{R}$. However, the ATM described the change in turbulence per unit of distances$\left(\frac{dk}{dx}\right)$, whereas the dissipation term $\epsilon = \frac{u_j'^3}{l}$ described the change in turbulence per unit of time$\left(\frac{dk}{dt}\right)$. To equate to the right units, it is assumed that the dissipation of turbulent energy over a certain period of time travels with the mean flow velocity $\bar{u}_j$ at the location the dissipation occurs. This gives:

$$\alpha \frac{k}{R} = \frac{1}{\bar{u}_j}\frac{u_j'^3}{l} \tag{4.4}$$

The above equation can be simplified into:

$$\alpha \frac{1}{2}\frac{u_j'u_j'}{R} = \frac{1}{\bar{u}_j}\frac{u_j'u_j'u_j'}{l}$$

$$\frac{\alpha}{2R} = \frac{u_j'}{\bar{u}_j}\frac{1}{l}$$

$$\alpha = \frac{u_j'}{\bar{u}_j}\frac{2R}{l} \tag{4.5}$$

Equation 4.5 depicts $\alpha$ as a dimensionless parameter. The value $\alpha$, following the derivation above, equals the product of the ratio between the fluctuating and the mean flow velocity $\left(\frac{u_j'}{\bar{u}_j}\right)$ and the hydraulic radius and a characteristic length$\left(\frac{2R}{l}\right)$. Equation 4.1 is supported by many studies (e.g. Tennekes & Lumley, 1972; George, 2013) thus modelling turbulence as defined by equation 4.1 (4.5) should benefit the validity of the ATM. However, the ATM, as introduced in section 3.4 assumes a constant value for the dissipation coefficient $\alpha$, whereas equation 4.5 describes the turbulence dissipation coefficient $\alpha$ as a function of the ratio between the fluctuating and the average flow velocity. The only way $\alpha = constant$ in equation 4.5 is when $\frac{u_j'}{\bar{u}_j} = constant$. This is almost never the case[9] because the flow fluctuations $u_j'$ (and thus turbulence) can change in a flow where the mean flow velocity $\bar{u}_j$ remains constant (Nakagawa & Nezu, 1987; Xingkui & Fontijn, 1993; Hofland, 2005). Validation of the ATM with empirical data will show whether the assumption that $\alpha = constant$ will approximate reality sufficiently to model turbulent energy levels in BFS flow.

---

[9] $\alpha = \frac{u_j'}{\bar{u}_j}\frac{2R}{l}$ can be constant with varying $\frac{u_j'}{\bar{u}_j}$ when the characteristic length scale $l$ varies exactly in the opposite direction. This is possible, but very unlikely (Uijttewaal, 2015). The term $\frac{u_j'}{\bar{u}_j}$ is constant for equilibrium turbulent energy levels (section 3.5).

## 4.6 Concluding remarks

In this chapter, an attempt was made to theoretically validate the ATM using existing literature and proven formulae. A literature study showed that multiple authors concluded that the reduction of mean flow energy is related to the increase of turbulent energy. The literature analysis did not make clear if it is valid to assume that 100% of the mean flow energy loss is converted into turbulent energy. Using the turbulent energy equation, it was shown in this chapter that the production of turbulence is exactly proportional to the reduction of mean flow energy under a set of assumptions. However, this neglects (among other things) the viscous stresses between the mean flow and the walls which can result in a mean flow energy loss that is not converted into turbulence. Whether the assumptions on which the ATM is based are applicable in real life situations is explored in the empirical validation.

Literature presents multiple ways of modelling turbulence dissipation. No instances in literature were found of modelling dissipation as a relaxation term similar to the ATM. If the $\alpha$ coefficient in the ATM is not assumed to be constant in space, then the dissipation term of the ATM can confirm with the dissipation term as described by the theory of large scale to smaller scale eddy dissipation. The lack of scientific papers presenting turbulence dissipation as a relaxation function is possibly an indication that a constant dissipation parameter for $\alpha$ might result in inaccurate modelling of turbulence. Comparison with empirical data will give more insight in the accuracy of modelling the turbulence dissipation using a constant value for $\alpha$ in the ATM.

# 5 Validation data collection

## 5.1 Introduction

To test whether the assumptions discussed in the previous chapter approximate reality sufficiently, the ATM is compared to empirical data. This chapter will describe what data is required for the ATM to run, what data confirms to these criteria, the quality of these selected data, and the uncertainties in the selected data. First, an assessment is made of the required data to run and validate the ATM. Using this assessment, experimental data is selected to use in the validation. The experimental data is divided into data needed to run the ATM (section 5.3 and 5.4) and data needed to validate the ATM (section 5.5). The experimental data are presented and discussed to get an idea about the experimental circumstances and limitations. An uncertainty analysis of the experimental data is made to assess the accuracy of the validation data.

## 5.2 Data requirements for the Arcadis Turbulence Model analysis

### Introduction

To validate the model output of the ATM, the output of the ATM needs to be compared to the turbulent energy levels that occurred during experiments $(\bar{k})$. In order to gather the right experimental datasets, first an assessment is made of the data required to run and validate the ATM. Figure 20 shows a schematization of the required ATM input data. The figure also schematizes how the ATM is validated using experimental measurements. In the following text, the data requirements for validating and running the ATM are treated separately.
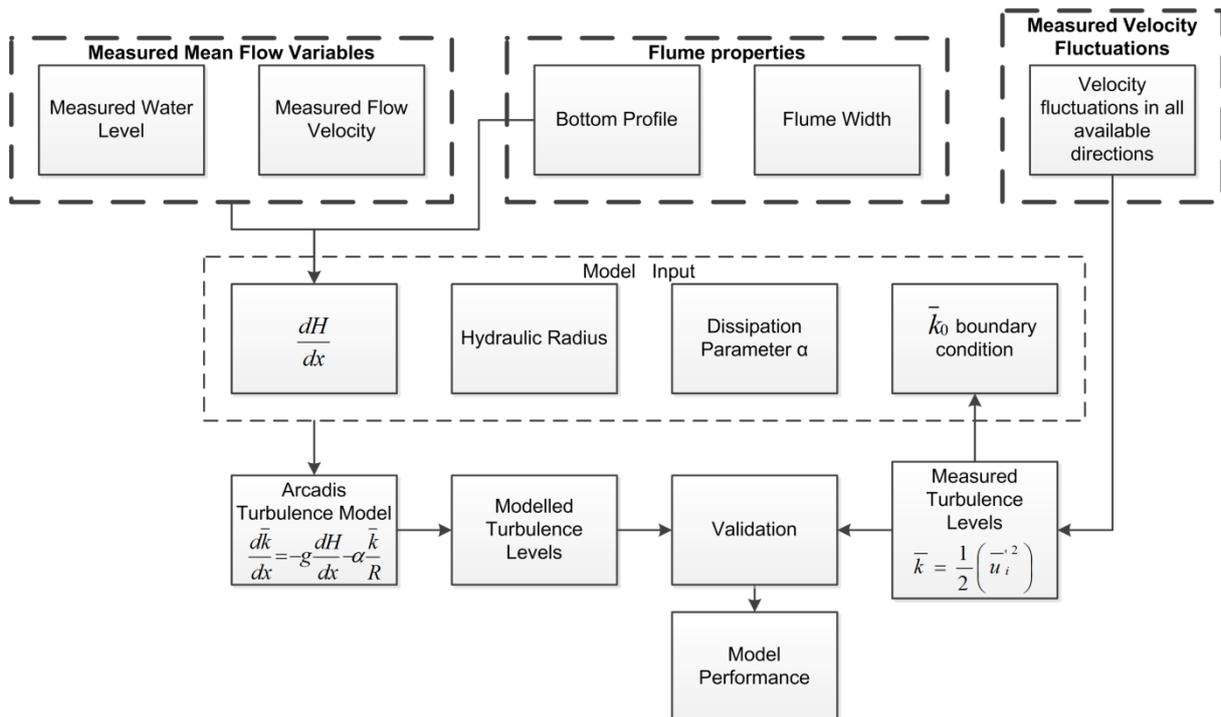


Figure 20 Flow chart showing ATM input and validation data[10]

### ATM validation data requirements

The ATM calculates depth averaged turbulent energy. In order to say something about the accuracy of the ATM's calculated turbulent energy levels, validation data is needed including

---

[10] The hydraulic radius is calculated using the flume width $B$ and the water depth $h$. However, in order to preserve the readability of all flow charts, this relation is left out.

measured depth averaged turbulent energy levels $(\bar{k})$ at multiple locations on top and downstream of the BFS.

Data about the (depth averaged) velocity fluctuations $\bar{u}_i'$ are often measured in experiments. This data can be used in the formula:

$$\bar{k} = \frac{1}{2}(\bar{u}_i')^2 \tag{3.3}$$

The resulting $\bar{k}$ is compared to the ATM output to say something about its validity.

### ATM input data requirements

The input variables for the ATM can be discerned looking at equation 3.11:

- the change in head level $\frac{dH}{dx}$
- the hydraulic radius $R$
- the dissipation coefficient $\alpha$
- an boundary conditions turbulence value[11] $k_0$

The methods used to calculate the input data are discussed below:

In order to calculate the change in head level, the flow velocity $(\bar{\bar{u}})$, water depth $(h)$ and elevation $(z)$ need to be known for the whole study area of the BFS flow. The head level can then be calculated using the formula 2.2:

$$H = z + h + \frac{1}{2}\frac{\bar{\bar{u}}^2}{g} \tag{2.2}$$

The hydraulic radius $R$ (m) is needed as input into the ATM. The hydraulic radius $R$ is calculated using:

$$R = \frac{h \times B}{2 \times h + B} \tag{5.1}$$

Appendix J explains the exact method used to calculate the hydraulic radius (a somewhat deviating method is used that can also be applied during the preliminary design phase but still accurately approximates the actual hydraulic radii).

The dissipation coefficient $\alpha$ is a calibration coefficient in the ATM. The dissipation coefficient is a new coefficient, and therefore, no experimental data contains information about the value of $\alpha$ (in chapter 6 a number of dissipation coefficient alternatives are proposed that can be used to run the ATM).

---

[11] Because the ATM only calculates the change in turbulent energy, an upstream boundary condition $k_0$ needs to be known in order for the ATM to find the absolute turbulent energy levels.

An upstream boundary turbulence value $\bar{k}_0$ is needed. Because the output of the ATM is compared to measured turbulent energy $\bar{k}$, $\bar{k}_0$ can be found by extracting the measured turbulent energy level at the upstream edge of the study area.

Table 2 summarizes the required flow variables needed to run and validate the ATM.

**Table 2 ATM variables and the section where they are discussed**

| Variable | Used for: | Discussed in: | What is discussed? |
|---|---|---|---|
| $h$ | Calculating the input variable $\dfrac{dH}{dx}$ | Section 5.3: & 5.4 | Section 5.3: analysis of variable Section 5.4: uncertainty in the variable |
| $\bar{\bar{u}}$ | Calculating the input variable $\dfrac{dH}{dx}$ | Section 5.3: & 5.4 | Section 5.3: analysis of variable Section 5.4: uncertainty in the variable |
| $R$ | Input variable into the ATM | Appendix J | Approximation of $R$ using data available during preliminary design phase and accuracy of this approximation |
| $\bar{u}'$ | Computing turbulent energy levels $\bar{k}$ to validate the ATM | Section 5.5 | Analysis and uncertainty of the variable |
| $\alpha$ | Input variable into the ATM | Chapter 6 | Possible alternatives |

## 5.3 Data analysis

### Introduction

The ATM is validated on experimental data. Because during this graduation assignment, no experiments were performed, experimental data to run and validate the ATM was collected from literature. A summary of the available data and applicability to the ATM can be found in appendix K. Eight experimental datasets were gathered from various sources. The experiments from Nakagawa & Nezu (1987) (two different experiments), Xingkui & Fontijn (1993) and Hofland (2005) proved usable for the validation procedure. The work of Hofland (2005) was performed using the experimental data from De Ruijter (2004), thus information was also extracted from the master thesis of De Ruijter (2004).

### Experimental conditions
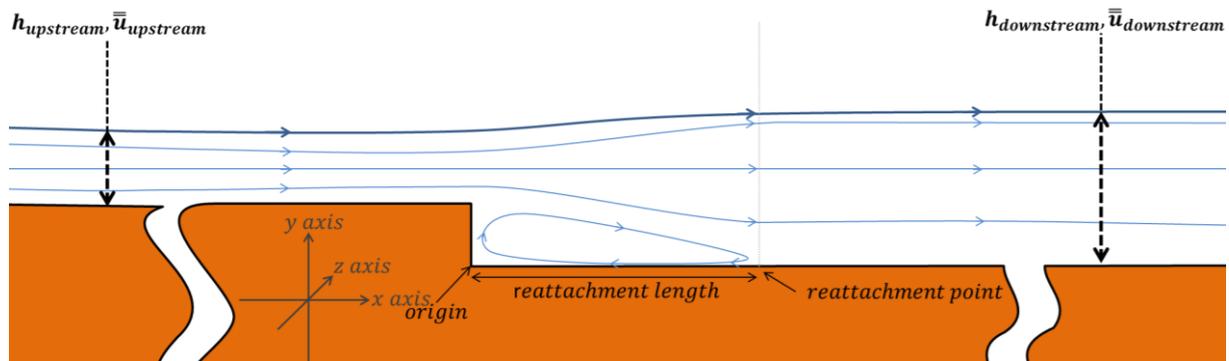


Figure 21 Measurement locations of selected experimental data; $x = 0$ at origin

Table 3 Experimental setup of the studies used for turbulence data. Question marks indicate data that were unavailable.

| Author | | Xingkui, 1993 | Hofland, 2005 | Nakagawa ST1, 1987 | Nakagawa ST3, 1987 |
|---|---|---|---|---|---|
| Flume properties | Width (m) | 0.4 | 0.495 | 0.3 | 0.3 |
| | Length (m) | 14 | 20 | 8 | 8 |
| Flow properties | $h_{upstream}$ (m) | 0.083 | 0.116 | 0.037 | 0.085 |
| | $h_{downstream}$ (m) | 0.166 | ? | 0.058 | 0.106 |
| | $\bar{\bar{u}}_{upstream}$ (m/s) | 0.606 | 0.580 | ? | ? |
| | $\bar{\bar{u}}_{downstream}$ (m/s) | 0.303 | ? | 0.142 | 0.221 |
| | Discharge (m³/s) | 0.0201 | 0.0318 | 0.0025 | 0.0070 |
| | Specific discharge (calculated) (m²/s) | 0.0503 | 0.0673 | 0.0082 | 0.0234 |
| | Froude$_{upstream}$ | 0.67 | 0.56 | ? | ? |
| | Froude$_{downstream}$ | 0.24 | ? | 0.19 | 0.22 |
| | Reynolds | 50000 | 66000 | 8200 | 23400 |
| Step properties | BFS height $(h_{step})$ (m) | 0.070 | 0.067 | 0.020 | 0.020 |
| | Reattachment length $(x/h_{step})$ | 10 | 12 | 6.3 | 5.2 |
| Bedlayer | Grain size downstream of step (m) | 0.033 | 0.0178 | smooth | smooth |
| | Mobility | glued | moving & glued | n.a. | n.a. |
| | Step roughness | smooth flat concrete | wood | smooth | smooth |
| | Chezy$_{downstream}$ (calculated) | 27.3 | 30.6 | 69.1 | 76.4 |
| Measurements | Equipment used | Laser Doppler Anemometer | Laser Doppler Anemometer | Laser Doppler Anemometer | Laser Doppler Anemometer |
| | Location first measurement $(x/h_{step})$ | 0 | -0.45 | -1 | -1 |
| | Location last measurement $(x/h_{step})$ | 25.7 | 15.3 | 12 | 12 |
| | Number of measurements | 7 | 11 | 13 | 13 |

Table 3 shows the experimental set up for the different studies that will be used to validate the ATM. It is unknown where measurements upstream and downstream were exactly located along the flume. However, every study did state that the measurement upstream is located on top of the step and the measurement downstream is located downstream of the reattachment point. Note that all four experiments were performed under different conditions (e.g. differences in discharge, bottom roughness, water height, etc.). The Froude numbers were calculated in the papers using the formula:

$$F = \frac{\bar{\bar{u}}}{\sqrt{gh}}$$
(5.2)

The Reynolds numbers were calculated in the papers using:

$$R_e = \frac{\bar{\bar{u}}h}{\nu}$$
(5.3)

Where $\nu$ equals the kinematic viscosity: $10^{-6}$ (m²/s). Note that it does not matter whether $h_{upstream}$ and $\bar{\bar{u}}_{upstream}$ or $h_{downstream}$ and $\bar{\bar{u}}_{downstream}$ is used for the calculation of the Reynolds number because due to the conservation of mass, and a constant flume width, the specific discharge $q = h_{upstream} \times \bar{\bar{u}}_{upstream} = h_{downstream} \times \bar{\bar{u}}_{downstream}$ (m²/s) is constant. For all selected experiments, the Reynolds number is large, thus all selected experiments were performed under fully turbulent flows.

The Chezy coefficient was not given in the papers. The Chezy coefficient is calculated in this study using:

$$C = \frac{1}{n} h_{downstream}^{1/6} \qquad (5.4)$$

Where $n$ equals the Manning coefficient (s/m$^{1/3}$), which is either looked up in a table, or calculated following the formula of the The Rock Manual (2007):

$$n = 0.048 D_{50}^{1/6} \qquad (5.5)$$

Where $D_{50}$ equals the characteristic sieve size of the stones on the bottom of the flume. For the studies of Xingkui & Fontijn (1993) and Hofland (2005) the bottom was covered with grains, and equation 5.5 is used to calculate the Manning coefficient. Nakagawa & Nezu (1987) stated that the flume is built using flat and smooth walls, it is therefore assumed that the flume consisted of smooth plastic, for which the Manning coefficient equals 0.009 (Engineering Toolbox, 2015).

### General remarks about the experimental conditions

In the study of Nakagawa & Nezu (1987), two flume experiments were performed using the same flume setup for two different discharges. These experiments were called ST-1 and ST-3. Both experiments are treated separately in this thesis.

The studies of Xingkui and Fontijn (1993) and Hofland, (2005) measured the velocity profiles at only one location in the flumes. In order to get the velocity profiles at varying distances from the step, the location of the step was varied. The same uniform subcritical flow conditions were set for the varying location of the step. This made sure the velocity profiles correspond to the same flow configuration. The error margins in the measured variables due to small differences in flow conditions are discussed in the next section.

The study of Hofland (2005) used a step with a height of 0.12 m. However, downstream of the step, the bed grains increased the bottom elevation. The effective step height was reduced to 0.067 m due to this increased bottom elevation.

All selected experiments were performed under subcritical flow conditions. Therefore, the ATM will be discussed only for subcritical flow conditions. More research is required to say something about the ATM under supercritical flow conditions.

### Intermediate measurement locations

The water depth $h$ and mean flow velocity $\bar{\bar{u}}$ are used to calculate the change in head level[12] $\left(\frac{dH}{dx}\right)$. The papers of the selected experiments presented multiple measurements of these flow variables (figure 22).

---

[12] The measurements $h_{upstream}, h_{downstream}, \bar{\bar{u}}_{upstream}$ and $\bar{\bar{u}}_{downstream}$ were not used as input into the ATM because the exact measurement locations were unknown for these measurements.
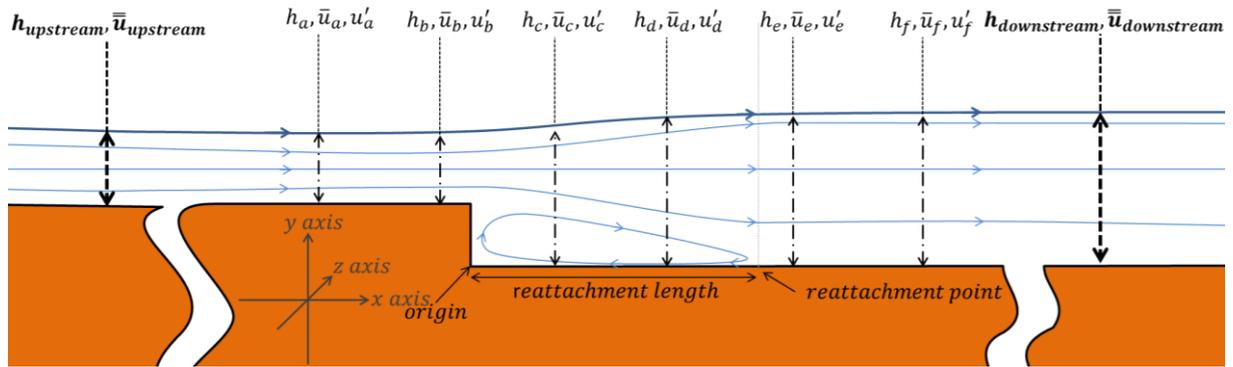
Figure 22 Measurement locations of selected experimental data

Figure 22 shows an approximation[13] of measurement location of the water depth $(h_{a,b,...})$ and the mean (time averaged) and fluctuating velocity profiles $(\bar{u}_{a,b,...}, u'_{a,b,...})$. These intermediate measurement locations are extracted from graphs in the different papers of the selected experiments. Appendix L gives a description of the method used to extract the water depths, and the mean and fluctuating velocity profiles from the graphs in the papers. To illustrate how the data is presented in the papers, one of the graphs from the experiment of Xingkui & Fontijn (1993) is depicted in figure 23.
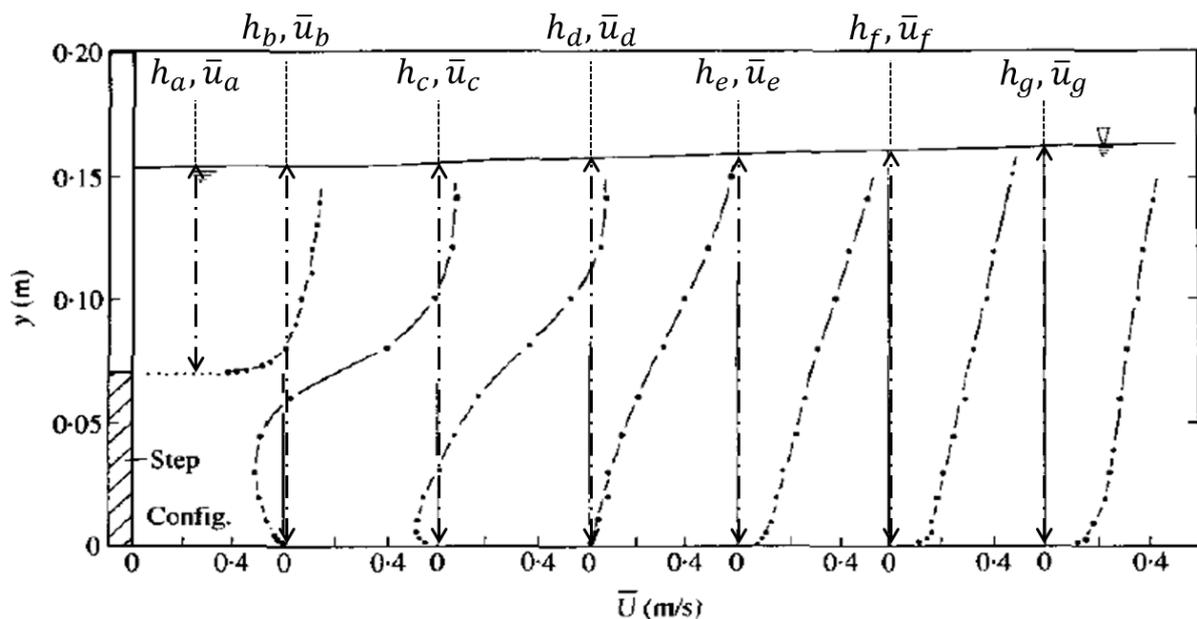


Figure 23 Example of graph used to extract flow velocity $\bar{u}$ and water depth $h$ (Xingkui & Fontijn 1993, p. 306)

### Missing data

The study of Hofland (2005) did not present the water depths at the intermediate measurement locations in the flume (only values for $h$ upstream and downstream are known). Without water depth information, the change in head level cannot be calculated. The missing water depth data is therefore computed using the conservation of mass. De Ruijter (2004) stated that the experiments were performed using a discharge of 31.8 l/s (measured on top of the step). The extracted flow velocities $\bar{u}_{a,b,...}$ from the graphs of Hofland (2005) are depth integrated. The corresponding water depth for each velocity measurement is then found using:

---

[13] Figure 21 only shows an approximation because the actual measurement locations are different for each dataset.

$$h_{a,b,\dots} = \frac{0.0318}{\bar{\bar{u}}_{a,b,\dots} \times B} \qquad\qquad (5.6)$$

Where 0.0318 is the discharge in the flume in (m³/s), $\bar{\bar{u}}_{a,b,\dots}$ the depth integrated velocity profiles extracted from the graphs (m/s), and $B$ the width of the flume (m). It is known that the discharge actually fluctuated during different velocity profile measurements. The effects of the uncertainty within the data due to the assumption of conservation of mass for the Hofland (2005) experiment are presented in the next section.

### Extracted data

The extracted intermediate water depths $h_{a,b,\dots}$ and mean flow velocities $\bar{\bar{u}}_{a,b,\dots}$ of the selected experiments are depicted in this section. The fluctuating flow profiles $\bar{u}'_{a,b,\dots}$ are also extracted. These will be discussed in section 5.5.
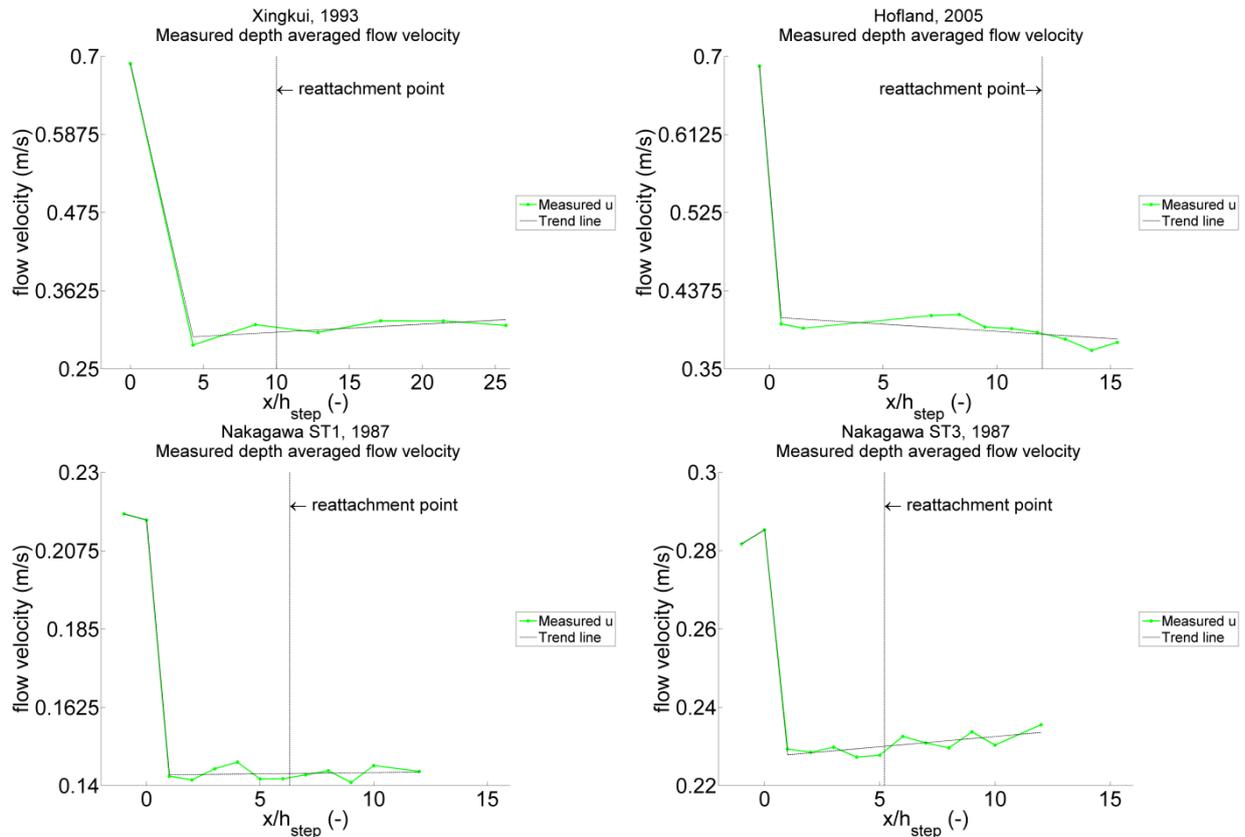


Figure 24 Depth integrated flow velocities including trend lines[14]

Figure 24 shows the extracted, time averaged depth integrated flow velocities. Every selected experiment shows a sudden decrease in depth averaged flow velocity downstream of the step. The sudden decrease in depth averaged flow velocity is the result of an integration over the whole water depth, including the recirculation zone just downstream of the end of the step (figure 25).

---

[14] All graphs depicted in this thesis are normalized by the step size $\left( x / h_{step} \right)$ in order to compare the different experimental results. In the graphs, $x$ is the distance from the origin (figure 13) and $h_{step}$ the height of the BFS as depicted in table 3.
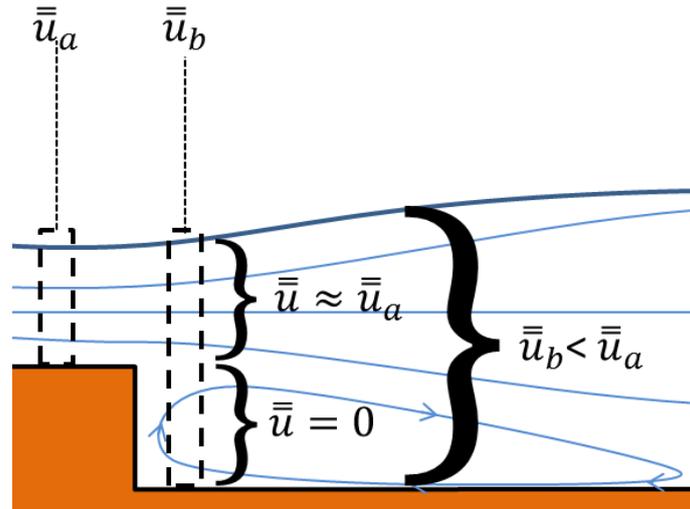
Figure 25 Sudden decrease in depth averaged flow velocity due to presence of a recirculation zone

A trend line is added to figure 24 to show the general trend of the flow velocity graphs after the initial sudden decrease. Weak acceleration is found for the experiments of Xingkui and Fontijn (1993) and Nakagawa & Nezu (1987) ST-3. On the other hand, weak deceleration is found for the studies of Hofland (2005) and Nakagawa & Nezu (1987) ST-1[15]. It is believed that the velocity measurements fluctuate within a certain margin. Therefore, the weak accelerations and decelerations could also be the result of uncertainty in the measurements.

The extracted water depth measurements are given below.
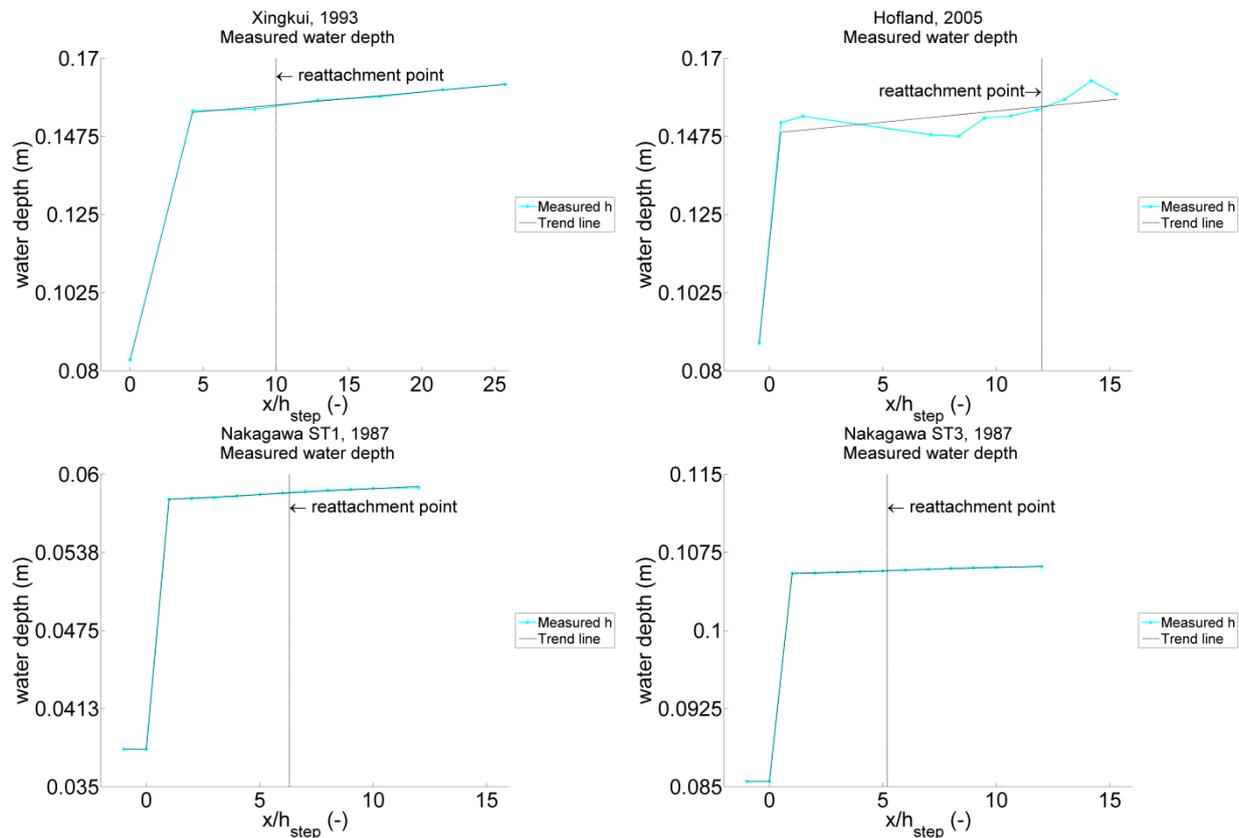


Figure 26 Water depth at the measurement locations including trend lines

---

[15] Possible phenomena that force water acceleration and deceleration downstream of the step are discussed in more detail in section 6.4.

Figure 26 shows the measured water depths at the measurement locations. The sudden decrease in depth averaged flow velocity is accompanied with a sudden increase in water depth for all experiments. The water depth measurements for all selected experiments show a trend of increasing water depth after the first sudden jump (even downstream of the reattachment point). The increase in water depth after the first jump is most likely related to the mean flow energy loss, which is discussed in section 6.4. Note that an increase in water depth should be accompanied with a decrease in flow velocity when the mass is preserved (assuming no change in flume width). However, figure 24 shows both flow deceleration and acceleration. This seems to indicate that the mass was either not preserved during the experiments, or the measurements were affected by sources of uncertainty.

## 5.4 Uncertainty in the experimental data used as input for the ATM

### Introduction

Uncertainty in the experimental data is an important factor to consider. As a first indication of the uncertainty in the measured variables, the discharge at each measurement location is calculated. The fluctuations in the measured discharge will give an idea about the size of uncertainty in the measurements. Next possible sources of uncertainty are proposed. A conservative estimate is then made about the effect of these sources of uncertainty on the measurements.

### Discharge fluctuations

To say something about the uncertainty in the measurement data, the discharge is calculated at each measurement location using the data from figure 24, 26 and the flume widths (given in table 3). The fluctuations in the measured discharge will give an idea about the size of uncertainty in the measurements. The discharge fluctuations will also give an indication of the sources of uncertainty affecting the measurements. In order to compare the discharge fluctuations for the difference selected experiments, the fluctuations are normalized. Normalization is performed by dividing the discharge by the explicitly in the papers stated discharge (as depicted in table 3). If the measurements are not affected by sources of uncertainty, and the discharge remained constant in between measurement locations, than the normalized discharges should equal unity at every measurement location.
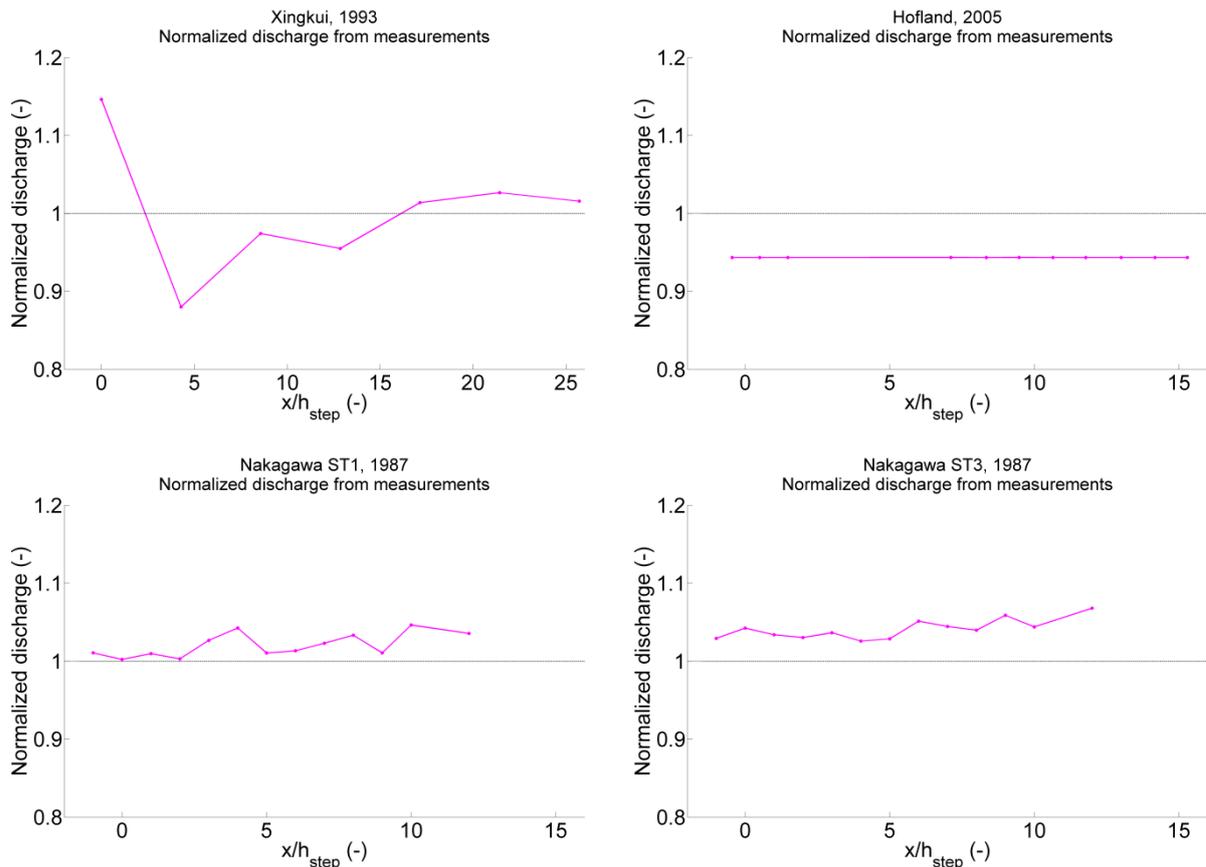
**Figure 27** Discharge calculated using extracted water depth and flow velocities. Discharge is normalized by dividing the discharge by the explicitly stated discharge in the papers (table 3)

The selected experiments (with the exception of the experiment of Hofland, 2005) show chaotic discharge fluctuations of up to 17% of the stated discharge (thus sources of uncertainty most likely affected the measurements during the experiments). Also note that all experiments with the exception of Xingkui & Fontijn (1993) seem biased. This might indicate that the authors of the papers used a different method for finding the discharge during the experiments (different from multiplying depth averaged flow velocity with the water depth and flume width to compute the discharge).

The discharge of the experiment of Hofland (2005) does not seem to fluctuate in between measurement locations. Because the water depth $h$ was calculated using the conservation of mass, the calculated discharge, per definition, does not fluctuate for Hofland (2005). This does not mean the measurements were not affected by sources of uncertainty for the experiment of Hofland (2005). The hypothesis that measurements are affected by sources of uncertainty for the experiment of Hofland (2005) is confirmed by the fact that the calculated discharge (figure 27) deviates from the given discharge (table 3). Thus the measurements of all selected experiments are most likely affected by measurement errors.

### Sources of uncertainty
Constant discharge is expected when every measurement of water depth and time and depth averaged flow velocity is 100% accurate. Thus, the extracted water depths and flow velocities are most likely affected by sources of uncertainty. Several sources of uncertainty are considered:

1. Uncertainty in the measurement data due to fluctuations in discharge when the experiments were performed

2. Uncertainty in water depth measurements due to local variations in water depth as a result of undulations
3. Uncertainty in the flow velocity measurements due to incorrect usage of the laser Doppler anemometer
4. Uncertainty in the flow variables due to tracing the graphs in the papers by hand

In the following text these sources of uncertainty are elaborated.

*1. Uncertainty in the measurement data due to fluctuations in discharge*
Nakagawa & Nezu (1987) stated that the measurements of the instantaneous flow velocity satisfied continuity within an error margin of 5%. De Ruijter (2004) who helped conduct the experiments of Hofland (2005) stated that during their experiments, their measured discharge fluctuated within a margin of 2 l/s. Their discharge on top of the step during their experiments equalled 31.8 l/s. This gives a relative fluctuation in discharge of 6.3%. Note that these fluctuations in discharge could be a measurement error, or it could be the result of an inability to very accurately set the discharge of the pump feeding the flume with water. Xingkui & Fontijn (1993) did not mention a fluctuation in discharge during its measurements, however, figure 27 clearly shows that for the experiment of Xingkui & Fontijn (1993) the measured discharge fluctuates.

The fluctuation in the discharge in between measurements due to an inability to very accurately set the discharge of the pump feeding the flume with water is problematic. Figure 28 shows an example of measuring water depths when discharges fluctuate between measurement locations. Measurements were performed at different locations under a slightly varying discharge. The water depth change $(h_b - h_a)$ under flow conditions that fluctuated in between measurements will show an increase in the water depth that is much larger than the actual increase due to the presence of the step (e.g. discharge equals 7 l/s when measuring $h_b$ whereas the previous measurement was performed under a discharge of 6 l/s).
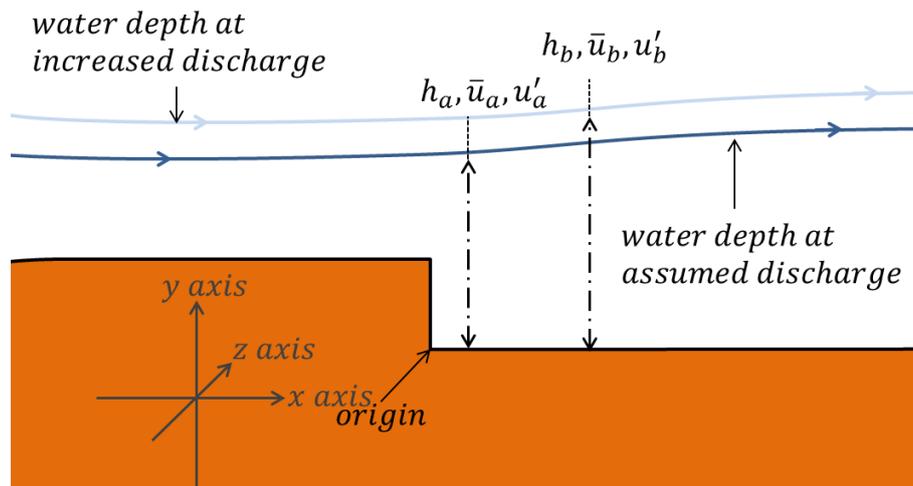


Figure 28 Example of wrong measurement due to a change in discharge between measurements

Conservation of mass between the two measurement location is now no longer valid. As a result, the change in water depth due to the presence of the step is possibly not accurately represented by the change in measured water depths. However, it is very hard to determine whether the fluctuations in discharge as depicted in figure 27 is the result of actual change in discharge in between measurements, or the result of measurement errors in water depth and flow velocity

profiles. Measurement errors in water depth and flow velocity could also result in a fluctuation in discharge, while the actual discharge during the experiments remained constant.

If it is assumed that the pump feeding the flume with water could be accurately set at a constant discharge, then it is still possible to find fluctuations in discharge due to measurement error in the water depth and flow velocity profiles. The accuracy of the water depth measurements and the accuracy of the flow velocity profile measurements using a laser Doppler anemometer are therefore discussed.

*2. Uncertainty in water depth measurements due to local variations in water depth*
The accuracy of the water height measurements are estimated to be in the order of magnitude of several millimetres by De Ruijter (2004). Moreover, local variations in water depth as a result of undulations just downstream of the step could amount to several centimetres of error in the water depth measurements. However, figure 26 shows a smooth change in water depth measurements without large outliers, thus it is unlikely that the water depth measurements were affected by a source of uncertainty that resulted in an independent fluctuation of several centimetres.

*3. Uncertainty in the flow velocity measurements due to incorrect usage of the laser Doppler anemometer*
The velocity measurements were all performed using a laser Doppler anemometer (LDA). The expected measurement error of the LDA depends on its calibration and correct setup of the system (Tropea, 1995). No data are available for the uncertainty margins as the result of using the LDA for the selected experiments. Tropea (1995) mentioned LDA uncertainty margins in the order of magnitude of micrometres, under the conditions that the LDA was setup and calibrated correctly. The uncertainty margin of several micrometres is much smaller than the uncertainty margins in the water depth measurements. However, the uncertainty margin might be bigger when the LDA is incorrectly set up or calibrated.

*4. Uncertainty in the flow variables due to tracing the graphs in the papers by hand*
Because the flow velocity and water depths are extracted from graphs, some uncertainty is contained in the extracted variable due to the extraction process itself. The flow velocity profiles and water depths were extracted by tracing the graphs in the papers by hand (aided by the computer, appendix L). Because the extraction process was performed by hand, human error is likely contained in the extracted data.

### Quantifying the uncertainty in the measurements
Because little data is available to quantify the uncertainty, it is only possible to get a rough estimate of the uncertainty in the measurements. The effect of each of the four identified sources of uncertainty were estimated using literature. This resulted in a conservative[16] estimate of the size of the uncertainty. The size of uncertainty in the measurements are quantified in appendix M. Table 4 summarizes the uncertainty quantification.

---

[16] Conservative because it is assumed that the error in the measurements is not auto-correlated. This results in a larger estimation of the uncertainty.

Table 4 Quantification of uncertainty in the measurements

| Author | Xingkui, 1993 | Hofland, 2005 | Nakagawa ST1, 1987 | Nakagawa ST3, 1987 |
|---|---|---|---|---|
| Water depth measurements uncertainty | ± 6.74% | ± 15.36% | ± 17.76% | ± 9.69% |
| Flow velocity measurements uncertainty | ± 1.6% | ± 1.79% | ± 2.29% | ± 2.24% |
| Discharge uncertainty | ± 9.3% | ± 17.32% | ± 20.90% | ± 12.07% |

The quantification of the measurement uncertainty reveals that especially the water depth measurements are somewhat uncertain. As a result, the discharge uncertainty is also quite large. However, as mentioned above, these uncertainty estimates are conservative.

When the uncertainty in the water depth and flow velocity measurements is taken into account, then it is quite possible that the experiments were performed under more or less constant discharge (appendix M) for all experiments except Xingkui & Fontijn (1993). This means that uncertainty source 1 might be less of a problem then first anticipated (except for the Xingkui & Fontijn, 1993 experiment). Because these uncertainty estimates are considered conservative, the measured data is still deemed usable for validating the ATM. However, the uncertainty in the input data should be kept in mind when reviewing the ATM results in chapter 7.

## 5.5 Turbulent energy measurements and the uncertainty margins

### Introduction

In this section, an uncertainty analysis is performed on the validation data. First, however, a more detailed explanation is given how turbulent energy levels are calculated using flow velocity fluctuations in only 2 dimensions. Because depth and width averaged turbulent energy levels contain, per definition, the turbulent fluctuations in all three dimensions, a method is introduced to approximate the flow velocity fluctuations in the third dimension. The sources of uncertainty affecting the flow velocity fluctuations are discussed after that. Finally, the measured turbulent energy levels are presented and discussed along with the uncertainty margins of the measured turbulent energy levels. This will give an overview of the accuracy of the measured turbulent energy levels.

### Calculating the turbulent energy using measured flow velocity fluctuations in only 2 dimensions

Turbulent energy $\bar{k}$ for the different studies is calculated using equation 3.3.

$$\bar{k} = \frac{1}{2}(\bar{u}_i')^2 \qquad\qquad (3.3)$$

The velocity fluctuation in $x$ and $y$ direction are given by the selected studies, but not in the $z$ direction (see figure 13 for the definition of the coordinate system). Because the ATM models the turbulence as a depth, width and time averaged value, the velocity fluctuations in $z$-direction also need be taken into account when calculating the measured turbulent energy levels (used to validate the ATM). Turbulence isotropy is sometimes assumed to find the velocity fluctuations in all directions (Nakagawa & Nezu, 1987; Brodkey, 1995; Wilczek, Stevens, & Meneveau, 2014). Anetor, et al. (2011) stated that the $\kappa - \epsilon$ models assume isotropy of turbulence. The velocity fluctuations in $z$ direction are therefore approximated by the assumption that $\bar{u}_x'^2 \sim \bar{u}_y'^2 \sim \bar{u}_z'^2$. Assuming $\bar{u}_x'^2 \sim \bar{u}_y'^2 \sim \bar{u}_z'^2$, is true then:

$$\overline{u_z'}^2 \approx \frac{1}{2}\left(\overline{u_x'}^2 + \overline{u_y'}^2\right) \tag{5.7}$$

Or in other words, the flow fluctuations squared in $z$ direction approximately equal the average of the flow velocities squared in $x$ and $y$ direction. This reduces equation 3.3 to:

$$\overline{k} = \frac{1}{2}\left(\overline{u_x'}^2 + \overline{u_y'}^2 + \overline{u_z'}^2\right)$$

$$\overline{k} = \frac{1}{2}\left(\overline{u_x'}^2 + \overline{u_y'}^2 + \frac{1}{2}\left(\overline{u_x'}^2 + \overline{u_y'}^2\right)\right)$$

$$\overline{k} = \frac{1}{2}\left(\frac{3}{2}\overline{u_x'}^2 + \frac{3}{2}\overline{u_y'}^2\right)$$

$$\overline{k} = \frac{3}{4}\left(\overline{u_x'}^2 + \overline{u_y'}^2\right) \tag{5.8}$$

**Uncertainty sources affecting the flow velocity fluctuations**

In the previous section the uncertainties expected in the ATM input data were discussed. The same sources of uncertainty are considered for the flow velocity fluctuations.

The following sources of uncertainty will most likely <u>not</u> affect the flow velocity fluctuations:

1. The flow velocity fluctuations are closely related to the turbulence in a flow. Turbulence in a flow is not dependent on the discharge of the flow (chapter 4). Therefore, it is expected that (small) fluctuations in discharge will have little to no effect on the flow fluctuations $\overline{u_i'}$.

2. The flow velocity fluctuations are not affected by the measurement uncertainties in the water depth.

The following sources of uncertainty <u>do</u> affect the flow velocity fluctuations:

3. Incorrect setup of the LDA measurement equipment will affect the instantaneous flow velocity measurements. Incorrectly measuring the instantaneous flow velocity will result in incorrect flow velocity fluctuation measurements (equation 3.2).

4. The uncertainty due to extraction of data from graphs also affects the flow velocity fluctuations measurements because every value for $\overline{u_i'}$ is found by extracting and integrating $u_i'$ from a graph in the papers.

Because the measured flow velocity fluctuations are solely used to calculate the measured turbulent energy levels, the uncertainty analysis is directly applied to the measured turbulent energy levels. The effect of the two sources of uncertainty were estimated similarly to section 5.4. In appendix N the size of the uncertainty in the turbulent energy measurements are quantified. In the next sections the measured turbulent energy levels including their uncertainty margins are presented.

A source of uncertainty that was not taken into account is the possibility that that the fluctuations in $z$ direction are not represented accurately by equation 5.8. However, the applicability of equation 5.8 is supported by literature (Nakagawa & Nezu, 1987; Brodkey, 1995; Wilczek, Stevens, & Meneveau, 2014). Because equation 5.8 is supported by literature, and it is hard to

quantify the error resulting from applying equation 5.8, it is assumed that equation 5.8 is correct for this study.

### Measured Turbulent energy

Figure 29 shows the measured turbulent energy (calculated using equation 5.8) for the different studies including the uncertainty margins of the measured turbulent energy. The general shape of the turbulent energy levels for the different experiments are discussed here. Thereafter the implications of the uncertainty limits are discussed.
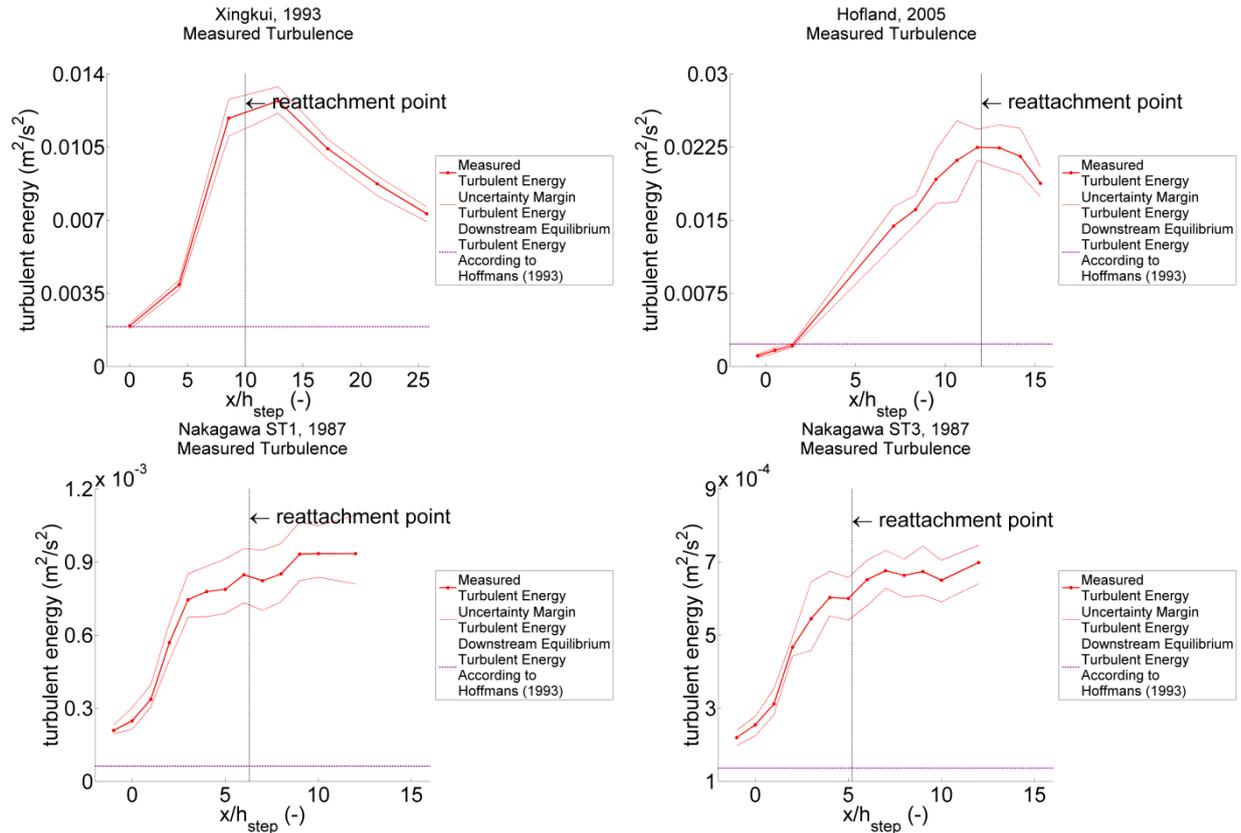


Figure 29 Measured depth averaged turbulent energy for the different selected experiments including the uncertainty margin[17]

In chapter 3 it was proposed that the turbulent energy increases until the reattachment point and dissipates further downstream. The experiments of Xingkui & Fontijn (1993) and Hofland (2005) roughly show this pattern. The Nakagawa & Nezu (1987) experiments show a less clear pattern. Turbulent energy seems to increase until the reattachment point, but no clear dissipation is detected downstream of the reattachment point. On the contrary, turbulence seems to increase even downstream of the reattachment point for the Nakagawa & Nezu (1987) experiments. The reason for the lack of turbulence dissipation for the experiments of Nakagawa & Nezu (1987) is

---

[17] Note that the experiment performed by Xingkui & Fontijn (1993) has very little measurement locations (only 7) and that the experiment of Hofland (2005) (performed by De Ruijter, 2004) has a large gap with no measurements between $x/h_{step} = 1$ and $x/h_{step} = 7$.

most likely related to the continuation of turbulence production downstream of the reattachment point. The cause of this is discussed in more detail in the next chapter[18].

Most of the measurements for the selected experiments were performed in or near the recirculation zone. This means that the dissipation of turbulent energy, which is expected to happen at large distances downstream of the reattachment point (Nakagawa & Nezu, 1987), is only partly represented in the measurements depicted here. Figure 29 shows the expected equilibrium turbulent energy level downstream of the reattachment point, as calculated using the formula of Hoffmans (1993). Assuming the formula of Hoffmans (1993) is correct, then all experiments have not yet reached their equilibrium turbulent energy level at the downstream edge of the study area. The experiments of Xingkui & Fontijn (1993) and Hofland (2005) do show a trend of turbulence levels approaching the equilibrium turbulence level downstream of the reattachment point. The Nakagawa & Nezu (1987) experiments probably do not show decreasing turbulence levels because the measurement locations were located close to the step, causing the production of turbulence to be larger than the dissipation up until the downstream edge of the study area. Because little validation data is available that shows decreasing turbulence levels, validating how the ATM models dissipation downstream of the reattachment point will be challenging.

Nakagawa & Nezu (1987) experiments contain 10 up to 100 times less turbulent energy compared to the other selected experiments. This is most likely related to the fact the other experiments were performed in a rough flume, whereas the Nakagawa & Nezu (1987) experiments were performed in a flume with smooth walls, which could explain the difference between the found absolute turbulent energy values.

### Turbulent energy uncertainty limits
Figure 29 also shows the uncertainty limits of the measured turbulent energy levels. The uncertainty margins of the measured turbulent energy levels are small enough to be able to accurately conclude whether the ATM output confirms with the measured turbulent energy levels or not. Therefore, the measured turbulent energy levels, as depicted above will be used in the validation of the ATM without reserve.

## 5.6 Concluding remarks
Multiple information sources were consulted to gather experimental data that is usable for the validation. This resulted in the selection of four experiments that confirmed to the data requirements. The analysis of the data extracted from the four experiments indicated that the experimental data might have been affected by multiple sources of uncertainty. This led to the conclusion that one should keep the uncertainty of the water depth and flow velocity measurements in mind when reviewing the ATM results in chapter 7. The uncertainty analysis of the validation data showed that the measured turbulent energy values has small uncertainty margins. This data is therefore used in the validation of the ATM without reserve.

---

[18] Short explanation: Flow velocity differences (in $y$ direction) that still exist downstream of the reattachment point result in internal viscous stresses in the flow; internal viscous stresses cause turbulence.

# 6 Arcadis Turbulence Model input alternatives

## 6.1 Introduction

The goal of this chapter is to explain how the experimental data is used to calculate the input data that will be used to run the ATM. Multiple methods are considered to calculate the ATM input data in this chapter. Figure 20 shows the relations between measured flow variables, input data and validation data.
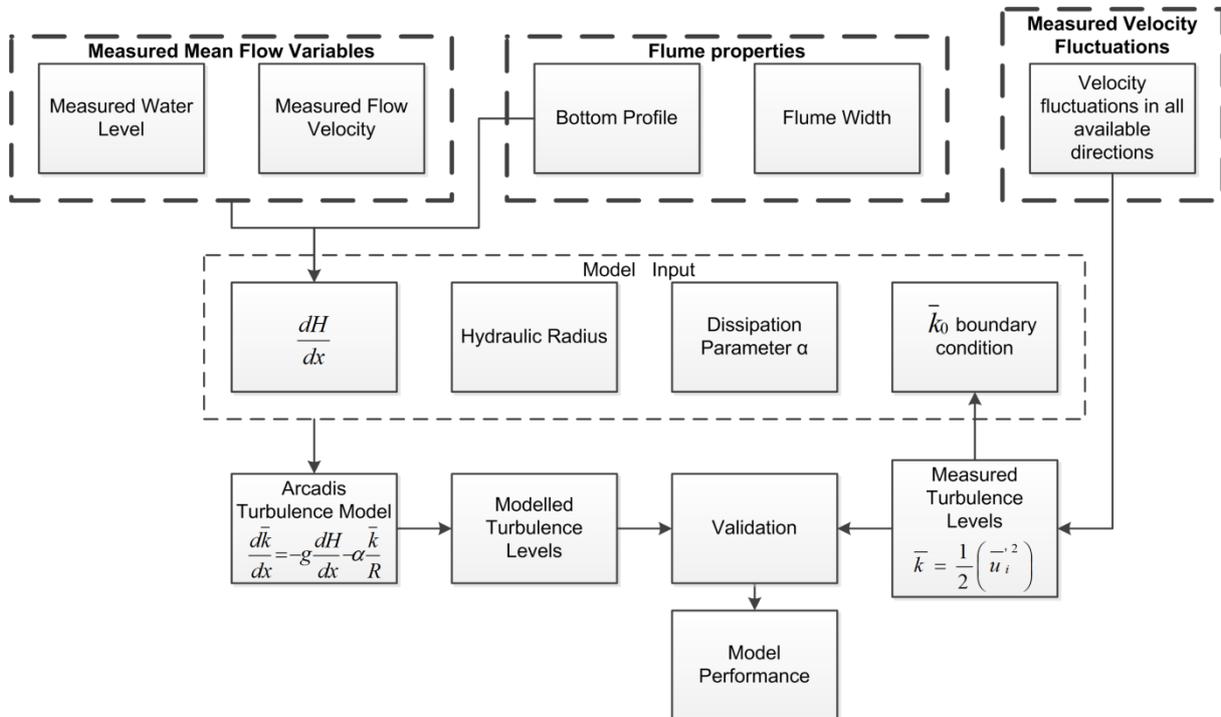


Figure 20 Flow chart showing ATM input and validation data

Figure 30 shows how the input variables relate to the ATM and the BFS. The term $\bar{k}_0$ can be interpreted as a boundary condition, $\alpha$ and $R$ as constants, and the head levels as a variable input. Take note that the turbulent energy depicted in the figure below has different units than the head levels and water levels.
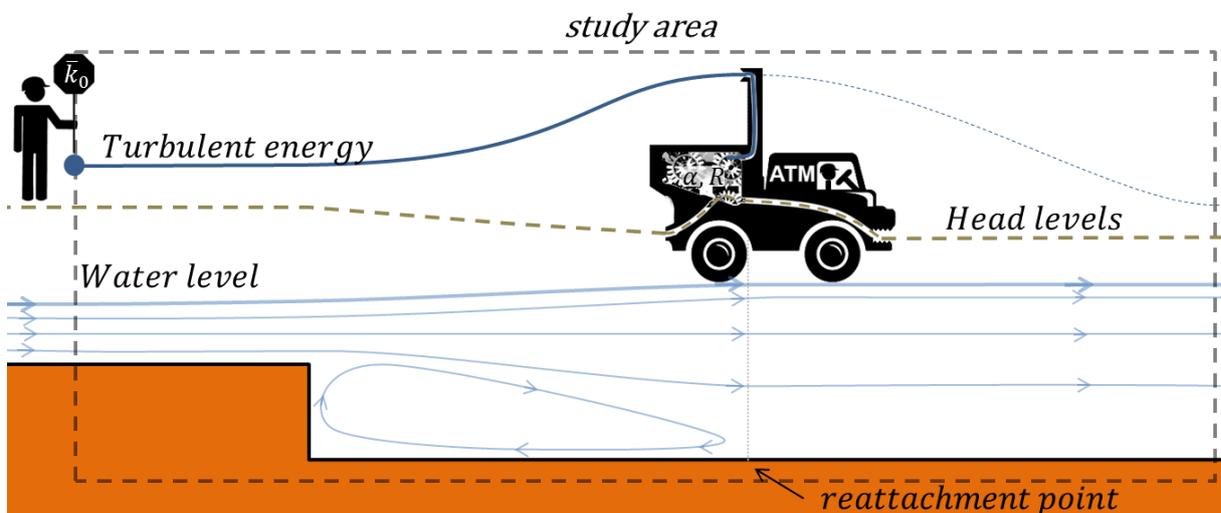


Figure 30 Relation between input variables, ATM output and the BFS

The dissipation coefficient $\alpha$ is a new parameter for which no measurement data is available. Therefore, three dissipation coefficient alternatives are suggested that are tested. Next, it is described what method is used to calculate the head levels using the measured water depth and flow velocities. Thereafter, an alternative method for finding the head level loss downstream of a BFS is proposed that uses the conservation of momentum. Finally, two methods are discussed to find a value for the incoming upstream turbulent energy $\bar{k}_0$. Table 5 shows the input variables, the number of alternatives that are considered and the section where they are discussed.

Table 5 ATM input alternatives and the section where they are discussed

| Variable | Number of alternatives considered | Discussed in: | What is discussed? |
|---|---|---|---|
| $\alpha$ | 3 | Section 6.3 | Three $\alpha$ alternatives based on the dissipation coefficient of Hoffmans (1993), no dissipation and calibrated dissipation |
| $\dfrac{dH}{dx}$ | 4 | Section 6.4: & 6.5 | Section 6.4: Three head level input alternatives based on the measured head levels Section 6.5: One head level alternative based on the conservation of momentum |
| $R$ | 1 | Appendix J | Formula and accuracy of approximation |
| $\bar{k}_0$ | 2 | Section 6.6 | Two $\bar{k}_0$ alternatives based on measured turbulence and equilibrium turbulence |

At the end of this chapter it will be clear what input alternatives are considered for the ATM runs. The ATM is then validated by comparing the output of the different runs to the measured turbulent energy values in chapter 7.

In order for the ATM to calculate absolute turbulent energy levels, a method is also required to solve the ATM differential equation. Therefore, first a numerical solution for the ATM differential equation is given before the input alternatives are discussed in this chapter.

## 6.2 Arcadis Turbulence Model numerical solution
### Introduction
A numerical solution for the ATM is needed because the ATM analytical solution (appendix G) can only use constant head level change as input $\left(\dfrac{dH}{dx} = constant\right)$. This section will discuss the method used to numerically solve the ATM.

### Forward Euler method
The Arcadis turbulence model is given by:

$$\frac{d\bar{k}}{dx} = -g\frac{dH}{dx} - \alpha\frac{\bar{k}}{R}$$

(3.11)

Equation 3.11 is a is a first order linear nonhomogeneous, differential equation. Multiple methods for numerically solving this type of equation exists. One of the most simple methods for numerically solving equation 3.11 is the forward Euler method. The Euler method is based on the fact that a differential equation $\frac{d}{dx}$ can be approximated by a finite step size $dx = \Delta x$ for small enough values of $\Delta x$. Applied to the ATM, this results in the following numerical equation:

$$\frac{d\bar{k}}{\Delta x} = -g\frac{dH}{\Delta x} - \alpha\frac{\bar{k}}{R}$$

$$d\bar{k} = \left(-g\frac{dH}{\Delta x} - \alpha\frac{\bar{k}}{R}\right)\Delta x$$

$$\bar{k}_{n+1} = \bar{k}_n + d\bar{k} = \bar{k}_n + \left(-g\frac{dH}{\Delta x} - \alpha\frac{\bar{k}_n}{R}\right)\Delta x$$

$$\bar{k}_{n+1} = \bar{k}_n - g(H_{n+1} - H_n) - \alpha \frac{\bar{k}_n}{R} \Delta x \qquad (6.1)$$

Where $\Delta x$ is a very small distance (m) and $\bar{k}_{n+1}$ is the turbulent energy at a distance $\Delta x$ downstream from the upstream turbulent energy value $\bar{k}_n$.

### Determining $\Delta x$

The step size $\Delta x$ is set at $\frac{1}{1000} h_{step}$ for all of the selected experiments. In appendix P the analytical and numerical solution of the ATM are compared. It is shown that the numerical solutions deviates only very little from the analytical solution when using a step size of $\frac{1}{1000} h_{step}$. The numerical ATM was also run using $\frac{1}{10000} h_{step}$ (to test the applicability of the forward Euler method when using non-constant change in mean flow energy ). The difference between ATM output using $\frac{1}{1000} h_{step}$ and using $\frac{1}{10000} h_{step}$ was negligibly small.

## 6.3 Arcadis Turbulence Model dissipation coefficient alternatives

### Introduction

In order to run the ATM, an assumption is necessary about the dissipation coefficient $\alpha$. Three different values for $\alpha$ are considered:

1. $\alpha = \frac{1}{1.21^2}$ (dissipation coefficient based on Hoffmans, 1993)
2. $\alpha = 0$ (no dissipation)
3. Calibrating $\alpha$ using the measured turbulence levels

Note that all three dissipations coefficient alternatives are constant in time and space. Chapter 4, showed that a dissipation coefficient that is variable in space and/or time might approximate reality better. The validation of the ATM with empirical data in chapter 7 will show whether the assumption that $\alpha = constant$ will approximate reality sufficiently to accurately model turbulent energy levels in BFS flow.

The reasons for choosing these three dissipation coefficient alternatives are discussed below.

*1. Dissipation coefficient following the dissipation of Hoffmans (1993)*

The dissipation coefficient $a = \frac{1}{1.21^2}$ follows from the Hoffmans (1993) formula for equilibrium stationary uniform turbulence (discussed in section 3.5). This dissipation coefficient alternative is based on the assumption that dissipation of turbulence under non-uniform conditions can be approximated by the dissipation coefficient under equilibrium flow conditions.

*2. No dissipation*

The dissipation coefficient $a = 0$ results in neglecting dissipation altogether. As was discussed in chapter 3 this will result in a never ending increase in turbulence for flows that continuously lose energy. This alternative is based on the assumption that the dissipation between the step and the reattachment point can be neglected. By neglecting turbulence dissipation, the maximum possible turbulence is found, which can then be compared to the measured turbulence to see how much the turbulent energy values are affected by turbulence dissipation. Downstream of the reattachment point, this model alternative will probably be less applicable for the experiments that show a decrease in turbulence downstream of the reattachment point.

*3. Calibrated dissipation*

The dissipation coefficient $\alpha$ is also calibrated based on the experimentally measured turbulent energy levels. After calibration, the ATM will fit the measured turbulent energy better. By comparing the different found values for $\alpha$, conclusions can be drawn about the applicability of the dissipation coefficient in the ATM. The calibration method and results are discussed in section 7.5.

## 6.4 Determining the head levels using the experimental measurements

### Introduction

Equation 6.1 needs a value for the head levels $H$ at increments of $\Delta x$. To calculate the head levels, the flow velocity $\bar{\bar{u}}$, water depth $h$ and elevation $z$ are needed at every increment $\Delta x$. This section will discuss how, using the measured variables presented in chapter 5, the measured head levels[19] are calculated. First, the applicability of the formula of Bernoulli to calculate the measured head levels is discussed. This discussion reveals that an adjusted Bernoulli formula is needed for calculating the head levels of a non-uniform flow velocity profile. An adjusted Bernoulli formula is introduced, and the non-uniformity of the flow velocity profiles of all selected experiments are discussed. A side step follows, where some questions that were raised in chapter 5 are answered using the adjusted Bernoulli formula in an example calculation. The experimentally measured head levels (calculated using the adjusted Bernoulli formula) are presented and discussed thereafter. In order to obtain head level values at increments of $\Delta x$, a number of methods are then proposed to interpolate the measured head levels.

### Head levels for non-uniform flow velocity profiles

The ATM needs the change in head level $\left(\frac{dH}{dx}\right)$ as input. Head levels are generally calculated using the formula of Bernoulli. However, this formula is based on a number of assumptions. In the coming text, the applicability of the Bernoulli formula for calculating the experimental head levels is discussed.

In chapter 2 the formula of Bernoulli was introduced to calculate the head levels in a flow:

$$H = z + h + \frac{1}{2}\frac{\bar{\bar{u}}^2}{g} \tag{2.2}$$

Because equation 2.2 will be applied to calculate the energy loss between two cross sections, the assumption of conservation of mean flow energy is discarded from the start. It is known that energy is lost between the step and the reattachment point, and equation 2.2 is applied to value how much energy is lost. Equation 2.2 also assumes stationary flow. During all the selected experiments, stationary flow was achieved before the measuring commenced, so this assumption is also valid.

In chapter 2 it was already mentioned that the Bernoulli equation also contains a correction coefficient $\alpha_{Bern}$ that deviates from 1 depending on how much the flow velocity profile (as a function of the depth) deviates from an uniform profile. Assuming a two dimensional flow (neglecting deviations in the width of the flume), the correction coefficient $\alpha_{Bern}$ can be calculated using the formula (Battjes, 1990):

---

[19] The term measured head levels is used to refer to the head levels found using the measured flow variables as discussed in chapter 5. In the next section, the momentum head levels are introduced as an alternative to the measured head levels.

$$\alpha_{Bern} = \frac{1}{h} \int_0^h (\bar{u}/\bar{\bar{u}})^3 \, dy \qquad (6.2)$$

Where $h$ equals the water depth (m), $\bar{u}$ the (time averaged) flow velocity in the flow direction (m/s) at a certain depth $y$, $\bar{\bar{u}}$ the time and depth averaged flow velocity (m/s), and $y$ the distance from the bottom of the flume to the location of $\bar{u}$ (m). When $\alpha_{Bern} \neq 1$ then the head levels are calculated using:

$$H = z + h + \alpha_{Bern} \frac{1}{2} \frac{\bar{\bar{u}}^2}{g} \qquad (6.3)$$

Figure 31 shows the measured mean flow velocity ($\bar{u}$) as a function of the depth for multiple cross section for the experiment of Xingkui & Fontijn (1993).
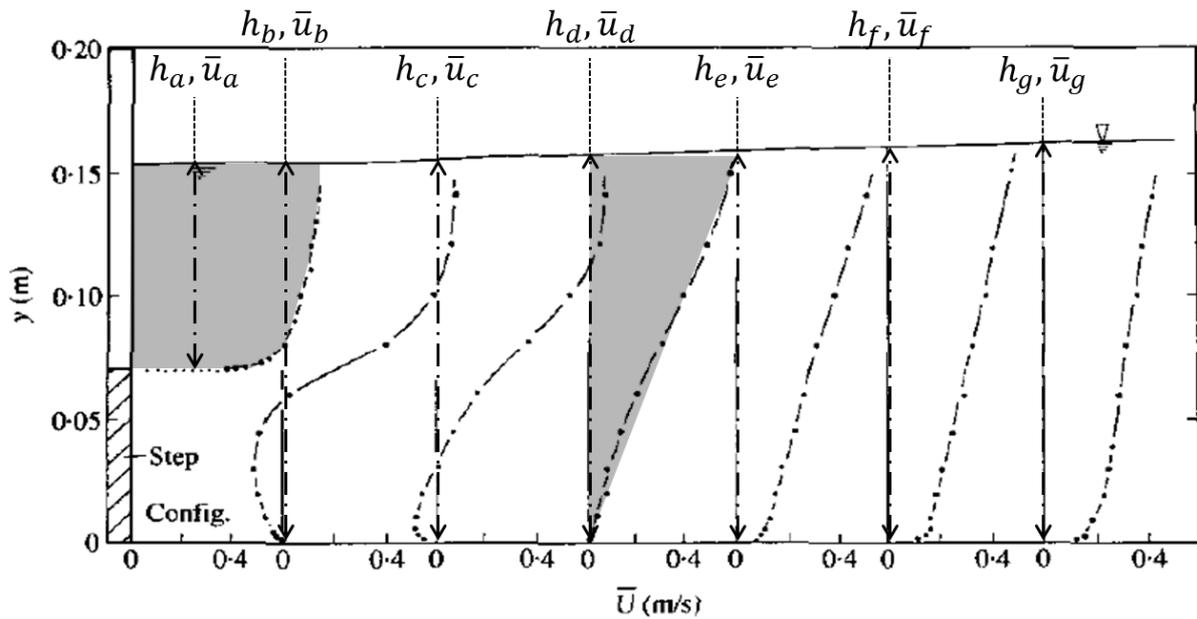


Figure 31 Flow velocity profile at multiple location in the flume as measured during the experiments of Xingkui & Fontijn (1993, p. 306)

Figure 31 shows a log-law (almost uniform) velocity profile on top of the step (first curve from the left). The reattachment point was located at cross section $d$ for the experiment of Xingkui & Fontijn (1993). Note that at this cross section the velocity profile shows an almost triangular shape. The velocity profiles of all cross sections downstream of the step show non-uniform shapes. Thus the assumption of an uniform velocity profile cannot be made downstream of the step and the Bernoulli formula should be adjusted using $\alpha_{Bern}$. The other selected experiments show similar non-uniform velocity profiles downstream of the step. Therefore, for all the selected experiments, the head levels are calculated using the measured $\alpha_{Bern}$. The found value of $\alpha_{Bern}$ at each measurement location is given in figure 32.
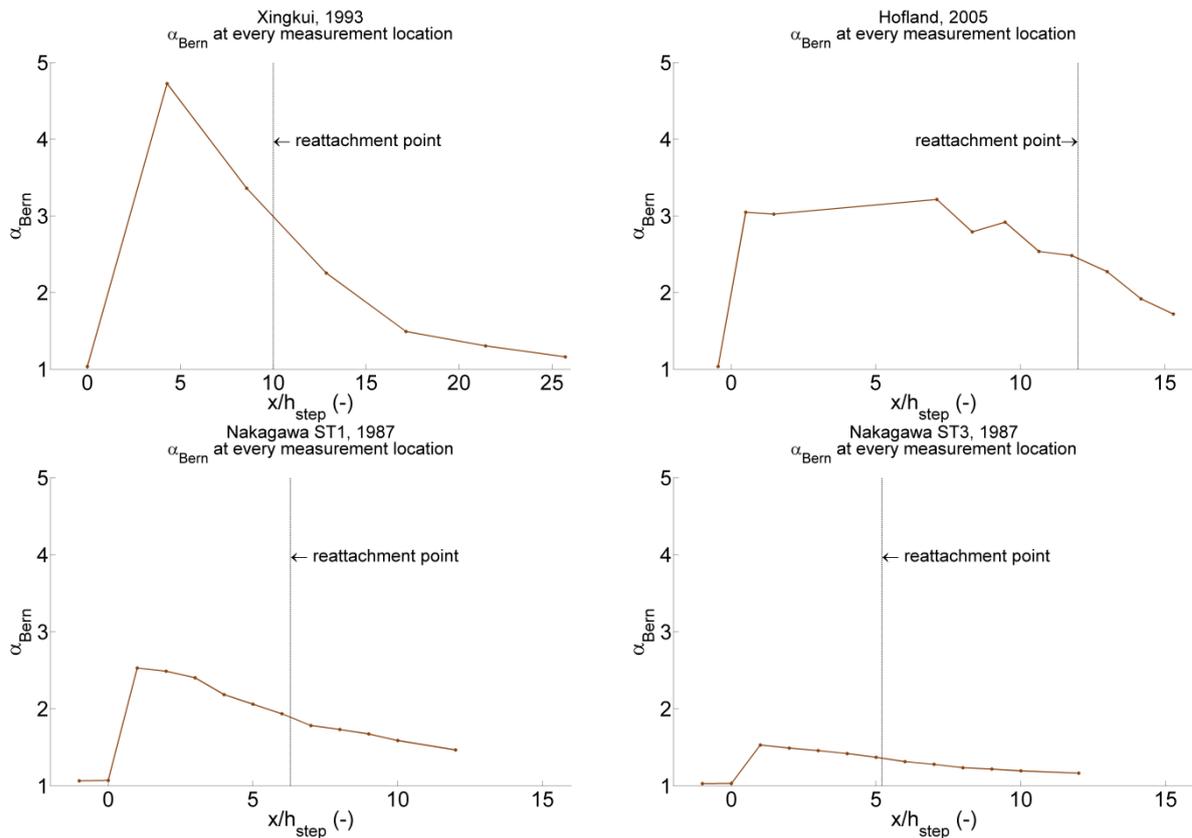
**Figure 32** The values for $\alpha_{Bern}$ at the measurement locations for the selected experiments calculated using formula 6.2

For every experiment, it can be seen that directly downstream of the step $\left(x/h_{step} > 0\right)$ the value of $\alpha_{Bern}$ is suddenly increased. This indicates that directly downstream of the step, the flow profile is suddenly significantly different from an uniform flow profile. The deviations from the uniform flow profile is caused by the presence of the recirculation zone. In the recirculation zone (figure 13) the flow velocity significantly differs from the depth average flow velocity on top of the step (the recirculation zone includes negative flow velocities). Thus, just after the step, the flow velocity profile consists of an upper part very similar to the flow profile on top of the step, and a lower (recirculation zone) part that includes negative flow velocities. These profiles together result in a non-uniform flow velocity profile (as can be seen starting from cross section $b$ in figure 31). It can also be seen that at the reattachment point, the value for $\alpha_{Bern}$ is still larger than 1 for all selected experiments.

This phenomena affects the turbulence in the flow downstream of the reattachment point. At the reattachment point, the flow velocity profile is still non-uniform. Downstream of the reattachment point, the flow velocity profile reverts back to a log-law profile. Due to the change in flow velocity profile, the flow experiences internal viscous stresses. Internal viscous stresses cause turbulence in a flow. Thus, downstream of the reattachment point, additional turbulence is produced on top of the production of turbulence due to wall friction. This deviates from the ideas that practitioners have about turbulence production (Voortman, 2015).

Chapter 5 showed increasing water depths downstream of the reattachment point. By considering non-uniform flow velocity profiles in the Bernoulli equation, a physical explanation can be given why the water depth rises even downstream of the reattachment point. This is shown with an example calculation in the following section.

### Increase in water depth due to non-uniform flow velocity profile change

In chapter 5 it was noted that the water depth increased downstream of the reattachment point. This was unexpected because it was assumed that downstream of the reattachment point, the flow does not decelerate anymore, resulting in a constant water depth. The phenomena of increasing water depths downstream of the reattachment point is clarified using the flow schematisation in figure 33.

Let's assume that a BFS flow has a water depth of 0.1 m, a depth averaged flow velocity of 0.5 m/s, a specific discharge $q = 0.05$ m²/s and a $\alpha_{Bern\,f} = 2$ at the reattachment point.
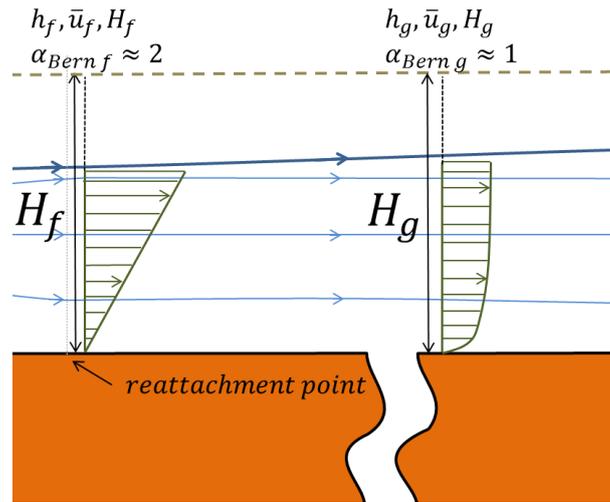


Figure 33 Graphical depiction of change in water profile downstream of the reattachment point

The head level can then be calculated using equation 6.3:

$$H_f = 0.1 + 2 \times \frac{1}{2} \frac{0.5^2}{g} = 0.1255\,m$$

Now let's assume that downstream of the reattachment point no energy is lost, mass is preserved, a log-law velocity profile develops that closely resembles $\alpha_{Bern\,g} \approx 1$ and no change occurs from subcritical to supercritical flow or vice versa. The water depth can then be found by solving the following equation:

$$H_g = h_g + 1 \times \frac{1}{2} \frac{\left(\frac{q}{h_g}\right)^2}{g} = 0.1255\,m$$

Where the subscript $g$ now indicates a location downstream of the reattachment point where the flow has returned to an approximate uniform flow velocity profile, thus $\alpha_{Bern\,g} \approx 1$. Solving above equation for subcritical flow gives $h_g = 0.116$ m and $\bar{\bar{u}}_g = 0.431$ m/s. Thus, as the result of a non-uniform velocity profile reverting to a uniform flow profile, the water depth increases and flow velocity decreases (downstream of the reattachment point).

Internal viscous friction could cause the mean flow to loose energy between location $f$ and $g$, $H_g < 0.1255$ and as a result, $h_g < 0.116$ for subcritical flow (Cruise, Sherif, & Singh, 2007). As mentioned previously, internal viscous frictions result in the production of turbulence. Thus when more turbulence is produced due to the change in flow velocity profile, the water depth is increased less. Wall friction could also result in energy loss between location $f$ and $g$, and thus a smaller increase in $h_g$.

Using this information, the BFS schematisation is adjusted slightly:
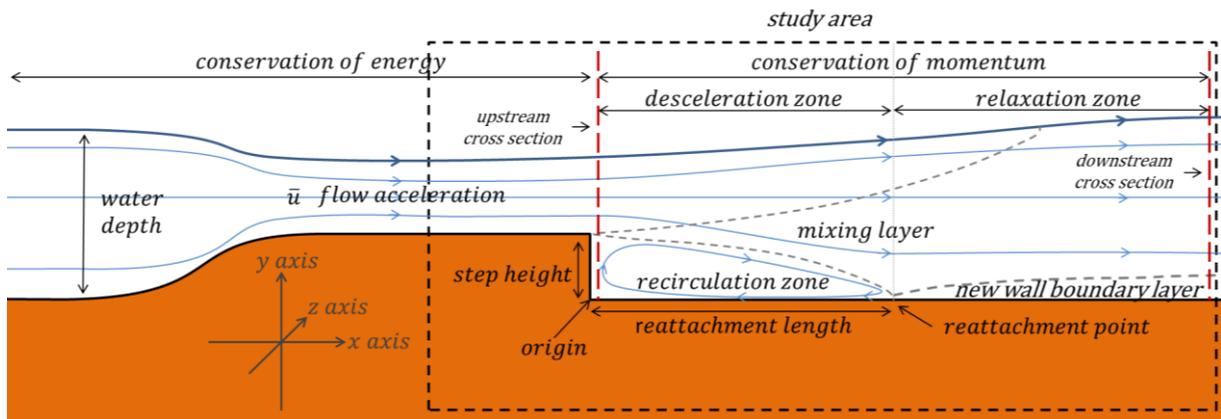


**Figure 34 Schematisation of BFS flow including changing water level downstream of the reattachment point**

Figure 34 shows the new BFS flow schematisation. In this new schematisation, the relaxation zone downstream of the reattachment point shows an increase in water depth due to the flow velocity profile reverting back to a log-law velocity profile. The increase in water level downstream of the reattachment point depends on the level of non-uniformity of the flow velocity profile at the reattachment point ($\alpha_{Bern}$). The increase (or decrease) in water level downstream of the reattachment point is also dependent on the energy loss of the mean flow (due to bed friction and internal viscous stresses).

The exact location where the flow velocity approximates a log-law profile again (and thus no change in water depths occurs due to change in flow velocity profile) is unknown for the selected studies. Nakagawa & Nezu (1987) did mention for their experiments that at approximately 20 step heights, the water level did not change anymore.

No decreasing levels of turbulent energy were found downstream of the reattachment point for the experiments of Nakagawa & Nezu (1987). This study hypothesizes that due to the change from non-uniform to a uniform flow velocity profile, internal viscous frictions produce turbulence. This production is more or less equal to the dissipation of turbulent energy, resulting in more or less constant turbulent energy levels downstream of the reattachment point for the experiments of Nakagawa & Nezu (1987). Possibly, the turbulent energy dissipation is related to the bottom roughness. This could explain the difference between the turbulence dissipation during the Xingkui & Fontijn (1993) and Hoffmans (1993) experiments compared to the turbulence dissipation during the Nakagawa & Nezu (1987) experiments.

### Head levels from measurements

For all selected experiments, the head levels are calculated using equation 6.3. Figure 35 shows the head levels for each measurement location of the selected experiments.
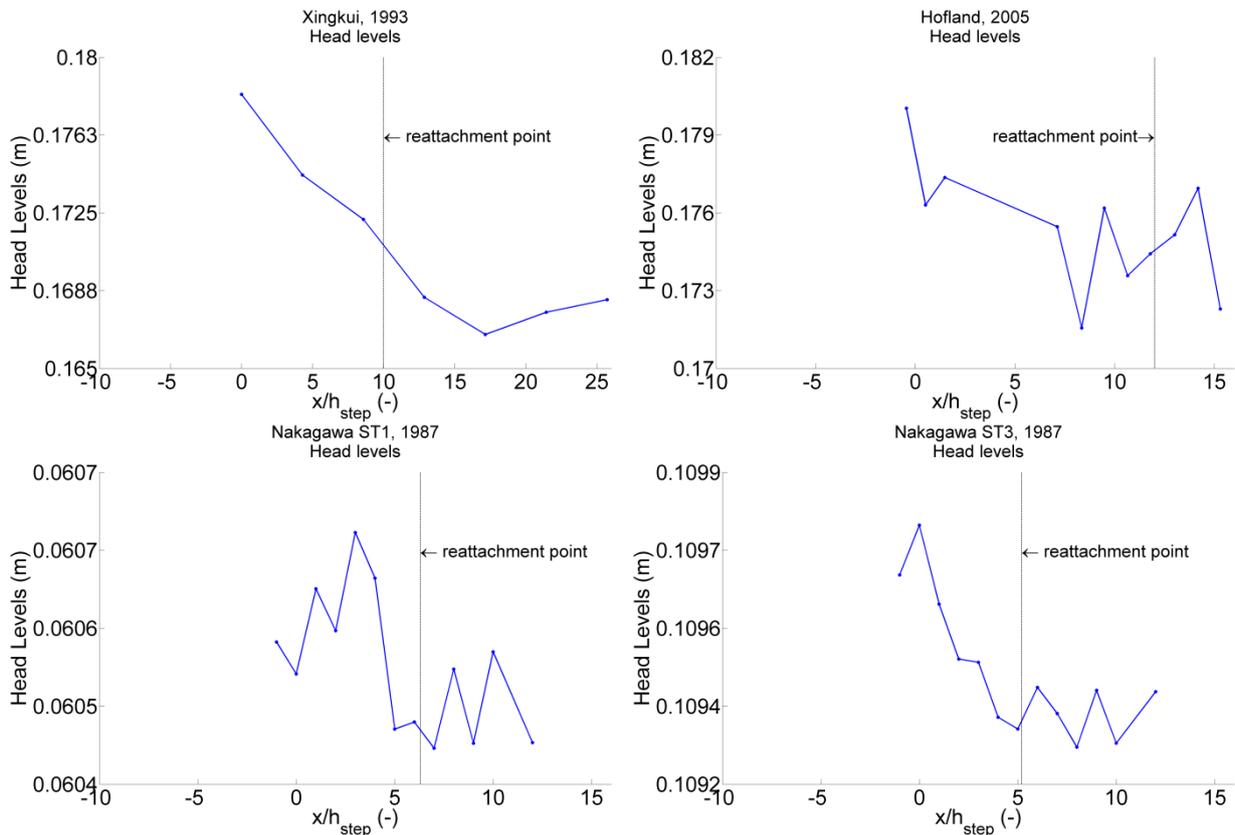
**Figure 35 Head levels calculated using the water depth, flow velocity and $\alpha_{Bern}$ coefficient**

Because figure 35 shows the measured head levels, all sources of mean flow energy loss are incorporated in these figures (internal viscous stress, bottom and wall friction, etc.). All experiments roughly show a pattern of decreasing mean flow energy in the flow direction. This is expected because the presence of the step and bottom friction are reducing the mean flow energy, resulting in a declining head levels in the flow direction. All experiments show both temporary increases and decreases head levels. Especially the increases in mean flow energy are not very likely. No phenomena are known that could add energy to the water in the flume beside the pump recirculating the water through the flume, which is located much further downstream. It is concluded that the head level fluctuations are probably the result of the errors in the water depth and flow velocity measurements. The uncertainty in the head levels is quantified in appendix Q. This uncertainty analysis conforms that the head levels are affected by the uncertainty in the measured flow variables.

Pay attention to the scale of the measured head levels for the selected experiments. For the experiments of Xingkui & Fontijn (1993) and Hofland (2005), the head levels fluctuate in the order of magnitude of several centimetres. On the other hand, both experiments performed by Nakagawa & Nezu (1987) show head levels that fluctuate in the order of magnitude of only tenths of millimetres. This is something to consider when reviewing the results presented in this thesis.

## Head level shapes

The ATM requires head levels $H$ at increments of $\Delta x$. Thus, in between the measurement location, the head levels need to be interpolated. However, the measured head levels show a chaotic pattern than include many temporarily increases in mean flow energy. Therefore, beside simply interpolation in between the measured (raw) head levels, two other interpolation methods are considered that smooth out the fluctuations in the head level measurement:

1. Raw measured head levels
2. Linear head levels
3. Polynomial head levels
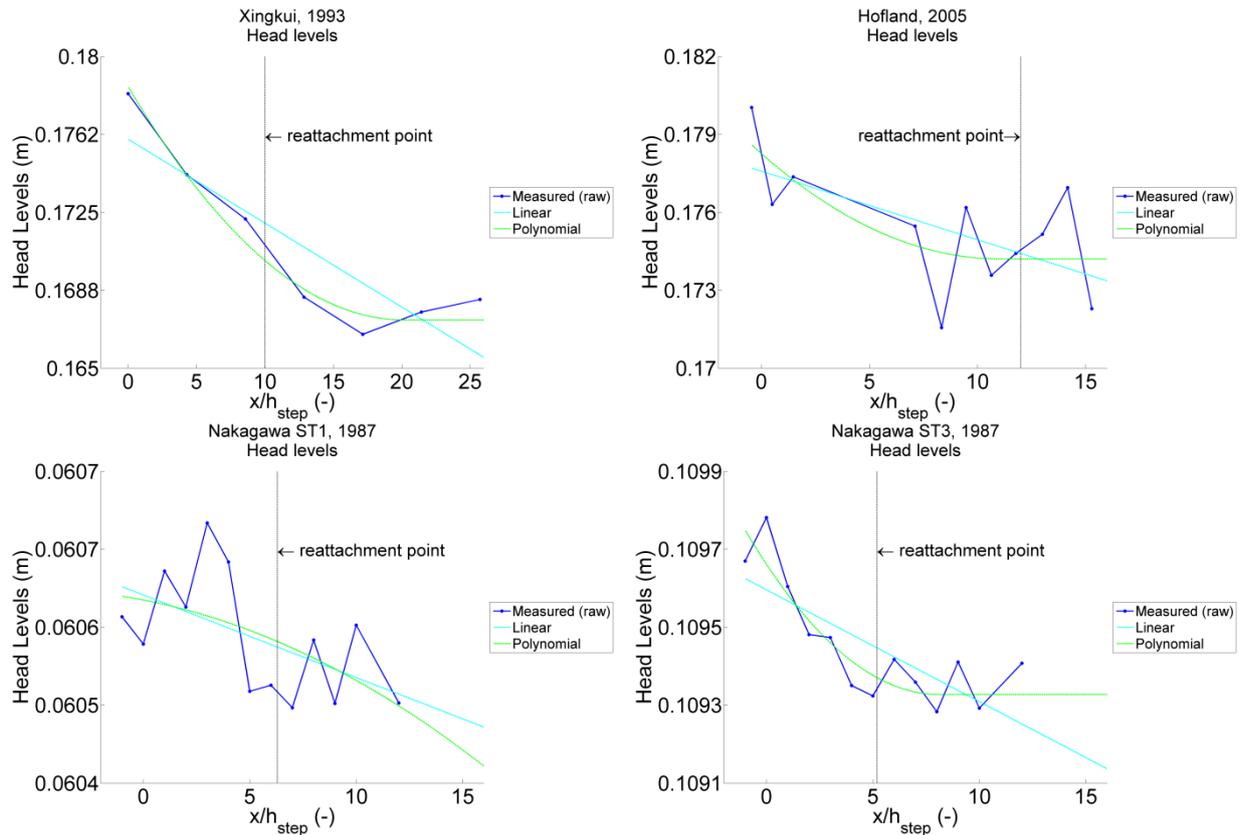


Figure 36 Head level shape interpolation alternatives for the selected experiments

*1. Raw measured head levels*

Because a value for the head level is needed at every increments of $\Delta x$, a constant rate of change is assumed in between the measured head levels (as was already depicted in figure 35; the straight blue lines in between the blue dots). This head level shape is considered because it does not force a certain shape on the head levels. However, when put into the ATM, the resulting turbulent energy levels should be handled with some reserve because of the unrealistic shape of these head levels.

*2. Linear head levels*

Downstream of the step, the flow decelerates and looses energy. The linear head level shape is based on the assumption that this energy loss occurs at the same rate up until the downstream edge of the study area (located downstream of the reattachment point).

*3. Polynomial head levels*

The polynomial head level shape is based on the following assumption: The speed differences between the water flowing over the step, and the water flow in the recirculation zone is larger near the step than further downstream (figure 31). These speed differences in the flow result in more viscous friction and thus more mean flow energy loss near the step compared to further downstream. After fitting the measured head level data with a polynomial function, all experimental data showed this relation except for the Nakagawa and Nezu (1987) ST-1 experiment, which showed a gradual energy loss at the step, and rapid energy loss near the reattachment point. The Nakagawa and Nezu (1987) ST-1 polynomial head level shape is still used because it is unclear whether the deviating shape is the result of measurement errors, or if the flow during the Nakagawa and Nezu (1987) ST-1 experiment actually showed a different energy loss pattern compared to the other experiments.

A more detailed description of the interpolation methods, is given in appendix S. In this appendix it is shown that the polynomial interpolation method best approximates the measured head levels for al experiments except Nakagawa and Nezu (1987) ST-1.

## Distinction between the ATM and the head level schematisation

Note that the ATM does not actually prescribe a method for obtaining the head level change $\frac{dH}{dx}$. The above described alternative head level shapes are not part of the ATM schematisation. If accurate measurements of the head levels are available at every increment of $\Delta x$, then no assumptions about the shape of the head levels are needed, and a numerical solution for the ATM can be found using equation 6.1. Alternatively, if a function of $\frac{dH}{dx}$ is available, the ATM can be solved analytically without the need for the numerical forward Euler method. However, the selected experiments did not give a function for $\frac{dH}{dx}$ or very accurate head levels $H$ at every increment of $\Delta x$. Therefore assumptions about the shape of the head levels are needed.

## Conclusion

This section discussed how the measured flow variables (water height, flow velocity) are used to calculate the head levels in the flume during the experiment. It was shown that the flow velocity profile at the measurement locations downstream of the step are non-uniform. Therefore, the adjusted Bernoulli formula is used to calculate the head levels in the flume. The resulting head levels showed a chaotic pattern. However, a general trend of decreasing mean flow energy could be recognised in this chaotic pattern for all selected experiments. In order to reduce the chaotic head level pattern, two smoothing methods were introduced. The ATM will be run using the head level alternatives, as schematized in figure 37.

Figure 37 shows what data the ATM needs to calculate the turbulent energy, the alternative inputs that are discussed thus far, and the data used to validate the ATM.
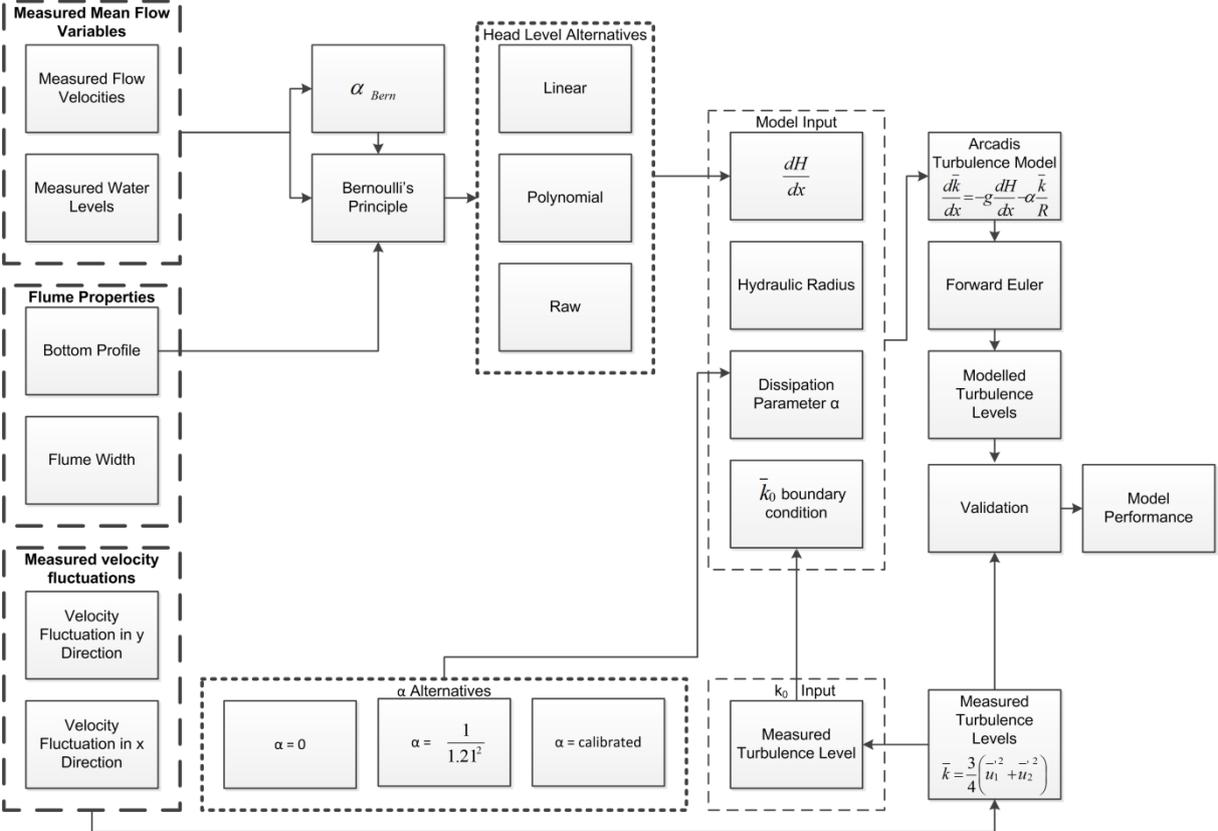


Figure 37 Schematization of input, output and validation of the ATM

In appendix Q an uncertainty analysis can be found of the measured head level input. The uncertainty analysis confirms that the head levels are affected by the uncertainty in the measured flow variables. The measured head levels (raw, linear, polynomial) will be used as input into the ATM. However, one should keep in mind that the measured head level input is affected by a number of sources of uncertainty, which can affect the accuracy of the ATM.

## 6.5 Determining the head levels using the conservation of momentum

### Introduction

Figure 37 shows that to run the ATM, measured values for the water depth and flow velocities on top of and downstream of the step at multiple locations are needed. However, the ATM is intended as a rapid assessment tool for finding the depth averaged turbulent energy in a flow. The rapid assessment tool is intended to be applied, for example, to calculate depth average turbulence as input for the design of bed protection. In such a scenario, it is unlikely that measurements of the water depth, flow velocity and incoming turbulence are available for the flow situation that the ATM is applied to. Moreover, the uncertainty analysis of the measured flow variables (appendix M) indicate that the experimental measurement data contain large uncertainties. Therefore, in the following text a method is described to find the mean flow energy loss (required as input into the ATM) using as little (uncertain) measurement data as possible. It is expected that running the ATM using both the measured head level alternatives as well as momentum head level alternative (discussed in this section) will result in more substantiated conclusions about the ability of the ATM to estimate turbulent energy levels in a flow.

In the following text, first an explanation is given how the conservation of momentum will be used to calculate the water depth at a downstream location. This discussion will show that that the non-uniformity of the flow velocity profile should be taken into account in order to accurately apply the conservation of momentum. The water depths and flow velocity at the downstream location, calculated using the conservation of momentum, are compared to their measured counterparts. This will give insight in what way the two methods for finding the flow variables deviate from one another. A short explanation how the momentum head levels are calculated, follows. Then, the momentum and measured head levels are compared to each other in order to explain dissimilarities between the head levels found using the two methods. Using the conservation of momentum will results in only two flow energy levels, one on top of the step and one at the most downstream measurement location. After the comparison between the measured and momentum head levels, the method used to find the intermediate momentum head levels is discussed. Lastly, a short discussion is given about the difference in accuracy between the measured and momentum head levels.

### Calculating the water height and flow velocity using the conservation of momentum

In order to apply the conservation of momentum, two cross sections need to be determined for which the momentum can be calculated. Conservation of momentum between the two cross sections depicted in figure 34 is therefore assumed. In the following text, it is shown that the conservation of momentum between these two cross sections is not applicable for two of the selected experiments because of non-uniform flow velocity profiles. Therefore, a more accurate method is suggested (similar to the adjusted Bernoulli equation) that takes into account the non-uniformity of the flow velocity profile.

To calculate the mean flow energy loss due to the BFS, the conservation of momentum between the two cross sections depicted in figure 34 is assumed. Chapter 2 described how the momentum at a cross section is calculated:

$$M = \frac{1}{2}\rho_w g h^2 + \rho_w \beta h \bar{\bar{u}}^2 \qquad (2.5)$$

For non-uniform flow velocity profiles, the momentum equation needs a value for $\beta$ to find the correct momentum of the flow. In appendix E is it described how the value for $\beta$ can be approximated for the cross section at an infinitesimal distance downstream of the step. By applying this method, only the water depth, flow velocity (on top of the step) and step height are required to calculate the momentum at an infinitesimal distance downstream of the step.

The cross section located furthest downstream should ideally be located somewhere where $\beta \approx$ 1. This way, no information about the uniformity of the flow velocity profile is needed to calculate the momentum at the downstream location. If it is assumed that the flow velocity profile at the downstream edge of the study area is approximately uniform ($\beta \approx 1$), then the water height at the downstream edge of the study area can then be calculated by solving:

$$h_{downstream} = \frac{M_{upstream} - \frac{1}{2}\rho_w g (h_{downstream})^2}{\rho_w \frac{q^2}{h_{downstream}^2}} \qquad (2.7)$$

Where $M_{upstream}$ equals the momentum just downstream of the step (N/m). Note that the above equations assumes that no momentum is lost due to bottom friction or other phenomena.

However, figure 32 ($\alpha_{bern}$) already showed that at the downstream edge of the study area, the measured flow velocity profile is not approximately uniform for all of the selected experiments[20]. To check the applicability of equation 2.5 and 2.7, the beta coefficient of the flow velocity profiles on top of the step and at the most downstream measurement location are presented below.

Table 6 $\beta$ coefficient found for the most downstream measurement location of all selected experiments

| Author | | Xingkui, 1993 | Hofland, 2005 | Nakagawa ST1, 1987 | Nakagawa ST3, 1987 |
|---|---|---|---|---|---|
| **Velocity profile uniformity** | $\beta_{step}$ | 1.01 | 1.01 | 1.03 | 1.01 |
| | $\beta_{downstream\ edge}$ | 1.05 | 1.24 | 1.16 | 1.06 |
| | Location last measurement $(x/h_{step})$ | 25.7 | 15.3 | 12 | 12 |

Table 6 shows that on top of the step, the flow velocity profile of all experiments are approximately uniform $(\beta_{step} \approx 1)$, thus equation 2.5 can be used to calculate the momentum at an infinitesimal distance downstream of the step. However, at the most downstream measurement location the experiments of Hofland (2005) and Nakagawa and Nezu (1987) ST-1 show a flow velocity profile with $\beta_{downstream\ edge} > 1$. For these experiments, the assumption of an uniform flow velocity profile is not valid. When the most downstream measurement location has a non-uniform flow velocity profile, then equation 2.7 cannot be used to calculate the water depth at the downstream measurement location. Therefore, an alternative method is proposed to calculate the water depth at the most downstream measurement location. This alternative method uses the conservation of momentum, conservation of mass, and the $\beta_{downstream\ edge}$ coefficient to compensate for the non-uniformity of the flow velocity profile:

$$h_{downstream\ edge} = \frac{M_{upstream} - \frac{1}{2}\rho_w g\left(h_{downstream\ edge}\right)^2}{\rho_w \beta_{downstream\ edge} \frac{q^2}{h^2_{downstream\ edge}}} \qquad (6.4)$$

Equation 6.4 is very similar to equation 2.7 but now, the non-uniformity of the flow velocity profile at the most downstream measurement location is taken into account. Using equation 6.3, the water depth, flow velocity, and head level at the downstream measurement location is calculated. These variables are presented next.

## Comparing the measured and momentum water depths and flow velocities
The differences between the measured flow variables, and the flow variables using the conservation of momentum, are discussed in the following text. This will give insight in what way the two methods for finding the flow data (water height, flow velocity) deviate from one another.

To calculate the water heights and flow velocities at the most downstream measurement location using the conservation of momentum, the water depth and flow velocity at a certain location upstream are needed. It is chosen to simply use the first measured water depth and flow velocity as input. These measured variables contain error, as was already discussed in chapter 5, so the

---

[20] On a side note, $\beta$ and $\alpha_{Bern}$ are both very similar expressions of the non-uniformity of the flow velocity profile, but $\alpha_{Bern}$ is more sensitive to non-uniformity than $\beta$. Both terms are calculated using the formula: $\left[\alpha_{Bern} or\ \beta = \frac{1}{h}\int_0^h (\bar{u}/\bar{\bar{u}})^{ii}\ dy\right]$. However, for $\beta$, $ii = 2$ whereas for $\alpha_{bern}$, $ii = 3$. Thus for the same non-uniform flow velocity profile $\alpha_{bern} > \beta > 1$. Still for log-law flow velocity profiles, it is often assumed that $\alpha_{bern} \approx \beta \approx 1$.

resulting downstream water depths and flow velocities might not be accurately estimated due to the uncertainty in the water depth and flow velocity on top of the step.

Using the conservation of momentum, conservation of mass, the first measured values for water depth and flow velocity, and equation 2.5 and 6.4, the following water depths and flow velocities are found.
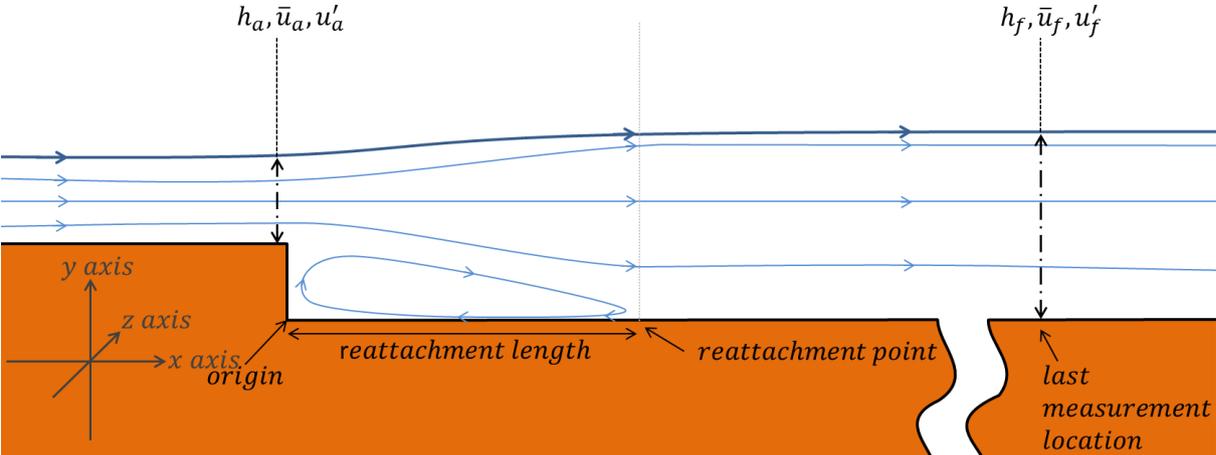


Figure 38 Locations of measured water depth and flow velocity to calculate and validate the conservation of momentum

Table 7 Flow variables and head levels measured and calculated using the conservation of momentum.

| Author | | Xingkui, 1993 | Hofland, 2005 | Nakagawa ST1, 1987 | Nakagawa ST3, 1987 |
|---|---|---|---|---|---|
| **Measured variables** | Measured $h_a$ (m) | 0.083 | 0.087 | 0.038 | 0.086 |
| | Measured $h_f$ (m) | 0.162 | 0.160 | 0.059 | 0.106 |
| | Measured $\bar{\bar{u}}_a$ (m/s) | 0.689 | 0.689 | 0.218 | 0.282 |
| | Measured $\bar{\bar{u}}_f$ (m/s) | 0.312 | 0.379 | 0.144 | 0.236 |
| | "Measured" $H_a$ (m) | 0.1782 | 0.1800 | 0.0606 | 0.1096 |
| | "Measured" $H_f$ (m) | 0.1683 | 0.1722 | 0.06049 | 0.1094 |
| | $\Delta H$ (m) | -0.00640 | -0.00774 | -0.00010 | -0.00026 |
| **Conservation of momentum** | Calculated $h_{f\,mom}$ (m) | 0.165 | 0.164 | 0.059 | 0.106 |
| | Calculated $\bar{\bar{u}}_{f\,mom}$ (m/s) | 0.347 | 0.370 | 0.141 | 0.226 |
| | Calculated $H_{f\,mom}$ (m) | 0.1721 | 0.1758 | 0.0603 | 0.1095 |
| | $\Delta H_{mom}$ (m) | -0.00608 | -0.00422 | -0.00032 | -0.00017 |

Table 7 Shows the measured water depths and flow velocities and the calculated water depth and flow velocity using the conservation of momentum and mass at the most downstream measurement location. The measured versus momentum water depth $\left(h_f, h_{f\,mom}\right)$ shows a difference of up to 2.5% (up to 4 mm) for the selected experiments. This is quite reasonable because, the uncertainty of the depth measurements for the different experiments ranged up to 18% (table 4). The measured versus momentum flow velocities $\left(\bar{\bar{u}}_f, \bar{\bar{u}}_{f\,mom}\right)$ deviate up to 11.2% (several cm/s). This is worse than the uncertainty contained within the flow velocity measurements (up to 2.3%, table 4). The most likely cause of the deviating flow velocity measurements is the fluctuations in discharge contained in the measured data. Equation 6.4 assumes conservation of momentum and mass, whereas chapter 5 showed that due to

measurement errors, the "measured" discharge[21] fluctuates. Considering the uncertainty in the measured data, the water heights and flow velocities (at the most downstream location) found by applying the conservation of momentum are reasonably close to the measured values.

### Comparing the measured and momentum head levels

The conservation of momentum is used to calculated the water depth and flow velocity at the most downstream measurement location. This data is then used to calculate the mean flow energy loss, which will be used as input into the ATM. The momentum and measured head levels are compared to each other in order to explain dissimilarities between the head levels found using the two methods.

The momentum head levels $(H_{f\,mom})$ are given in table 7. The momentum head levels are found by inserting the momentum water depth and flow velocity $h_{f\,mom}$ and $\bar{\bar{u}}_{f\,mom}$ in the adjusted formula of Bernoulli (6.3). The momentum head level $(H_{f\,mom})$ is calculated using the measured non-uniformity coefficient $\alpha_{Bern}$ at the most downstream measurement location (to take into account the non-uniformity of the flow velocity profile there). The total energy loss due to the presence of the step (according to the conservation of momentum) can be calculated by subtracting $H_{f\,mom}$ from $H_a$, this results in $\Delta H_{mom}$ as shown in table 7. Table 7 also depict $\Delta H$, which is the difference between the first and last measured head level (as shown in figure 36).

For the experiment of Xingkui & Fontijn (1993), the mean flow energy loss is almost equal when using the measured ($\Delta H$) or momentum ($\Delta H_{mom}$) head levels. For the experiments of Hofland (2005) and Nakagawa and Nezu (1987) ST-3, measured and momentum head level change ($\Delta H, \Delta H_{mom}$) deviate up to 43% of each other, and for the experiment of Nakagawa and Nezu (1987) ST-1, a deviation of 200% is even found. These deviations are not unexpected because as discussed earlier, the measurement data contains a certain level of uncertainty. Also, the conservation of momentum only takes into account the mean flow energy loss due to flow deceleration. Other sources like wall friction are not taken into account. This is most likely the reason why the mean flow looses less energy according to the momentum head levels than according to the measured head levels. The exception to this rule is the experiment of Nakagawa and Nezu (1987) ST-1. However, take in mind that the measured head levels for this experiments have a somewhat unrealistic shape. This might explain the deviating results for this experiment.

It is unclear whether the momentum or measured head levels better approximate the actual mean flow energy during the experiments. Therefore both methods are assumed to be equally valid measures of the mean flow energy loss (used as input into the ATM).

### Momentum head level shape

The momentum head levels are only know at two locations, on top of the step $(H_a)$ and at the most downstream measurement location $(H_{f\,mom})$. In order to use these head levels as input into the ATM, head levels $H$ at increments of $\Delta x$ need to be known. Therefore, it is assumed that between the step and the most downstream measurement location, the momentum head levels have a constant rate of energy loss. The resulting head levels are compared to the measured head levels in figure 39.

---

[21] Computed using the measured water depth and flow velocity
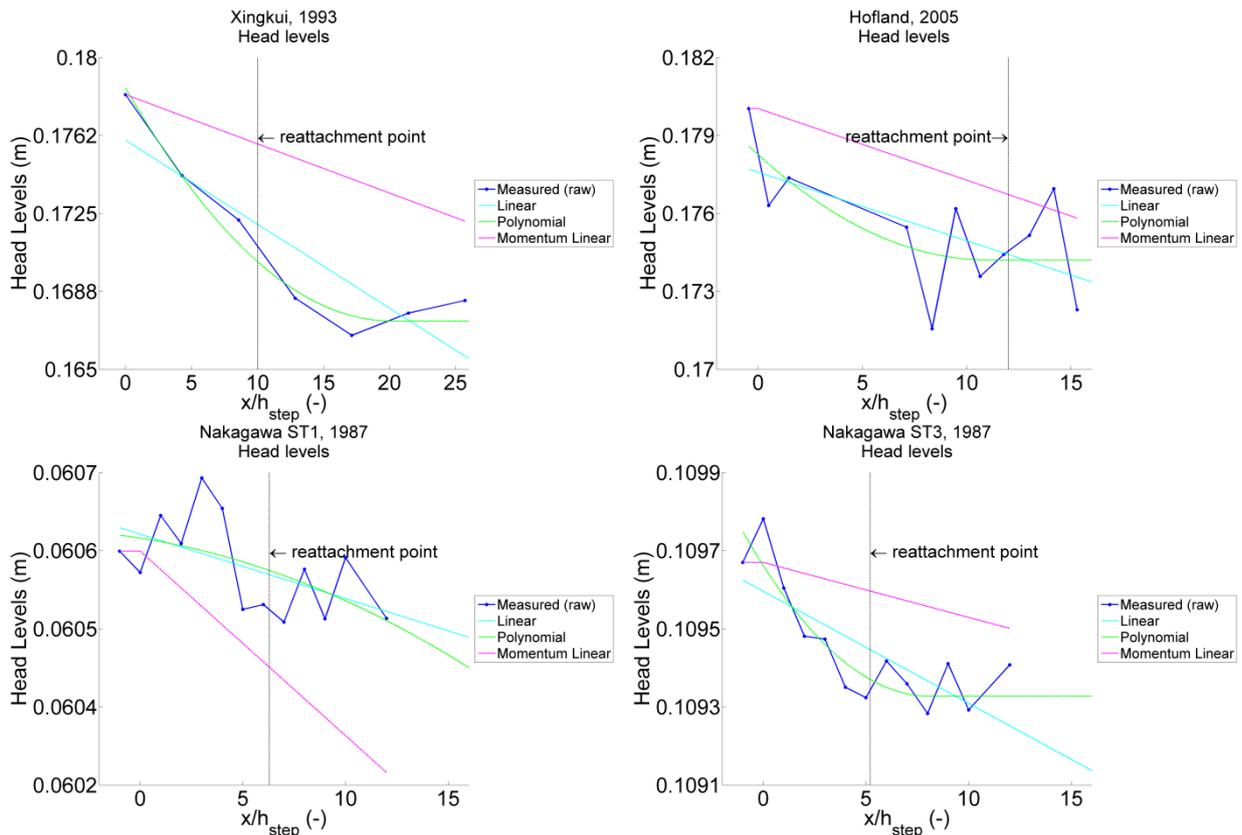
**Figure 39** Head levels of the selected experiments following from the measured variables and following from the conservation of momentum

In appendix Q it is shown that the momentum head level shapes are contained within the uncertainty margins of the measured head levels.

Note that an infinite amount of other shapes are possible that connect the upstream head level ($H_a$) with the downstream momentum head level ($H_{f\ mom}$). A possible alternative is for example a polynomial head level shape (discussed in the previous section), where the mean flow energy loss rate initially starts high, but reduces further downstream. However, this shape (or any other shape) is not considered for the momentum head levels because of two reasons: First, only the head level at the end of the step and at the most downstream measurement location are known. An infinite number of polynomials could be drawn through these points that would all have a 100% match with these momentum head levels. Thus no accurate shape of the (momentum) polynomial can be determined without using additional (measurement) data. Second, a great number of model alternatives are already considered. Also considering different momentum head level shape alternatives is not expected to help answer the research questions of this thesis.

### Accuracy of measured and momentum head levels

Four head level alternatives are now under consideration:

1. Raw measured head levels
2. Linear head levels
3. Polynomial head levels
4. Momentum head levels

The analyses above revealed a difference between the measured and momentum head levels. So what method is expected to approximate reality best? The measured head levels are based on

multiple measurements in between the top of the step and the most downstream located measurement location. All measured head levels show a global decreasing trend. This gives some confidence in the measured data because it shows a pattern that is expected to occur for decelerating flow. On the other hand, the conservation of momentum is based on some fundamental laws of physics and it at least guarantees the conservation of mass in between measurement locations. However, it is known that the momentum head levels do not take into account the mean flow energy loss due to bottom friction. The head levels following from the conservation of momentum will be used as an alternative to the measured head levels as input in the ATM because all four alternatives have their advantages and disadvantages. It is currently unknown whether the head levels following from the conservation of momentum or the measured head levels represent reality more accurately. The results from the empirical validation in the next chapter will shed some light on this question.

### Conclusion
This section introduced an alternative method to calculate the mean flow energy loss for flow over a BFS. It was shown that the non-uniformity of the flow velocity profile should be taken into account in order to accurately apply the conservation of momentum. The water depth and flow velocities found using the conservation of momentum were compared to their measured counterparts. This revealed that the momentum flow variables corresponded reasonably well with the measured water depths. The momentum head levels underestimated the mean flow energy loss when compared to the measured head levels for three out of the four experiments. This is most likely related to the fact that the momentum head levels only take into account the mean flow energy loss due to flow deceleration. It remains unknown whether the measured or momentum head levels more accurately represent reality. Therefore all four head level alternatives are considered in the validation of the ATM.

## 6.6 Determine the upstream incoming turbulent energy
### Introduction
In order to calculate the turbulent energy levels following equation 6.1, an initial boundary condition for the turbulent energy at the upstream edge of the study area ($\bar{k}_0$) needs to be known. Two alternatives are proposed:

1. Using the upstream measured turbulent energy
2. Assuming upstream incoming equilibrium turbulence levels

Both alternatives are discussed below.

*1. Extracting the upstream incoming turbulent energy from the measured turbulent energy levels*
In chapter 5 it was already discussed that this initial value $\bar{k}_0$ could simply be extracted from the measured turbulent energy used to validate the ATM. The experimentally measured turbulent energy level at the most upstream measurement location is then used as input into the ATM.

*2. Calculating the upstream incoming equilibrium turbulent energy*
The measured turbulent energy can be used to find a value for the input variable $\bar{k}_0$. However, during the design phase of a hydraulic structure, the incoming turbulent energy might not be available. Thus, this energy is also approximated in a different way.

When no other large flow disturbances (e.g. hydraulic structures) are located closely upstream of the BFS, then it can be assumed that the incoming flow is primarily defined by the flow conditions of the channel. Moreover, when the flow through the channel upstream of the BFS can be more or

less classified as uniform and stationary, then according to Hoffmans (1993), under stationary uniform equilibrium flow conditions, turbulent intensity is also in equilibrium. The formula of Hoffmans (1993) can then be applied to find the incoming equilibrium turbulent energy ($k_e$). The method used to determine the equilibrium turbulent energy $k_e$ for the selected experiments (as depicted in the table below) is discussed in appendix T.

Table 8 Comparison between measured incoming turbulent energy $\bar{k}_0$ and equilibrium turbulence $\bar{k}_e$ following from the formula of Hoffmans (1993)

| Author | | Xingkui, 1993 | Hofland, 2005 | Nakagawa ST1, 1987 | Nakagawa ST3, 1987 |
|---|---|---|---|---|---|
| Incoming turbulent energy | $\bar{k}_0$ measured (m$^2$/s$^2$) | 0.00190 | 0.00110 | 0.00021 | 0.00022 |
| | $\bar{k}_e$ from Hoffmans (1993) (m$^2$/s$^2$) | 0.00190 | 0.00120 | 0.00017 | 0.00021 |

Table 8 shows the measured incoming turbulent energy and the equilibrium turbulent energy for the flow conditions on top of the step. The found equilibrium turbulent energy levels correspond very well with the measured turbulent energy levels for all selected experiments. Thus the formula of Hoffmans (1993) (and the assumption of equilibrium turbulence) appears to be a good alternative to using the measured turbulent energy as input into the ATM. Note that these four experiments were al performed under laboratory conditions[22].

## 6.7 Concluding remarks

This chapter showed how the experimentally measured data is used to run the ATM. The forward Euler method is used to numerically solve the ATM. Three dissipation coefficient alternatives are proposed that will all be used in the next chapter to check the accuracy of the ATM in estimating the turbulent energy levels. It was shown that the non-uniform flow velocity profiles downstream of the step should be taken into account when calculating the mean flow energy levels. The head levels that followed from the water depth and flow velocity measurements showed a chaotic pattern. In order to get more realistic head levels, two smoothing methods were proposed. These smoothing methods ensured that the measured mean flow energy levels showed a pattern that better corresponded with the expected change mean flow energy downstream of a BFS. A second method for determining the mean flow energy loss downstream of a BFS was proposed using the conservation of momentum. All four measured and momentum head levels have their advantages and disadvantages. Because it is unknown which of these four head level input alternatives represent reality more accurately, all four head level methods will be used in the validation of the ATM.

Figure 40 connects all measured data and input alternatives in one schematisation (including the momentum head levels). In the next chapter these input alternatives will be used to run and validate the ATM.

---

[22] When applying the formula of Hoffmans (1993) to a real life scenario, uncertainties (for example in accurately determining the Chezy coefficient) might result in a less accurate approximation of the incoming turbulence.
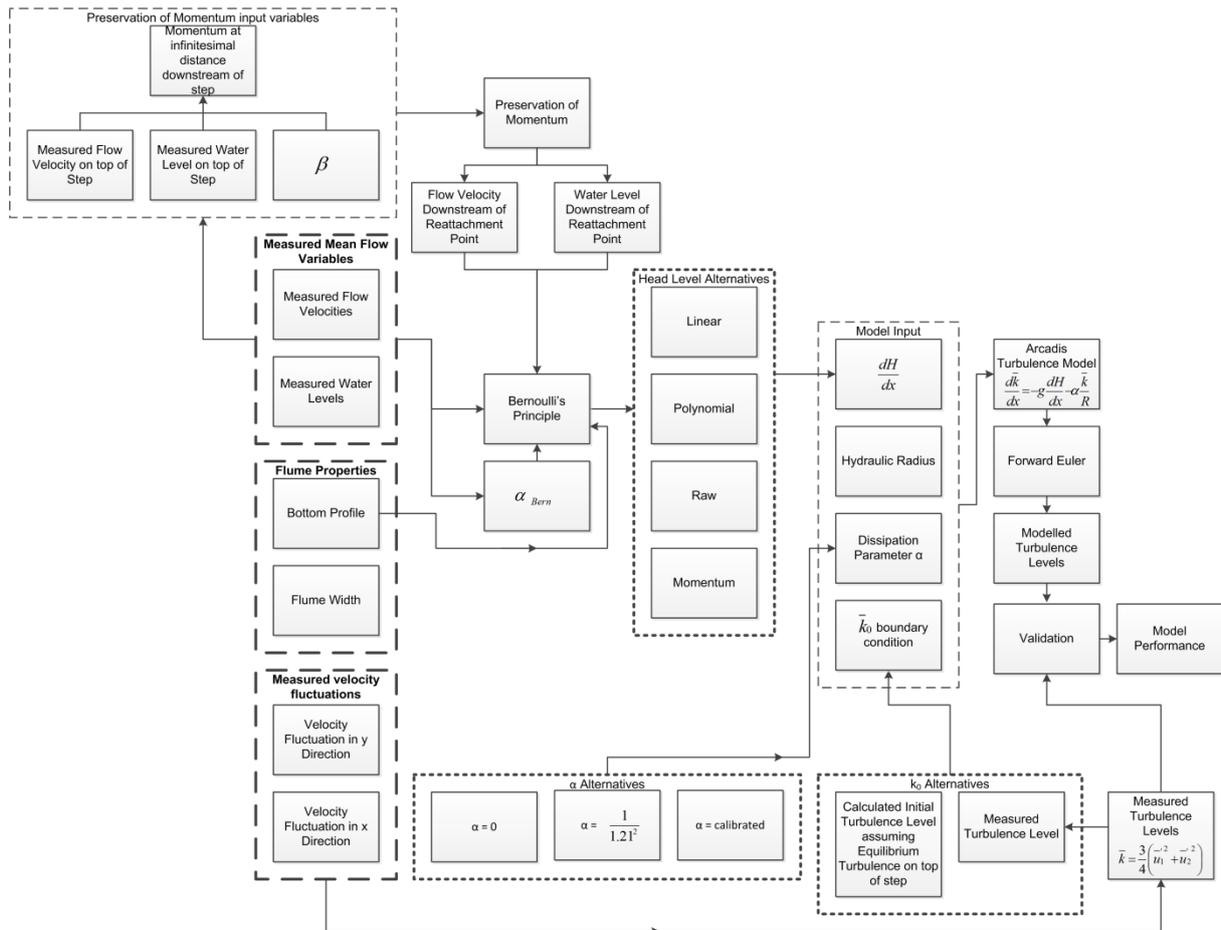
Figure 40 Schematization of input, output and validation of the ATM including the input alternatives when using as little measured data as possible[23]

---

[23] Note that when using the conservation of momentum to calculate the flow variables downstream of the reattachment point, the non-uniformity term $\alpha_{Bern}$ downstream of the reattachment point is still taken into account.

# 7 Arcadis Turbulence Model empirical validity and sensitivity analysis

## 7.1 introduction

In chapter 5 the data used to validate the ATM was introduced. Chapter 6 explained how this data will be used to run the ATM. In this chapter the results of the ATM empirical validation are presented and discussed. Because a large number of input alternatives are considered in the empirical validation of the ATM, the empirical validation is also a sensitivity analysis. Using the results of the empirical validation, the performance of the ATM is judged. Recommendations about improving the ATM are then given. However, first a selection is made of all input alternatives that will be analysed in the empirical validation because it is not sensible to present all possible input alternative combinations as will be explained below.

## 7.2 Arcadis turbulence model alternatives for the empirical validation

### Introduction

In the previous chapter, the input alternatives for the dissipation coefficient, head levels, and incoming turbulence were discussed. The following text will explain why it is useful to consider cases (instead of every input alternative combination) for the coming sensitivity analysis.

Investigating every input alternative combination results in 96 model outputs to consider. Presenting all 96 alternative combinations will not contribute to answering the research questions (as will be explained below). Therefore, three case scenarios are constructed, each with a certain goal in mind:

- A Base case consisting of the input variable combination that is expected to perform best a priori
- A No Dissipation case that assumes turbulence is not dissipated within the study area
- A Calibrated Dissipation case for which the dissipation coefficient $\alpha$ is calibrated using the measured turbulent energy levels

First the schematisation of the cases are discussed using the Base case as an example, the other cases are discussed thereafter. This section is concluded with some remarks about using these cases to validate the ATM.

### Base case

The Base case is schematised in the figure below.
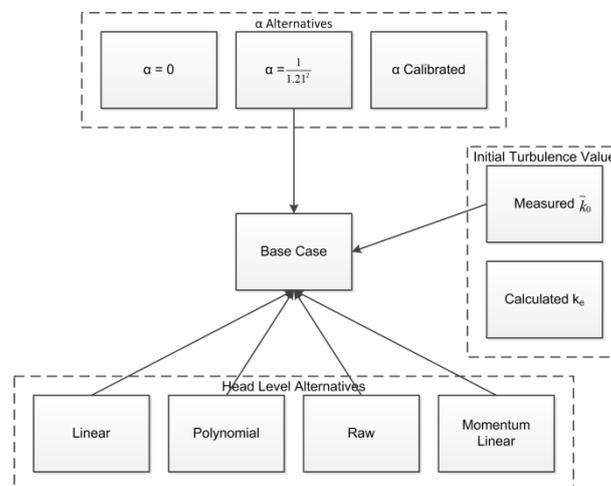


Figure 41 Base case alternative schematisation

Figure 41 shows the three categories of input variable alternatives. The arrows pointing towards the central square indicate that a specific input alternative is considered for that case. Every case scenario will be applied to every selected experiment, thus each case will result in at least 4 different graphs (one for each experiment).

The Base case is the input combination that is expected to perform best of all cases based on the information available before the sensitivity analysis is actually performed (a priori). The input alternatives considered for the Base case are expected to perform best because of the following reasons:

The Base case scenario assumes that the dissipation of turbulence under non-equilibrium conditions can best be approximated by the dissipation under equilibrium conditions as defined by Hoffmans (1993). Because little to no information is available about the dissipation coefficient $\alpha$, $\alpha = \frac{1}{1.21^2}$ (based on the equilibrium turbulence dissipation of Hoffmans, 1993) is initially deemed as the best approximation of this coefficient. It is known that turbulence dissipates (chapter 4). Thus, the $\alpha = 0$ alternative is expected to perform worse than a dissipation coefficient alternative that does take into account turbulence dissipation. The calibrated $\alpha$ alternative will definitely outperform the other two dissipation coefficient alternatives, so initially it would be expected that the calibrated $\alpha$ alternative is the preferred dissipation alternative for the Base case. However, the dissipation coefficient $\alpha$ cannot be calibrated without first running the ATM, which is in violation with the design philosophy of the Base case: picking the input alternatives that are expected to perform best, before actually running the sensitivity analysis. Therefore, for the Base case, the dissipation coefficient based on the work of Hoffmans (1993) is only considered.

For the Base case, the initial incoming turbulent energy (upstream of the step) is set at the first measured turbulent energy ($\bar{k}_0$). By doing so, the first calculated turbulent energy output from the ATM will show a 100% match with the measured turbulent energy. The alternative, using the calculated equilibrium turbulent energy following from the formula of Hoffmans (1993) can deviate (slightly) from the measured turbulent energy (table 8). Thus the measured turbulent energy $\bar{k}_0$ is expected to perform best and is therefore chosen for the Base case.

All four head level alternatives are considered for the Base case. As was mentioned previously, it is unknown whether the head levels during the experiments are best represented by the measured or the momentum head levels. All four head level alternatives could in theory be the best performing. Therefore, all four head level alternatives are considered in the Base case.

The Base case (as described above) will result in 4 graphs (one for each head level alternative) for each of the selected experiments . This results in a total of 16 graphs. In order to balance the number of figures, and the readability of these figures, it is chosen to present four figures (one for each of the selected experiments) containing four graphs (one for each head level alternative) for the Base case.

## No Dissipation case
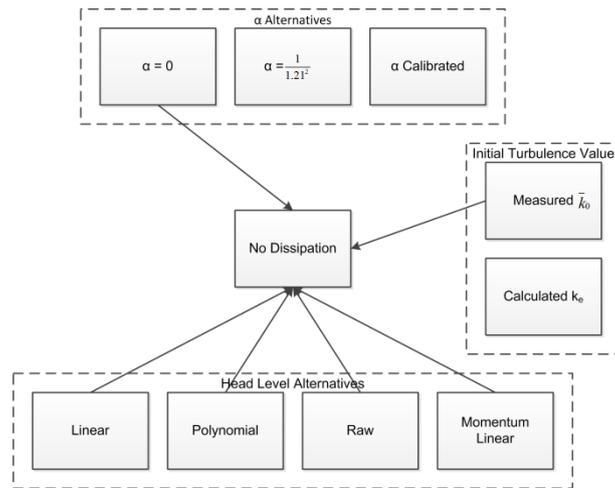


Figure 42 No Dissipation case alternative schematisation

Figure 42 shows the No Dissipation case. For this case, instead of the dissipation coefficient based on the work of Hoffmans (1993), turbulence dissipation is left out altogether ($\alpha = 0$). Physically, turbulence is expected to dissipate due to internal viscous stresses. This case however neglects this dissipation to find the most extreme turbulent energy levels. The No Dissipation case will give the upper limit of the turbulent energy that can be expected in the flow (according to the ATM). This upper limit might be useful as an alternative to the flat rules of thumb as discussed in chapter 1.

## Calibrated Dissipation case
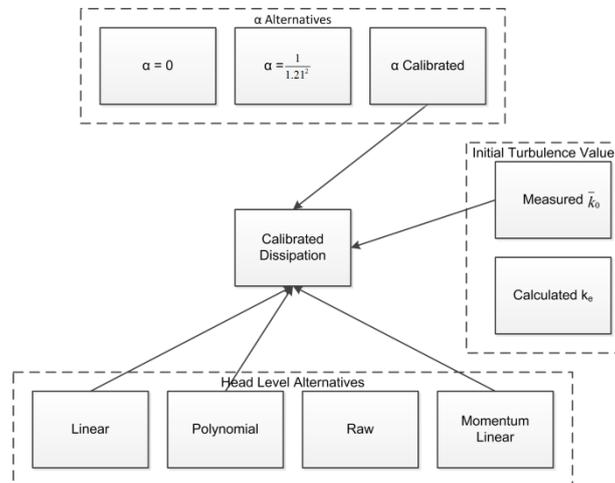


Figure 43 Calibrated Dissipation case alternative schematisation

The third case calibrates the dissipation coefficient using the measured turbulent energy. After calibration, the different ATM's will fit the measured turbulent energy better. The goal of calibrating the dissipation coefficient $\alpha$ is to find a relation between the experimental conditions and the calibrated dissipation coefficient $\alpha$. Based on the results of this case, recommendations will be given about setting the dissipation coefficient. The exact calibrated procedure used to calibrate the dissipation coefficient $\alpha$ will be discussed in section 7.5.

Unlike the Base case, for the Calibrated Dissipation case the raw measured head levels are omitted. It was chosen not the calibrate the raw measured head levels because no useful

information would result from this exercise. The raw measured head levels contain locations were the mean flow energy is increasing. The ATM models turbulence production as a function of the loss of mean flow energy. When the mean flow energy (wrongly) shows an increasing pattern, the ATM translates this into a (wrong) destruction of turbulent energy. Thus beside the turbulence dissipation due to relaxation, turbulence is also destroyed due to wrong head level input data. Therefore, when calibrating the ATM based on this data, lower values of $\alpha$ will be found (compared to using other head level input data). The resulting $\alpha$ coefficients will not result in new insights because they are greatly affected by the wrong head level input data.

### Remarks related to the case studies

Note that none of the cases described above uses the calculated equilibrium turbulent energy $\bar{k}_e$ as the initial incoming turbulent energy. In fact, all above cases were also calculated using the equilibrium turbulent energy $\bar{k}_e$ as the initial incoming turbulent energy. However, the resulting ATM output did not visually deviate from the ATM output when using the first measured turbulent energy level $\bar{k}_0$ as the incoming turbulent energy. This result is expected because, as table 8 shows, only very small differences exist between the first measured turbulent energy $\bar{k}_0$ and the equilibrium turbulent energy $\bar{k}_e$. The equilibrium turbulent energy $\bar{k}_e$ alternative will therefore not be presented or discussed in this thesis. One can assume that $\bar{k}_0$ and $\bar{k}_e$ can be used interchangeably.

## 7.3 Sensitivity and validity of the Arcadis Turbulence model: Base case

### Introduction

This section will present and discuss the result of the ATM Base case. The setup of this section is as follows: First the graphs depicting the ATM results for the case under consideration are presented. Then the ATM results are discussed, with a focus on the shape and size of the calculated turbulent energy levels[24] compared to the measured turbulent energy levels. Lastly, conclusions are drawn about the performance of the ATM based on the presented graphs[25].

---

[24] When the texts refers to the calculated turbulent energy, it refers the ATM output using the specific head level input alternative under review.

[25] For your convenience, figure 39 and the coming ATM results are also depicted in appendix U. It is suggested to tear appendix U out of this report in order to review the coming graphs side by side with the head level alternatives.

## Base case
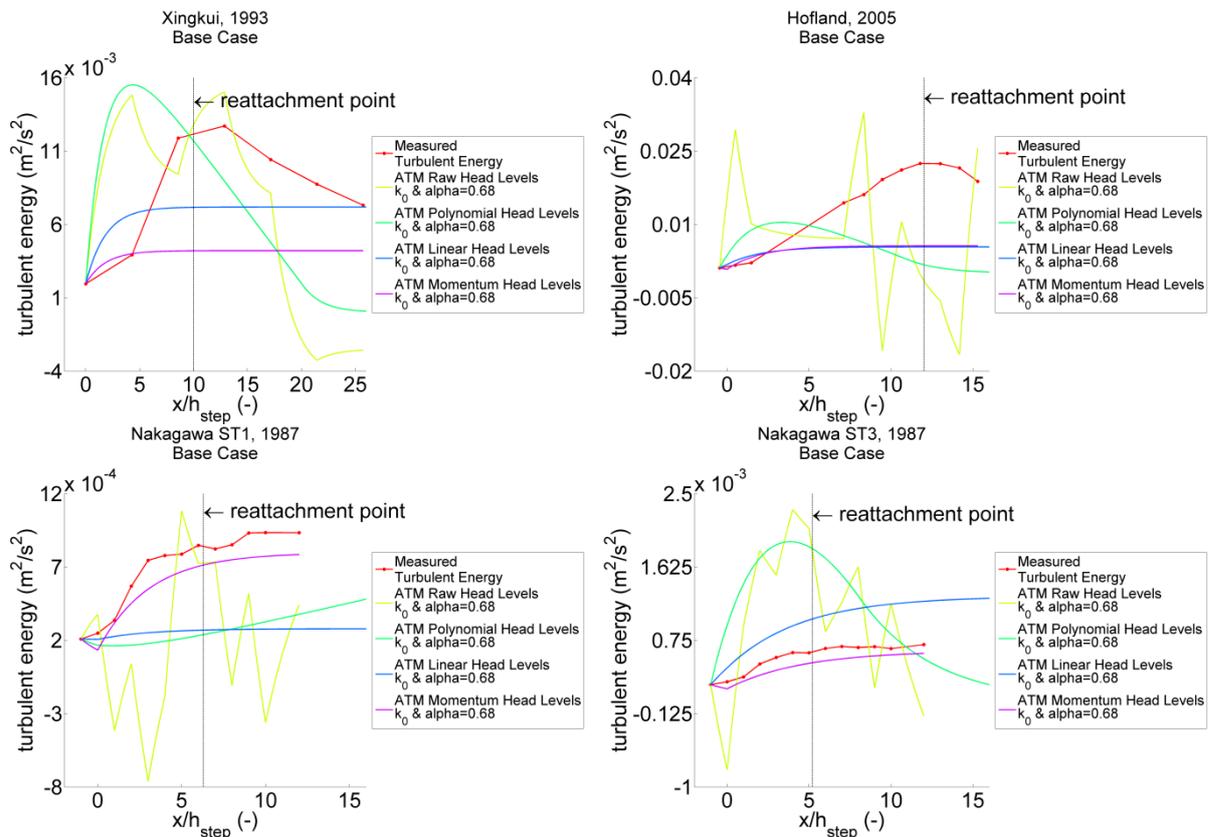


Figure 44 Comparison between measured turbulent energy and ATM output for the Base case

Figure 44 shows the results of running the ATM using the Base case input. The measured turbulent energy is also presented in figure 44 in order to compare the ATM output with the experimentally measured turbulence. In the coming text, the ATM results for each head level alternative is discussed separately.

### Base case: ATM using raw head level input

When looking at the ATM results using the raw head levels, a number of things can be noticed. The chaotic pattern that is observed in the raw head levels (Figure 36) is translated in a chaotic pattern in the calculated turbulent energy. The chaotic pattern of calculated turbulent energy conflicts with the laws of physics. All selected experiments show calculated turbulent energy levels that contain one or more negative values. This is the result of the ATM modelling (additional) turbulence dissipation when the mean flow shows a pattern of increasing energy levels. Because turbulence is calculated by taking the square of the flow velocity fluctuations (chapter 3), negative turbulent energy levels are not possible.

*Magnitude*

The ATM, using raw head levels, does not show a clear pattern of over or underestimation for the selected experiments. The ATM results for the experiments of Hofland (2005) and Nakagawa and Nezu (1987) ST-1 show an underestimation of the turbulent energy, whereas to other experiments show on average an overestimation. This could be the result of the ATM assumptions not approximating reality sufficiently in different ways for the different experiments. The other head level alternatives will shed some more light on this. Note that the order of magnitude of the turbulence estimation using this head level alternative (and all other head level alternatives) is on par with the measured turbulence.

*Shape*
Beside the absolute values of the calculated turbulent energy levels, the shape of the calculated turbulent energy levels is also compared to the shape of the measured turbulent energy levels. When using the raw head levels as input, the shapes of the calculated turbulent energy levels are chaotic. It cannot be said that the calculated turbulent energy approximate the shape of the measured turbulent energy levels.

## Base case: ATM using polynomial head level input
The ATM Base case results when using polynomial head levels show different patterns. The calculated turbulent energy levels are now much smoother due to the smooth polynomial head level input. Because of the much smoother head level input, the calculated turbulent energy does not show any negative values anymore.

*Shape*
Different shapes of calculated turbulent energy levels are found for the different experiments. The calculated turbulent energy levels for the experiments of Xingkui & Fontijn (1993), Hofland (2005) and Nakagawa and Nezu (1987) ST-3 show a pattern of increasing turbulent energy up until a location upstream of the reattachment point, and a decrease in turbulent energy downstream of that. For the experiment of Nakagawa and Nezu (1987) ST-3, the peak is located very close to the reattachment point. On the other hand, the calculated turbulent energy levels for the experiment of Nakagawa and Nezu (1987) ST-1 shows increasing turbulent energy levels without any valleys or peaks.

All above described calculated turbulent energy level shapes can be explained by looking at the shape of the polynomial head levels. First consider the way the ATM calculates the turbulent energy levels. The production of turbulent energy is a function of the change in mean flow energy $\frac{dH}{dx}$. The dissipation of turbulence is a function of the turbulence itself. A flow that is losing energy at a constant rate will also increase its turbulent energy. Because the dissipation is a function of the turbulence itself, an increase in turbulent energy also results in an increase in the dissipation rate. This continues until $-g\frac{dH}{dx} = \alpha\frac{k}{R}$. At this point, assuming the mean flow continues to lose energy at a constant rate, the turbulent energy has reached an equilibrium. The size of this equilibrium is determined by the rate of energy loss of the mean flow $\left(\frac{dH}{dx}\right)$ and the dissipation coefficient $\alpha$. Now consider the results of an ATM run using polynomial head level input (figure 45).
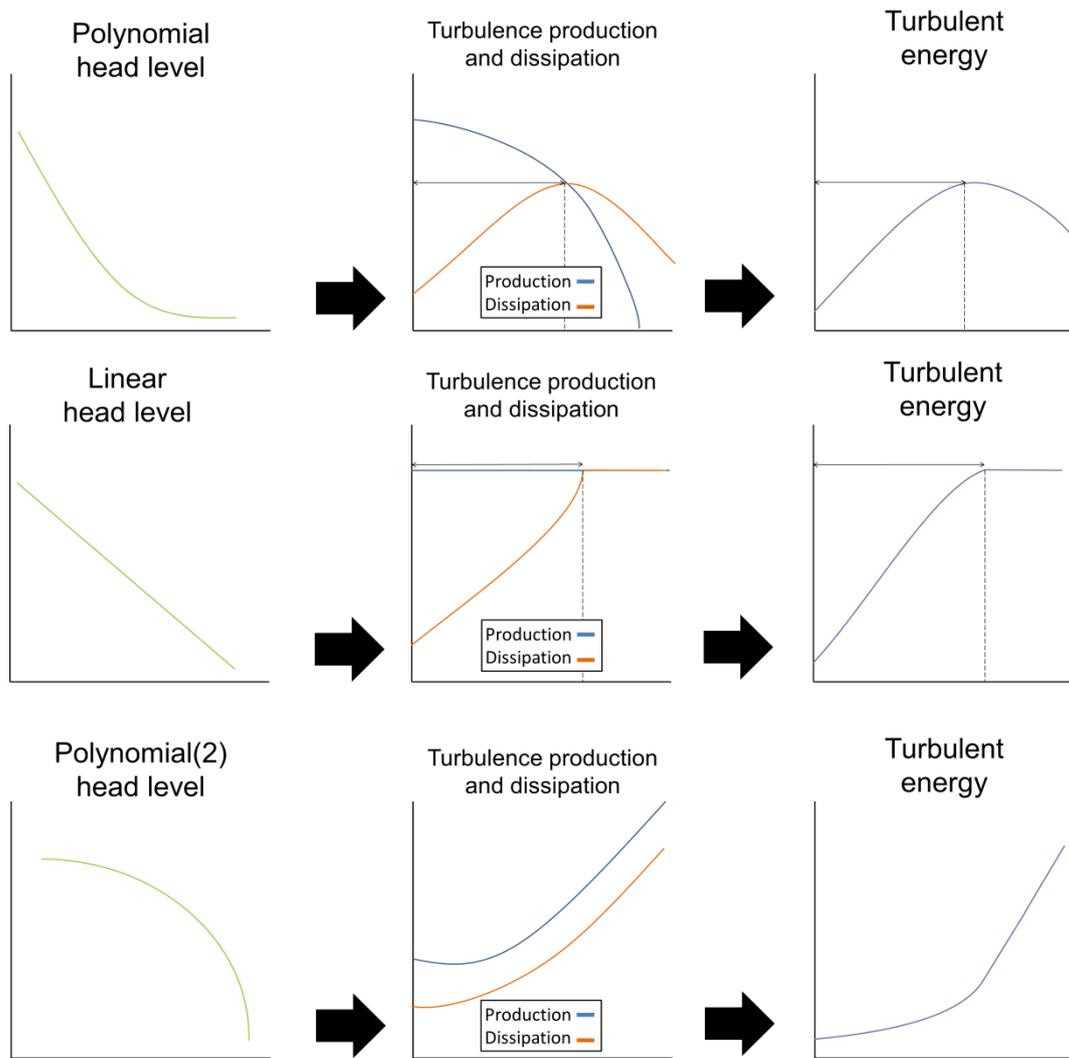
**Figure 45 Relation between head level shape, turbulence production and dissipation and the absolute turbulent energy levels as calculated by the ATM**

Figure 45 shows the relation between the head level shape, the turbulence production and dissipation, and the resulting turbulent energy estimation as computed by the ATM. All measured polynomial head levels, with the exception of the Nakagawa and Nezu (1987) ST-1 experiment show a decreasing rate of mean flow energy loss in the flow direction. At a certain location (at the maximum calculated turbulent energy level), the production of turbulence equals the dissipation. Downstream of this location, the rate of mean flow energy loss becomes smaller and smaller, thus less and less turbulence is produced. However, the absolute turbulent levels are still high, thus the turbulent energy dissipation is still large. This results in decreasing turbulent energy levels downstream of location of the maximum calculated turbulent energy level. For the experiments of Hofland (2005) and Xingkui & Fontijn (1993), the rate of mean flow energy loss (and thus the rate of turbulence production) equals the rate of turbulence dissipation upstream of the reattachment point. For the experiment of Nakagawa and Nezu (1987) ST-3 the rate of mean flow energy loss equals the rate of turbulence dissipation roughly at the reattachment point. For the experiment of Nakagawa and Nezu (1987) ST-1, the mean flow first only loses a little energy, but the energy loss becomes bigger and bigger, further downstream of the step. The dissipation of turbulence is therefore always smaller than the production of turbulence, thus no peaks or valleys in the calculated turbulent energy level are found for this head level input.

*Magnitude*

When using polynomial head levels, the ATM on average underestimates the turbulent energy levels for the experiments of Hofland (2005) and Nakagawa and Nezu (1987) ST-1 and overestimates on average the turbulent energy levels for the other experiments (similar to the results using the raw head levels). This indicates a miss match between the production and dissipation of the calculated turbulent energy levels. Some hypothesis about this miss match are discussed at the end of this section.

## Base case: ATM using linear head level input

The ATM Base case when using linear head levels as input, results in smooth calculated turbulent energy levels as output. The calculated turbulent energy levels show a pattern of increase turbulent energy levels without valleys or peaks for all selected experiments.

*Magnitude*

The ATM using linear head levels underestimates the turbulent energy levels for all experiments except Nakagawa and Nezu (1987) ST-3. This is a change in trend because now the results for the experiment of Xingkui & Fontijn (1993) also underestimates the turbulent energy, whereas for the previous discussed head level alternatives, it consistently overestimated turbulence. This could be related to the fact that the linear head level smoothing technique is less accurate in approximating the actual measured head levels then the polynomial smoothing technique (appendix S). Note that the calculated turbulent energy levels only show increasing turbulence, not decreasing turbulence. The reason for this is discussed in the following text.

*Shape*

All calculated turbulent energy levels follow only one pattern, increasing turbulent energy levels downstream of the step. No decrease in turbulence are found in the ATM results using this head level alternative. The reason for this is easily explained by looking at figure 45. When a constant rate of mean flow energy loss is put into the ATM, the turbulent energy levels move to an equilibrium value, and then remain constant at this value. When this equilibrium value is greater than the starting turbulent energy level, the turbulence is increased until the equilibrium is reached. Vice versa, when the equilibrium value is lower than the starting turbulent energy level, turbulence levels are decreased until the equilibrium is reached. An initial increase in turbulence up to a maximum value and decreasing levels downstream of the maximum, as can be seen in the measured turbulent energy levels of the experiment of Xingkui & Fontijn (1993) and Hofland (2005) cannot be modelled using the ATM in combination with a constant rate of energy loss and a constant dissipation coefficient. This can indicate that the assumption of a constant mean flow energy loss rate is incorrect or that the constant dissipation coefficient $\alpha$ is incorrect. At the end of this section, this observation is discussed further.

## Base case: ATM output using momentum head level input

The last head level alternative that is analysed for the Base case is the momentum head level alternative. As discussed previously, this head level alternative is based on the assumption of conservation of momentum and conservation of mass. Because the momentum head levels also assume a constant mean flow energy loss, the limitations of the linear head level alternative, as discussed above, also apply to this alternative.

*Shape*

The calculated turbulent energy levels using the momentum head levels as input show a shape similar to the calculated levels using linear head level: increasing turbulent energy levels for the whole flume downstream of the step. However, contrary to the linear head levels, the ATM using

momentum head levels does a decent job estimating the turbulent energy levels for the experiments of Nakagawa and Nezu (1987). This could indicate that the conservation of momentum actually better represent the mean flow energy loss downstream of a BFS than the experimentally measured mean flow energy loss for those studies.

*Magnitude*

As mentioned above, the ATM using momentum head levels does a decent job estimating the turbulent energy levels for the experiments of Nakagawa and Nezu (1987). However, it still underestimates the turbulent energy levels. In fact, the ATM results for all selected experiments underestimated the turbulent energy levels when using the conservation of momentum. Two causes for this can be hypothesised. First, it is possible that the momentum head levels do not accurately enough represent the actual occurring mean flow energy loss. On the other hand, it is also possible that the dissipation coefficient based on the dissipation of Hoffmans (1993) is incorrect. The Calibrated Dissipation case will shed some more light on this.

## Conclusions

The ATM output using raw head levels as input resulted in chaotic calculated turbulent energy levels both when dissipation was considered and neglected. Moreover the calculated turbulent energy levels, using the raw head levels, contained negative values for the turbulent energy which is physically impossible. It is believed that due to measurement error, the head levels show this chaotic behaviour. The ATM is based (among other things) on the principle that free flowing water can only loose energy. The raw head levels are therefore less (not) usable as input into the ATM.

The smoothed head level input (linear or polynomial) resulted in calculated turbulent energy levels that are at least physically possible. However, the shape of the head level input defines the ATM output possibilities. When constant mean flow energy loss is assumed (linear and momentum head levels), than the ATM in its present form is unable to model both an increase and decrease in computed turbulent energy. Using polynomial head levels, it is possible to both model increasing and decreasing turbulence levels. However, there still exists a notable discrepancy between model and measurement (even when taking into account the measured turbulent energy uncertainty[26]). The calibration of the dissipation coefficient $\alpha$ will show whether a change in the dissipation coefficient can compensate this discrepancy.

The ATM output using momentum head levels and the dissipation coefficient of Hoffmans (1993) corresponded reasonably well with the measured turbulent energy levels up until the reattachment point for the experiments of Nakagawa and Nezu (1987). Calibrating the dissipation coefficient will show whether a reasonably fit can also be found for the other experiments using the linear or momentum head levels.

Three head level alternatives show potential as input for the ATM to accurately estimate the turbulent energy levels. The ATM results using the momentum head levels already somewhat accurately estimate the turbulent energy levels up to the reattachment point for two of the selected experiments. After calibration the ATM might also accurately estimate turbulent energy levels up until the reattachment point using linear head level input. Therefore, this input alternative is also considered. However, because of the assumed constant rate of mean flow energy loss for these head levels, these head level alternatives will not result in ATM output with both increasing and decreasing turbulent energy levels (figure 45). On the other hand, The ATM

---

[26] The uncertainty in the measured turbulent energy levels were taken into account for the analysis of the ATM results. However, in order to preserve readability of the figures, the uncertainty margins of the measured turbulent energy are not depicted in the case graphs.

output using the polynomial head level alternatives showed the ability to roughly reproduce the shape of the measured turbulent energy levels. Using polynomial head levels, a notable discrepancy between ATM estimated and measured turbulent energy exists. The calibration of the ATM using all three head level alternatives will show whether a change in dissipation coefficient can fix the above mentioned limitations. However, first the results of the No Dissipation case are presented to show that taking dissipation into account improves the ATM accuracy.

## 7.4 Sensitivity and validity of the Arcadis Turbulence model: No Dissipation case

### No Dissipation case results

For the No Dissipation case, turbulence dissipation is neglected altogether. In the following section the accuracy of the ATM when dissipation is neglected is investigated.
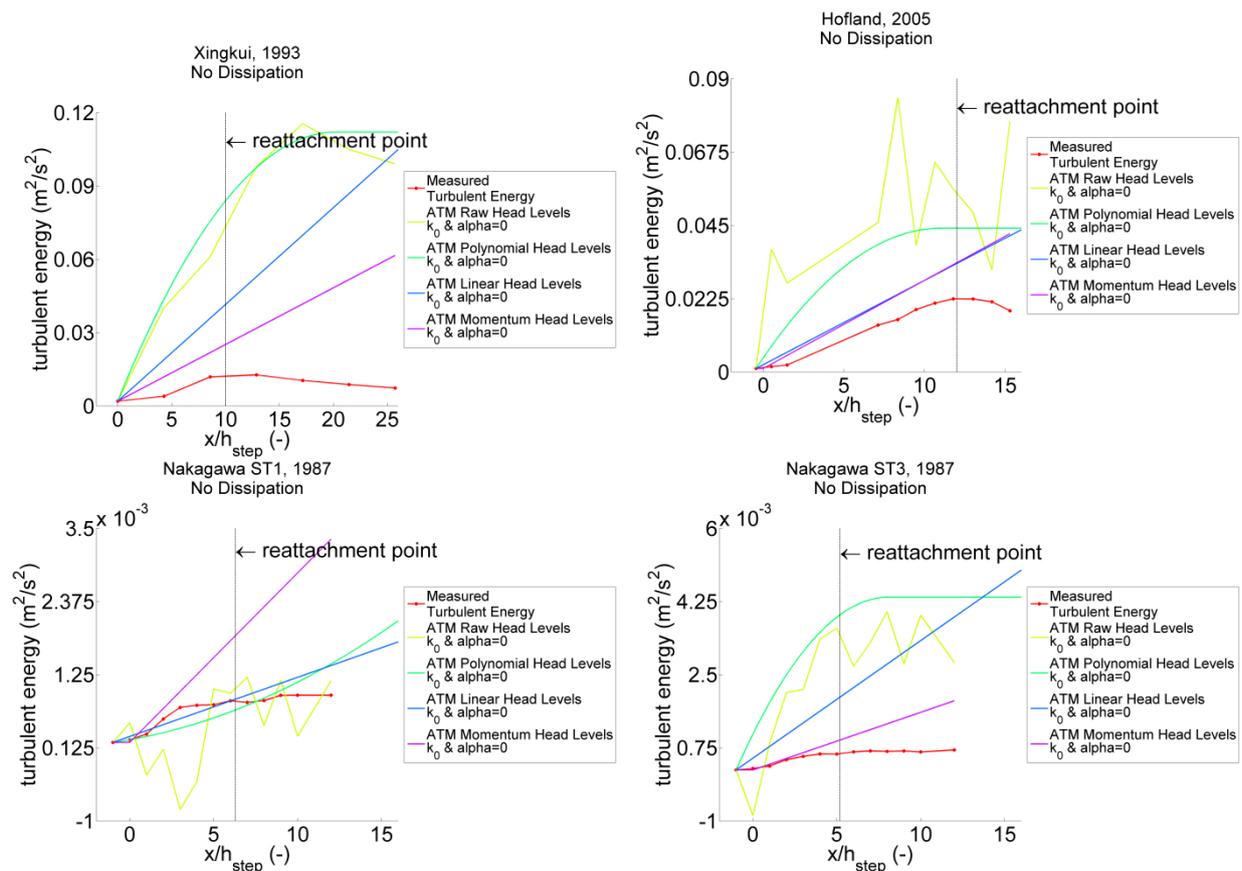


Figure 46 Comparison between measured turbulent energy and ATM output for the No Dissipation case

Because most head level alternatives for the No Dissipation case show similar patterns, it is chosen not to discuss each head level alternative separately. Instead the general trends and noteworthy results are discussed below.

*Raw head levels*

When the dissipation of turbulence is neglected, ATM outputs, with the exception of the ATM using raw head level input, show a pattern of increasing or constant turbulent energy levels. The ATM using raw head levels as input still show decreasing turbulent energy levels as the result of the increase in mean flow energy levels, which ATM incorrectly translates into a decrease of the turbulent energy.

*Xingkui & Fontijn (1993), Hofland (2005), and Nakagawa and Nezu (1987) ST-3*

The ATM results of the experiments of Xingkui & Fontijn (1993), Hofland (2005), and Nakagawa

and Nezu (1987) ST-3 all overestimate the turbulent energy levels. The calculated turbulent energy levels using the linear and momentum head levels show a constant increase in turbulent energy, which is inversely proportional to the constant rate of mean flow energy loss. The polynomial calculated turbulent energy levels show a pattern of increasing turbulent energy levels that flattens out further downstream, which also corresponds to an inversely proportionality with the polynomial head levels. Overestimation of the calculated turbulent energy is expected because by neglecting the turbulence dissipation, turbulence can only increase in energy, thus overestimation is bound to happen.

*Nakagawa and Nezu (1987) ST-1*
The ATM results of the experiments of Nakagawa and Nezu (1987) ST-1 under and overestimate the turbulent energy levels depending on the head level alternative used as input. Even when neglecting the dissipation of turbulence, the ATM output using linear or polynomial head levels underestimates the turbulent energy levels up until the reattachment point, which is in contrast to the large overestimation for all other selected experiments. This underestimation is most likely the result of the somewhat strange raw head levels that were found for the experiment of Nakagawa and Nezu (1987) ST-1. The ATM results using the momentum head levels overestimate the turbulent energy levels for all selected studies. This can be beneficial because using this approach will at least guarantee (for the selected experiments) that the turbulent energy is not underestimated.

## Conclusions

All selected experiments with the exception of Nakagawa and Nezu (1987) ST-1 showed overestimation of the turbulent energy levels when dissipation is neglected, this can indicate that either dissipation cannot be neglected, or that production of turbulence is overestimated. Moreover, when neglecting turbulence dissipation, the calculated turbulent energy levels can only increase in downstream direction, not decrease. The measured turbulent energy levels show both increasing and decreasing turbulent energy levels. Therefore it is concluded that, to accurately model turbulent energy levels over the whole study area, turbulence dissipation should be taken into account.

## 7.5 Sensitivity and validity of the Arcadis Turbulence model: Calibrated Dissipation

### Introduction

The goal of calibrating the dissipation coefficient $\alpha$ is to review the relation between the experimental conditions and the calibrated dissipation coefficient $\alpha$ for the different head level alternatives. Based on the results of this case, recommendations will be given about setting the dissipation coefficient, and how the ATM can be improved. First, the calibration procedure is explained. Then the results of the calibrated ATM are discussed per head level input alternative. Using the linear and momentum head level alternatives cannot result in both increasing and decreasing turbulent energy levels. Therefore, the ATM using these head level inputs is also calibrated using only the measured turbulent energy levels up until the found maximum. This will illustrate the ability of the ATM to estimate only the increasing part of the turbulent energy levels in BFS flow.

### Calibrating the ATM

The ATM is calibrated for each head level alternative by running the model a number of times. For each model run, a different value for the dissipation coefficient $\alpha$ is chosen. Each model run is than compared to the measured turbulent energy levels to say something about the goodness of

fit between the calculated and measured turbulent energy. The goodness of fit is calculated using the coefficient of determination. The coefficient of determination is interpreted as the proportion of the variance in the measured turbulent energy levels that is predictable from the ATM output (StatTrek, 2015; appendix R). The ATM run that showed the best goodness of fit (coefficient of determination closest to 1) is selected as the calibrated model.

The ATM is run for a range of $\alpha$ values. The range of $\alpha$ values is defined by three constants, the smallest $\alpha$ to consider, the largest $\alpha$ to consider, and the number of intermediate values between the smallest and largest $\alpha$ value. The smallest value that is considered for the calibration is simply set at zero. That way, the No Dissipation case is in consideration when the best fitting model is searched for. Negative values for $\alpha$ are illogical. This would mean that turbulence is not dissipated, but produced even when the mean flow does not lose energy. The largest considered $\alpha$ value is set by running the calibration and looking at the found $\alpha$ coefficients. When the best goodness of fit is found for an $\alpha$ equal to the set maximum value for $\alpha$, then the maximum value for $\alpha$ is increased. This process is repeated until the $\alpha$ coefficient corresponding to the calibrated ATM is no longer equal to the maximum set value for $\alpha$. As much intermediate values as possible need to be considered in order to find the best calibrated model. However, there is a limit to the number of intermediate values that can be considered due to the required computation time. The following range of dissipation coefficients resulted in a good balance between accuracy and computation time: $\alpha = [0, 0.01, 0.02 \cdots 5.98, 5.99, 6]$.

For the head level input alternatives that are unable to model both increasing and decreasing levels of turbulence (linear and momentum head level input alternatives), an additional calibration procedure is used. The ATM for these head levels is also calibrating using only the part of the measured turbulent energy levels that show increasing turbulence. This will result in a calibrated model that is better able to estimate the turbulence energy levels up to a maximum (but unable to accurate estimate the decrease in turbulent energy downstream of this maximum).

## Calibrated Dissipation case results
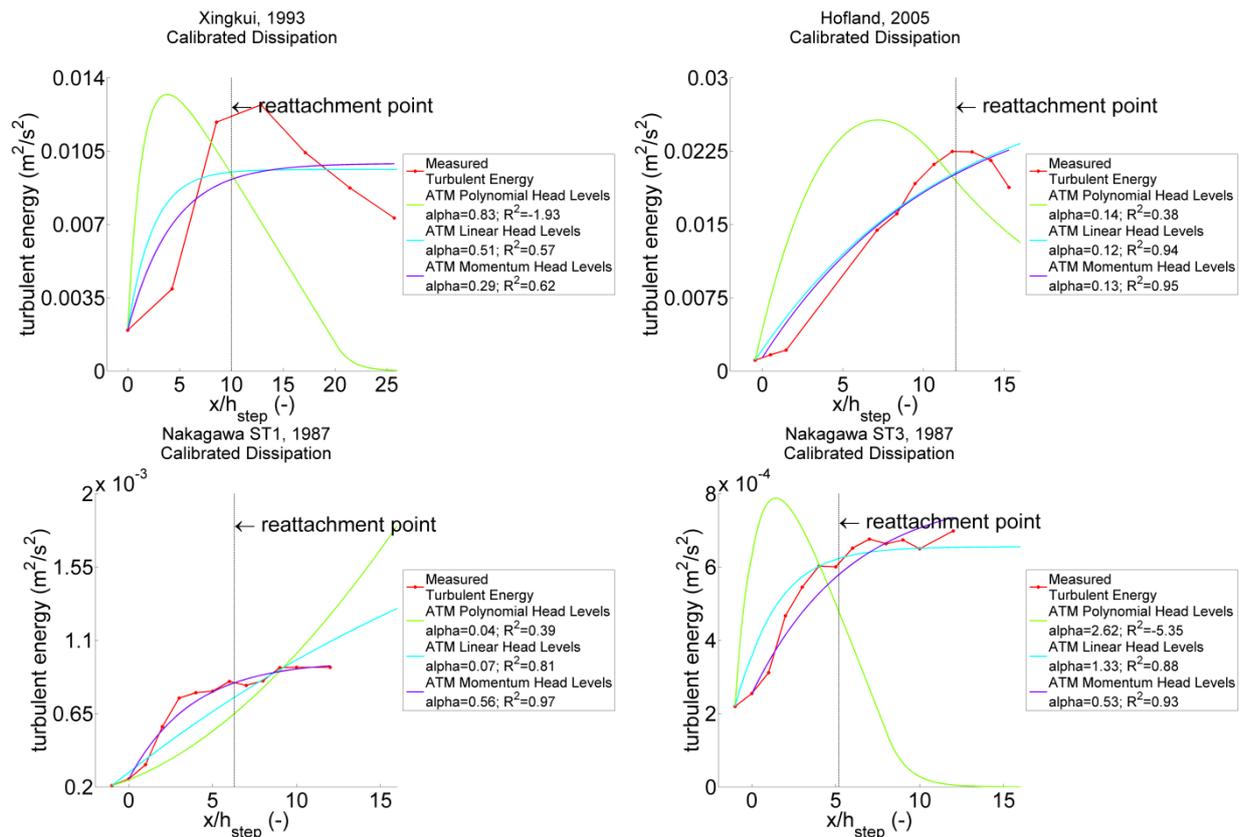


Figure 47 Comparison between measured turbulent energy and ATM output for the Calibrated Dissipation case

Table 9 All dissipation coefficients $\alpha$ after calibration and their corresponding coefficients of determination

| Author | | Xingkui, 1993 | Hofland, 2005 | Nakagawa ST1, 1987 | Nakagawa ST3, 1987 |
|---|---|---|---|---|---|
| Calibrated using all measured turbulent energy values | $\alpha$ polynomial head level input | 0.83 | 0.14 | 0.04 | 2.62 |
| | $R^2$ polynomial head level input | -1.93 | 0.38 | 0.39 | -5.35 |
| | $\alpha$ linear head level input | 0.51 | 0.12 | 0.07 | 1.33 |
| | $R^2$ linear head level input | 0.57 | 0.94 | 0.81 | 0.88 |
| | $\alpha$ momentum head level input | 0.29 | 0.13 | 0.56 | 0.53 |
| | $R^2$ momentum head level input | 0.62 | 0.95 | 0.97 | 0.93 |

## Calibrated Dissipation case: ATM output using polynomial head level input

Calibrating the ATM using the polynomial head levels as input resulted in the worst ATM performance (compared to the other head level input alternatives). All calculated turbulent energy levels (except the Nakagawa and Nezu (1987) ST-1 experiment) show a rapid increase in turbulent energy, that peaks before the reattachment point, and an even faster dissipation of turbulence downstream of this peak. Although the shape of the turbulent energy using the polynomial head level input somewhat resembles the shape of the measured turbulent energy levels, for the experiments of Xingkui & Fontijn (1993) and Hofland (2005), the peak is modelled more upstream than the measured turbulence peak. The ATM results for the experiment of Nakagawa and Nezu (1987) ST-3 also shows a calculated turbulent energy with a peak and rapid dissipation downstream of the peak, whereas the measured turbulent energy for this experiment does not have a peak. This results in very bad model accuracy. The shape of the ATM output using polynomial head level input can be explained using figure 48.
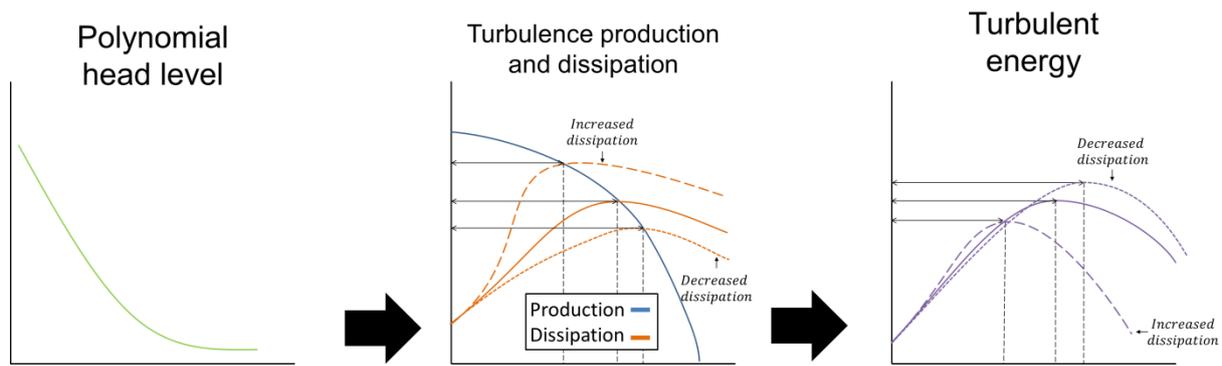
**Figure 48 Relation between head level shape, turbulence production and dissipation and the absolute turbulent energy levels as calculated by the ATM, dashed lines show effect of increasing or decreasing the dissipation coefficient $\alpha$**

The ATM turbulent energy levels using polynomial head input for the experiments of Xingkui & Fontijn (1993) and Nakagawa and Nezu (1987) ST-3 overestimated the turbulent energy levels (see figure 44 and 46). In order to find a better model, the dissipation coefficient $\alpha$ is increased to counteract the overestimation of the calculated turbulent energy levels. However, as figure 48 shows, an increase in the dissipation coefficient $\alpha$ also results in an upstream displacement of the turbulent energy peak. Vice versa, when turbulence is underestimated (experiment of Hofland, 2005), after calibration the dissipation term is decreased and the turbulence peak is moved downstream. Thus after calibration, the magnitude of the modelled turbulence better fits the measured turbulence, but the shape of the modelled turbulence is distorted at the same time. This is a limitation of the ATM in its present form. Suggestions for improving the ATM in order to resolve this limitation are given in section 7.6.

The results for the Nakagawa and Nezu (1987) ST-1 experiment are different. Due to the shape of the polynomial head level input, the production of turbulence is always larger than the dissipation (figure 45). This results in the ATM modelling increasing turbulent energy levels, as can be seen in figure 47. However, the measured turbulent energy levels for the experiment of Nakagawa and Nezu (1987) ST-1 show exactly the reverse pattern: an initial rapid increase in turbulent energy, that settles at a constant value further downstream. This results in a bad fit between measured and calculated turbulent energy levels.

Because the calibrated ATM using polynomial head level input showed bad performance, the resulting $\alpha$ dissipation terms are not analysed any further.

### Calibrated Dissipation case: ATM output using linear and momentum head level input

The ATM results using linear and momentum head level input are discussed at the same time because they both show similar results.

The calibrated ATM using linear or momentum head level input shows good up to great fit with the measured turbulent energy levels (figure 47). The ATM applied to the experiment of Xingkui & Fontijn (1993) resulted in the least fitting model. This is the result of the linear head level change input being unable to model increasing and decreasing turbulence levels within the same figure. All other experiments show only little or no decrease in turbulent energy levels. Thus for those experiments it is less of a problem that the head level input does not allow for both an increase and decrease in turbulent energy levels. As a result, the calibrated models for the other experiment are quite accurate.

The resulting $\alpha$ dissipation terms are not analysed yet for the ATM linear and momentum head level alternatives because the used calibration method does not take into account the inability of

these models to predict both increasing and decreasing turbulent energy levels. In order to better compare the dissipation coefficients found after calibrating the ATM using linear and momentum head level input, the different calibration method is first applied (as discussed at the beginning of this section). For this calibration method, the ATM is calibrated using the measured turbulent energy levels up until the maximum measured energy level. This will make sure that the found dissipation coefficients are not distorted because the measured turbulent energy levels show both increasing and decreasing turbulent energy levels, whereas the head level input does not allow for this behaviour. The new calibration method resulted in the following graphs:
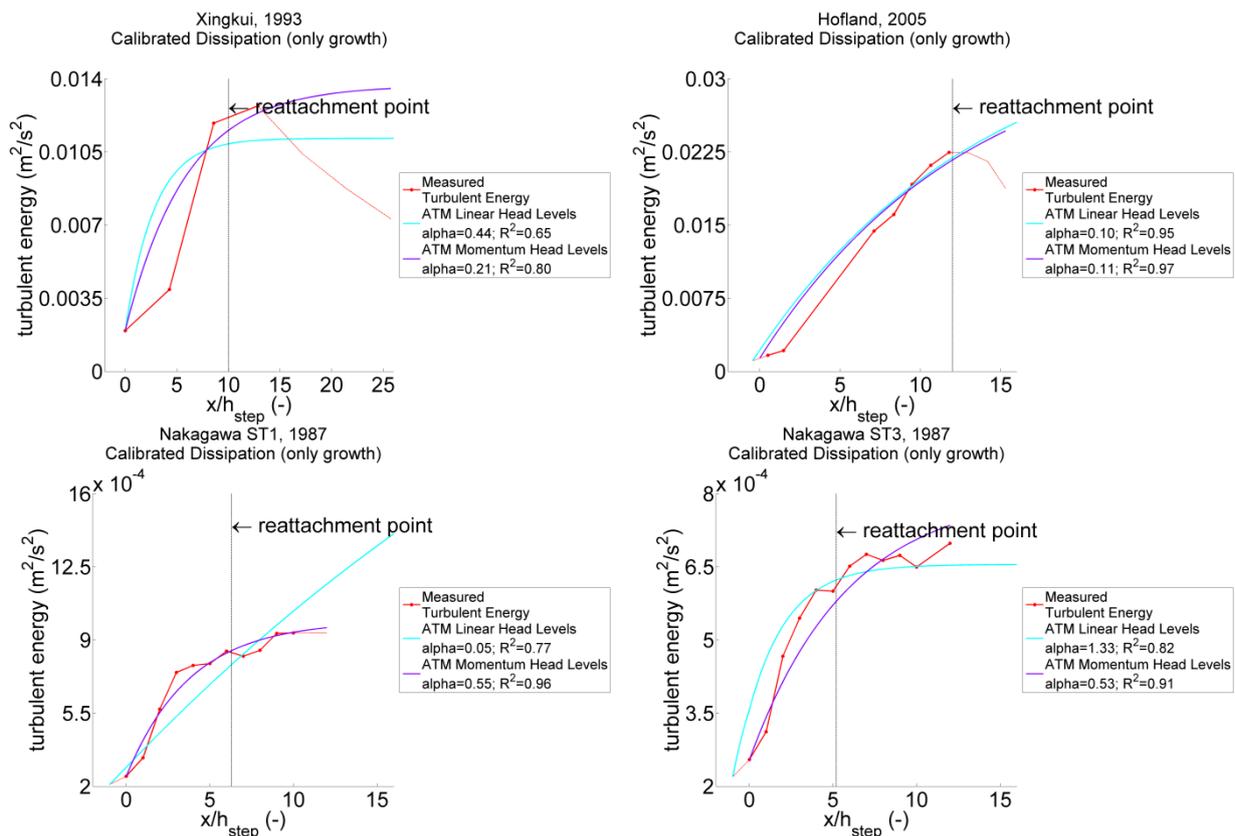


Figure 49 Comparison between measured turbulent energy and ATM output for the Calibrated Dissipation case only considering the measured turbulent energy levels up until the maximum value

Table 10 All dissipation coefficients $\alpha$ after calibration (using only measured turbulent energy levels up until the maximum) and their corresponding coefficient of determination

| Author | | Xingkui, 1993 | Hofland, 2005 | Nakagawa ST1, 1987 | Nakagawa ST3, 1987 |
|---|---|---|---|---|---|
| Calibrated using measured turbulent energy values up until the maximum value | $\alpha$ linear head level input | 0.44 | 0.10 | 0.05 | 1.33 |
| | $R^2$ linear head level input | 0.65 | 0.95 | 0.77 | 0.82 |
| | $\alpha$ momentum head level input | 0.21 | 0.11 | 0.55 | 0.53 |
| | $R^2$ momentum head level input | 0.80 | 0.97 | 0.96 | 0.91 |

By omitting the measured decrease in turbulent energy, the ATM results for the experiment of Xingkui & Fontijn (1993) now also shows a reasonably good fit with the measured turbulent energy levels up until around the reattachment point. The results in figure 49 indicate that the ATM is at least able to accurately approximate the turbulent energy levels up until the reattachment point when using linear or momentum head level input.

An indication that the ATM correctly approximates the physics behind turbulence generation and dissipation would be when the calibrated dissipation coefficient $\alpha$ can be related to flow properties of the experiments. It is hypothesised that the dissipation of turbulence is related to the bed roughness of the flume. The dissipation coefficients found when using linear head level input fluctuates without any clear pattern. For example, the studies of Xingkui & Fontijn (1993) and Hofland (2005) were both performed with a rough bottom, but the calibrated dissipation coefficient of turbulence equalled 0.44 for Xingkui & Fontijn (1993) and 0.10 for Hofland (2005). The experiment of Nakagawa and Nezu (1987) ST-1 and ST-3 were performed under similar conditions (with the exception of an increase in discharge), but the calibrated dissipation coefficient deviate greatly (table 11). Thus the ATM results using linear head level input do not show a relation between bottom roughness and the ATM dissipation coefficient.

The dissipation coefficients found when using momentum head level input does show consistency. The studies of Xingkui & Fontijn (1993) and Hofland (2005) were both performed using a rough bottom and resulted in calibrated dissipation coefficient of 0.21 and 0.11 respectively. The experiment of Nakagawa and Nezu (1987) ST-1 and ST-3 were performed using a smooth bottom and resulted in calibrated dissipation coefficients of 0.55 and 0.53 respectively. For the rough bottom, much lower dissipation coefficients are found ($\alpha < 0.21$) than for the smooth bottom ($\alpha > 0.53$). This might indicate a relation between bottom roughness and the dissipation coefficient in the ATM. However, with only four different experiments, no hard conclusions can be made about the relation between the dissipation coefficient $\alpha$ and the flow conditions of the experiments. When more experiments are available, it is suggested to make a scatter plot of various flow variables (e.g. discharge, Reynolds number, bottom roughness, etc.) versus the found calibrated dissipation coefficients to find possible patterns between the flow conditions and the dissipation coefficients. One thing that can be concluded based on the calibrated $\alpha$ coefficients, is that it is unlikely that there exists a single value for $\alpha$ that can approximate the dissipation of turbulence, regardless of the flow conditions.

### Conclusions

This section discussed the results of calibrating the dissipation coefficient of the ATM using the different head level alternatives. This section confirmed that the ATM has a hard time modelling both increasing and decreasing turbulent energy levels accurately. The calibrated ATM using polynomial head level input resulted in sub optimal model performance due to the model inner workings as discussed in figure 48. If the ATM is to be used to accurately model both increases and decreases in turbulence, it should first be adjusted. The calibrated ATM using linear and momentum head levels results in a better fit with the measured turbulence. This goodness of fit is mainly achieved because the area where turbulent energy in the flow is increasing is accurately modelled. Smaller dissipation coefficients are found for the experiments performed in a flume with a rough bottom compared to a flume with a smooth bottom. This indicates that it is unlikely that there exists a single value for $\alpha$ that can describe the dissipation of turbulence.

## 7.6 Final remarks and recommendations for improving the Arcadis Turbulence Model

### Summarizing the results

In figure 50 the results of most ATM alternatives are plotted in one figure. Figure 50 shows for each of the model alternatives how much the ATM estimated turbulent energy levels deviates from the measured turbulent energy levels at the reattachment point. Figure 50 is normalized by dividing the estimated turbulent energy levels by the measured turbulent energy levels at the

reattachment point. Because the raw head levels are defying the laws of physics, the ATM results using the raw head levels are not shown in figure 50.
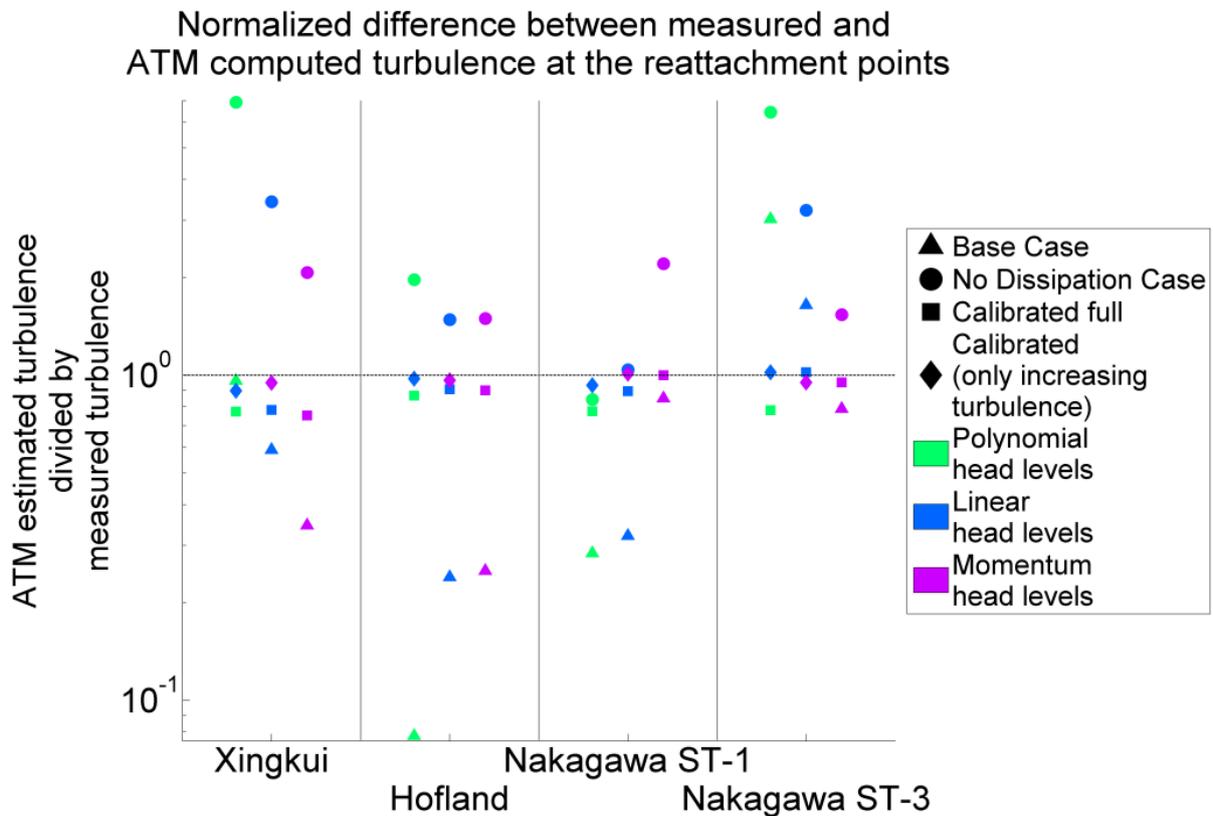


Figure 50 Performance of the ATM estimating the turbulent energy at the reattachment point. Note the log scale of the y-axis.

Figure 50 shows that the calibrated ATM using linear and momentum head levels perform best overall at estimating the turbulent energy at the reattachment point.

### Goal of the ATM

The ATM is intended to be used as a rapid assessment tool to estimate turbulent energy at multiple locations in a flow. Applying the ATM could be more accurate than using rules of thumb because the ATM takes into account the production and dissipation of turbulence in a flow. However, in its present form, the ATM is not able to consistently and accurately estimate turbulent energy downstream of the reattachment point for the selected experimental data.

The raw measured head level input data results in unrealistic destruction of turbulent energy due to sudden increases in mean flow energy. Therefore, a smoothing method is needed to achieve more realistic head level values. The polynomial smoothing function seemed to best represent the physics behind mean flow energy loss. The polynomial smoothing function also fitted best with the measured head levels. However inserting the polynomial head levels into the ATM resulted in less than accurate ATM turbulent energy levels, even when the dissipation coefficient was calibrated. When a constant rate of mean flow energy loss (linear and momentum head levels) is used as input, the ATM was able to accurately estimate the turbulent energy levels. But using a constant rate of mean flow energy loss as input into the ATM results in the ATM being unable the model decreasing turbulent energy levels. An important question should now be raised: is the inability of the ATM to accurately estimate turbulent energy levels the result of inaccurate input data, or the result of the limitations of the ATM in its present form? It is expected

that both the input data and the ATM limitations play a role in the unsatisfactory estimated turbulent energy levels.

### The ATM dissipation coefficient

The ATM models dissipation as a relaxation function. The theoretical validation of the ATM (chapter 4) showed that the dissipation coefficient of the ATM could confirm with the theory of large scale to smaller scale eddy dissipation when:

$$\alpha = \frac{u_j'}{\bar{u}_j} \frac{2R}{l} \tag{4.5}$$

For all runs of the ATM depicted in this chapter, it was assumed that $\alpha = constant$ over the whole flume. Equation 4.5 however, relates the dissipation coefficient $\alpha$ to the ratio between the flow velocity fluctuations $u_j'$ and the mean flow velocity $\bar{u}_j$. This ratio will fluctuate in space. A constant dissipation coefficient was used in ATM runs presented in this chapter to check whether the assumption that $\frac{u_j'}{\bar{u}_j} \frac{2R}{l} = constant$ would approximate reality sufficiently. Based on the results presented in this chapter, this seems not to be the case. A different definition of the dissipation coefficient $\alpha$ is therefore needed. It is recommended to use equation 4.5 as a start to formulate a new dissipation coefficient for the ATM. The calibration of the dissipation coefficient $\alpha$ also showed a possible relation between the bottom roughness and the dissipation coefficient. It is recommended that in future research this is also taken into account when redesigning the ATM. The introduction of two separate dissipation terms might improve the ATM. One dissipation term then affects the turbulence produced due to flow deceleration. The other dissipation term affects the turbulence produced due to wall friction.

### The ATM production term

The ATM assumes that 100% of the mean flow energy loss is converted into turbulent energy. Chapter 4 already showed that the mean flow can loose energy which is not converted into turbulent energy as the result of friction with a wall. Let's assume for a moment that the ATM overestimates the production of turbulent energy. Let's also assume that the polynomial head levels best approximate the actual mean flow energy loss that occurred during the experiments. During the calibration of the ATM using polynomial head levels, the overestimation of turbulence production is compensated by assuming a larger dissipation coefficient $\alpha$. However, the larger dissipation coefficient $\alpha$ results in the turbulent energy peak moving upstream (figure 48). Moreover, the increased dissipation coefficient results in in a very rapid decrease in turbulent energy downstream of the turbulent energy peak. The ATM results for three out of the four selected experiments showed exactly this pattern in figure 47. A solution would be to adjust the ATM to convert less than 100% of the mean flow energy loss into turbulence. More experiments are required in order to validate this hypothesis.

### Head level input data

The measured head levels contained large uncertainty limits (appendix Q). These uncertainty limits translated into large uncertainties in the ATM output (appendix V). Conclusions based on ATM results using the measured head levels (raw, linear or polynomial) as input should therefore be handled with some reserve. However, this chapter did show that the ATM using measured head levels as input found turbulent energy levels that were in the same order of magnitude as the measured turbulent energy. The large uncertainty in the ATM output should therefore not be a reason to reject the ATM results altogether.

ATM results using momentum head level input were more certain (appendix V). For the Base case, using the conservation of momentum in the ATM resulted in a somewhat accurate estimation of the turbulent energy for two out of the four experiments. The calibration of the ATM using momentum head level input resulted in dissipation coefficients that could be linked to the flume bottom roughness. The uncertainty analysis (appendix V), and the more consistent ATM output using momentum head level input gives confidence in the accuracy of the momentum head levels representing the actual mean flow energy loss.

Recommendations about performing new experiments are given in chapter 9.

**Usability of the ATM in its present from**
The ATM is able to reasonably accurately estimate the turbulent energy levels up until the reattachment point (figure 50). An approximation of the turbulent energy levels at the reattachment point is usable in the preliminary design of hydraulic structures. The next chapter gives an explanation how the ATM in its present form can be used in the preliminary design of hydraulic structures.

# 8 Applying the Arcadis Turbulence Model in practice

## 8.1 Introduction

Chapter 7 discussed the performance of the ATM. It was revealed that the ATM using momentum head level input was able to estimate the turbulent energy levels up until the reattachment point with reasonable accuracy after calibration (figure 50). Estimating the turbulent energy at the reattachment point can be beneficial in the preliminary design phase. This can give a more substantiated estimate of turbulence in a flow compared to a rule of thumb. Moreover, at the reattachment the largest turbulence is often found (chapter 5). Therefore, in this chapter, a method is discussed how the ATM can be applied in practice to approximate the turbulent energy levels at the reattachment point. The method described in this chapter can only be used to calculate the turbulent energy levels at the reattachment point downstream of a BFS under subcritical flow conditions.

In the following text, first all formulae are introduced that are needed to calculate the turbulent energy at the reattachment point during the preliminary design phase. Because in the preliminary design phase, very little measurement data is available, the ATM is run a bit different from chapter 7. The results of the ATM turbulent energy levels at the reattachment point are compared to the measured values to say something about the accuracy of this application of the ATM. Finally, it is shown how the ATM results can be used in the design of loose rock bottom protection.

## 8.2 Formulae needed to apply the Arcadis turbulence model in practice

### ATM input data

The flow situation to which the ATM is applied is defined below.
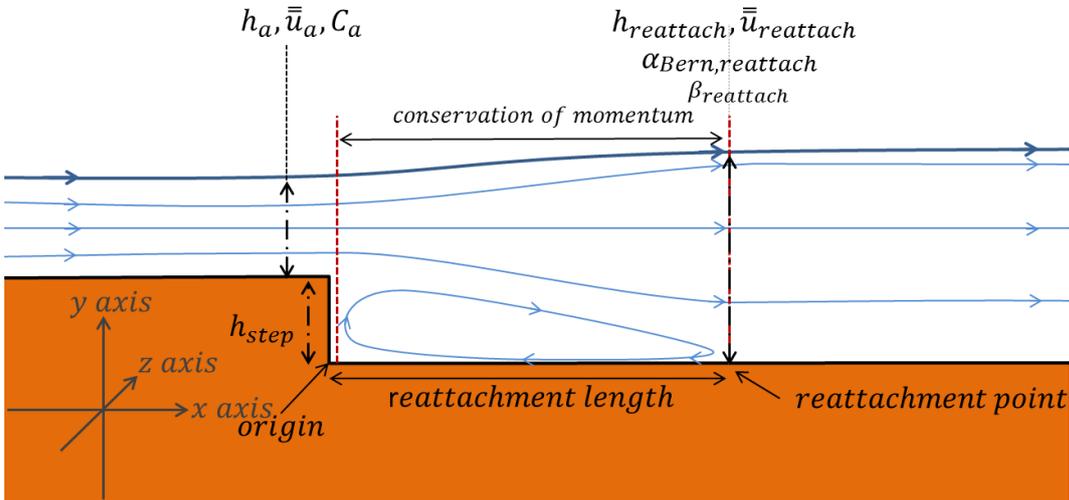


Figure 51 BFS flow situation for which ATM can be used to calculate turbulent energy levels at the reattachment point

The ATM is given by :

$$\frac{d\bar{k}}{dx} = -g\frac{dH}{dx} - \alpha\frac{\bar{k}}{R} \tag{3.11}$$

In order to run the ATM, information is needed about the hydraulic radius $R$, the dissipation coefficient $\alpha$ and the change in head level $\frac{dH}{dx}$. Additionally, the incoming turbulent energy $\bar{k}_0$ is also needed (chapter 6).

The dissipation coefficient $\alpha$ is set at 0. This is done in order to get a conservative estimation of the turbulent energy at the reattachment point. Figure 50 shows that applying the ATM for the No

Dissipation case ($\alpha = 0$) using momentum head level input results in consequent overestimation of the turbulent energy in the flow. It is believed that overestimating the turbulence is less problematic then underestimating turbulence because an underestimation of the turbulence could result in unexpected damages to a hydraulic structure. This reduces the ATM to:

$$\frac{d\bar{k}}{dx} = -g\frac{dH}{dx} \tag{8.1}$$

Equation 8.1 simply states that the production of turbulence equals the mean flow energy loss. No dissipation is considered up until the reattachment point. The hydraulic radius is therefore not required in order to run the ATM.

The incoming turbulent energy $\bar{k}_0$ can be approximated by the equilibrium turbulent energy level $\bar{k}_e$, as discussed in section 6.6:

$$\bar{k}_e = \bar{\bar{u}}_a{}^2 c_0^2 \frac{g}{C_a{}^2} \tag{3.14}$$

To find the equilibrium turbulent energy levels, the flow velocity $\bar{\bar{u}}_a$ and Chezy coefficient on top of the step need to be known ($c_0^2 = 1.21^2$, Hoffmans, 1993). It is assumed that the flow velocity $\bar{\bar{u}}_a$ and water depth $h_a$ on top of the step are known in the preliminary design phase. The Chezy coefficient can be calculated using the following formula:

$$C_a = \frac{1}{n}h_a{}^{1/6} \tag{5.4}$$

It is assumed that the Manning coefficient $n$ is known on top of the step in the preliminary design phase[27]. Appendix T shows how the equilibrium turbulent energy levels $\bar{k}_e$ are calculated using equation 3.14 for the selected experiments.

### Approximating the head levels in the flume

The change in head level $\frac{dH}{dx}$ is needed as input into the ATM. The head levels in a flow can be calculated using the adjusted Bernoulli formula:

$$H = z + h + \alpha_{Bern}\frac{1}{2}\frac{\bar{\bar{u}}^2}{g} \tag{6.3}$$

The water depth $h_a$ and flow velocity $\bar{\bar{u}}_a$ are assumed to be known on top of the step. If it is also assumed that the rate of mean flow energy loss downstream of the BFS is constant up until the reattachment point, then only the water depth $h_{reattach}$, flow velocity $\bar{\bar{u}}_{reattach}$ and the reattachment length are needed to calculate the change in head level $\frac{dH}{dx}$. This is done using the conservation of momentum. Because at the reattachment point the flow velocity profile is not uniform yet, a value for $\alpha_{Bern}$ at the reattachment point is also needed. The method for finding the non-uniformity coefficient $\alpha_{Bern}$ in the preliminary design phase is discussed below.

### Using the conservation of momentum at the reattachment point

In order to find the water depth $h_{reattach}$ and flow velocity $\bar{\bar{u}}_{reattach}$, the conservation of momentum and mass is used. The water depth at the reattachment point can be found using the following formula:

---

[27] Assuming the upstream incoming turbulent energy is defined by the step roughness.

$$h_{reattach} = \frac{M_a - \frac{1}{2}\rho_w g (h_{reattach})^2}{\rho_w \beta_{reattach} \frac{q^2}{h_{reattach}^2}} \qquad (6.3)$$

The flow velocity $\bar{\bar{u}}_{reattach}$ is then simply found by assuming conservation of mass:

$$\bar{\bar{u}}_{reattach} = \frac{h_a \times \bar{\bar{u}}_a}{h_{reattach}}$$

Equation 6.3 also needs the momentum $M_a$ of the flow at an infinitesimal distance downstream of the step. This momentum can be calculated using the following formula:

$$M_a = \frac{1}{2}\rho_w h_b^2 + \rho_w h_a \bar{\bar{u}}_a^2 \qquad (2.6)$$

Here $h_b = h_a + h_{step}$.

### Finding the non-uniformity coefficients $\alpha_{Bern}$ and $\beta_{reattach}$

Equation 6.3 requires the non-uniformity coefficient $\beta_{reattach}$. The non-uniformity coefficient $\alpha_{Bern}$ is also needed in the Bernoulli formula. A new method is suggested to approximate the values of $\alpha_{Bern}$ and $\beta_{reattach}$.

A relation exists between the value for non-uniformity coefficient at the reattachment point and the ratio between the water depth on top of the step $h_a$ and the step size $h_{step}$. This relation can be made visible using a scatter plot.
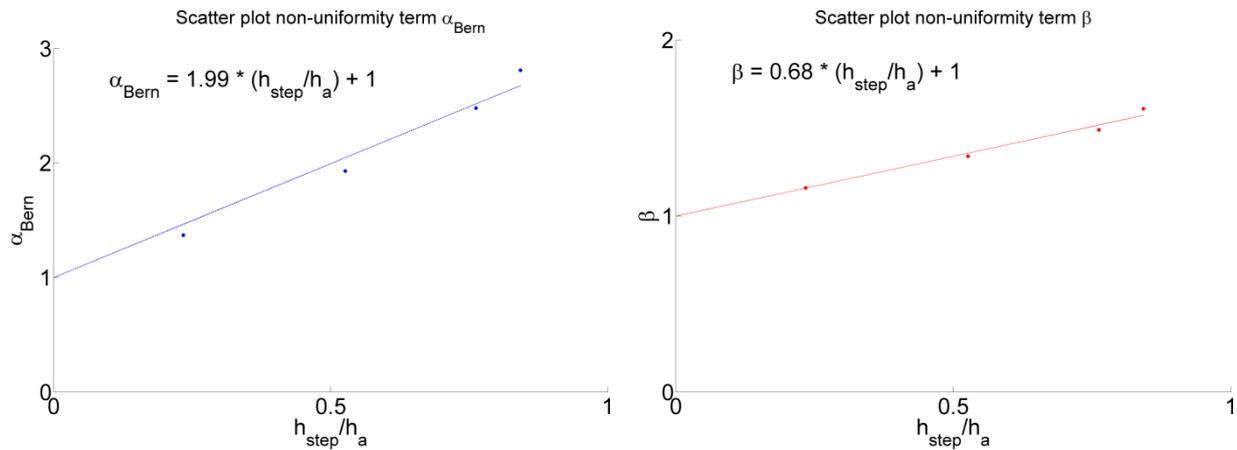


Figure 52 Scatter plots of the non-uniformity coefficients at the reattachment point versus the ratio between $h_{step}$ and $h_a$

Figure 52 is constructed using the flow velocity profiles and water depths of the four selected experiments (Xingkui & Fontijn, 1993; Hofland, 2005; and Nakagawa & Nezu, 1987). In figure 52, the step/water-depth ratio $(h_{step}/h_a)$ is plotted against the non-uniformity coefficients. Figure 52 shows a very clear relation between the step water depth ratio $(h_{step}/h_a)$ and the non-uniformity coefficients $\alpha_{Bern}$ and $\beta_{reattach}$. This relation is caused by the fact that the relative step height affects the size of the recirculation zone. The size of the recirculation zone in turn affects the non-uniformity of the flow at the reattachment point. Because a relation exists between $\alpha_{Bern}$, $\beta_{reattach}$ and $h_{step}/h_a$, and both $h_{step}$ and $h_a$ are assumed to be known during the preliminary design phase, it is also assumed that $\alpha_{Bern}$ and $\beta_{reattach}$ at the reattachment point can be

calculated during the preliminary design phase. The relation depicted in the figure above should be handled with reserve for $(h_{step}/h_a) > 1$.

### Reattachment length

Only one variable is left which is needed to calculate the turbulent energy level at the reattachment point during the preliminary design phase: the reattachment length. Both Nakagawa and Nezu (1987) and Hofland (2005) discussed the relation between properties of the flow (Reynolds number, Froude number etc.) and the location of the reattachment point downstream of a BFS. However, no clear relation was found by those authors. In engineering practice, a reattachment length of $x/h_{step} = 10$ is often used. In the following calculation it is assumed that the reattachment length is located at $x/h_{step} = 10$. When a more substantiated estimation of the reattachment length is available during the preliminary design phase, it is recommended to use the substantiated estimation instead of the engineering practice.

## 8.3 Accuracy of the Arcadis Turbulence Model when applied during the preliminary design phase

Using the above described method, the ATM is used to calculate the turbulent energy at the reattachment point. This resulted in in following table:

Table 11 Comparing measured and ATM calculated turbulent energy at the reattachment point

| Author | | Xingkui, 1993 | Hofland, 2005 | Nakagawa ST1, 1987 | Nakagawa ST3, 1987 |
|---|---|---|---|---|---|
| Turbulent energy at reattachment point | $\bar{k}$ measured (m$^2$/s$^2$) | 0.0127 | 0.0225 | 0.0009 | 0.0007 |
| | $\bar{k}$ ATM calculated (m$^2$/s$^2$) | 0.0231 | 0.0213 | 0.0021 | 0.0016 |

Table 11 shows that for three out of the four selected experiments, the ATM run as described above overestimates turbulent energy up to 130%. Considering that the ATM was run using only the water depth and flow velocity on top of the step and turbulence dissipation is neglected, these results are reasonably good. For the experiment of Hofland (2005), an underestimation of the turbulent energy of roughly 5% was found when using the ATM. This is very close to the actual measured turbulent energy at the reattachment point. An underestimation of 5% is deemed small enough to not jeopardize the stability of a hydraulic structure, especially considering that applying rules of thumb can result in even larger underestimations of turbulence (Voortman, 2015).

Based on the results of table 11, it is concluded that the ATM can estimate the maximum occurring turbulent energy levels downstream of a BFS with some accuracy. In the worst case scenario (experiment of Hofland, 2005), the ATM underestimates to turbulent energy by only 5% (based on the selected experiments). Overestimation of turbulent energy the flow is less problematic because an overestimation of the turbulence will most likely not result in an unstable designs of hydraulic structures as the result of the inaccurate turbulence estimations[28].

## 8.4 Using the Arcadis Turbulence Model to design loose rock bottom protection

Turbulent energy levels are required in the design of loose rock bed protection. Appendix C introduces the design formula of Pilarczyk (1995) which is often used to determine the required

---

[28] It was deliberately chosen to minimize underestimation of the turbulence as much as possible (achieved by neglecting dissipation). This was done so that the model is biased in its error direction ("often" overestimation, but only very little underestimation). Having a model that is biased in its error direction is beneficial because it is then known that the actual occurring turbulence in the flow is equal to the estimate turbulence; or less. This actually reduces the uncertainty margins of the turbulence estimations.

size of the loose rock. In the design formula of Pilarczyk (1995) a correction coefficient $k_t{}^2$ is included to take into account the turbulence in the flow. An 100% increase in the correction coefficient $k_t{}^2$ results in an 100% increase in the size of the required loose rock. The correction coefficient $k_t{}^2$ is calculated in the following way:

$$k_t{}^2 = \left(\frac{1 + 3r}{1.3}\right)^2 \tag{8.2}$$

Where $r$ equals the depth averaged turbulent intensity (-). Depth averaged turbulent intensity is defined as:

$$r = \frac{\sqrt{\bar{k}}}{\bar{u}} \tag{8.3}$$

Using equation 8.2 and 8.3, the $k_t{}^2$ can be calculated. This was done for the ATM estimation of turbulence, the actual measured turbulence at the reattachment point and the turbulence levels as follow from the rules of thumb presented in the Rock Manual (2007). The results are depicted in the table below.

Table 12 Values for the correction coefficient $k_t{}^2$ measured in the flume at the reattachment point, calculated using the ATM and following the rule of thumb given in the Rock Manual (2007)

| Author | Xingkui, 1993 | Hofland, 2005 | Nakagawa ST1, 1987 | Nakagawa ST3, 1987 |
|---|---|---|---|---|
| $\bar{k}$ measured (m²/s²) | 0.0127 | 0.0225 | 0.0009 | 0.0007 |
| $\bar{k}$ ATM calculated (m²/s²) | 0.0231 | 0.0213 | 0.0021 | 0.0016 |
| $r$ measured (-) | 0.3087 | 0.3952 | 0.2154 | 0.1162 |
| $r$ ATM calculated (-) | 0.4160 | 0.3847 | 0.3245 | 0.1758 |
| $r$ rule of thumb (Rock Manual, 2007) | 0.6000 | 0.6000 | 0.6000 | 0.6000 |
| $k_t{}^2$ measured (-) | 2.195 | 2.826 | 1.603 | 1.076 |
| $k_t{}^2$ ATM calculated (-) | 2.990 | 2.745 | 2.305 | 1.381 |
| $k_t{}^2$ following rules of thumb | 4.639 | 4.639 | 4.639 | 4.639 |

Table 13 Typical turbulence levels according to the Rock Manual (p. 651, 2007)

| Situation | Turbulence level | |
|---|---|---|
| | Qualitative | Turbulence intensity, $r$ |
| Straight river or channel reaches | normal (low) | 0.12 |
| Edges of revetments in straight reaches | normal (high) | 0.20 |
| Bridge piers, caissons and spur-dikes; transitions | medium to high | 0.35 – 0.50 |
| Downstream of hydraulic structures | very high | 0.60 |

Table 12 shows the turbulent intensity $r$ and turbulence correction factor $k_t{}^2$ as follows from the turbulent energy levels calculated by the ATM and measured in the flume. The $k_t{}^2$ factor only deviates up to 30% when comparing measured and calculated values. Also note that the ATM underestimates the turbulence correction factor by 3% for the experiment of Hofland (2005).

The Rock Manual (2007) contains a table showing the typical turbulent intensity levels (rules of thumb) after a hydraulic structure (table 13). These rules of thumb are currently used in the

preliminary design phase in combination with formula 8.2 to calculate the $k_t{}^2$ (Voortman, 2015). The Rock Manual (2007) advises to use a turbulence intensity of 0.60 after hydraulic structures. The resulting $k_t{}^2$ values are depcited in table 12.

The ATM overestimated the $k_t{}^2$ values by up to 30% when compared to $k_t{}^2$ calculated using the measured turbulence levels. The rules of thumb were also used to calculate $k_t{}^2$ values. Compared to the measurements, the rules of thumb overestimated $k_t{}^2$ by up to 330%. Thus, for the experiments studied in this thesis, the ATM is able to significantly more accurately estimate the turbulence intensity and $k_t{}^2$ values compared to the rules of thumb. Moreover the method described in this chapter is easy to apply and only requires little data. Thus the ATM can be a viable alternative to using rules of thumb when calculating the effect of turbulence on loose rock bed protection. However, it is advised to perform more research using different experimental conditions in order to ascertain that the ATM performance is consistent.

Figure 53 shows how much difference applying the ATM instead of the rules of thumb can make on the required stone weight[29] when designing loose rock bed protection.
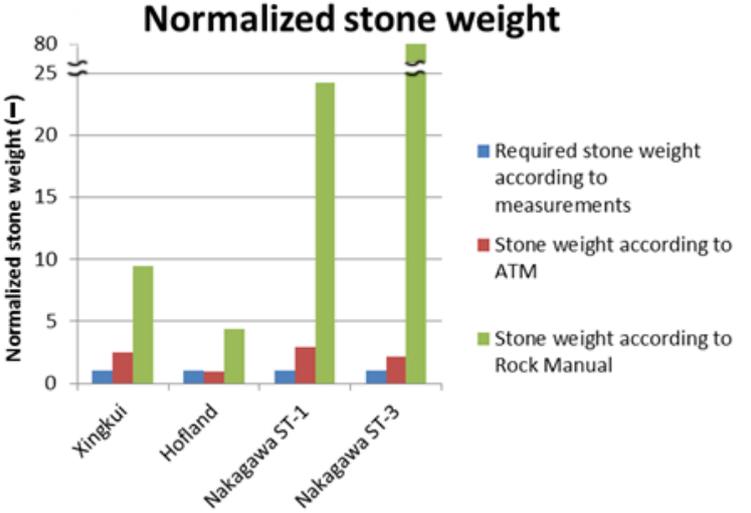


Figure 53 Normalized required stone weight according to ATM and rules of thumb. Stone weight according to measurements is set at unity.

## 8.5 Concluding remarks

This chapter showed how the ATM can be used in the preliminary design phase. The ATM can be run using very little measurement data by applying the conservation of mass, conservation of momentum and using the relation between the water depth ratio $\left(h_{step}/h_a\right)$ and the non-uniformity coefficients ($\alpha_{Bern}$ and $\beta_{reattach}$). The resulting turbulent energy levels approximate reality within the same order of magnitude (underestimation of 5% up to overestimation of 130%). The ATM is already usable to estimate the upper limit of turbulence at the reattachment point during the preliminary design phase (for subcritical backward facing step flow). Using the ATM output results in up to 3 times heavier stones compared to the stone weight design based on the experimentally measured turbulence. This is significantly more accurate then applying rules of thumb, which results in stone weights up to 80 times heavier. Thus the ATM could be a more accurate alternative to using rules of thumb when calculating the effect of turbulence on loose rock bed protection.

---

[29] Assuming the relations: stone weight = (stone size)$^3$

# 9 Conclusion, discussion and recommendations

## 9.1 Introduction
This chapter will conclude the thesis. The conclusions will present the final ideas about the ATM and will reflect on the goal of this thesis. Thereafter, a number of issues are discussed. These issues were not explicitly discussed in the previous chapters, but are important to mention. Finally, recommendations are given for future research.

## 9.2 Conclusion
### Research goal and questions
An estimation of the turbulent intensity in a flow is needed when designing hydraulic structures. Not taking turbulence intensities into account can result in the destruction of the designed hydraulic structure. The Arcadis Turbulence Model, as discussed in this thesis is intended as a rapid assessment tool to estimate turbulent energy in a quick way, more accurately than rules of thumb, and more easy to apply than complicated $k - \varepsilon$ models.

The objective of this study was to test the theoretical and empirical validity of the ATM as a rapid assessment tool for the flow conditions of a wide channel with a backward facing step. The goal was reached by answering the three research questions.

### 1. What is the theoretical validity of the ATM?
The ATM assumes that 100% of the mean flow energy loss is converted into turbulent energy. Multiple scientific sources state that the reduction of mean flow energy is related to the increase of turbulent energy. This partly validates the assumption of the ATM. The mean flow can lose energy due to wall friction which is not completely converted in turbulence. Thus the assumptions that 100% of the mean flow energy loss is converted into turbulent energy is questionable. Using the turbulent kinetic energy equation, it was shown that the production of turbulence is exactly proportional to the reduction of mean flow energy under a set of assumptions. This means that the turbulent kinetic energy equation can confirm with the production term of the ATM. However, neglecting the mean flow energy loss due to viscous stresses with the boundaries seems questionable. Neglecting the mean flow energy loss due to viscous stresses with the boundaries can result in overestimation of the produced turbulence (as was hypothesized in the empirical validation, section 7.6).

No instances in literature were found of modelling dissipation as a relaxation term similar to the ATM. The dissipation coefficient of the ATM can confirm with the dissipation coefficient as described by the theory of large scale to smaller scale eddy dissipation under the assumptions of a variable dissipation coefficient $\alpha$. However, in this thesis, it was researched whether setting the dissipation coefficient $\alpha$ at a constant value will approximate reality sufficiently. This seemed not to be the case according to the empirical validation (section 7.6).

### 2.What is the accuracy of the ATM turbulence estimations compare to experimental measurements of BFS turbulence?
The empirical validation resulted in a number of observations. First of all, the input data to run the ATM is not very certain. Without applying smoothing techniques, the input data contains physically impossible measurements (e.g. no conservation of mass, figure 27; sudden increases in mean flow energy, figure 35). Moreover, the choice of smoothing technique determines the ATM outcome. This made it challenging to objectively asses the empirical validity of the ATM using the measured input data. Alternatively, ATM input was calculated using the conservation of momentum. This resulted in a bit more confidence in the input data. However, the conservation of

momentum does not take into account a number of phenomena (e.g. mean flow energy loss due to bottom friction and sediment transport).

When it was assumed that dissipation of turbulence follows the dissipation coefficient of Hoffmans (1993), then the ATM was able to approximate the order of magnitude of the turbulence. However, there still exists a notable discrepancy between model and measurement (figure 44). This could indicate that downstream of a BFS, turbulence is dissipated at a different rate than the dissipation coefficient based on the work of Hoffmans (1993). Calibrating the dissipation coefficient using the measured turbulent energy levels made it clear that the ATM has general issues modelling the right turbulent energy levels and shapes in its present form (figure 47). The ATM especially has a hard time modelling both increasing and decreasing turbulent energy levels accurately. The ATM was able to approximate the turbulent energy levels up until the reattachment point reasonably accurate after calibration (figure 49).

The inability of the ATM to accurately estimate turbulent energy levels over the whole flume is concluded to be the result of inaccurate input data and the current way the ATM calculates turbulent energy. The results of the empirical validation and the uncertainty analysis indicate that the used input data is not perfect. More accurate experimental data is required to make sure that the discrepancies between the experimentally measured and ATM calculated turbulent energy levels are the result of the limitations of the ATM, and not the result of measurement errors in the input and validation data (in the recommendations section, new experiments are proposed). Moreover, in its present form, the dissipation and production terms of the ATM cause an inability to accurately model turbulent energy peaks at the right location. This will probably be resolved by letting go of the assumption of a constant dissipation coefficient $\alpha$ in time and space and changing the production term to account for mean flow energy loss not being 100% transformed into turbulent energy.

The fact that turbulence can be produced downstream of the reattachment point due to non-uniform flow velocity profiles (on top of the turbulence production due to bottom friction) is an important finding. This could explain why for the study of Nakagawa and Nezu (1987), turbulence is not reduced immediately downstream of the reattachment point. Due to the non-uniformity of the flow, more energy is contained in the flow than would be found when assuming uniformity. Therefore, the non-uniformity of the flow velocity profile is an important factor to take into account when considering mean and turbulent energy in a flow.

### 3. How can the ATM be applied in the preliminary design phase?

At the reattachment point downstream of a BFS the largest turbulence is often found (Nakagawa & Nezu, 1987; Xingkui & Fontijn, 1993; Kasagi & Matsunaga, 1995; Hofland,2005). In the preliminary design phase, the largest value of turbulence is used in the design of hydraulic structures. During the empirical validation of the ATM it was shown that the ATM was able to estimate the turbulent energy levels at the reattachment point with reasonable accuracy. Therefore it can be beneficial to use the ATM in the preliminary design phase.

The data requirements of applying the ATM in the preliminary design phase are low. Using the water depth and flow velocity on top of the step, the turbulence energy at the reattachment point can be calculated. The resulting turbulent energy levels approximate reality within the same order of magnitude (underestimation of 5% up to overestimation of 130%; table 11). The ATM is usable to estimate the upper limit of turbulence at the reattachment point during the preliminary design phase. Using the ATM output results in up to 3 times heavier stones compared to the stone weight design based on the experimentally measured turbulence. This is significantly more

accurate then applying rules of thumb, which results in stone weights up to 80 times heavier (figure 53).Thus the ATM can be a more accurate alternative to using rules of thumb when calculating the effect of turbulence on loose rock bed protection. However, these results were achieved using experimental data not intended for validating the ATM. Therefore these results should be handled with some reserve. More research is required before the ATM can be confidently used to accurately design loose rock bed protection in, for example, the final design phase of a hydraulic structure.

### Objective
The goal of this thesis is to test the validity of the ATM for the flow conditions of a wide channel with a backward facing step. This thesis concluded that the ATM in its present form is able to reasonably accurately estimate the turbulent energy levels up until the reattachment point. It also showed how the ATM in its present form can be applied in the preliminary design phase to estimate the required stone size for loose rock bed protection. The resulting bed protection design using the ATM output is more accurate then applying rules of thumb. In chapter 1 the ATM was introduced as a rapid assessment tool that would potentially combine the ease of rules of thumb with the more accurate measures of turbulence found using complex turbulence models. The results of this thesis indicate that the ATM is not there yet. The ATM has a hard time modelling the right shape of the turbulent energy levels. The accuracy of the ATM estimations is also bad downstream of the reattachment point. The results of this thesis did show the potential of the ATM to become a great assessment tool for turbulence in a flow during the preliminary design phase. In order for the ATM to become a more accurate rapid assessment tool, more research is required though.

## 9.3 Discussion
A number of issues related to this research are mentioned below.

### Measured turbulent energy levels
It was shown in this thesis that for the depth averaged mean flow energy levels, the non-uniformity of the flow will affect the found energy levels. The measured turbulent energy levels were also depth averaged. Taking into account the non-uniformity of the measured turbulent energy levels might result in increased levels of turbulent energy. If it is assumed that the non-uniformity coefficient of the turbulent energy can be calculated similar to the non-uniformity coefficient of the mean flow energy ($\alpha_{Bern}$), than non-uniformity coefficients up to 1.25 are found for the measured turbulent energy. This is much smaller than the non-uniformity of the mean flow energy, but it might still be significant. It is advised that future research takes the non-uniformity of the measured depth averaged turbulent energy into account.

The flow velocity fluctuations (used to calculate the turbulent energy) were measured using a Laser Doppler Anemometer (LDA). This measuring device only has a limited measuring resolution. Therefore, the flow velocity fluctuations which manifested itself over a distance smaller than the LDA measurement resolution are not measured correctly. This means that the measured turbulent energy might be somewhat smaller than the actual turbulent energy in the flow because the smallest velocity fluctuations are not taken into account.

### Non-uniformity in z-direction
In this research, uniformity in $z$-direction was assumed. Some remarks can be made about this assumption. The LDA measured flow velocity fluctuations in the centre of the flume. Moreover, it only measured the flow fluctuations in $x$ and $y$-direction. It is therefore unknown how large and uniform the flow velocity fluctuations are in the $z$-direction. The validity of assuming uniformity in

$z$-direction is therefore unknown. It is unlikely that the flow fluctuations are completely uniform in the $z$-direction because the presence of the wall will result in smaller flow velocity fluctuations near the wall. However, turbulence isotropy is often assumed in literature (Nakagawa & Nezu, 1987; Brodkey, 1995; Wilczek, Stevens, & Meneveau, 2014), thus this assumption was also made to approximate the fluctuations in $z$-direction.

### Equilibrium turbulence

The equilibrium turbulence levels were calculated using the formula of Hoffmans (1993). The calculated equilibrium turbulent energy levels approximated the measured turbulent energy on the step closely. However, some remarks should be made. It is unknown for which flow scenario's the formula of Hoffmans (1993) is applicable. No terms are present in the formula that take into account slope, discharge, water height, flow velocity, Froude number etc. Therefore, the formula should be handled with some reserve in practice.

### Bernoulli equation

The Bernoulli equation, as presented in this thesis, assumed parallel stream lines. However, as shown in chapter 6, at certain sections the head level is calculated while the water depth is changing. Changes in water depth result in non-parallel stream lines. Thus, the Bernoulli formula might not find the correct mean flow energy values at these locations. However, the change in water depth is very small, thus it is assumed that the Bernoulli equation, as applied in this thesis approximates reality sufficiently.

### Uncertainty analysis

In the previous chapters, some remarks were made about the uncertainty in the measured data and the ATM output. These uncertainties were estimated based on some remarks in the papers and some best guesses because data was lacking for more accurate uncertainty estimations. Therefore the uncertainty analyses presented in the appendices should be handled with some reserve. A number of possible sources of uncertainty (e.g. uncertainty in the non-uniformity coefficients, uncertainty in the hydraulic radius, etc.) were also not taken into account. However, it is still believed that the uncertainty analyses give a good idea about how the uncertainties affecting the ATM input and output.

### Experimental circumstances

The ATM was tested using the experimental data from the selected experiments. These experiments were not performed with the intention to validate the ATM. Moreover, the experiments used to validate the ATM lacked a number of flow situations. All experiments were performed without a sloping channel and the experiments only contained subcritical flow. It is therefore still unclear how the ATM performs for sloped and/or supercritical flow conditions.

## 9.4 Recommendations

Based on the results of the ATM validation as presented in this thesis, and the experience of working with the ATM for over half a year, a detailed recommendation can be given for the continuation of this research.

### New experiments

The results of the of the empirical validation and the uncertainty analyses indicate that the used input data is not perfect. New flume experiments are needed to obtain accurate and diverse experimental data usable to validate and redesign the ATM. This will make sure that the discrepancies between the experimentally measured and ATM calculated turbulent energy values

are the result of the limitations of the ATM, instead of measurement errors in the input and validation data. The following experimental setup is proposed:

Experiments in larger flumes are preferred in order to minimize the error in measurements that are uncorrelated with scale. The instantaneous flow velocity field and the water depth should be measured at as much locations as possible and over a long distance in the flume preferably up until the point where the turbulence downstream of the reattachment point has reached a new equilibrium. The resulting data will give a good idea how turbulence after a BFS reverts back to an equilibrium value (this data was lacking in this thesis). By measuring the instantaneous flow velocity field and the water depth at many locations, the change in head levels in the flume can be accurately calculated. Special attention should be given to the accuracy of the instantaneous flow velocity field and the water depth measurements. Preferably, probability density functions (PDF's) should be created for each measurement location. These PDF's can then be used to say something about the uncertainty in the input (head levels) and output of the ATM. It is advised to perform multiple experiments that have different flume bottom roughness's. This will give a clearer picture how turbulent energy levels in BFS flow relate to the bottom roughness. This information can then perhaps be used to adjust the ATM production and dissipation terms. This thesis showed that the uniformity of the flow velocity profile can affect the turbulence production and that the step/water-depth ratio is related to the non-uniformity of the flow velocity profile at the reattachment point. It is therefore advised that experiments are performed for varying step/water-depth ratios in order to say something about the change in turbulent energy levels by varying this ratio. The ATM has only been validated in this thesis for subcritical flow conditions. Experiments that include supercritical flow conditions should be performed in order so say something about the accuracy of the ATM under these conditions. The above described experiments can be used to validate and redesign the ATM. Note that the data resulting from these experiments are also very usable in many other studies about turbulence. The time and money required to perform these experiments will pay itself back because the resulting dataset can be used in turbulence research for many years to come.

### Validate and redesign the ATM

The ATM can be validated and redesigned when all (or just parts) of the experimental data described above are available. It is advised to first run the ATM in its present form using the newly required input and validation data. If the ATM output then over or underestimates the turbulent energy levels (at least up until the reattachment point), the production term of the ATM should be adjusted. If the turbulence dissipation downstream of the reattachment point is too small or too large, and/or the maximum turbulent energy level according the ATM is located too far up or downstream, then the dissipation term of the ATM should be adjusted. After adjusting the ATM, and a good fit is found between the ATM and the measured turbulent energy levels for multiple experiments, it is then advised to relate the dissipation and production terms to the flow properties of the experiments (e.g. discharge, Reynolds number, bottom roughness, etc.). Finding relations between the flow properties and the production and dissipation terms of the ATM will pave the way for using the ATM in the preliminary design of hydraulic structures during which little measurement data is available.

Finally, the ATM could also be validated for flow situations other than BFS flow, in order to make the ATM more generally applicable.

# Bibliography

Adrian, R. J., Christensen, K. T., & Liu, Z. C. (2000). Analysis and interpretation of instantaneous turbulent velocity fields. *Experiments in fluids*, 275-290.

Andreopoulos, Y., & Honkan, A. (1996). Experimental techniques for highly resolved measurements of rotation, strain and dissipation-rate tensors in turbulent flows. *Measurement Science and Technology, 7*(10), 1462-1476.

Anetor, L., Osakue, E., & Odetunde, C. (2011). Reduced mechanism approach of modeling premixed propane-air mixture using ANSYS Fluent. *Engineering Journal, 16*(1), 67-86.

Auton, T. R. (1987). The lift force on a spherical body in a rotational flow. *Journal of Fluid Mechanics, 183*, 199-218.

Battjes, J. (1990). *Vloeistofmechanica b70: Collegehandleiding.* Retrieved 6 19, 2015, from http://repository.tudelft.nl/: http://repository.tudelft.nl/view/ir/uuid%3A3ed3e49e-cfd8-4e69-9790-f66a5370f0b3/

Bezuijen, A., & Vastenburg, E. W. (2012). *Geosystems: Design Rules and Applications.* Boca Raton: CRC Press.

Bijker, E. W. (1967). *Some considerations about scales for coastal models with movable bed.* Delft: Delft Hydraulics Laboratory.

Blake, W. K. (1970). Turbulent boundary-layer wall-pressure fluctuations on smooth and rough walls. *Journal of Fluid Mechanics, 44*(04), 637-660.

Brodkey, R. S. (1995). *The phenomena of fluid motions. Courier Corporation.* North Chelmsford: Courier Corporation.

Burden, T. (2008). *Chapter 5. Mean Kinetic Energy*. Retrieved 5 8, 2015, from KTH Royal Institute of Technology: http://www2.mech.kth.se/courses/5C1218/KineticE.pdf

Chen, W. F., & Liew, J. R. (2012). *The civil engineering handbook.* Boca Raton: CRC Press.

Cheng, L., Draper, S., & An, H. (2014). *Scour and Erosion: Proceedings of the 7th International Conference on Scour and Erosion.* Perth: Crc Press.

Coleman, N. L. (1972). The drag coefficient of a stationary sphere on boundary of similar spheres. *La Houille Blanche, 1*, 17-22.

Construction Industry Research, Information Association, Civieltechnisch Centrum Uitvoering Research en Regelgeving (Netherlands), & Centre d'études maritimes et fluviales (France). (2007). *The Rock Manual* (Vol. 683). London: Ciria.

Cruise, J. F., Sherif, M. M., & Singh, V. P. (2007). *Elementary hydraulics. .* Toronto: Thomson Learning.

De Gunst, M. (1999). *Steenstabiliteit in een turbulente stroming achter een afstap.* Delft University of Technology: Delft.

De Ruijter, R. (2004, 11 1). *Master Thesis: Turbulence structures affecting stone stability in backward-facing step flow.* Retrieved 5 21, 2015, from repository.tudelft.nl: http://repository.tudelft.nl/view/ir/uuid%3Ae0998d8d-497a-4720-b393-803c207dcb16/

Dessens, M. (2004, 8 1). *The influence of flow acceleration on stone stability.* Retrieved 2 24, 2015, from repository.tudelft.nl: http://repository.tudelft.nl/view/ir/uuid%3A17f63722-b650-4207-b71d-1ef657f75a0b/

Einstein, A. (1916). Die grundlage der allgemeinen relativitätstheorie. *Annalen der Physik, 354*(7), 769-822.

Einstein, H. A., & El-Samni, E. S. (1949). Hydrodynamic forces on a rough wall. *Reviews of modern physics, 21*(3), 520-524.

Engineering Toolbox. (2015). *Manning's Roughness Coefficient*. Retrieved 5 21, 2015, from engineeringtoolbox.com: http://www.engineeringtoolbox.com/mannings-roughness-d_799.html

George, W. K. (2013). *Lectures in Turbulence for the 21st Century.* Göteborg: Chalmers University of Technology.

Greenblatt, D., & Wygnanski, I. J. (2000). The control of flow separation by periodic excitation. *Progress in Aerospace Sciences, 36*(7), 487-545.

Griendhouthandel. (2015). *(BRUSHWOOD) PRODUCTS*. Retrieved 3 4, 2015, from Griendhouthandel.nl: http://www.griendhouthandel.nl/en/products/

Hoan, N. T. (2008, 11 3). *Master Thesis: Stone stability under non-uniform flow.* Retrieved 2 17, 2015, from repository.tudelft.nl: http://repository.tudelft.nl/view/ir/uuid%3Afbf294c2-0cae-4a04-8dac-d07e051a6081/

Hoffmans, G. (1993). *A study concerning the influence of the relative local turbulence on local-scour holes.* Delft: Rijkswaterstaat, DWW.

Hoffmans, G. (2012). *The influence of turbulence on soil erosion* (Vol. 10). Delft: Eburon Uitgeverij BV.

Hofland, B. (2005). *Rock and roll: Turbulence-induced damage to granular bed protections.* Delft: Delft University of Technology.

Hunt, J. C., Wray, A. A., & Moin, P. (1988). *Eddies, streams, and convergence zones in turbulent flows.* Stanford: NASA.

Jongeling, T., Blom, A., Jagers, H., Stolker, C., & Verheij, H. (2003). *Ontwerpmethodiek granulaire verdedigingen.* Delft: Deltares (WL).

Kasagi, N., & Matsunaga, A. (1995). Three-dimensional particle-tracking velocimetry measurement of turbulence statistics and energy budget in a backward-facing step flow. *International Journal of Heat and Fluid Flow, 16*(6), 477-485.

Kim, H., Kline, S. J., & Reynolds, W. C. (1971). The production of turbulence near a smooth wall in a turbulent boundary layer. *Journal of Fluid Mechanics, 50*(1), 133-160.

Kim, J., Choi, J. I., & Sung, H. J. (2002). Relationship between wall pressure fluctuations and streamwise vortices in a turbulent boundary layer. *Physics of Fluids, 14*(2), 898-901.

Klingmann, B. G., & Alfredsson, P. H. (1989-1993). Turbulent spots in plane Poiseuille flow—Measurements of the velocity field. *Physics of Fluids A: Fluid Dynamics, 2*(12), 2183-2195.

Laufer, J. (1954). *The structure of turbulence in fully developed pipe flow.* Washington: National Bureau of Standards.

Lermusiaux, P. (2011). *Numerical Fluid Mechanics*. Retrieved 5 7, 2015, from ocw.mit.edu: http://ocw.mit.edu/courses/mechanical-engineering/2-29-numerical-fluid-mechanics-fall-2011/lecture-notes/MIT2_29F11_lect_28.pdf

Maynord, S. T. (1995). Corps Riprap Design Guidance for Channel Protection. In S. T. Maynord, C. R. Thorne, S. R. Abt, F. B. Barends, S. T. Maynord, & K. W. Pilarczyk, *River, Coastal and Shoreline Protection: Erosion Control using Riprap and Armourstone.* John Wiley & Sons.

Mohammadi, B., & Pironneau, O. (1993). *Analysis of the k-epsilon turbulence model.* Paris: INRIA.

Morison, J. R., Johnson, J. W., & Schaaf, S. A. (1950). The force exerted by surface waves on piles. *Journal of Petroleum Technology, 2*(05), 149-154.

Moskvitch, K. (2014, 8 5). *Fiendish million-dollar proof eludes mathematicians.* Retrieved 5 7, 2015, from nature.com: http://www.nature.com/news/fiendish-million-dollar-proof-eludes-mathematicians-1.15659

Nakagawa, H., & Nezu, I. (1987). Experimental investigation on turbulent structure of backward-facing step flow in an open channel. *Journal of Hydraulic Research, 25*(1), 67-88.

Nallasamy, M. (1987). Turbulence models and their applications to the prediction of internal flows: a review. *Computers & Fluids, 15*(2), 151-194.

Nikora, V. I., & Smart, G. M. (1997). Turbulence characteristics of New Zealand gravel-bed rivers. *Journal of Hydraulic Engineering, 123*(9), 764-773.

Patnaik, P. C., Pande, P. K., & Vittal, N. (1992). Drag coefficient of a stationary sphere in gradient flow. *Journal of Hydraulic Research, 30*(3), 389-402.

Pilarczyk, K. W. (1995). Simplified unification of stability formulae for revetments under current and wave attack. In S. T. Maynord, C. R. Thorne, S. R. Abt, F. B. Barends, S. T. Maynord, & K. W. Pilarczyk, *River, coastal and shoreline protection: erosion control using riprap and armourstone.* John Wiley & Sons.

Ragheb, M. (2013, 4 1). *Fluid Mechanics, Euler and Bernoulli Equations.* Retrieved 5 18, 2015, from mragheb.com: http://mragheb.com/NPRE%20475%20Wind%20Power%20 Systems/Fluid%20Mechanics%20Euler%20and%20Bernoulli%20Equations.pdf

Rijkswaterstaat. (2015). *De Oosterscheldekering.* Retrieved 6 17, 2015, from rijkswaterstaat.nl: http://www.rijkswaterstaat.nl/water/feiten_en_cijfers/dijken_en_keringen/oosterschelde kering/

Rijkswaterstaat. (2015). *De Oosterscheldekering is een waterkering in Nederland ID313515.* Retrieved 6 17, 2015, from beeldbank.rws.nl: https://beeldbank.rws.nl/ MediaObject/Details/313515

Rijkswaterstaat. (2015). *DWW 228 24 Waddenzee zeedijk tussen Wierum en Holwerd ID330087.* Retrieved 6 7, 2015, from beeldbank.rws.nl: https://beeldbank.rws.nl/MediaObject/ Details/DWW_228_24_Waddenzee_zeedijk_tussen_Wierum_en_Holwerd_330087

Schiereck, G. J. (2004). *Introduction to bed, bank and shore protection.* Delft: CRC Press.

Sheng, J., Meng, H., & Fox, R. O. (2000). A large eddy PIV method for turbulence dissipation rate estimation. *Chemical engineering science, 55*(20), 4423-4434.

Shields, A. (1936). Application of similarity principles and turbulence research to bed-load movement. *Soil Conservation Service.*

Song, T., & Chiew, Y. M. (2001). Turbulence measurement in nonuniform open-channel flow using acoustic Doppler velocimeter (ADV). *Journal of Engineering Mechanics, 127*(3), 219-232.

Soulsby, R. (1997). *Dynamics of marine sands: a manual for practical applications.* London: Thomas Telford.

StatTrek. (2015). *Coefficient of Determination*. Retrieved 7 14, 2015, from StatTrek.com: http://stattrek.com/statistics/dictionary.aspx?definition=coefficient_of_determination

Steenstra, R. S. (2014, 3 13). *Master Thesis: Incorporation of the effects of accelerating flow in the design of granular bed protections.* Retrieved 2 17, 2015, from repository.tudelft.nl: http://repository.tudelft.nl/view/ir/uuid%3A60aa407c-0e87-46b6-97bc-34c0fe3a6183/

Stenen. (2015). *Ardenner grijs breuksteen*. Retrieved 6 23, 2015, from Tuinsteentjes.com: http://tuinsteentjes.com/?product=ardenner-grijs-breuksteen-60-90

Stoutjesdijk, T., Kleine, M. d., Ronde, J. d., & Raaijmakers, T. (2012). *Stormvloedkering Oosterschelde: ontwikkeling ontgrondingskuilen en stabiliteit bodembescherming, Hoofdrapport.* Delft: Deltares.

Tennekes, H., & Lumley, J. L. (1972). *A first course in turbulence.* Cambridge: MIT press.

Townsend, A. A. (1970). Entrainment and the structure of turbulent flow. *Journal of Fluid Mechanics, 41*(1), 13-46.

Tropea, C. (1995). Laser Doppler anemometry: recent developments and future challenges. *Measurement Science and technology, 6*(6), 605-619.

Tuin, H. G., Voortman, H. G., Kamp, R. A., Seinen, W., Vrijling, J. K., & Van der Toorn, A. (2014). An integral feasibility study of a new weir in the lower Rhine. *River Flow 2014* (pp. 2519-2526). Laussane: CRC Press.

Uchiyama, T. (2006). *Comprehensive List of Researchers "Information Knowledge"*. Retrieved 6 24, 2015, from http://is.nagoya-u.ac.jp/: http://is.nagoya-u.ac.jp/research/Pid=29_jhc_data_en.html

Uijttewaal, W. (2015, 9 10). Internal correspondance during graduation at Arcadis. (J. Hoeve, Interviewer)

Van Noortwijk, J. M., & Klatter, H. E. (1999). ptimal inspection decisions for the block mats of the Eastern-Scheldt barrier. *Reliability Engineering & System Safety, 65*(3), 203-211.

Voortman, H. (2015, 8 24). Internal correspondance during graduation at Arcadis. (J. Hoeve, Interviewer)

Voortman, H. G. (2013). *Semi-analytic model for turbulence in open channel flow.* Amersfoort: Arcadis (internal document).

Weisstein, E. W. (2015). *Least Squares Fitting*. Retrieved 7 13, 2015, from mathworld.wolfram.com: http://mathworld.wolfram.com/LeastSquaresFitting.html

Wilczek, M., Stevens, R. J., & Meneveau, C. (2014). Spatio-temporal spectra in the logarithmic layer of wall turbulence: large-eddy simulations and simple models. *Journal Fluid Mechanics, 769*, 1-12.

Xingkui, W., & Fontijn, H. L. (1993). Experimental study of the hydrodynamic forces on a bed element in an open channel with a backward-facing step. *Journal of fluids and structures, 7*(3), 299-318.

Yang, C. T., & Wang, L. K. (2014). *Advances in Water Resources Engineering* (Vol. 14). Springer.

# Appendix A: Bottom protection alternatives

## Loose rock bed protection

Loose rock bed protection is one of the most applied and simple to construct methods of bed protection. Bed protection using loose rock is very easy to realize and the equipment necessary to place the rocks in the river bed are available almost everywhere. Loose rock bed protection will need a filter gradient to reduce winnowing of the underlying sediment (Schiereck, 2004).



Appendix figure 1  Loose rock which can function as bed protection (Stenen, 2015)

## Fascine mattress

Fascine mattress are traditionally used in the Netherlands as part of a bottom protection. Fascine mattress are made out of willow faggots but they can be made from any vegetation that is flexible and strong enough. When the fascine mattresses continuously stay under water during their lifetime, they can last up to a hundred years before needing replacement. Winnowing of the sediment underneath the mattresses is reduced by placing a reed mat or geotextile under the mattress. (Schiereck, 2004). Often, fascine mattresses are applied in combination with loose rock bed protection and geotextile for a robust protection of the bottom.



Appendix figure 2 Fascine mattress with a reed mat underneath. Loose rock is put on top the mattress (Griendhouthandel, 2015)

## Placed blocks and asphalt

Water beds can also be protected by placed blocks or asphalt. Placed blocks are large size boulders that are placed tightly against each other with smaller gravel and sand in between to keep them in place. This configuration can yield very good protection, provided the elements are placed with skill and care (Schiereck, 2004). Water beds under large hydraulic loads can be protected from scour by using asphalt. Constructing asphalt scour protection requires special equipment and regular inspection for damage is necessary, but a well-designed, constructed and maintained asphalt bed protection is very strong and reliable (Schiereck, 2004). Asphalt bed protection is used beside the large placed concrete blocks directly downstream of the Oosterschelde storm surge barrier.



Appendix figure 3 Placed blocks (basalton) bed protection (Rijkswaterstaat, 2015)

## Composite mattresses

Composite mattresses govern some alternative bed protection designs not discussed above. When large areas have to be protected or other factors cause the regular bed protection methods to be inadequate, alternative bed protections are designed. Examples are compositions of concrete block mats, geotextile and steel slags (Van Noortwijk & Klatter, 1999), or a combination of a geometrically closed filters and geotextiles that ascertained lifespan of the bed protection larger than the lifespan of geotextiles alone, in combination with the easy of construction of geotextiles (Schiereck, 2004).
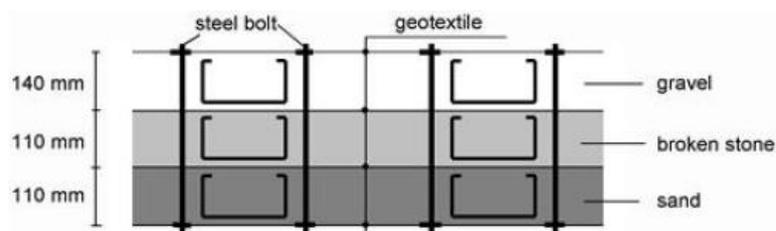


Appendix figure 4  A combination of a geometrically closed filters and geotextiles (Schiereck, 2004, p. 280).

## Appendix B: Forces acting on granular bed protection

The hydraulic load on a grain in general and the forces due to turbulent flow on a grain in particular are discussed here. Looking at the horizontal force, vertical force and moment equilibrium of a single grain in turbulent flow is also called the Izbash approach (Schiereck, 2004). This approach, along with additions found in more recent studies are discussed below.

### Mobilizing forces on a grain
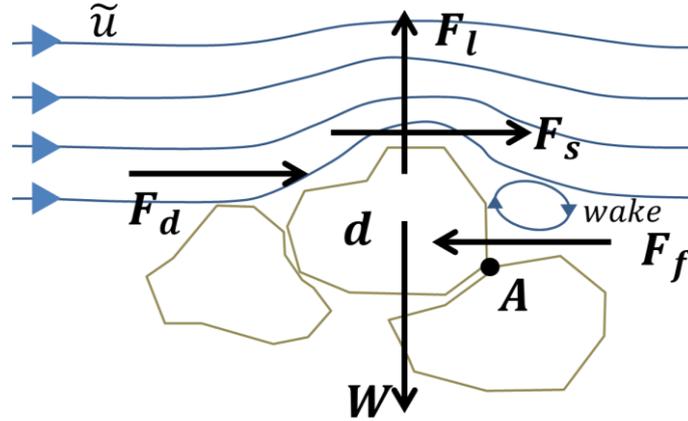


Appendix figure 5 forces on single grain, based on Schiereck (2004)

The primary mobilizing forces on a grain under turbulent flow are the drag force $F_d$, the shear force $F_s$ and the lift force $F_l$ (Schiereck, 2004; Hofland, 2005; Hoan, 2008; Steenstra, 2014). The shear force $F_s$ is the force acting on the grain as a result of friction (due to speed difference) between the flow and the grain. The grain experiences a shear stress due to water flowing over the grain. Viscous stresses are the primary driving horizontal force when particle Reynolds number $Re_*$ is smaller than 3.5 (Hofland, 2005; Hoan, 2008). For Reynolds number larger than 3.5, the laminar flow separates from the particle and a small wake occurs behind the top of the grain. Because of the lower pressure in the wake of the particle compared to the pressure in front of the particle, a net force is observed, $F_d$. At higher Reynolds numbers {$Re_* > 500$ (Hoan, 2008) or $Re_* > 1000$ (Hofland, 2005)} viscous stresses becomes negligible and the horizontal force on the particle is dominated by the drag force. The shear and drag forces are respectively given by:

$$F_s = \frac{1}{2} C_s \rho_w \tilde{u}|\tilde{u}|A_s \tag{B.1}$$

$$F_d = \frac{1}{2} C_d \rho_w \tilde{u}|\tilde{u}|A_d \tag{B.2}$$

Where $C_s$ and $C_d$ are shear and drag coefficients (-), $\rho_w$ the density of water (kg/m³), $\tilde{u}$ the instantaneous flow velocity near the grain, and $A_s$ and $A_d$ the area of the grain affected by shear and drag forces respectively ($A_s$ parallel to flow direction, $A_d$ perpendicular to flow direction). The area $A_{s,d}$ can be the entire projected area or the exposed part of it (Hofland, 2005). The shear and drag coefficients are dependent on the particle Reynolds number, but for large Reynolds numbers the coefficient are almost constant (Hofland, 2005).

The lift force $F_l$ is the result of the increased flow velocity above the grain relative to the flow velocity underneath the grain. The Bernoulli law states that an increase in flow velocity equals a reduction of pressure. This results in a lower pressure working on top of the particle compared to the bottom of the particle, thus a net lift force. Hofland (2005), simplified the formula of Auton

(1987) for the lift force on a sphere in inviscid, rotational flow. This transformation resulted in the following familiar equation:

$$F_l = \frac{1}{2} C_l \rho_w \tilde{u}^2 A_l \qquad\qquad (B.3)$$

Where $C_l$ is the lift coefficients (-), and $A_l$ the area of the particle affected by the lift force (parallel to the flow direction). $A_l$ can be the plan area of the stone or a representative area around the protruding stone (Hofland, 2005). Different definitions of $A_l$ result in different lift coefficents $C_l$.

"A negative $v$ (flow velocity in negative $y$ direction, see figure 13) directly creates larger drag forces. It can be conceived as that a downward directed flow increases the exposed area of the stone, and hence increases the drag force (…) downward directed flow creates negative (stabilising) lift forces" (Hofland, 2005, p. 85-86). So the drag force is also affected by the vertical flow velocity. However, Hofland (2005) does not propose an adjusted drag formula incorporating this.

### Stabilizing forces on a grain
The force $W$ equals the gravitational force of the particle (Schiereck, 2004). Because the particle is submerged, the relative weight is used:

$$W = V(\rho_r - \rho_w)g \qquad\qquad (B.4)$$

Where $W$ equals the gravitational force (N), $V$ equals the volume of the particle (m³), $\rho_r$ equals the density of the particle (kg/m³) and $g$ equals the gravitational constant (m/s²).

$F_f$ equals the friction force working on the particle due to friction with the underlying particles. $F_f$ is a balancing force that counters the mobilizing forces (Schiereck, 2004). The gravitational force $W$ and friction force $F_f$ are also shown in appendix figure 5.

### Determining the flow velocity affecting the grain
The mobilizing forces $F_s$ $F_d$ and $F_l$ are all a function of the flow velocity squared. However, due to the assumption of zero flow velocity at the surface of the grain, it is unclear which flow velocity is used to calculate the forces. The flow velocity near the bed has a large vertical gradient making the coefficients of the shear, drag and lift forces very sensitive to the choice of the y-coordinate (Hofland, 2005). The coefficients depend on the flow pattern around the bed particle and the method of estimating $\tilde{u}$ (Hoan, 2008). Several different methods of estimating $\tilde{u}$ have been used. Einstein and El-Samni (1949) determined the lift coefficients by measuring the flow velocity at 0.35 grain diameters above the theoretical wall. Coleman (1972) measured the flow velocity $\tilde{u}$ at the centre of the grain (sphere), but noted that: "This definition is slightly in error for a sphere on a boundary, because in this case the skin friction forces which make up part of the total drag are not symmetrically distributed over the sphere" (Coleman, 1972, p. 17). Patnaik, Pande, and Vittal (1992) also calculated $\tilde{u}$ at the centre of the particle and furthermore concluded that: "… among the various reference velocities adopted by different investigators in the past, the velocity at the centre level of the sphere (…) appears more suitable" (Patnaik, Pande, & Vittal, 1992, p. 401).

## Force and moment balance
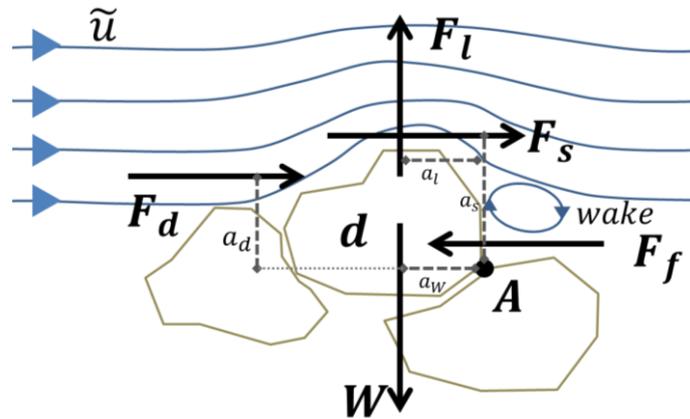


Appendix figure 6, forces and moments on single grain, based on Schiereck (2004) $a_d, a_w, a_s$ and $a_l$ are the distances to the rotation point of the similarly named forces

For a grain to remain stationary on the bed, the net forces and moments of the grain should be zero. The horizontal shear and drag forces will be cancelled by the horizontal friction force when the grain is stationary. The lift force will be cancelled out by the gravitation force and the vertical components of the friction force. The shear and drag forces can also have an vertical component that are cancelled by the gravitational force and friction force, assuming the vertical component of the shear and drag force is directed to the water surface. Appendix figure 6 also shows the rotation point $A$ of the grain. The mobilizing forces are expected to generate a clockwise moment. This moment is balanced by the gravitational force generating a counter-clockwise moment. In formula notation above is given by (assuming no vertical components for the drag and shear forces):

$$\left.\begin{aligned} \sum H &= 0: F_{s,d} = F_f \\ \sum V &= 0: F_l = W \\ \sum M &= 0: F_{s,d,l} \times a_{s,d,l} = W \times a_w \end{aligned}\right\} \rho_w \tilde{u}_c{}^2 d^2 \propto (\rho_r - \rho_w)gd^3 \quad \text{(B.5)}$$

Where $a_{s,d,l,w}$ equals the distance perpendicular to the force towards the rotation point (m), $d$ the characteristic grain diameter (m) and $\tilde{u}_c$ equals the instantaneous flow velocity for which $f_l = W$ (m/s). Equation B.5 based on Schiereck (2004, p. 49).

Equation B.5 states that for a grain that is just stationary, the critical flow velocity is proportional to:

$$u_c \propto (\rho_r - \rho_w)gd \qquad \text{(B.6)}$$

All formulae on grain stability contain some form of to this proportionality (Schiereck, 2004).

## Variable flow velocity due to turbulence
The formulas for the shear, drag and lift forces use the velocity measured at a certain location above the grain. In turbulent flow, the fluctuation of the flow velocity near the bed can have the same order of magnitude as the average flow velocity (Hofland, 2005). The flow velocity near the bed can be characterized as containing a mean and a fluctuating part as defined in the main text. The formulae for shear, drag and lift can be adjusted to incorporate a mean flow, and the deviations from this mean flow. The total mobilizing forces on a grain are than given by:

$$F_{s,d,l} = \bar{F}_{s,d,l} + \acute{F}_{s,d,l} \tag{B.7}$$

Where $\bar{F}_{s,d,l}$ equals the forces as the result of the mean flow (N), and $\acute{F}_{s,d,l}$ the forces as the result of the instantaneous velocity fluctuations. Hofland (2005) defined the drag force $\acute{F}_d$ as the result of the fluctuating velocity profile:

$$\acute{F}_d \propto \bar{u}\acute{u} + \frac{1}{2}\acute{u}^2 - \frac{1}{2}\sigma(\tilde{u})^2 \tag{B.8}$$

With $\tilde{u}$ the total instant flow velocity (m/s), $\sigma$ the standard deviation, $\bar{u}$ the time average flow velocity (to average out turbulent fluctuations) (m/s) and $\acute{u}$ the fluctuating flow velocity (m/s).

The lift force $\acute{F}_l$ can be written similarly according to Steenstra (2014):

$$\acute{F}_l \propto \bar{u}\acute{u} + \frac{1}{2}\acute{u}^2 - \frac{1}{2}\sigma(\tilde{u})^2 \tag{B.9}$$

Radecke & Schulz-DuBois (1988) as referenced by Hofland (2005) and Hoan (2008) defined a different formula for the fluctuating part of the lift force:

$$\acute{F}_l \propto a\bar{u}\acute{u} + b\bar{u}\acute{v} \tag{B.10}$$

Where $\acute{v}$ equals the deviations of the mean flow in vertical direction (m/s), $\acute{u}$ equals the deviations of the mean flow in horizontal direction (m/s), and $a$ and $b$ are factors for coefficients. The first term originates from the linear expansion of equation B.3 using equation 3.1 and neglecting the higher order terms. "The second term is due to the fact that the instantaneous flow direction does not have to be horizontal like the mean flow. Therefore, the instantaneous force in line with the velocity can have a vertical component" (Hofland, 2005, p. 22).

From formula B.8 and B.9 it follows that the fluctuating part of the flow velocity can exert a mobilizing force in the same order of magnitude as the time averaged flow velocity. The fluctuation part of the flow velocity is therefore important to consider when studying particle mobilization. The forces $\acute{F}_d$ and $\acute{F}_l$ are also called the quasi steady forces (Hofland, 2005; Hoan, 2008; Steenstra, 2014).

### Accelerating flow
Beside flow velocity, the acceleration of flow also exerts a net force on a particle due to pressure differences, see Appendix figure 7.
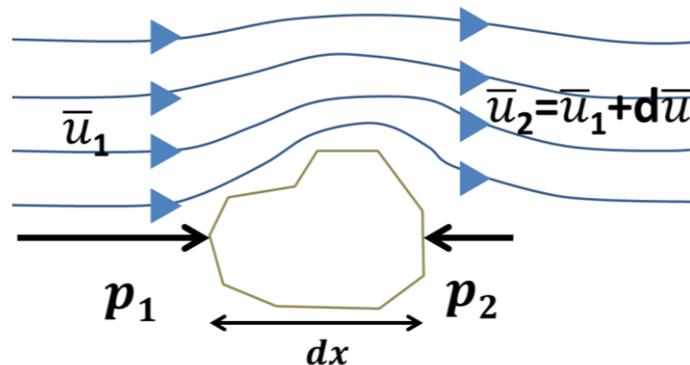


Appendix figure 7, Flow acceleration over a single grain, (based on Dessens, 2004)

Due to an increase in flow velocity over the particle, the pressure at the end of the particle is

lower than the pressure at the beginning, resulting in a net force in the flow direction. The combination of the drag force $F_d$ on the particle and the force exerted on the particle due to flow acceleration is often called the Morison equation (Steenstra, 2014). Dessens (2004) rewrote the formula of Morison, Johnson, and Schaaf (1950) in a more general form, the flow acceleration force in this general form equalled:

$$F_a = C_m \rho_w \bar{u} \frac{d\bar{u}}{dx} \tag{B.11}$$

Where $C_m$ equals the coefficient that accounts for the effects of flow acceleration.

It is important to note that turbulence intensities and the Reynolds stress decrease in accelerating flow and increase in decelerating flow, when compared with those in uniform flow (Song & Chiew, 2001). As was already mentioned by Steenstra (2014), an accelerating flow will therefore be accompanied by a reduced fluctuating drag and lift force. Vice versa, a decelerating flow (which results in an increased turbulence intensity) will be accompanied by an "acceleration" force $F_a$ that is directed in the opposite direction of the drag force $F_d$, effectively reducing the net drag force. This means that flow acceleration as a mobilizing force is always accompanied by a decrease in the turbulence mobilizing forces and flow deceleration as a stabilizing force is always accompanied by an increase in the turbulence mobilizing forces. Huijsmans (2006) measured stone stability under accelerating flow and found results indicating that under certain conditions, flow acceleration actually resulted in a more stable bed (possibly due to a decrease in turbulence).

### Turbulence wall pressure

Beside the steady forces due to mean flow and the quasi steady forces due to fluctuating flow, a third force generating mechanism is affecting a grain under turbulent flow, the turbulence wall pressures (Hofland, 2005). Within the boundary layer, flow over either rough or smooth walls is turbulent when the flow outside of the boundary layer is turbulent (Blake, 1970; Kim, Kline, & Reynolds, 1971). Turbulent flow can be described in terms of individual events or streamline patterns, for example by defining turbulence as a large set of vortices (Hunt, Wray, & Moin, 1988). Generation of wall pressure fluctuations is associated with the streamwise vortices in the vicinity of the wall (Kim, Choi, & Sung, 2002). The temporal changes in flow speeds as a result of turbulent vortices change the pressure on the wall following Bernoulli's law. Turbulence wall pressure fluctuations, when integrated over a stone, will result in net forces on the stone (Hofland, 2005).
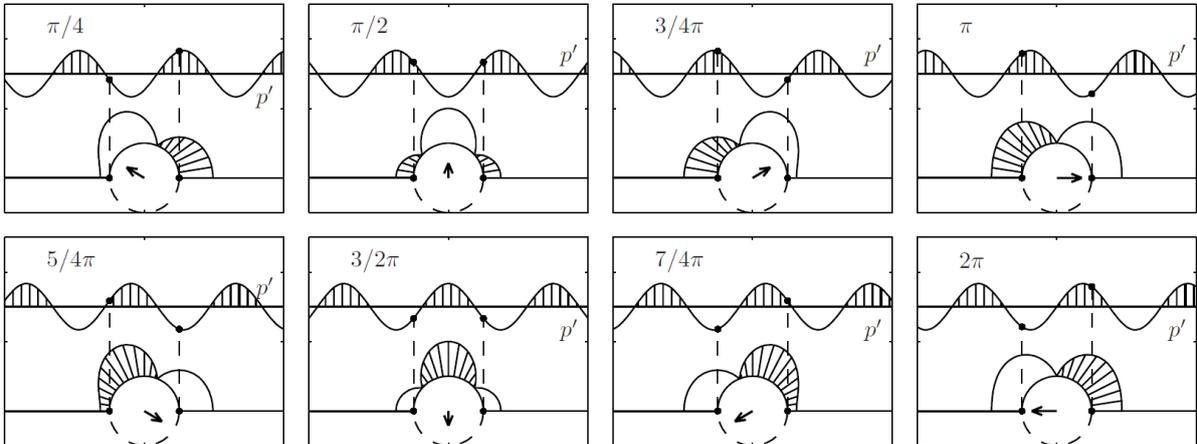


Appendix figure 8, Change of the integrated force on a stone due to a convected frozen pressure field (Hofland, 2005, p. 101)

The figure above shows the resulting net force on a particle as a vortex moves over the particle. A vortex is transported along with the average flow direction, causing the vortex to influence a particle according to the 8 steps shown above. The force vector covers all directions, including the direction where it generates the largest moment around the rotation point of the stone (Hofland, 2005). Thus, the turbulence wall pressure theoretically has the ability to act as a mobilizing force. For an explanation of how vortices result in an extra drag and lift force on the particle, refer to Hofland (2005, p. 94-100). Hofland (2005) found that the turbulence wall pressure becomes more important for particles that are only little exposed to flows but where the flow is highly turbulent, whereas the quasi steady forces discussed above are more important for more exposed particles.

### Dominant forces for the initiation of granular scour

The mobilizing forces described above can all initiate granular scour. However, the relative size of the mobilizing forces described above differ. At higher Reynolds numbers {$Re_* > 500$ (Hoan, 2008) or $Re_* > 1000$ (Hofland, 2005)} viscous stresses becomes negligible (Burden, 2008) and the horizontal force on the particle is dominated by the drag force. Thus the shear force is not relevant for the initiation of granular material under high Reynolds numbers but the drag force is. The lift force showed similar magnitudes as the drag force according to Hofland (2005) but the lift force can become negative under certain flow conditions. This results in larger drag forces but also a stabilizing lift force. It is concluded that the lift and drag force are important forces to consider in granular scour, but the effects of the lift forces are less straight forward than the drag forces.

In turbulent flow, the fluctuation of the flow velocity near the bed can have the same order of magnitude as the average flow velocity (Hofland, 2005). Therefore, the fluctuating components of the drag and lift forces are relevant forces when considering the initiation of granular scour.

The extra force due to acceleration appears to be of the same order as the force due to the flow velocity. Therefore, when looking at the stone stability in an accelerated flow, it is important to take the force generated by the acceleration into account (Dessens, 2004).

Hofland (2005) found that the turbulence wall pressure becomes more important for particles that are only little exposed to flows but where the flow is highly turbulent, whereas the quasi steady forces are more important for more exposed particles. Exposed grains are most likely to initiate movement due to a larger area $A_{d,l}$ on which the drag and lift forces work. Therefore, for the initiation of granular scour, turbulence wall pressure is less relevant to consider because it is only important for particles that are only little exposed to flows, whereas the first grains to start moving are the most exposed ones.

## Appendix C: The adjusted Shields parameter leading to bed protection design

To assess the stability of loose rock as bed protection, the Shields parameter (Shields, 1936) is most often used. The Shields parameter is defined as the ratio between shear stress and the submerged weight and characteristic sieve size of the sediment (The Rock Manual, 2007).

$$\Psi = \frac{\tau}{(\rho_r - \rho_w)gD} \qquad \qquad \text{(C.1)}$$

Where $\Psi$ is the Shields parameter (-), $\tau$ the bed shear stress (N/m²), $\rho_r$ and $\rho_w$ the density of the stone and water respectively (kg/m³), g the gravitational constant (m/s²), and $D$ the characteristic sieve size of the sediment (m).

The Shields parameter is based on a simplification of reality. Critical phenomena effecting loose rock transport that are not taken into account are: a changing depth or velocity profile, turbulence amplification, wave amplification, non-horizontal bed slope (The Rock Manual, 2007), flow acceleration, dynamic drag, and lift forces (Hofland, 2005). Multiple factors were developed to adjust the Shields parameter to take into account some of the above mentioned phenomena. A factor was introduced to incorporate the effects of waves on the mobility of stones based on the work of Bijker (1967). A factor was introduced to incorporate a sloping bed reducing the stabilizing forces of gravity on the bed protection, based on the work of Soulsby (1997). A factor was introduced to incorporate effects of turbulent flow on the mobility of bed protection. Also, a factor was introduced to incorporate effects of depth velocity profiles on the mobility of bed protection (The Rock Manual, 2007). This resulted in the following formula including all adjustment factors discussed above:

$$\frac{\bar{\bar{u}}^2/2g}{\Delta D} = k_{sl}k_t{}^{-2}k_w{}^{-1}\Lambda_h\Psi_{cr} \qquad \qquad \text{(C.2)}$$

Where $\bar{\bar{u}}$ equals the depth and time averaged flow velocity (m/s), g the gravitational constant (m/s²), $\Delta$ the relative buoyancy $\frac{\rho_r - \rho_w}{\rho_w}$ (-), $D$ the characteristic sieve size of the sediment (m), $k_{sl}$ the slope reduction factor (-), $k_t$ the turbulence amplification factor (-), $k_w$ the wave amplification factor, $\Lambda_h$ the depth of velocity profile factor (-), and $\Psi_{cr}$ the critical Shield parameter (-) (The Rock Manual, 2007).

Equation C.2 has been used as the basis for stability formulae to help design granular bed protection, see for example Pilarczyk (1995) or Maynord, (1995). A number of adjusted critical Shields formulae have been suggested by various authors, most of them only suitable for the design of loose rock bed protection, and they tend to give quite different results in terms of required stone size (The Rock Manual, 2007). As an example, the design formula of Pilarczyk (1995) is discussed, which has been used extensively for the design of bed protection under current attack (The Rock Manual, 2007). Pilarczyk (1995) defined the following formula:

$$D = \frac{\phi_{sc}}{\Delta}\frac{0.035}{\Psi_{cr}}k_h k_{sl}{}^{-1}k_t{}^2\frac{\bar{\bar{u}}^2}{2g} \qquad \qquad \text{(C.3)}$$

Where D equals the characteristic size of the protection element (m), $D = D_{50}$ for armourstone, $\phi_{sc}$ equals a stability factor (-), and $\bar{\bar{u}}$ equals the depth and time averaged flow velocity.

Pilarczyk (1995) uses the following formula to determine $k_t$

$$k_t = \frac{1 + 3r}{1.3} \qquad\qquad\qquad (C.4)$$

Where $r$ equals the relative turbulence intensity (-).

The Rock Manual (2007) advises $k_t^2 = 1$ for normal turbulence, $k_t^2 = 2$ for sharp outer bends, and $k_t^2 > 2$ for the additional turbulence as the result of propeller jet velocities. When assuming that all other factors remain the same, than the effect of the different turbulence levels can easily be found using equation C.3. For a flow situation with an sudden increase in turbulence (and ceteris paribus) the required stone diameter is increased by 100%. An increase of 100% in stone diameter results in an increase of 800% in required stone mass (mass $\propto$ diameter$^3$).

## Appendix D: Differentiating the Bernoulli formula

The Bernoulli formula is given by:

$$H = z + h + \frac{1}{2}\frac{\bar{\bar{u}}^2}{g}$$

Differentiating in the flow direction gives

$$\frac{dH}{dx} = \frac{dz}{dx} + \frac{dh}{dx} + \frac{d}{dx}\left(\frac{1}{2}\frac{\bar{\bar{u}}^2}{g}\right)$$

Assume $\bar{\bar{u}}^2 = J$, then by applying the chain rule:

$$\frac{d}{dx}\left(\frac{1}{2}\frac{\bar{\bar{u}}^2}{g}\right) = \frac{1}{2g}\frac{d}{dx}(J)$$

$$\frac{1}{2g}\frac{d}{dx}(J) = \frac{1}{2g}\frac{dJ}{d\bar{\bar{u}}}\frac{d\bar{\bar{u}}}{dx}$$

$$\frac{dJ}{d\bar{\bar{u}}} = \frac{d\bar{\bar{u}}^2}{d\bar{\bar{u}}} = 2\bar{\bar{u}}$$

Which gives:

$$\frac{dH}{dx} = \frac{dz}{dx} + \frac{dh}{dx} + \frac{1}{g}\bar{\bar{u}}\frac{d\bar{\bar{u}}}{dx}$$

## Appendix E: Calculating the momentum just downstream the step

In this appendix, a method will be described how the momentum at an infinitesimal distance downstream of a BFS can be approximated.

The formula for momentum in a (horizontal) flow is given by (Battjes, 1990):

$$M = \frac{1}{2}\rho_w g h^2 + \rho_w \beta h \bar{\bar{u}}^2$$

Where $M$ equals the momentum (N/m), $\rho_w$ equals the density of water (kg/m³), $g$ the gravitational constant (m/s²), $\bar{\bar{u}}$ equals the depth and time averaged flow velocity (m/s) and $\beta$ a coefficient that corrects the momentum for non-uniformity of the flow profile (-).

The $\beta$ coefficient for a 2 dimensional flow (neglecting variations in the width) is given by:

$$\beta = \frac{1}{h}\int_0^h (\bar{u}/\bar{\bar{u}})^2 \, dy$$

Where $h$ equals the water depth (m), $\bar{u}$ the (time averaged) flow velocity (m/s) at a certain depth $y$, $\bar{\bar{u}}$ the time and depth averaged flow velocity (m/s), and $y$ the distance from the bottom of the flume (m).

Assume water flowing over a BFS as depicted by appendix figure 9. Because of the log-law flow velocity profile of $\bar{u}_1$ (on top of the step), $\bar{\bar{u}}_1 \approx \bar{u}_1$(at any depth) and therefore $\beta \approx 1$ (on top of the step). Just downstream of the step, the flow velocity profile above the step has not yet adjusted to the increased water depth. It is hypothesized that just downstream of the step, the flow profile $\bar{u}$ remain intact (and equal to $\bar{u}_1$) for the water flowing above (but downstream of) the step (step part of the cross section). The water in the recirculation zone just downstream of the step is affected by the presence of the walls. Therefore, in practice it is often assumed that very close the step, the water is standing still in the recirculation zone, thus $\bar{u}_1 \approx 0$ in the recirculation zone part of the cross section.
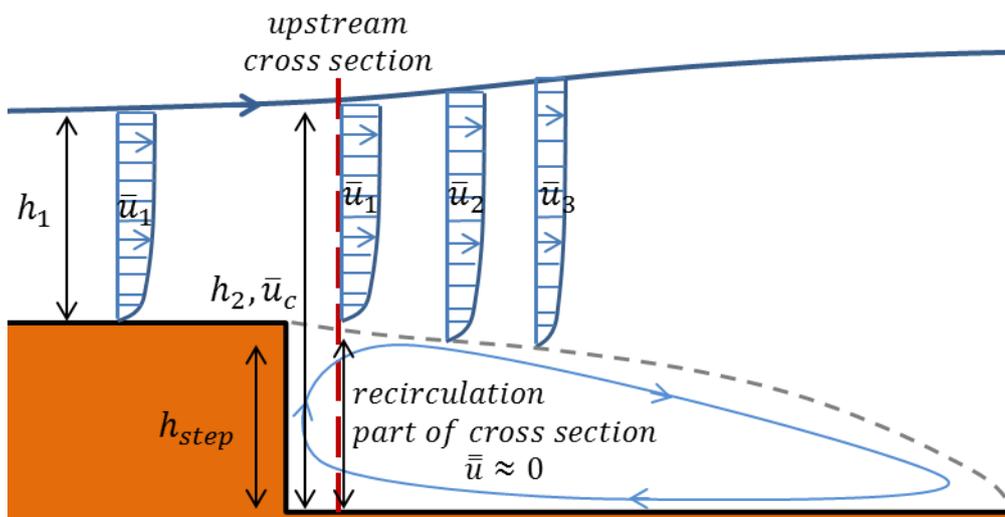


Appendix figure 9 Velocity profile at an infinitely small distance downstream of the step

For the flow situation described above, the momentum at the (red) cross section can be

calculated. First, the $\beta$ coefficient needs to be determined for the cross section. The flow velocity field at the cross section in appendix figure 9 is defined mathematically as:

$$\bar{u}_c = \begin{cases} 0, & y < h_{step} \\ \bar{\bar{u}}_1, & y \geq h_{step} \end{cases}$$

Where $\bar{u}_c$ is the time averaged flow velocity (m/s) (at the cross section) at a certain depth $y$, with $y = 0$ at the bottom of the flume, $y = h_2$ at the water surface (m). The term $\bar{\bar{u}}_1$ is the depth and time averaged flow velocity on top of the step (m/s). The depth and time averaged profile is used because it is assumed that the flow velocity on top of the step is roughly uniform, thus $\bar{\bar{u}}_1 \approx \bar{u}_1$. The depth and time averaged value for $\bar{u}_c$ then equals:

$$\bar{\bar{u}}_c = \frac{(h_{step} - 0) \times 0 + (h_2 - h_{step}) \times \bar{\bar{u}}_1}{h_2} = \left(1 - \frac{h_{step}}{h_2}\right) \times \bar{\bar{u}}_1$$

The formula for the $\beta$ coefficient is given by:

$$\beta = \frac{1}{h_2} \int_0^{h_2} (\bar{u}/\bar{\bar{u}})^2 \, dy$$

Filling in $\bar{\bar{u}}_c$ and $\bar{u}_c$ gives:

$$\beta = \frac{1}{h_2} \int_0^{h_2} (\bar{u}_c/\bar{\bar{u}}_c)^2 \, dy$$

First solve $\bar{u}_c/\bar{\bar{u}}_c$:

$$\bar{u}_c/\bar{\bar{u}}_c = \begin{cases} 0, & y < h_{step} \\ \dfrac{\bar{u}_c}{\left(1 - \dfrac{h_{step}}{h_2}\right) \times \bar{\bar{u}}_1}, & y \geq h_{step} \end{cases}$$

$\bar{u}_c = \bar{\bar{u}}_1$ for $y \geq h_{step}$ thus:

$$\bar{u}_c/\bar{\bar{u}}_c = \begin{cases} 0, & y < h_{step} \\ \dfrac{1}{\left(1 - \dfrac{h_{step}}{h_2}\right)}, & y \geq h_{step} \end{cases}$$

Squared gives:

$$(\bar{u}_c/\bar{\bar{u}}_c)^2 = \begin{cases} 0, & y < h_{step} \\ \dfrac{1}{\left(1 - \dfrac{h_{step}}{h_2}\right)^2}, & y \geq h_{step} \end{cases}$$

Filling above formula into the equation for $\beta$ gives:

$$\beta = \frac{1}{h_2} \left( \int_0^{h_{step}} (\bar{u}_c/\bar{\bar{u}}_c)^2 \, dy + \int_{h_{step}}^{h_2} (\bar{u}_c/\bar{\bar{u}}_c)^2 \, dy \right)$$

$$\beta = \frac{1}{h_2} \left( [0]_0^{h_{step}} + \left[ \frac{y}{\left(1 - \frac{h_{step}}{h_2}\right)^2} \right]_{h_{step}}^{h_2} \right)$$

$$\beta = \frac{1}{h_2} \left( 0 + \frac{h_2 - h_{step}}{\left(1 - \frac{h_{step}}{h_2}\right)^2} \right)$$

$$\beta = \frac{\frac{h_2 - h_{step}}{h_2}}{\left(1 - \frac{h_{step}}{h_2}\right)^2}$$

$$\beta = \frac{\left(1 - \frac{h_{step}}{h_2}\right)}{\left(1 - \frac{h_{step}}{h_2}\right)^2}$$

$$\beta = \frac{1}{\left(1 - \frac{h_{step}}{h_2}\right)}$$

The $\beta$ coefficient is now inserted into the formula of momentum in a flow:

$$M = \frac{1}{2}\rho_w g h_2^2 + \rho_w \beta h_2 \bar{\bar{u}}_c^2$$

$$M = \frac{1}{2}\rho_w g h_2^2 + \rho_w \frac{1}{\left(1 - \frac{h_{step}}{h_2}\right)} h_2 \bar{\bar{u}}_c^2$$

The term $\bar{\bar{u}}_c$ was defined as:

$$\bar{\bar{u}}_c = \left(1 - \frac{h_{step}}{h_2}\right) \times \bar{\bar{u}}_1$$

Thus:

$$M = \frac{1}{2}\rho_w g h_2^2 + \rho_w h_2 \frac{1}{\left(1 - \frac{h_{step}}{h_2}\right)} \left( \left(1 - \frac{h_{step}}{h_2}\right) \times \bar{\bar{u}}_1 \right)^2$$

$$M = \frac{1}{2}\rho_w g h_2^2 + \rho_w h_2 \frac{\left(1 - \frac{h_{step}}{h_2}\right)}{\left(1 - \frac{h_{step}}{h_2}\right)} \left(1 - \frac{h_{step}}{h_2}\right) \times \bar{\bar{u}}_1^2$$

$$M = \frac{1}{2}\rho_w g h_2^2 + \rho_w h_2 \left(1 - \frac{h_{step}}{h_2}\right) \times \bar{\bar{u}}_1^2$$

$$M = \frac{1}{2}\rho_w g h_2{}^2 + \rho_w(h_2 - h_{step}) \times \bar{\bar{u}}_1{}^2$$

Or in words, the momentum just downstream of the step is defined by a hydrostatic part $\frac{1}{2}\rho_w g h_2{}^2$ that acts over the whole water depth $h_2$ and a kinetic part $\rho_w(h_2 - h_{step}) \times \bar{\bar{u}}_1{}^2$ that is only present in the upper water column ($h_2 - h_{step}$ see appendix figure 9).

# Appendix F: Calculate the water depth using the conservation of momentum

Assume that the momentum of a flow at location 1, $M_1$ is known. For a location 2, down or upstream of location 2, the momentum is then given by:

$$M_2 = \frac{1}{2}\rho_w g(h_2)^2 + \rho_w h_2 \bar{\bar{u}}_2{}^2$$

The conservation of mass is given by:

$$q = \bar{\bar{u}}_1 \times h_1 = \bar{\bar{u}}_2 \times h_2$$

If the momentum is preserved than:

$$M_1 = M_2$$

This gives:

$$M_1 - \frac{1}{2}\rho_w g(h_2)^2 - \rho_w h_2 \bar{\bar{u}}_2{}^2 = 0$$

$$M_1 - \frac{1}{2}\rho_w g(h_2)^2 = \rho_w h_2 \bar{\bar{u}}_2{}^2$$

$$\frac{M_1 - \frac{1}{2}\rho_w g(h_2)^2}{\rho_w \bar{\bar{u}}_2{}^2} = h_2$$

Inserting conservation of mass:

$$\frac{M_1 - \frac{1}{2}\rho_w g(h_2)^2}{\rho_w \frac{q^2}{h_2^2}} = h_2$$

Above formula can be solved analytically, or using a program like Mathcad or Matlab. The solution is not depicted here because of its complexity.

# Appendix G: Finding an analytical solution for the Arcadis Turbulence Model

The ATM is used with the assumption of a constant turbulent energy production term:

$$\frac{d\bar{k}}{dx} = -gD - \alpha\frac{\bar{k}}{R}$$

Because the ATM is a nonhomogeneous differential equation, the homogenous and particular part are solved separately.

## The homogeneous part

$$\frac{d\bar{k}}{dx} = -\alpha\frac{\bar{k}}{R}$$

$$\frac{1}{\bar{k}}d\bar{k} = \frac{-\alpha}{R}dx$$

$$\ln \bar{k} = \frac{-\alpha}{R}x + T$$

Where $T$ equals an integration constant.

$$\bar{k} = e^{\frac{-\alpha}{R}x+T}$$

$$\bar{k} = e^T e^{\frac{-\alpha}{R}x}$$

$$\bar{k} = Ae^{-\frac{\alpha}{R}x}$$

Where $A$ is the rewritten integration constant $A = e^T$

## Particular part

Trial solution:

$$\bar{k}_{(part)} = B$$

Gives:

$$\frac{B}{dx} = -gD - \alpha\frac{B}{R}$$

$$0 = -gD - \alpha\frac{B}{R}$$

$$gD = -\frac{\alpha}{R}B$$

$$-\frac{gDR}{\alpha} = B$$

## Total solution

Combining the homogeneous and particular solution gives:

$$\bar{k} = Ae^{-\frac{\alpha}{R}x} - \frac{gDR}{\alpha}$$

The integration constant $A$ can be solved by assuming an initial value for $k$

Assume that $k(0) = \bar{k}_0$ then:

$$\bar{k}_0 = Ae^{-\frac{\alpha}{R}0} - \frac{gDR}{\alpha}$$

$$\bar{k}_0 = A - \frac{gDR}{\alpha}$$

$$\bar{k}_0 + \frac{gDR}{\alpha} = A$$

Thus the total solution is given by:

$$\bar{k} = \left(\bar{k}_0 + \frac{gDR}{\alpha}\right)e^{-\frac{\alpha}{R}x} - \frac{gDR}{\alpha}$$

Following are some checks to make sure the solution is correct:

Filling in $x = 0$ gives:

$$\bar{k} = \left(\bar{k}_0 + \frac{gDR}{\alpha}\right)e^{-\frac{\alpha}{R}0} - \frac{gDR}{\alpha}$$

$$\bar{k} = \left(\bar{k}_0 + \frac{gDR}{\alpha}\right)1 - \frac{gDR}{\alpha}$$

$$\bar{k} = k_0$$

Differentiating $\bar{k}$ gives:

$$\frac{d\bar{k}}{dx} = \frac{d}{dx}\left(\bar{k}_0 + \frac{gDR}{\alpha}\right)e^{-\frac{\alpha}{R}x} - \frac{d}{dx}\frac{gDR}{\alpha}$$

$$\frac{d\bar{k}}{dx} = -\frac{\alpha}{R}\left(\bar{k}_0 + \frac{gDR}{\alpha}\right)e^{-\frac{\alpha}{R}x}$$

$$-\frac{R}{\alpha}\frac{d\bar{k}}{dx} - \frac{gDR}{\alpha} = \left(\bar{k}_0 + \frac{gDR}{\alpha}\right)e^{-\frac{\alpha}{R}x} - \frac{gDR}{\alpha}$$

$$-\frac{R}{\alpha}\frac{d\bar{k}}{dx} = k + \frac{gDR}{\alpha}$$

$$\frac{d\bar{k}}{dx} = -\frac{\alpha}{R}\frac{gDR}{\alpha} - \frac{\alpha}{R}\bar{k}$$

$$\frac{d\bar{k}}{dx} = -gD - \frac{\alpha}{R}\bar{k}$$

Thus a correct solution was found

## Appendix H: Reducing the Arcadis Turbulence Model to the model of Hoffmans

The ATM is given by:

$$\frac{d\bar{k}}{dx} = -g\frac{dH}{dx} - \alpha\frac{\bar{k}}{R}$$

Under stationary uniform turbulent flow with a gradual sloping bed turbulence reaches an equilibrium where it does not change as a function of the distance anymore. Due to the turbulence flowing into the study area $k > 0$. This gives:

$$-g\frac{dH}{dx} = \alpha\frac{\bar{k}}{R}$$

Under stationary uniform flow under a slope, the change in head levels equals the bottom friction due to Chezy:

$$-g\frac{dH}{dx} = g\frac{\bar{\bar{u}}^2}{C^2}$$

Thus:

$$g\frac{\bar{\bar{u}}^2}{C^2} = \alpha\bar{k}$$

$$\bar{k} = \frac{1}{\alpha}\frac{g}{C^2}\bar{\bar{u}}^2$$

Turbulence intensity is given by:

$$r = \frac{\sqrt{\bar{k}}}{\bar{\bar{u}}}$$

Equilibrium turbulence intensity under stationary, uniform flow is given by (Hoffmans,1993):

$$r_0 = c_0\frac{\sqrt{g}}{C}$$

Where $c_0 = 1.21$. Rewriting equilibrium turbulence intensity into equilibrium turbulent energy (combining the above two equations):

$$k_e = (r_0\bar{\bar{u}})^2$$

$$k_e = \left(c_0\frac{\sqrt{g}}{C}\right)^2\bar{\bar{u}}^2$$

$$k_e = c_0^2\frac{g}{C^2}\bar{\bar{u}}^2$$

$$k_e = c_0^2\frac{g}{C^2}\bar{\bar{u}}^2$$

Under stationary uniform flow under a slope the ATM is reduced to:

$$\bar{k} = \frac{1}{\alpha} \frac{g}{C^2} \bar{\bar{u}}^2$$

Equilibirum turbulence levels according to Hoffmans (1993) are given by:

$$k_e = c_0^2 \frac{g}{C^2} \bar{\bar{u}}^2$$

Thus $k = k_e$ when $\alpha = \frac{1}{c_0^2}$

## Appendix I: Deriving the ATM production term using the TKE

This appendix describes under what assumptions the production of turbulence according to the TKE confirms with the production of turbulence according to the ATM. The derivation presented in this appendix is divided into 5 steps:

1. Introduction of the turbulent and mean flow kinetic energy equations
2. Simplifying the TKE and MKE
3. Rewriting and simplifying the MKE
4. Linking the Bernoulli equation to the MKE equation
5. Relating the MKE to the TKE and to the production term of the ATM

### 1. Introduction of the turbulent and mean flow kinetic energy equations

The turbulent kinetic energy equation (TKE) is given by:

$$\frac{dk}{dt} + \bar{u}_j \frac{dk}{dx_j} = \frac{d}{dx_j}\left( -\frac{1}{\rho_w}\, \bar{p}u_i'\delta_{ij} - \frac{1}{2}u_i'u_i'u_j' + v\frac{dk}{dx_j} \right)$$
$$- u_i'u_j'\frac{d\bar{u}_i}{dx_j} - v\frac{du_i'}{dx_j}\frac{du_i'}{dx_j} \tag{I.1}$$
$$\delta_{ij}\begin{cases}0 \; if \; i \neq j \\ 1 \; if \; i = j\end{cases}$$

Where $k$ equals the turbulent energy in the flow (m²/s²), $t$ equals the time (s), $\bar{u}_i$ equals the time averaged flow velocity (m/s), $\rho_w$ equals the density of the fluid (kg/m³), $\bar{p}$ equals the root mean squared (RMS) pressure fluctuations (N/m²), $\delta_{ij}$ equals Kronecker delta (-), $u_i'$ equals the RMS velocity fluctuations (as discussed in section 3.2) (m/s), and $v$ equals the kinematic viscosity (m²/s). The subscripts $i$ and $j$ are free indices that can take on the values $x$, $y$, and $z$ corresponding to the three dimensions.

Equation I.1 depicts the kinetic energy of the velocity fluctuations in a flow. Similarly, the kinetic energy of the mean flow (MKE) can be found by taking the scalar product of the Reynolds averaged Navier-Stokes equation with the mean flow velocity (George, 2013). This results in:

$$\frac{dK}{dt} + \bar{u}_j \frac{dK}{dx_j} = \frac{d}{dx_j}\left( -\frac{1}{\rho_w}\, \bar{P}\bar{u}_i\delta_{ij} - \frac{1}{2}u_i'u_i'\bar{u}_i + v\frac{dK}{dx_j} \right)$$
$$+ u_i'u_j'\frac{d\bar{u}_i}{dx_j} - v\frac{d\bar{u}_i}{dx_j}\frac{d\bar{u}_i}{dx_j} + f \tag{I.2}$$
$$\delta_{ij}\begin{cases}0 \; if \; i \neq j \\ 1 \; if \; i = j\end{cases}$$

Where $K$ equals the kinetic energy of the mean flow $\left(K = \frac{1}{2}\bar{u}_i\bar{u}_i\right)$ (m²/s²), $t$ equals the time (s), $\bar{u}_i$ equals the time averaged flow velocity (m/s), $\rho$ equals the density of the fluid (kg/m³), $\bar{P}$ equals the time averaged pressure (N/m²), $\delta_{ij}$ equals Kronecker delta (-), $u_i'$ equals the time averaged velocity fluctuations (m/s), $v$ equals the kinematic viscosity (m²/s), and $f$ equals a source or sink term for kinetic energy (m²/s³) e.g. gravity adding energy to the flow by transforming potential into kinetic energy. The subscripts $i$ and $j$ are free indices that can take on the values $x$, $y$, and $z$ corresponding to the three dimensions.

### 2. Simplifying the TKE and MKE

The production term $u_i'u_j'\frac{d\bar{u}_i}{dx_j}$ in the TKE equation is assumed to be approximated by $-g\frac{dH}{dx}$ in the ATM. To give credibility to this assumption, the ATM is compared to the TKE equation. Because

the production of turbulent energy in the TKE equation is related to the loss of kinetic energy in the MKE equation, the MKE equation is also needed in the comparison.

The turbulent energy and mean flow energy equations can be rewritten to resemble the ATM. The ATM assumes stationarity and no additional transport beside advection is considered. When the same assumptions are applied to the TKE equation (I.1), the equation is reduced to:

$$\bar{u}_j \frac{dk}{dx_j} = -u_i'u_j' \frac{d\bar{u}_i}{dx_j} - v \frac{du_i'}{dx_j} \frac{du_i'}{dx_j} \tag{I.3}$$

Equation I.3 states that the change in turbulent energy per unit of distance is dependent on the production of turbulence (equal to the dissipation of mean flow energy) and the dissipation of turbulent energy due to viscous stresses.

Similarly the MKE equation is reduced to:

$$\bar{u}_j \frac{dK}{dx_j} = u_i'u_j' \frac{d\bar{u}_i}{dx_j} - \frac{d}{dx_j}\left(\frac{1}{\rho_w} \bar{P}\bar{u}_i\delta_{ij}\right) + f \tag{I.4}$$

The pressure transport term $-\frac{d}{dx_j}\left(\frac{1}{\rho_w} \bar{P}\bar{u}_i\delta_{ij}\right)$ is left into the equation for the mean flow energy.

This is done to retain an explanation for the transfer from kinetic into potential energy. Note that the viscous dissipation of the kinetic energy is left out here. This is done because the viscous dissipation of the kinetic energy of the mean flow is negligible at high (local) Reynolds numbers (Burden, 2008) and turbulent flows are accompanied by high Reynolds numbers (Hofland, 2005).

### 3. Rewriting and simplifying the MKE

Equation I.4 can be rewritten into the energy per volume of water per second by multiplying it with the density of water $\rho_w$. For the left hand side equation I.4 then becomes:

$$\rho_w\left(\bar{u}_j \frac{dK}{dx_j}\right) = \rho_w \bar{u}_i\bar{u}_i \frac{d\bar{u}_j}{dx_j} \tag{I.5}$$

The right hand side of equation I.4 (after multiplication with the density of water $\rho_w$) is written as:

$$\rho_w u_i'u_j' \frac{d\bar{u}_i}{dx_j} - \rho_w \frac{d}{dx_j}\left(\frac{1}{\rho_w} \bar{P}\bar{u}_i\delta_{ij}\right) \tag{I.6}$$

The whole equation can now be written as:

$$\rho_w \bar{u}_i\bar{u}_i \frac{d\bar{u}_j}{dx_j} + \frac{d\left(\bar{P}\bar{u}_i\delta_{ij}\right)}{dx_j} = \rho_w u_i'u_j' \frac{d\bar{u}_i}{dx_j} \tag{I.7}$$

Here the source or sink term for kinetic energy $f$ is assumed to be zero.

In equation I.7 the pressure term can be simplified. Expanding the pressure term in equation I.7 gives:

$$\frac{d\left(\bar{P}\bar{u}_i\delta_{ij}\right)}{dx_j} = \bar{P}\frac{d\left(\bar{u}_j\right)}{dx_j} + \bar{u}_j \frac{d(\bar{P})}{dx_j} \tag{I.8}$$

$\bar{P}\frac{d(\bar{u}_j)}{dx_j} = 0$ due to the assumption of incompressible flow (George, 2013). Equation I.7 can then be rewritten into:

$$\rho_w \bar{u}_i \bar{u}_i \frac{d\bar{u}_j}{dx_j} + \bar{u}_j \frac{d\bar{P}}{dx_j} = \rho_w u_i' u_j' \frac{d\bar{u}_i}{dx_j} \tag{I.9}$$

Note that equation I.9 still represents the mean flow kinetic energy for a stationary flow, neglecting transport of energy due to other velocity fluctuations or viscous effects. Under these assumptions, the production term of turbulent energy $\rho_w u_i' u_j' \frac{d\bar{u}_i}{dx_j}$ (right hand side of equation I.9) is still related to the change in mean flow energy (left hand side of equation I.9).

The ATM relates the production of turbulence to the mean flow energy loss. The ATM only considers the mean flow energy loss and turbulence production in the flow direction. Thus, uniformity is assumed in the $y$ and $z$ direction. For equation I.9 this mean $i = j = x$. Under the assumption of uniformity in the $y$ and $z$ direction, equation I.9 reduces to:

$$\rho_w \bar{u}_x \bar{u}_x \frac{d\bar{u}_x}{dx} + \bar{u}_x \frac{d\bar{P}}{dx} = \rho_w u_x' u_x' \frac{d\bar{u}_x}{dx} \tag{I.10}$$

The left side of equation I.10 is a rewritten version of the Bernoulli equation as will be shown below.

## 4. Linking the Bernoulli equation to the MKE equation

The formula of Bernoulli for an infinitely small particle along a streamline is given by:

$$E = \bar{P} + \frac{1}{2}\rho_w \bar{u}_x \bar{u}_x \tag{I.11}$$

Where $E$ equals the flow energy (J/m³) for this particle. Note that equation I.11 is only time averaged, and not depth (or width) averaged. The Bernoulli equation assumes no energy is lost and thus $E$=constant.

The formula of Bernoulli is rewritten into the same units as the MKE (equation I.10). This is achieved by differentiating equation I.10 in space (similar to appendix D) and multiplying it with the time averaged flow velocity:

$$\bar{u}_x \frac{dE}{dx} = \bar{u}_x \frac{\bar{P}}{dx} + \rho_w \bar{u}_x \bar{u}_x \left(\frac{d\bar{u}_x}{dx}\right) \tag{I.12}$$

The right hand side of equation I.12 now exactly equals the left hand side of the one dimensional MKE (equation I.10). So $\rho_w u_x' u_x' \frac{d\bar{u}_x}{dx}$ can be calculated using the change in mean flow energy according to Bernoulli:

$$\bar{u}_x \frac{dE}{dx} = \rho_w u_x' u_x' \frac{d\bar{u}_x}{dx} \tag{I.13}$$

The derivation up until this point showed that the MKE can be reduced to the Bernoulli equation under certain assumptions. This is expected because both formulas describe the mean flow energy, however, the MKE is more inclusive.

## 5. Relating the TKE to the production term of the ATM

Equation I.3 states that under certain assumptions turbulent energy can be defined as:

$$\bar{u}_j \frac{dk}{dx_j} = -u_i' u_j' \frac{d\bar{u}_i}{dx_j} - v \frac{du_i'}{dx_j} \frac{du_i'}{dx_j} \qquad (I.3)$$

When only considering the production of turbulent energy in equation I.3 and assuming uniformity in $x$ and $y$ direction, then equation I.3 is written as:

$$\bar{u}_x \frac{dk}{dx} = -u_x' u_x' \frac{d\bar{u}_x}{dx} \qquad (I.14)$$

Substituting equation I.13 into I.14 gives

$$\bar{u}_x \frac{dk}{dx} = -\bar{u}_x \frac{1}{\rho_w} \frac{dE}{dx} \qquad (I.15)$$

Rewritten in head level notation and dividing by $\bar{u}_x$ this gives:

$$\frac{dk}{dx} = -g \frac{dH}{dx} \qquad (I.16)$$

Which is exactly the turbulence production term in the ATM, quod erat demonstrandum.

### Remark about flow over a slope

The source term $f$ for kinetic energy of the mean flow is assumed to be zero in the above derivation. A possible source of kinetic energy is the transfer of potential energy into kinetic energy, e.g. water flowing down a slope. The horizontal gravity component then adds energy to the flow. Under this situation, the elevation above a reference plane $z$ (m) should be added to the head level $H$ to correctly depict the change of potential into kinetic energy.

## Appendix J: Calculating the hydraulic radius

The thesis stated that the hydraulic radius is calculated using the following formula:

$$R = \frac{h \times B}{2 \times h + B}$$

This definition for the hydraulic radius is inconvenient because it requires the water depth at each location where $R$ needs to be known. This complicates the ATM calculations. Moreover, in the preliminary design phase, the exact water depths after the BFS is unknown. Therefore, the hydraulic radius was in fact approximated in this thesis in the following way:

$$R = \begin{cases} \dfrac{h_{upstream} \times B}{2 \times h_{upstream} + B}, & x/h_{step} \leq 0 \\[2em] \dfrac{\left(h_{upstream} + h_{step}\right) \times B}{2 \times \left(h_{upstream} + h_{step}\right) + B}, & x/h_{step} > 0 \end{cases}$$

Where $h_{upstream}$ equals the water depth on top of the step (m), $h_{step}$ equals the BFS step height (m) and $B$ equals the flume width. Using this definition, the hydraulic radius is assumed to be constant on top of the step and constant downstream of the step. This definition of the hydraulic radius does not take into account the increase in water depth downstream of the step due to mean flow energy loss.

The mean flow has lost the most energy at the most downstream measurement location. For subcritical flow, mean flow energy loss results in an increase in the water depth (Cruise, Sherif, & Singh, 2007). At the most downstream measurement location the actual water depth will therefore deviate the most from the assumed water depth $h_{upstream} + h_{step}$. Thus the hydraulic radius approximation will deviate most from reality at the most downstream measurement locations. The hydraulic radius approximation and the hydraulic radius calculated using the actual most downstream measured water depth are depicted in the table below.

Appendix Table 1 Comparison between hydraulic radius approximation and the actual hydraulic radius at the most downstream measurement location

| Author | Xingkui, 1993 | Hofland, 2005 | Nakagawa ST1, 1987 | Nakagawa ST3, 1987 |
|---|---|---|---|---|
| $R_{downstream} = \frac{h \times B}{2 \times h + B}$ | 0.0897 | 0.0970 | 0.0423 | 0.0621 |
| $R_{approximation} = \frac{(h_{upstream} + h_{step}) \times B}{2 \times (h_{upstream} + h_{step}) + B}$ | 0.0867 | 0.0953 | 0.0418 | 0.0619 |

Appendix Table 1 shows that even at the most downstream measurement location, the approximated hydraulic radius confirms reasonably well with the actual hydraulic radius. It is therefore concluded that the hydraulic radius can be approximated using the method described above.

# Appendix K: Selection of experimental data usable to validate the ATM

Appendix Table 2 Experimental data available to this study

| Author | Procurement | Flow situation | Usable | Reason |
|---|---|---|---|---|
| Nakagawa & Nezu (1987) | Data extracted from paper | BFS flow | Yes | All data needed are available |
| Xingkui & Fontijn (1993) | Data extracted from dissertation | BFS flow | Yes | All data needed are available |
| Hofland (2005) | Data extracted from paper | BFS flow | Yes | All data needed are obtainable by assuming conservation of mass |
| Hofland2 (2005) | Data obtained from author (DVD's) | Uniform flow | No | No BFS flow |
| De Gunst (1999) | Data extracted from paper and downloaded from the internet | BFS flow | No | Experiment performed with a rigid lid |
| Jongeling et al. (2003) | Data obtained from Remco Steenstra (via email) | BFS flow (special) | No | Sloped BFS |
| Kasagi & Matsunaga (1995) | Data extracted from paper | BFS flow | No | Experiment performed with a rigid lid |
| Hoan (2008) | Data extracted from paper | Widening channel | No | No BFS flow |

A total of 8 experimental datasets were considered to use in the validation of the ATM. Out of the 8 experiments, only 3 experiments were usable to validate the ATM with.

The Hofland (2005) experimental data extracted from his dissertation lacked detailed information about the measured water heights during the experiments. This data was obtained by assuming conservation of mass during his experiments.

A second dataset was obtained from Bas Hofland. This dataset contained the raw measurements performed for flow over a flat rough bottom. This data was not used because it did not contain BFS flow data.

The studies of Kasagi & Matsunaga (1995) and De Gunst (1999) were performed in a flume containing a rigid lid. This made sure the water level during the experiments remained constant. One of the variables needed as input into the ATM is the change in head level $\left(\frac{dH}{dx}\right)$. For experiments performed using a rigid lid, the change in mean flow energy $\left(\frac{dH}{dx}\right)$ cannot be found using the change in flow velocity and water depth. Instead, the change in pressure on the rigid lid now gives value to the mean flow energy loss. Regrettably, both experiments did not present the pressure on the rigid lid as a function of the flow distance. Moreover, rigid lid will result in some additional mean flow energy loss due to friction with the lid. This makes it hard to compare ATM results using rigid lid data sets and ATM results using free surface data sets. Therefore, these data sets were not used to validate the ATM.

A BFS flow experiment was performed by Jongeling et al. (2003). However, for this experiment the end of the step was not followed by a sudden deepening of the flume. A more gradual slope (1:3) was used as transition between the step and the downstream flume bottom. This results in a reduction (disappearance) of the recirculation zone downstream of the step. Comparison between the ATM results using the data of Jongeling et al. (2003) and the ATM results using the other datasets would be hard due to the different BFS setups. Therefore, this dataset was not used in the validation.

The dataset of Hoan (2008) was not used because the experiment was not performed for BFS flow.

## Appendix L: Extracting velocity data from papers

The following papers were used to extract data from:

- Nakagawa & Nezu (1987)
- Xingkui & Fontijn (1993)
- De Ruijter (2004) & Hofland (2005)

All studies gave flow velocity data (mean $\bar{u}_i$ and fluctuating $u_i'$) as a function of the distance $x$ from the step and the height $y$ from the bottom of the flume, with $y = 0$ at the bottom of the flume downstream of the step. Depth averaged data is required as input for the ATM. The process of extracting and depth averaging the data from the graphs presented in the papers is discussed below. The water depth measurements were extracted from the papers using a method similar to the method described below.

Appendix figure 10 shows, as an example, the velocity fluctuations graph of the study of Xingkui & Fontijn (1993). To find the average flow velocity for each cross-section (A-G) a computer program was designed using Matlab. This program aided in the extraction process.



Distribution of turbulence intensities $u'$ (●) and $v'$ (○); run 1.
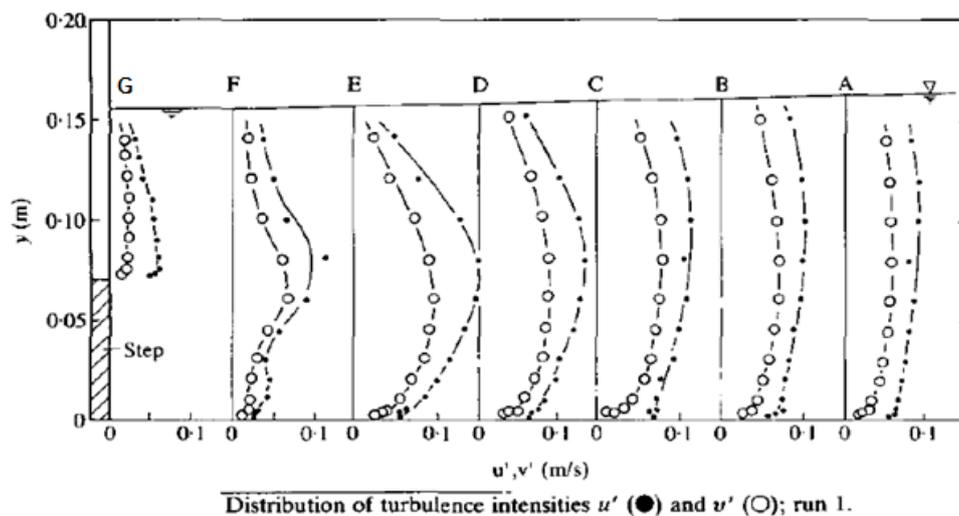
Appendix figure 10 Distribution of velocity fluctuations from the study of Xingkui & Fontijn (1993, p. 306)

The extraction process for each graph consisted of the following steps:

1. Determine how many pixels correspond with a certain measure of velocity in the graph
2. Determine how many pixels correspond with a certain measure of height in the graph
3. Measure the area of the velocity graph
4. Measure the water depth corresponding to the area measured in step 3
5. Divide the area by the water depth
6. Repeat step 1-5 three times to minimize measurement error
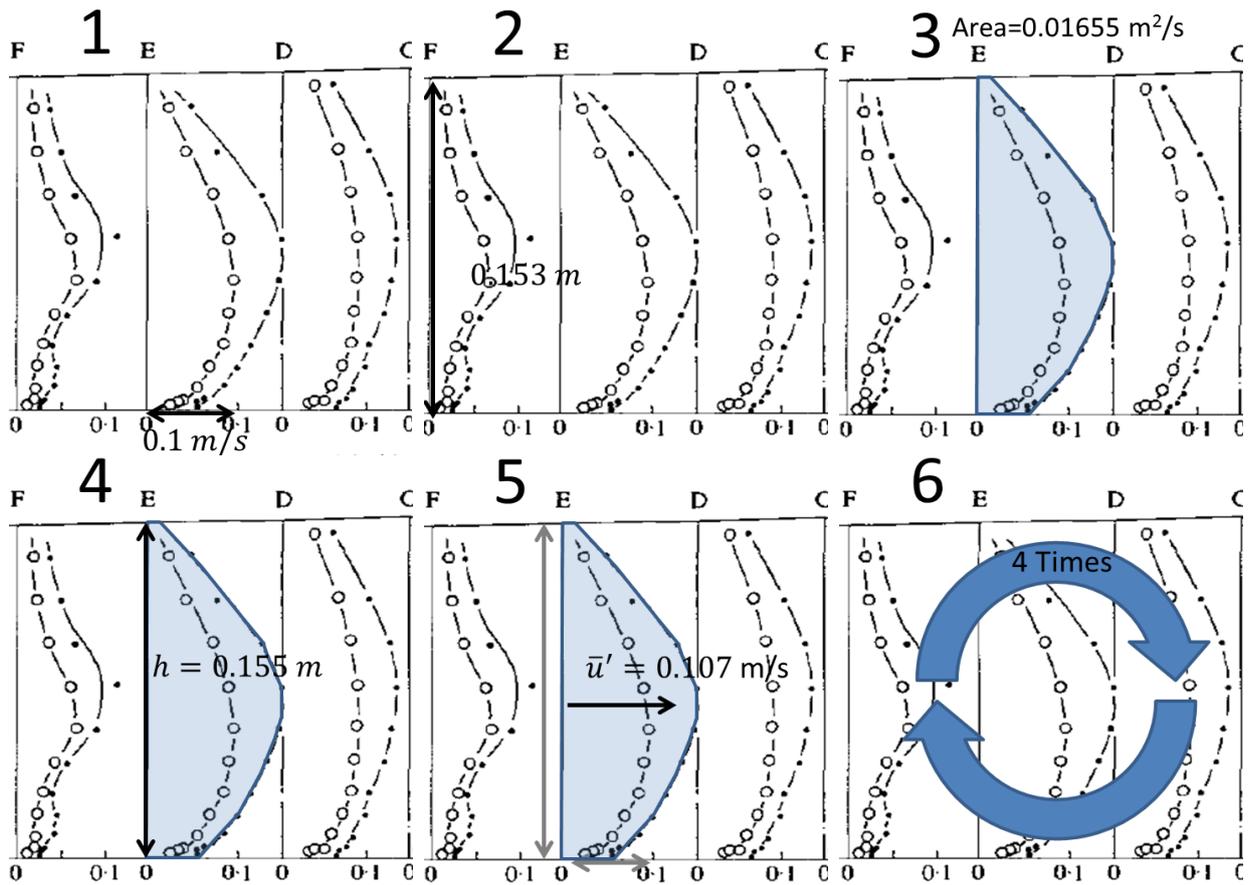
Appendix figure 11 Steps for the extraction of data from graphs

After step 6, the mean of the found depth averaged flow velocity is taken to find the final measurement at the cross section under consideration.

## Appendix M: Quantifying the uncertainty in the experimental data used as ATM input

In section 5.4 several sources of uncertainty were identified. The size of uncertainty in the measurements are quantified in the following text. Because little data is available to quantify the uncertainty, the quantification is performed based on a simple principle: Each measurement is assumed to have a certain uncertainty margin. The actual value of the variable $(h, \bar{\bar{u}})$ that was measured, is located within this uncertainty margin. Appendix figure 12 visually depicts the idea behind the uncertainty margins. The uncertainty margins will give an idea about how certain the measured variables actually are.
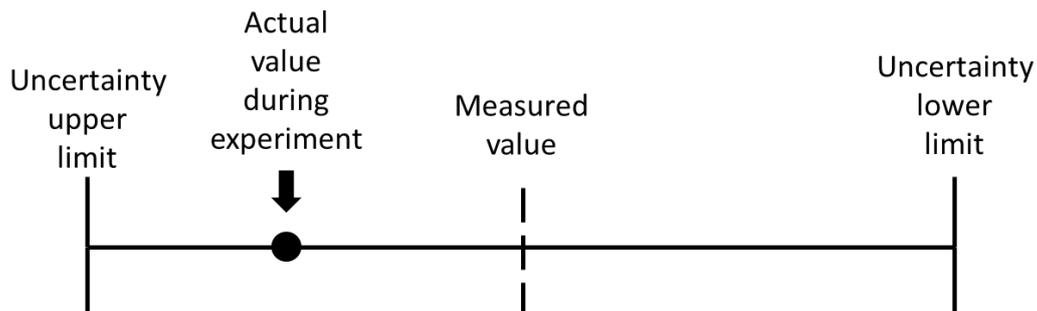


Appendix figure 12 Schematization of uncertainty limits of the measured variable

Because multiple sources of uncertainty can affect the same variable $(h, \bar{\bar{u}})$, uncertainty margins of different sources add up. In order to clearly define how the total uncertainty margins of each variable are calculated, a schematization of the total uncertainty margins is given in appendix figure 13.

*1. Uncertainty in the measurement data due to fluctuations in discharge*
The uncertainty in the measured variables as the result of fluctuations in the discharge in between measurement locations are hard to quantify. However, it will be shown below that, when all other sources of uncertainty are taken into account, the discharge fluctuations as shown in figure 27 can simply be the result of the uncertainty margins of the water depth and mean flow velocities. Therefore, it is hypothesized that this source of uncertainty is the result of the other sources of uncertainty.

*2. Uncertainty in water depth measurements due to local variations in water depth*
De Ruijter (2004) stated an expected measurement error of several millimetres up to several centimetres for the water depth measurements. However, figure 26 shows a smooth change in water depth measurements without large outliers, thus it is unlikely that the water depth measurements contained uncertainty margins several centimetres wide. As a worst case scenario, it is assumed that every water depth measurement has an uncertainty margin of $\pm 10 \ mm$ due to the accuracy of the water depth measurements.

*3. Uncertainty in the flow velocity measurements due to incorrect usage of the laser Doppler anemometer*
Tropea (1995) mentioned LDA uncertainty margins in the order of magnitude of micrometres, but only when the LDA is properly setup. For the extracted and integrated velocity measurements $\bar{\bar{u}}$ and $\bar{u}'_i$, an uncertainty margin of $\pm 1\%$ is assumed. The size of this uncertainty margin is based on the remark of Tropea (1995) that improper setup of the LDA measuring system can result in increased error in the measurements. The uncertainty margin of 1% is a best guess and is mainly set to investigate the effects of an uncertainty margin on discharge fluctuations. Larger or smaller

uncertainty margins than this 1% are quite possible, but the study limits itself to the assumption of this 1%.

*4. Uncertainty in the flow variables due to tracing the graphs in the papers by hand*
Appendix L describes the method used to extract data from the graphs in the papers. At each measurement location, the water depth and flow velocity (both mean and fluctuating) is extracted by hand. This procedure is repeated four times. The definitive value of the measurement under consideration is determined by taking the average of the four repeated measurements. The human measurement uncertainty margin due to tracing the graphs by hand, is determined to equal the minimum and maximum extracted value (where the minimum is set as the lower limit of the uncertainty margin, and the maximum is set as the upper limit of the uncertainty margin). This results in a measured value and its uncertainty limits, for each variable ($h, \bar{\bar{u}}, \bar{u}'_i$), at each measurement location.

*1,3,4. Uncertainty due to applying the conservation of mass*
The water depths for the experiment of Hofland (2005) were found by using the conservation of mass. The accuracy of the calculated water depth is dependent on the accuracy of the assumption that during the whole experiment, the discharge in the flume was actually equal to the stated 31.8 l/s. De Ruijter (2004) stated that the discharge was measured with an accuracy of 2 l/s. De Ruijter (2004) also stated that the discharge fluctuated in between measurements up to 2 l/s. this gives a total possible discharge fluctuation of $\pm 4$ l/s. Moreover, the uncertainty margin in the mean flow velocity measurements affects the uncertainty margin in the calculated water depths (using the conservation of mass). The following formula describes the uncertainty margin in the calculated water depths (using the conservation of mass) for the experiment of Hofland (2005):

$$h_{a,b,\dots} = \frac{0.0318 \pm 0.004}{(\bar{\bar{u}}_{a,b,\dots} \pm err) \times B} \qquad (M.1)$$

Where $h_{a,b,\dots}$ is the calculated water depth (m) at a certain measurement location, 0.0318 is the discharge in the flume in (m³/s), 0.004 the possible discharge fluctuation (m³/s) due to measurement errors or the inability to accurately set the pump discharge, $\bar{\bar{u}}_{a,b,\dots}$ the depth integrated velocity profiles as extracted from the graphs (m/s), $err$ the error in the mean flow velocity measurements due to the extraction process and the 1% assumed LDA error (m/s) and $B$ the width of the flume (m). Note that the lower uncertainty limit of $h_{a,b,\dots}$ is found by filling into equation M.1 $h_{a,b,\dots} = \frac{0.0318-0.004}{(\bar{\bar{u}}_{a,b,\dots}+err)\times B}$ and the upper uncertainty limit is found by filling in $h_{a,b,\dots} = \frac{0.0318+0.004}{(\bar{\bar{u}}_{a,b,\dots}-err)\times B}$.

*Schematisation of uncertainty margins*
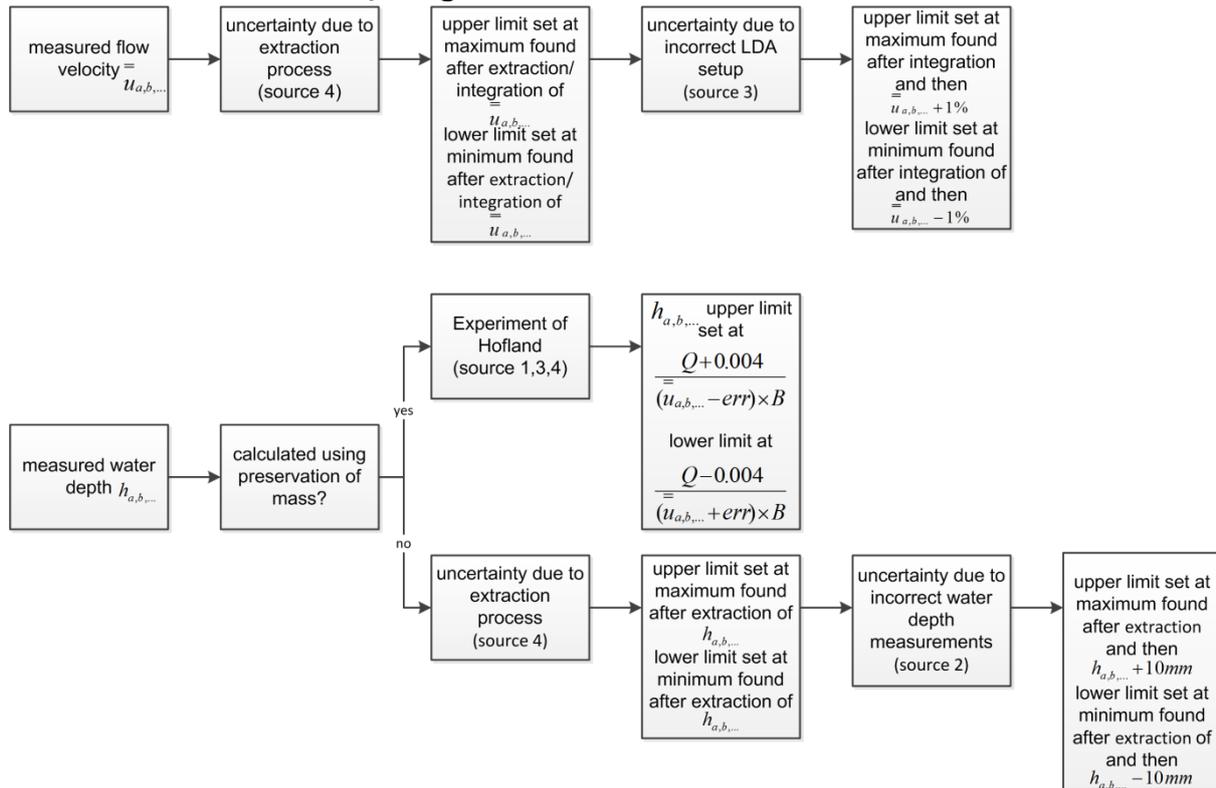


**Appendix figure 13 Schematization of determining uncertainty margins for the extracted variables**

## Graphs of water depth and flow velocity uncertainty limits

The extracted water depths and flow velocities, including the uncertainty limits are presented below.
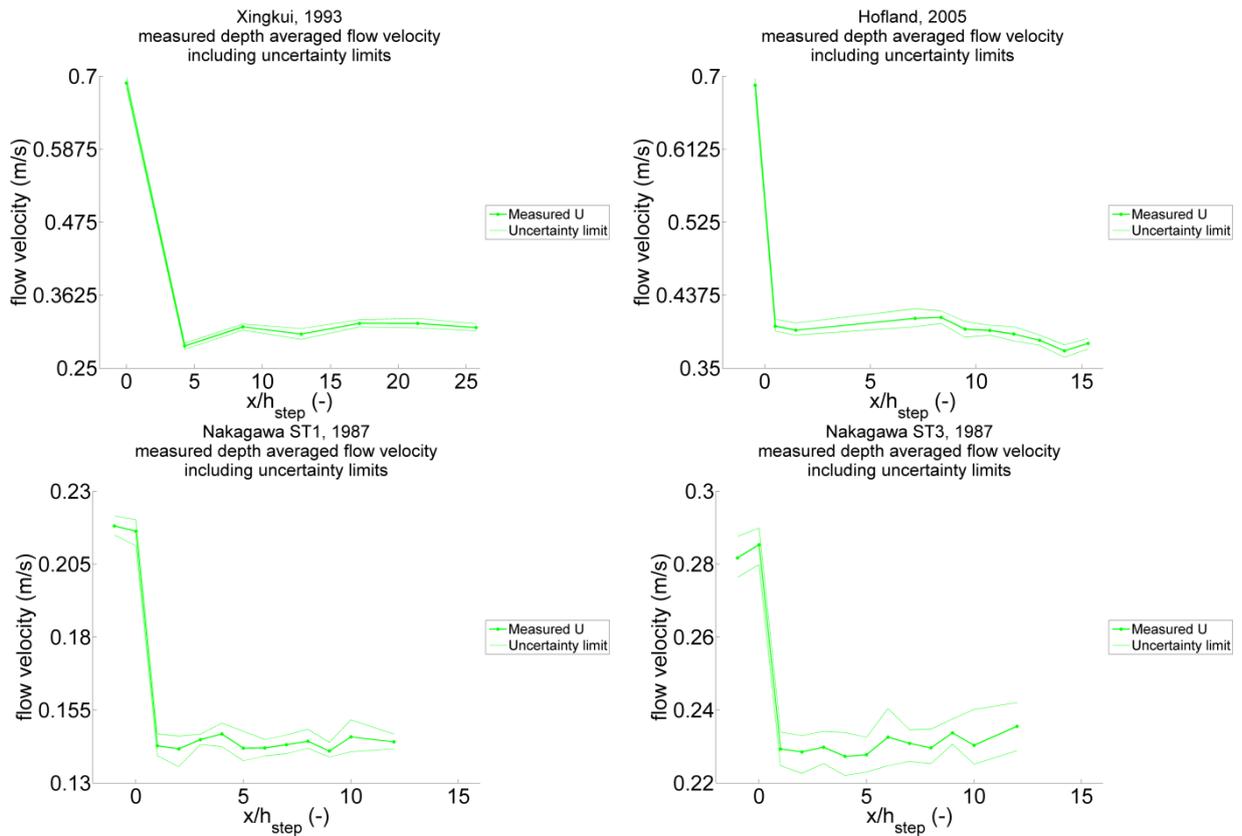


Appendix figure 14 Depth integrated flow velocity profiles including uncertainty limits, as described in appendix figure 13
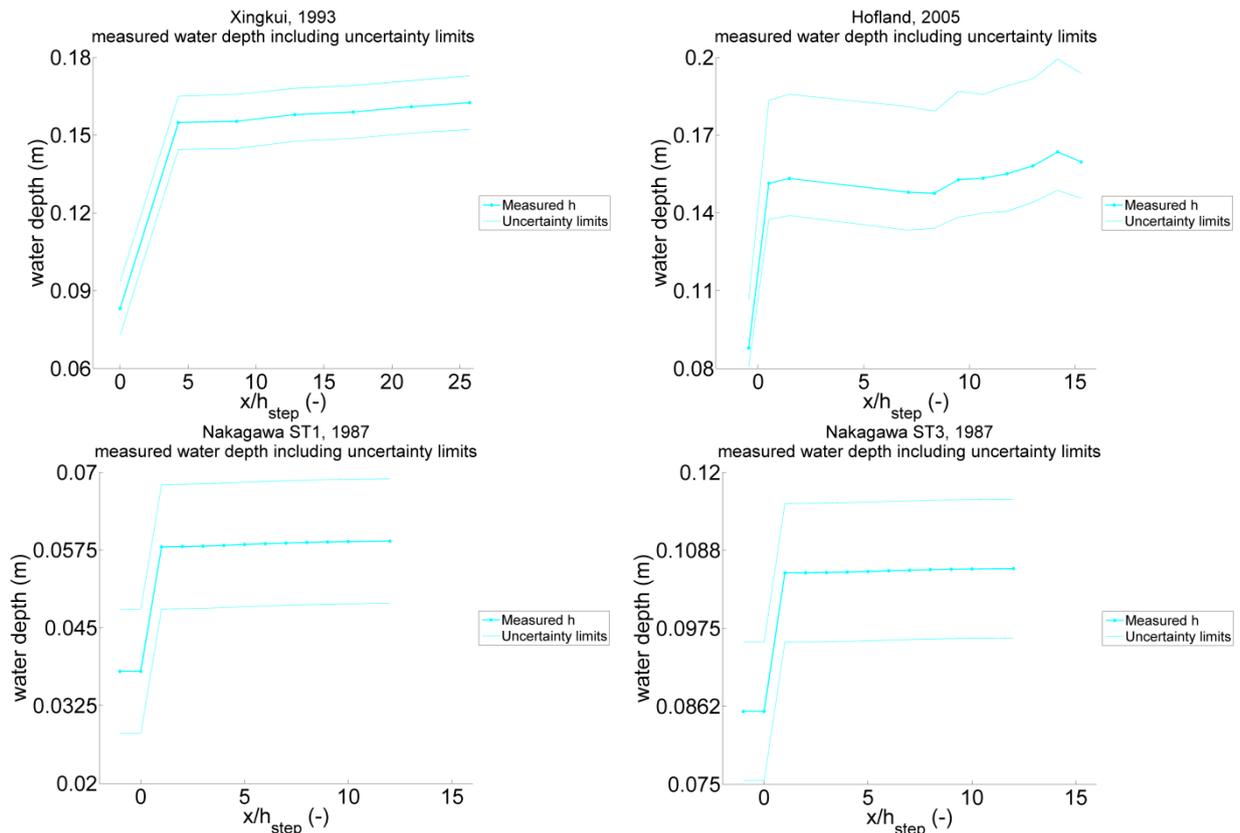
**Appendix figure 15 Water depth at the measurement locations including uncertainty limits, as described in appendix figure 13**

Appendix figure 14 and 15 show the uncertainty limits of the measured water depths and flow velocities. The uncertainty in the water depth measurements are relatively larger than the uncertainty in the depth integrated water velocity measurements. This is expected because the water depth measurement error is set at a flat 10 mm, which is quite large compared to the 1% expected error in the LDA measurements. Even including the uncertainty limits, the changes in water depth and flow velocity remain clearly visible. However, the uncertainty limits of especially the water depth measurements indicate that the measured variables are not that certain. This should be taken into account when reviewing the ATM results in chapter 7.

### Graphs of discharge uncertainty limits

Using the uncertainty limits of the mean flow velocities and water depths, the uncertainty margins of the discharge can be calculated. The upper and lower limits of the discharge are found by multiplying the upper and lower limits of the water depths with the upper and lower limits of the flow velocities respectively. Figure 27 (normalized discharge fluctuations) showed that the discharge fluctuated in between measurements. However, this could simply be the result of the uncertainty margins in the measurements. If the uncertainty margins in the discharge give the possibility that the discharge during every measurement was actually constant, then it's at least possible that the discharge fluctuations are not the result of a change in discharge in between the measurements. The discharge fluctuations, including the uncertainty margins are given below.
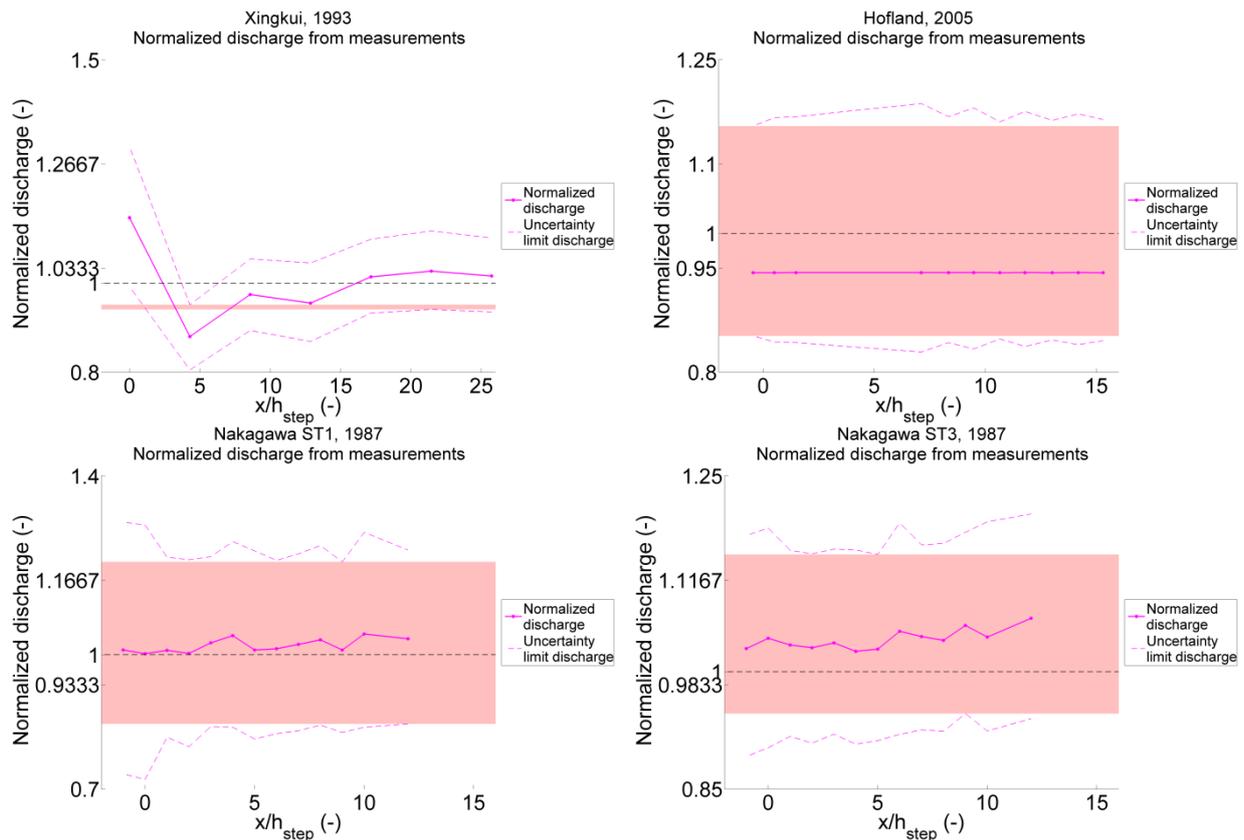
**Appendix figure 16** Discharge calculated using extracted water depth and flow velocities including the uncertainty limits, normalized by dividing the discharge by the explicitly stated discharge in the papers (table 3). Shaded area indicates the area in between the uncertainty limits where the discharge can be constant over the whole experiment.

The results of appendix figure 16 show that it is quite possible that the experiments were performed under more or less constant discharge when the uncertainty in the discharge (other than actual fluctuations in discharge in between measurement locations) is taken into account. The experiments of Nakagawa & Nezu (1987) and Hofland (2005) contain a large range in between which the discharge could have been constant for the whole experiment. The shaded area of the experiments of Xingkui & Fontijn (1993) is constructed after omitting the most upstream located discharge measurement. Even after omitting this measurement, the shaded are of the Xingkui & Fontijn (1993) experiment is still much smaller than the other experiments. This makes it less likely that the experiment of Xingkui & Fontijn (1993) was actually performed under constant discharge. The validation of the ATM using the Xingkui & Fontijn (1993) data (chapter 7) should therefore be reviewed with some more reserve.

## Appendix N: Quantifying the uncertainty in the measured turbulent energy levels

In the following text, it is explained how the uncertainty margins in the flow velocity fluctuations were determined. Thereafter, uncertainty margins of the turbulent energy levels are calculated using the flow velocity fluctuations uncertainty margins. The method for finding the uncertainty margins in the measured turbulent energy levels is also schematized in appendix figure 17.

*4. Uncertainty in the flow variables due to tracing the graphs in the papers by hand*

Every measurement for $\bar{u}_i'$ was extracted from a graph. The flow velocities are extracted using the same method as the extraction process for the mean flow (appendix L): the extraction is performed 4 times (by hand), the mean of the found velocity $\bar{u}_i'$ is set as the actual velocity, the minimum and maximum values found during the integration are set as the limits of uncertainty.

*3. Uncertainty in the flow velocity measurements due to incorrect usage of the laser Doppler anemometer*

Because all flow velocity measurements were done using a LDA, it is assumed that every measurement of the flow fluctuation $\bar{u}_i'$ contains an uncertainty margin due to the possible incorrect setup and usage of the LDA. As a worst case scenario the flow fluctuations $\bar{u}_i'$ are expected to contain a maximum error of 1% in either direction ($\bar{u}_i' \pm 1\%$). As was discussed the previous section, this value is a best guess.

The turbulent energy uncertainty margin following from the uncertainty in the flow fluctuations $\bar{u}_i'$ is then found using the formula:

$$\bar{k}_{uncertainty\ margins} = \frac{3}{4}\left((\bar{u}_x' \pm 0.01\bar{u}_x')^2 + \left(\bar{u}_y' \pm 0.01\bar{u}_y'\right)^2\right) \qquad (N.1)$$

Solving equation N.1 (Appendix O) gives:

$$\bar{k}_{uncertainty\ margins} = \bar{k} \pm \frac{1}{50}\bar{k} \qquad (N.2)$$

The upper and lower uncertainty limits of the measured turbulent energy are calculated by adding or subtracting $\frac{1}{50}k$ from the respectively the maximum and minimum value of the extracted and integrated turbulent energy level $\bar{k}$. Appendix figure 17 visually depicts how the measured turbulent energy, and its uncertainty margins are found.
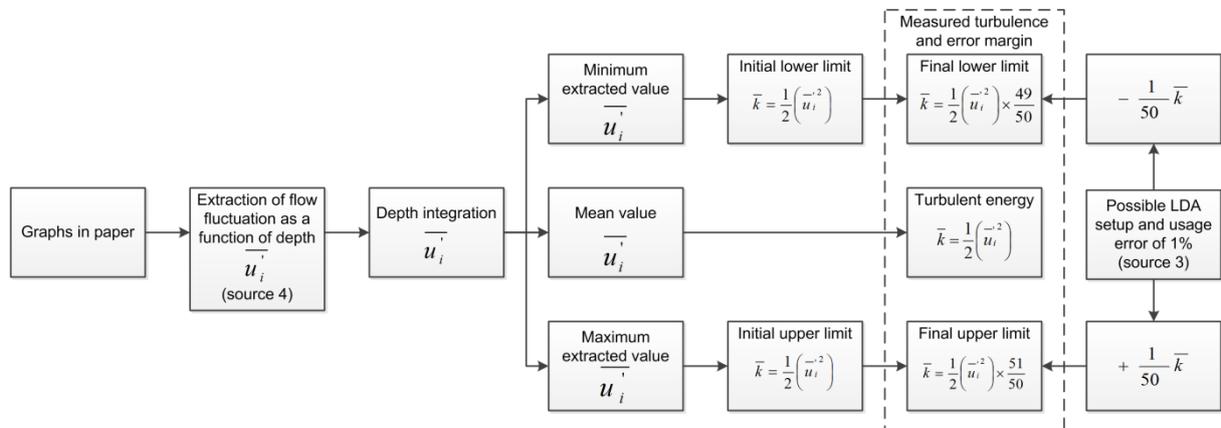


Appendix figure 17 Visual depiction of calculation of measured turbulent energy $k$ and its upper and lower limit uncertainty margin

## Appendix O: Deriving the Uncertainty margins of the turbulent energy

Assuming the depth averaged flow velocity fluctuations $\bar{u}'_i$ are affected by a measurement uncertainty of 1% and $\bar{u}'^2_x \sim \bar{u}'^2_y \sim \bar{u}'^2_z$, then the depth averaged turbulence uncertainty margins can be described in the following way:

$$\bar{k}_{uncertainty\ margins} = \frac{3}{4}\left((\bar{u}'_x \pm 0.01\bar{u}'_x)^2 + \left(\bar{u}'_y \pm 0.01\bar{u}'_y\right)^2\right)$$

$$\bar{k}_{uncertainty\ margins} = \frac{3}{4}\left((\bar{u}'_x \pm 0.01\bar{u}'_x)(\bar{u}'_x \pm 0.01\bar{u}'_x) + \left(\bar{u}'_y \pm 0.01\bar{u}'_y\right)\left(\bar{u}'_y \pm 0.01\bar{u}'_y\right)\right)$$

Assume "$\pm$" equals "$+$" and reintroduce "$\pm$" when derivation is finished

$$\bar{k}_{uncertainty\ margins} = \frac{3}{4}\left(\left(\bar{u}'^2_x + 2\bar{u}'_x 0.01\bar{u}'_x + (0.01\bar{u}'_x)^2\right) + \left(\bar{u}'^2_y + 2\bar{u}'_y 0.01\bar{u}'_y + \left(0.01\bar{u}'_y\right)^2\right)\right)$$

$$\bar{k}_{uncertainty\ margins} = \frac{3}{4}\left(\left(\bar{u}'^2_x + \bar{u}'^2_y\right) + \left(2\bar{u}'_x 0.01\bar{u}'_x + (0.01\bar{u}'_x)^2 + 2\bar{u}'_y 0.01\bar{u}'_y + \left(0.01\bar{u}'_y\right)^2\right)\right)$$

$$(0.01\bar{u}'_x)^2 = 0.0001\bar{u}'^2_x \ll \bar{u}'_x$$

$$\left(0.01\bar{u}'_y\right)^2 = 0.0001\bar{u}'^2_y \ll \bar{u}'_y$$

Thus:

$$\bar{k}_{uncertainty\ margins} = \frac{3}{4}\left(\left(\bar{u}'^2_x + \bar{u}'^2_y\right) + \left(2\bar{u}'_x 0.01\bar{u}'_x + 2\bar{u}'_y 0.01\bar{u}'_y\right)\right)$$

$$\bar{k}_{uncertainty\ margins} = \frac{3}{4}\left(\left(\bar{u}'^2_x + \bar{u}'^2_y\right) + \left(0.02\bar{u}'^2_x + 0.02\bar{u}'^2_y\right)\right)$$

$$\bar{k}_{uncertainty\ margins} = \frac{3}{4}\left(\bar{u}'^2_x + \bar{u}'^2_y\right) + \frac{3}{4}\left(0.02\bar{u}'^2_x + 0.02\bar{u}'^2_y\right)$$

Reintroduce "$\pm$" and $\bar{k}$:

$$\bar{k}_{uncertainty\ margins} = \bar{k} \pm \frac{3}{4}\left(\pm 0.02\bar{u}'^2_x \pm 0.02\bar{u}'^2_y\right)$$

Worst case scenario :

$$\pm\frac{3}{4}\left(\pm 0.02\bar{u}'^2_x \pm 0.02\bar{u}'^2_y\right) = \pm\frac{3}{4}\left(0.02\bar{u}'^2_x + 0.02\bar{u}'^2_y\right)$$

Thus:

$$\bar{k}_{uncertainty\ margins} = \bar{k} \pm \frac{3}{4}\left(0.02\bar{u}'^2_x + 0.02\bar{u}'^2_y\right)$$

# Appendix P: Validation of step size $\Delta x$ used for numerical Arcadis Turbulence Model

*This appendix uses an ATM case to validate the numerical step size $\Delta x$. For an explanation of the ATM cases, see section 7.2.*

In chapter 6 it was explained that the ATM differential equation is solved using the forward Euler method and a $\Delta x$ of $\frac{1}{1000} h_{step}$. To check the validity of applying the forward Euler using a step size of $\frac{1}{1000} h_{step}$, equation 6.1 is compared to the analytical solution of the ATM (appendix G). To compare the numerical and analytical solution of the ATM, the ATM needs to be run for a case that can be solved using both the analytical and numerical solution method. The following case adheres to this criteria:
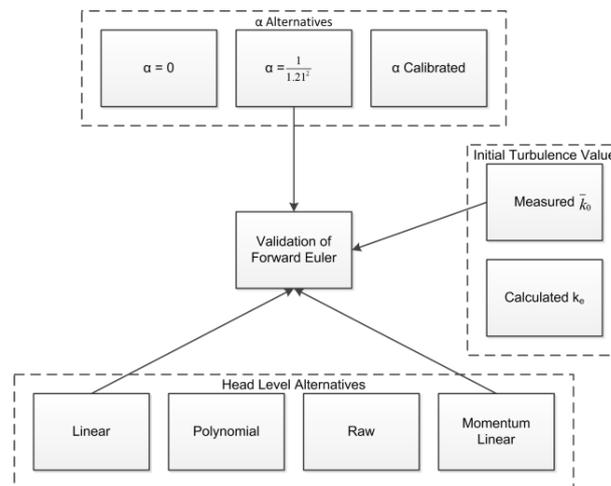


Appendix figure 18 Case description used to validate the forward Euler method

Appendix figure 18 shows the case that will be used to validate the forward Euler method. The linear and momentum head level input alternatives both model the mean flow energy loss at a constant rate $\left( \frac{dH}{dx} = constant \right)$. The analytical solution given in (appendix G) is also based on the assumption of a constant change in head level. Therefore both the analytical and numerical solution methods of the ATM can be used to calculate turbulent energy for the case described above. The polynomial head level input alternative has varying values for $\frac{dH}{dx}$, and can therefore not be used to compare the numerical and analytical ATM models (because the analytical solution can only be applied for $\frac{dH}{dx} = constant$).

The found turbulent energy levels of the Euler ATM confirmed almost exactly with the found turbulent energy levels of the analytical ATM when a step size of $\frac{1}{1000} h_{step}$ is used (root mean square error equalled $5.14 \times 10^{-7}$ (m²/s²)). Thus, the step size used in the forward Euler method is small enough to accurately approximate the analytical solution. No graph is presented of the results of both ATM solution methods because when plotted, the resulting turbulent energy levels (from the Euler ATM and the analytical ATM) did not visually deviate from one another, so presenting the graphs is pointless.

A second method was used to check whether the numerical step size of $\frac{1}{1000} h_{step}$ sufficiently approaches the analytical solution. For a number of model input alternatives, the ATM was run

using a step size of $\frac{1}{1000}h_{step}$ and $\frac{1}{10000}h_{step}$. The resulting turbulent energy levels were compared. The difference between running the model using a step size of $\frac{1}{1000}h_{step}$ or $\frac{1}{10000}h_{step}$ was very small ($\pm0.01\%$), thus it is concluded that the numerical step size of $\frac{1}{1000}h_{step}$ is sufficiently small.

## Appendix Q: Uncertainty analysis of the measured and momentum head levels

This appendix will show how the uncertainty in the measured flow velocity and water depth is translated into an uncertainty into the measured head levels.

The uncertainty margins of the measured head levels are calculated by inserting the upper and lower limits of the water depth and flow velocity measurements as depicted in appendix figure 14 and 15 into de Bernoulli equation (equation 6.3). This results in the following uncertainty margins:
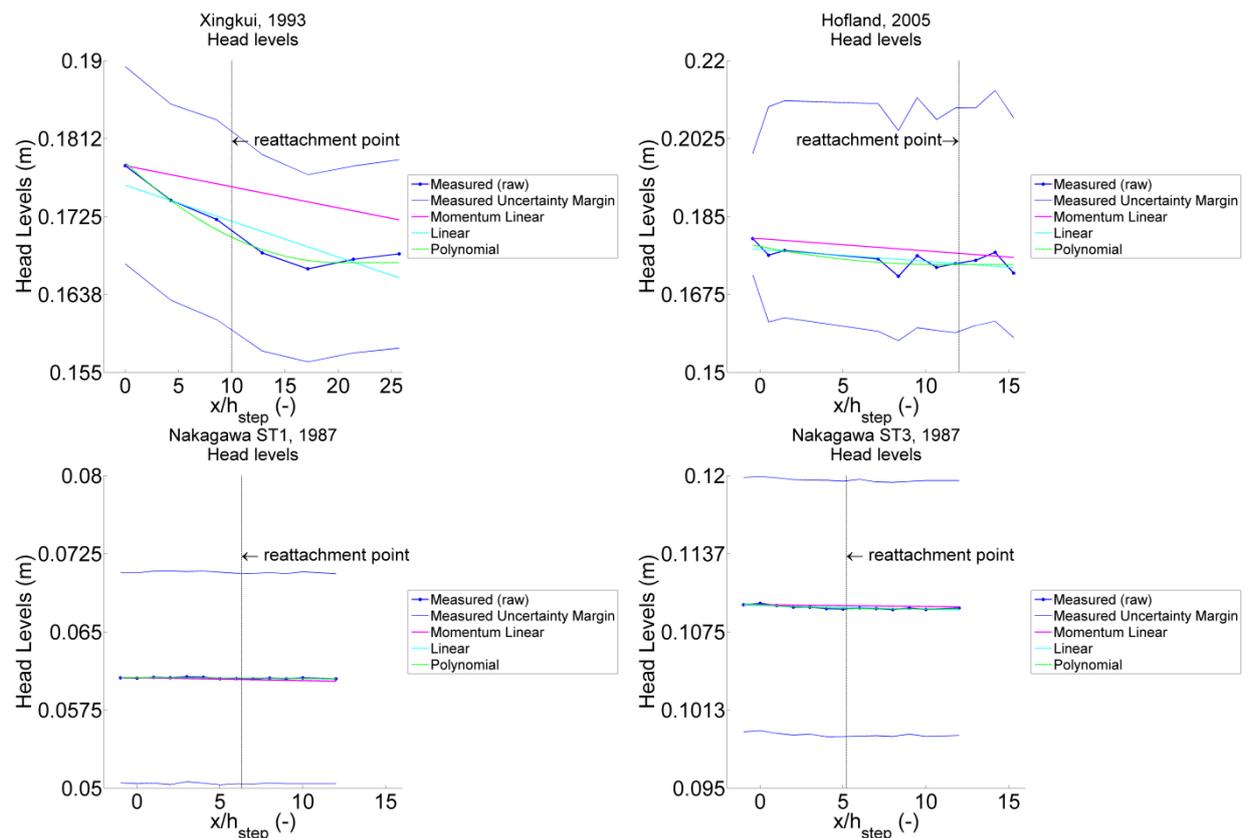


Appendix figure 19 Measured raw head levels including the uncertainty margins

Appendix figure 19 shows the upper and lower limits of the measured head levels. Assuming that the uncertainty margins set in chapter 5 are correct, than the actual head levels (that occurred during the experiments) are located in between the measured uncertainty margin as depicted in the above figure. Note that all head level alternatives (linear, polynomial and momentum) are located within the uncertainty margins of the measured head levels. Thus all head level alternative can potentially accurately represent the actual head levels as they occurred during the experiments.

Appendix figure 19 does make one thing clear, the shape and absolute values of the measured head levels are not very certain. For the experiments of Nakagawa and Nezu (1987) the shapes of the head level alternatives are barely visible anymore because of the large uncertainty margins. The uncertainty margins in the head level shapes of Xingkui & Fontijn (1993) and Hofland (2005) are relatively smaller. The cause of the large uncertainty in the Nakagawa and Nezu (1987) experiments is related to the assumed fixed uncertainty margin in the water depth measurements. It is assumed that, as a worst case scenario, the water depth was measured with an accuracy of $\pm$ 1 cm. This fixed 1 cm is relatively much larger for the experiments of Nakagawa

and Nezu (1987) (which measured water depths up to 11 cm) than for the other experiments (which measured water depths up to 16 cm). However, it is assumed that the $\pm$ 1 cm uncertainty margin in the water depth measurements is justified for all experiments because of the following reason: because the water depth measurements are assumed to be collected by hand (e.g. by using a Pitot tube), the uncertainty margins due to human error are likely to be independent of the experimental conditions, which justifies the used uncertainty margin.

The large uncertainty margin of the measured head levels do not mean that the measured head levels are not usable anymore. The uncertainty margins were found using the most extreme water depth and flow velocity uncertainty margins. Appendix figure 19 shows that for this worst case scenario, the head level uncertainty margins are quite big. However, the chance that theses extreme head level values actually occurred during the experiments is not very large because these are the uncertainty limits. Ideally, a probability density function is constructed for the water depth, flow velocity and head level measurements to say something about the data confidence interval. However, data is lacking to create a probability density function. The measured head levels (raw, linear, polynomial) were used as input into the ATM, but the resulting turbulent energy levels should be considered with the uncertainty margins of the measured head levels in mind.

## Appendix R: Coefficient of determination or R²

The coefficient of determination is interpreted as the proportion of the variance in the dependent variable that is predictable from the independent variable (StatTrek, 2015). In civil engineering, the coefficient of determination is often used to assess the predictive power of hydrological models. The coefficient of determination is then called the Nash–Sutcliffe model efficiency coefficient.

The coefficient of determination is calculated in the following way:

Assume a depend variable $y$ and an independent variable $x$. The independent variable $x$ tries to model the dependent variable $y$.

The Total Sum of Squares (TSS) of $y$ is given by:

$$TSS = \sum_i (y_i - \bar{y})^2$$

Where $i$ equals the number of realisations of $y$ and $\bar{y}$ the mean of $y_i$.

The Sum of Squares of Residuals (SSR) (deviation of $y_i$ from $x_i$) is given by:

$$SSR = \sum_i (x_i - y_i)^2$$

The coefficient of determination is then given by:

$$R^2 = 1 - \frac{SSR}{TSS}$$

The coefficient of determination ($R^2$) can range from 1 (perfect fit) down until – infinity. A number of characteristics values of $R^2$ exists. $R^2 = 1$ indicates a perfect relation between dependent and independent variables. $R^2 = 0$ indicates that the independent variable $x$ is only able to predict the mean of the dependent variable $y$. $R^2 = -1$ indicates a perfect inverse relation between $x$ and $y$, or in other words, when $x$ decreases, $y$ relatively increases by the same amount.

# Appendix S: Interpolation of head level data

## Interpolation method

In order to smooth out the chaotic fluctuations in the measured (raw) head levels, two interpolation methods were used. The linear shape of the head levels was found by fitting a polynomial with power 1 to the measured head levels. The optimal (straight) line was found by minimizing the square error between line and the raw head levels (Weisstein, 2015). Similarly the polynomial shape of the head levels was found by fitting a polynomial with power 2 to the measured raw head levels. Here, the optimal (polynomial) line was also found by minimizing the square error.

## Adjusting the polynomial head level shape

The polynomial interpolation method (figure 36) results in a small increase in head level for the last few measurements (located furthest downstream from the step) for all experiments except Nakagawa and Nezu (1987) ST-1. This is caused by the fact that a second degree polynomial cannot predict a constant value, thus after it finds a minimum, the head levels increase again. This is solved by fixing all polynomial head levels downstream of the minimum head level value at the minimum. This results in a constant head level after the minimum polynomial value is found. Appendix figure 20 depicts an example of the difference between the calculated polynomial (brown line) and the flattened polynomial (green line). To make the difference more clearly visible, the area between the lines is shaded yellow. The polynomials depicted in figure 36 are already flattened.
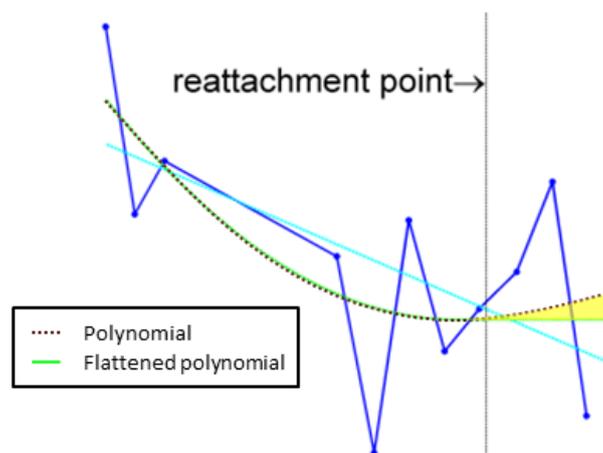


Appendix figure 20 Example of flattened polynomial (experiment of Hofland, 2005). Difference between regular and flattened polynomial is depicted by the yellow shaded area.

## Goodness of fit of interpolation methods

In order to say something about the quality of the interpolation methods, the goodness of fit between measured raw head levels and interpolated head levels are discussed. The goodness of fit is calculated using the coefficient of determination.

Appendix Table 3 shows the coefficient of determination for the linear and (flattened) polynomial interpolation method compared to the measured raw head levels. For further into about the coefficient of determination, see appendix R.

**Appendix Table 3** Coefficient of determination $(R^2)$ for the interpolation methods

| Author | | Xingkui, 1993 | Hofland, 2005 | Nakagawa ST1, 1987 | Nakagawa ST3, 1987 |
|---|---|---|---|---|---|
| **Interpolation method** | Linear (-) | 0.732 | 0.303 | 0.242 | 0.546 |
| | Polynomial (-) | 0.952 | 0.360 | 0.178 | 0.777 |

The coefficients of determination in appendix figure 3 show some interesting results. The general ability of the interpolation method to model the measured head levels is dependent on the size of the fluctuations in the measured head levels. The experiments of Xingkui & Fontijn (1993) and Nakagawa and Nezu (1987) ST-3 show the smallest fluctuations in head levels, and therefore have the best fitted interpolated head levels. The experiments of Hofland (2005) and Nakagawa and Nezu (1987) ST-1 show a much more chaotic pattern in the measured raw head levels and therefore also have much smaller goodness of fit. Note that the point of applying the interpolation methods is to achieve a more gradual decreasing head level shape without sudden fluctuations, thus coefficients of determination smaller than 1 (but larger than 0) are still acceptable. For all selected experiments except Nakagawa and Nezu (1987) ST-1, the polynomial interpolated head levels fit the measured head level better than the linear interpolated head levels. This indicates that for these experiments, the rate of mean flow energy loss is probably largest near the step, and is reduced further downstream. The measured head levels of the experiment of Nakagawa and Nezu (1987) ST-1 showed a bad fit with both the linear and polynomial interpolation methods. Due to the large irregular fluctuations in head level, it is hard to say anything about the shape of mean flow energy loss for this study beside that it has a general decreasing trend (downstream of an initial increase in mean flow energy).

The analysis of the coefficients of determination shows that for 3 out of the 4 selected experiments, the polynomial interpolation method outperforms the linear interpolation method. Thus, some change in the rate of mean flow energy loss is expected to occur between the step and the last measurement performed downstream of the step.

# Appendix T: Calculating the equilibrium turbulence levels on top of the step

Appendix H gave the following formula for equilibrium turbulence (based on equation 3.5: the formula of Hoffmans,1993):

$$k_e = c_0^2 \frac{g}{C^2} \bar{\bar{u}}^2$$

The equilibrium turbulence levels, as depicted in table 8, were calculated using this formula.

To calculate the value of $k_e$, a value for the Chezy coefficient $C$ and the depth averaged flow velocity $\bar{\bar{u}}$ needs to be known. The depth averaged flow velocity ($\bar{\bar{u}}$) in the above formula was simply set at the most upstream measured depth averaged flow velocity $\bar{\bar{u}}_a$ as depicted in figure 24. To find a value for the Chezy coefficient, equation 5.4 was used:

$$C = \frac{1}{n} h^{1/6} \qquad\qquad (5.4)$$

The formula for the Chezy coefficient requires a water depth $h$ and a value for the Manning coefficient $n$. The water depth $h$ was simply set at the most upstream measured water depth $h_a$ as depicted in figure 26. The Manning coefficient was determined using the description in the papers about the BFS roughness. The papers stated the following BFS roughness's:

Appendix Table 4 the BFS roughness and used Manning coefficients

| Author | Xingkui, 1993 | Hofland, 2005 | Nakagawa ST1, 1987 | Nakagawa ST3, 1987 |
|---|---|---|---|---|
| **Stated step roughness's** | smooth flat concrete | wood | smooth | smooth |
| **Determined Manning coefficients** | 0.011 | 0.009 | 0.009 | 0.009 |

Using this information and Engineering Toolbox (2015), the Manning coefficient for the BFS of the selected experiments were determined. For the experiment of Hofland (2005), it was assumed that the wooden step was laminated, resulting in a Manning coefficient for smooth plastic.

Note that the roughness's as depicted in appendix table 4 are different from the roughness's of the flume bed downstream of the BFS. This is caused by the fact that the grains placed on the bottom of the flume for the experiments of Xingkui & Fontijn (1993) and Hofland (2005) were not placed on top of the step, only downstream of the step. This results in a different Manning coefficient on top of the step compared to downstream of the step for these experiments.

# Appendix U: Head levels and ATM results

The graphs in this appendix are a copy of the graphs presented in the thesis. When reading the results in chapter 7, it is convenient to have a copy of the head levels and ATM results at hand. Therefore the results are printed here. Instructions: 1 Tear these pages out; 2 Read chapter 7.
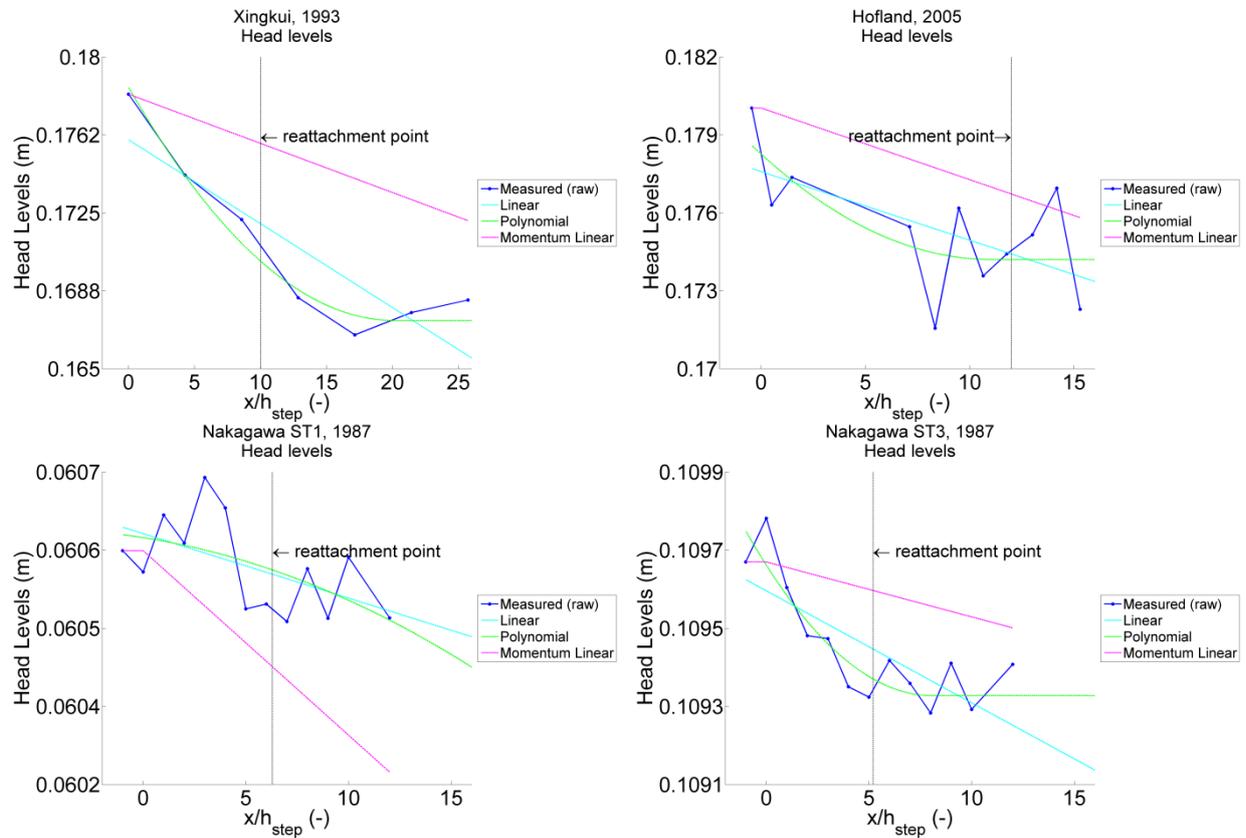


Figure 39 Head levels of the selected experiments following from the measured variables and following from the conservation of momentum
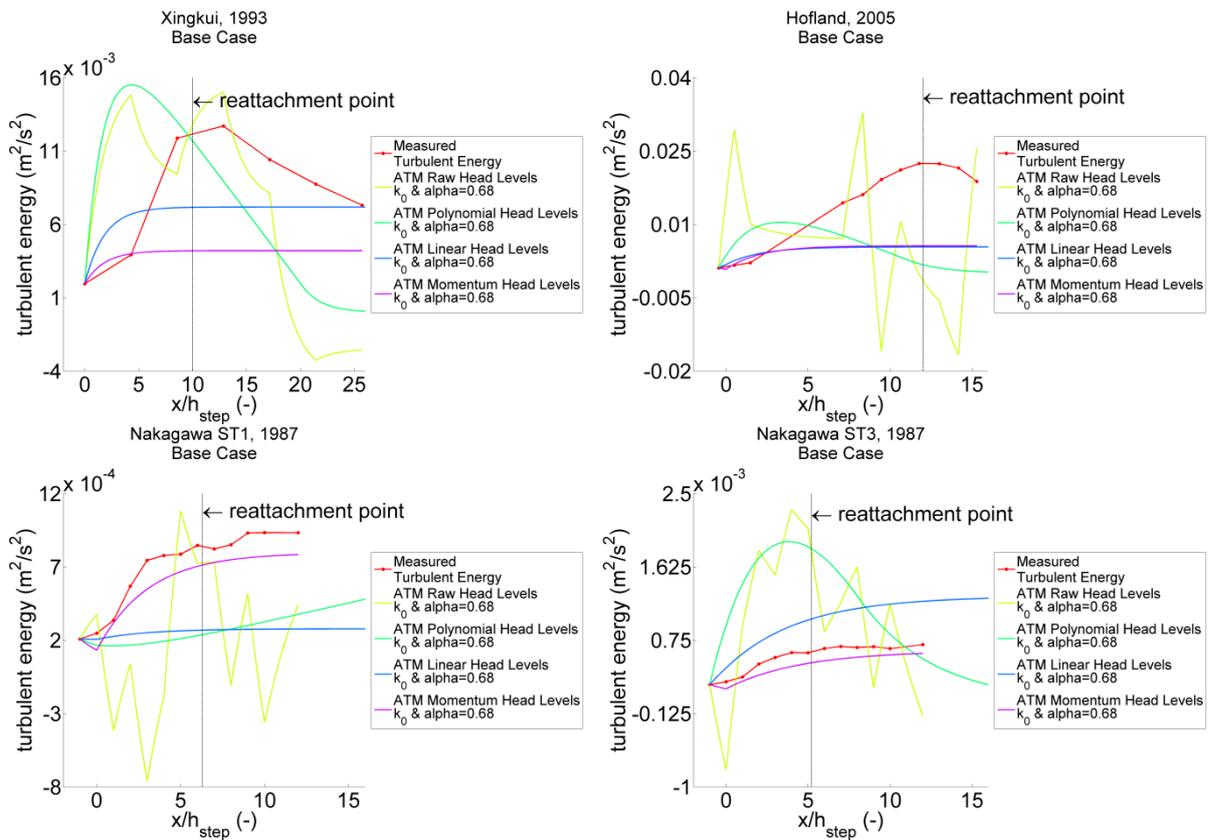
Figure 44 Comparison between measured turbulent energy and ATM output for the Base case
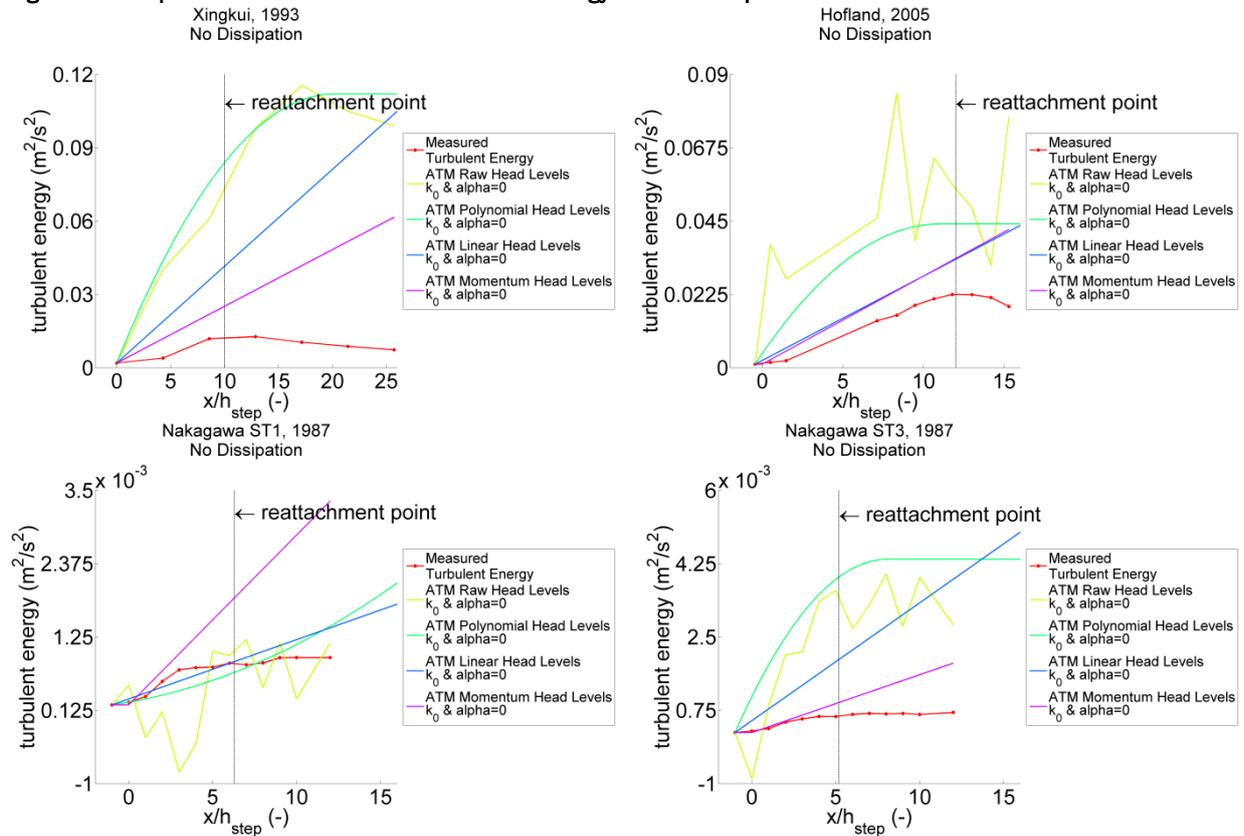


Figure 46 Comparison between measured turbulent energy and ATM output for the No Dissipation case

167
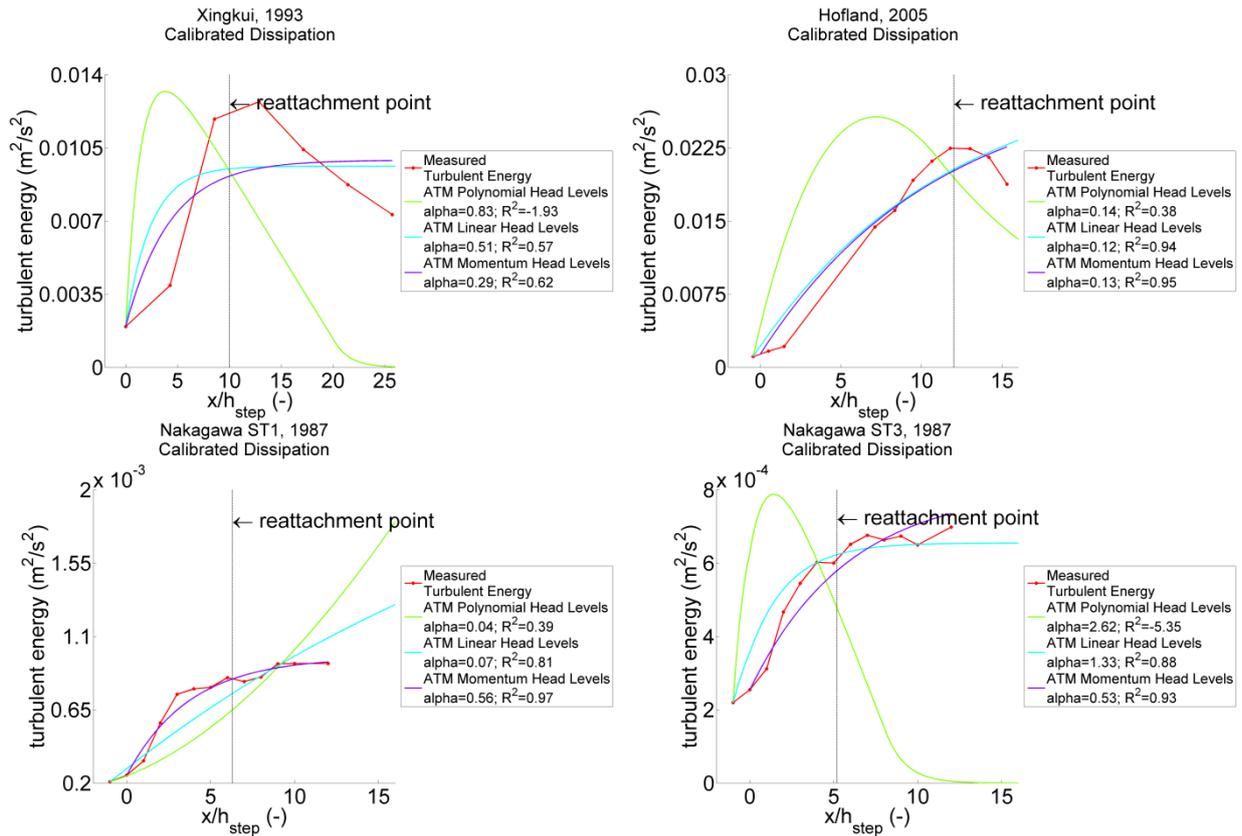
Figure 47 Comparison between measured turbulent energy and ATM output for the Calibrated Dissipation case



Figure 49 Comparison between measured turbulent energy and ATM output for the Calibrated Dissipation case only considering the measured turbulent energy levels up until the maximum value

168
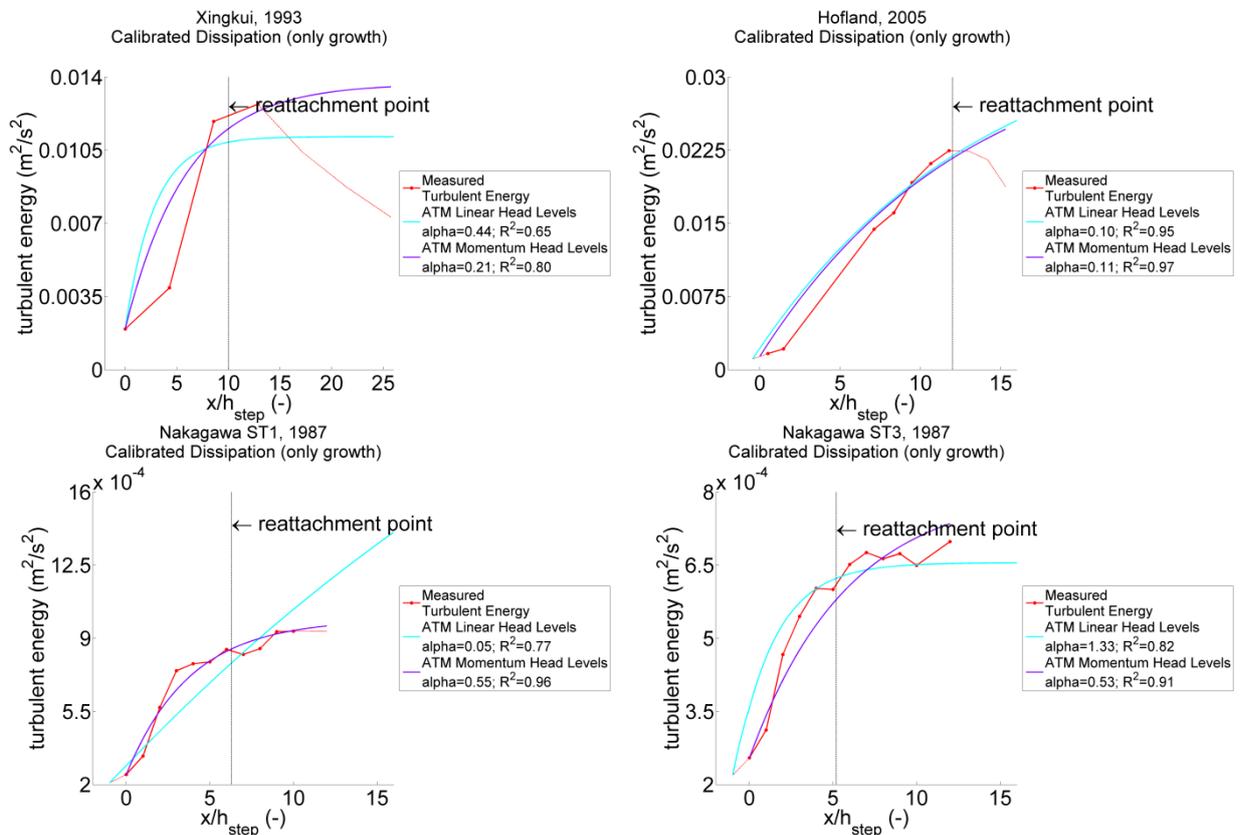
# Appendix V: Uncertainty analysis of the Arcadis Turbulence Model

## Introduction

In appendix Q the uncertainty margins of the head levels were discussed. These margins are used as the basis to get an idea of the uncertainty margins in the ATM output. The uncertainty in the ATM output is defined by minimum and maximum turbulent energy levels that follow from the uncertainty in the head level input. In the following text first the head level input that will be used in the uncertainty analysis is discussed. The ATM output resulting from the uncertain measured head level input is then discussed. The uncertainty of the ATM output as the result of uncertain momentum head level input is discussed thereafter.

## Head level input used  to calculate the uncertainty in the ATM

The measured head level uncertainty margins from appendix Q are repeated below with some additions.
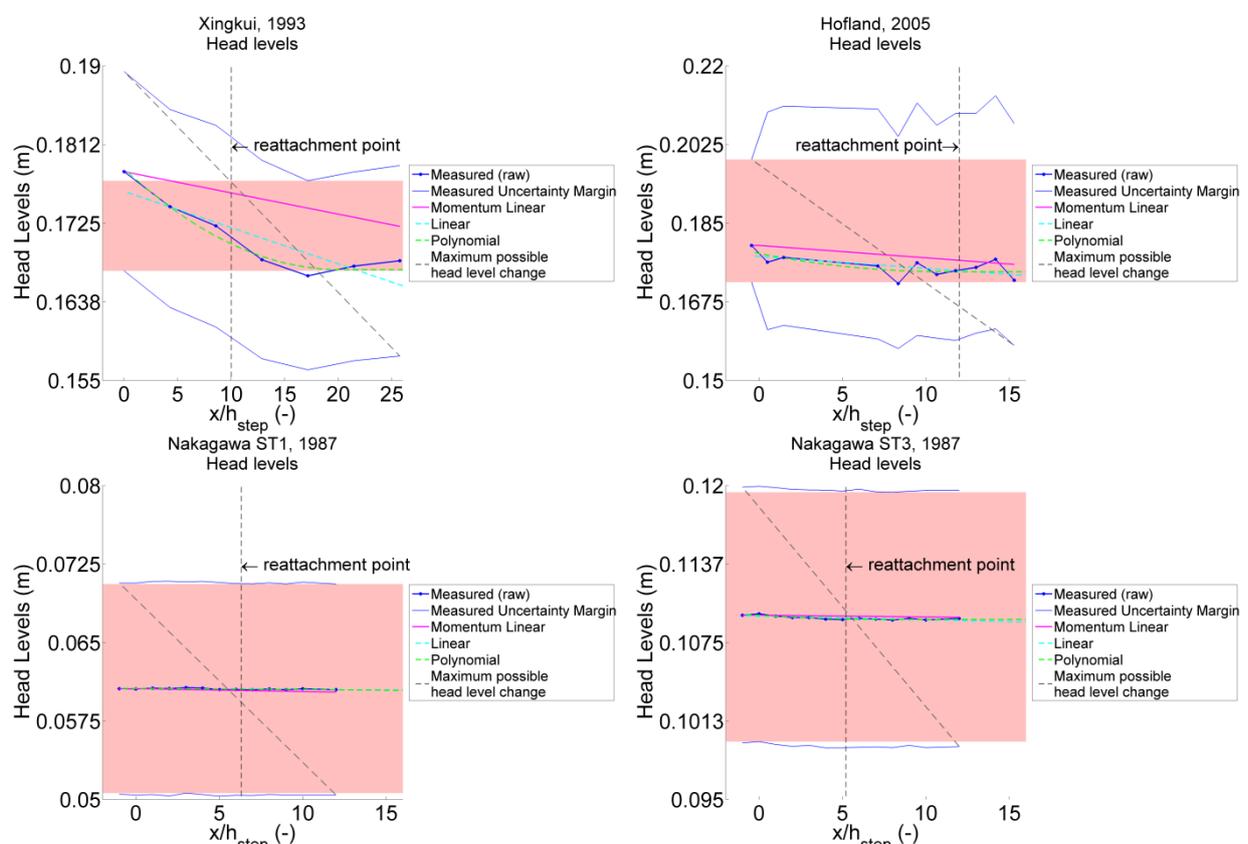


Appendix figure 21 Uncertainty limits of measured head levels. Shaded area indicates the region where constant head levels are possible.

Appendix figure 21 shows the uncertainty limits of the measured head level input. Two additions to figure appendix figure 21 are made (compared to appendix figure 19). First, the area where it's possible that no change occurred in the head levels is shaded. Second, the most extreme mean flow energy loss possible within the uncertainty margins of the measured head levels is depicted in the figure above. The two additions are related to the minimum and maximum uncertainty margin of the ATM output respectively. The minimum of the ATM output uncertainty margin is discussed using the shaded area in the figure above. The maximum of the ATM output uncertainty margin is discussed using the most extreme mean flow energy loss possible.

## The head level input used to find the minimum ATM uncertainty margin

Within the shaded area in Appendix figure 21, it is possible to draw a straight horizontal line at

any height, without crossing the uncertainty limits of the measured head levels. These straight lines represent head level inputs that give the possibility that no mean flow energy is lost when water flows over the BFS $\left(\frac{dH}{dx} = 0\right)$. Two hypothetical head level input alternatives that show no change in mean flow energy are depicted in appendix figure 22 (red lines). Physically, it is expected that downstream of a BFS mean flow energy is lost due to flow deceleration. However, the uncertainty margins of the measured head levels do allow for the possibility that no mean flow energy is lost. Therefore this assumption is used as input into the ATM for the minimum uncertainty limit. When no mean flow energy loss is put into the ATM, turbulence is only dissipated. If dissipation of turbulence is also assumed to be large, than the incoming turbulent energy will quickly be reduced to zero. This gives the lower limit of the ATM turbulent energy uncertainty margin. When it is assumed the mean flow does not lose any energy, and turbulence is dissipated, than the turbulent energy over the whole study is by approximation equal to zero for the minimum uncertainty margin.
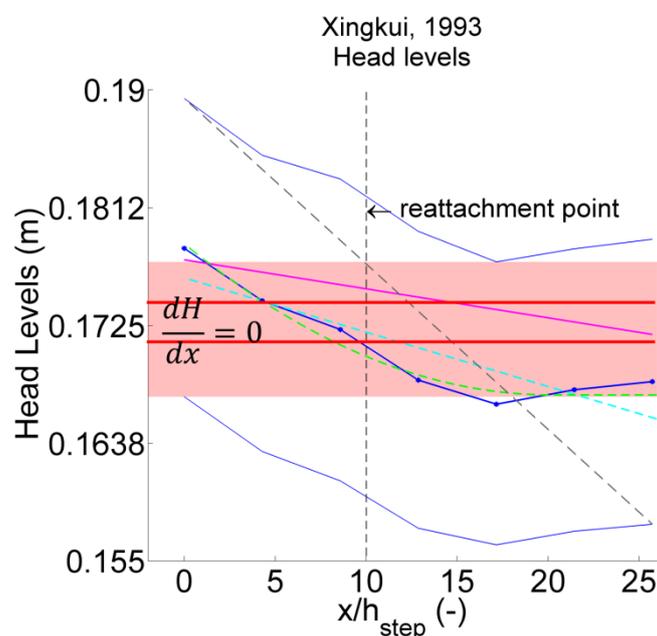


Appendix figure 22 Example of possible head level curves (red lines) that adhere to no change in mean flow energy

### The head level input used to find the maximum ATM uncertainty margin

Appendix figure 21 depicts a line (for each experiment) that connects the maximum upper limit of the head level uncertainty margin with the minimum lower limit of the head level uncertainty margin. This line represents to most extreme case of mean flow energy loss possible within the set uncertainty margins of the measured head levels. In this most extreme case, the measured incoming mean flow energy was underestimated and actually equalled the mean flow energy level at the upper uncertainty margin. Vice versa the measured outgoing mean flow energy level was greatly overestimated, and actually equalled the lower limit of the uncertainty margin. The total mean flow energy loss in this scenario will be as large as possible within the uncertainty margins of the measured head levels. This extreme mean flow energy loss is used to calculate the upper uncertainty margin of the ATM output. For the upper uncertainty margin, it is also assumed that no turbulence is dissipated. This will give the most extreme ATM output possible using the head level input.

**The ATM uncertainty margins   due to measured head level uncertainty**

The methods described above are used to calculate the minimum and maximum uncertainty margins of the ATM. This resulted in the following figures:
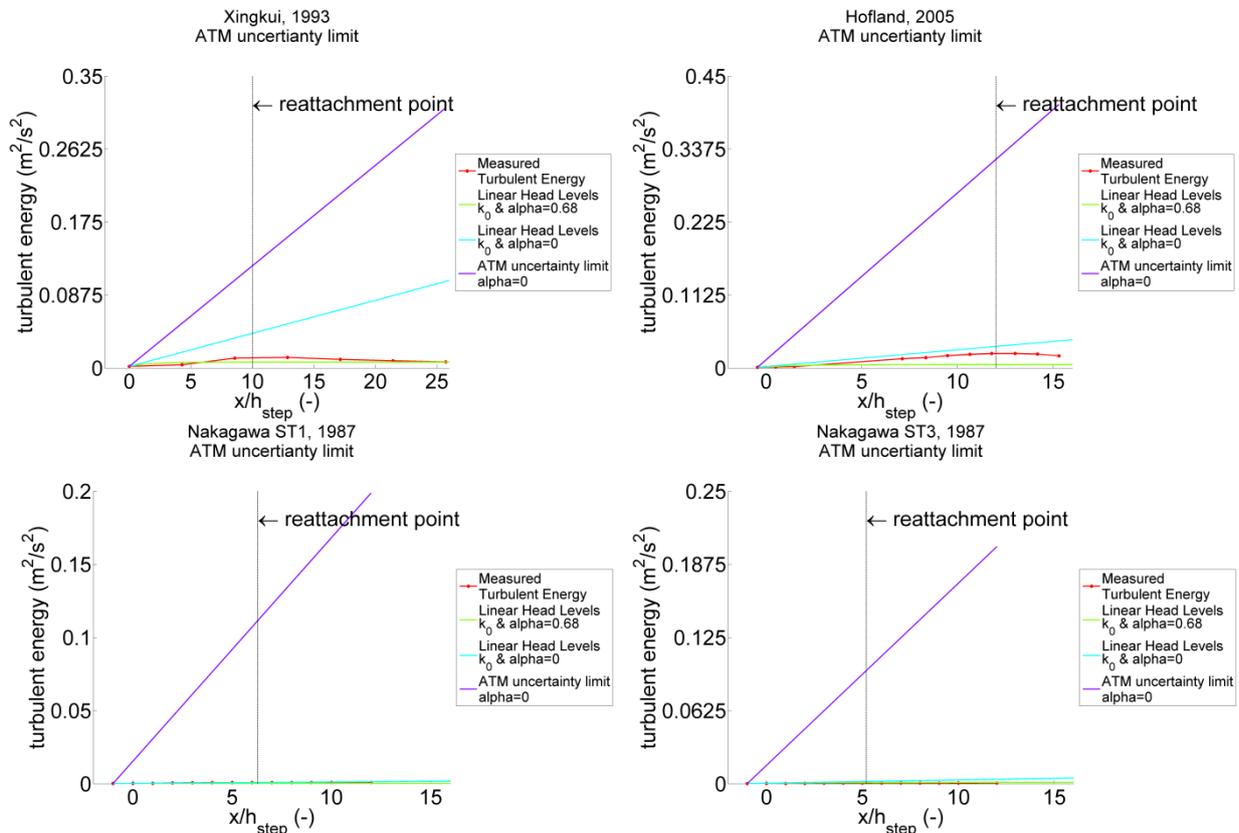


Appendix figure 23 Uncertainty limits of the ATM as a result of uncertainty in the measured head level input

Appendix figure 23 shows the maximum uncertainty limit for the ATM output as the result of the uncertainty in the ATM head level input. The minimum ATM uncertainty limit is not explicitly depicted in appendix figure 23. The minimum is simply located at $\bar{k} = 0$ because turbulence is not produced and it is assumed that the incoming turbulent energy is quickly dissipated. The measured turbulent energy levels, and the No Dissipation case turbulent energy levels using linear head level input are also depicted in the figure above to get an idea of the scale of the uncertainty limits for the ATM output. Note that the maximum uncertainty limit is overestimating the turbulent energy levels in varying degrees of magnitude. Especially the ATM runs for the Nakagawa & Nezu (1987) experiments are greatly overestimated. This indicates that the results ATM results for the Nakagawa & Nezu (1987) experiments are not very certain when using measured head level input.

The maximum uncertainty limit for the ATM output greatly overestimate the actually measured turbulent energy levels. This was of course expected. The extremely large mean flow energy loss used as input into the ATM results in extremely large turbulent energy levels as output. The uncertainty limit of the ATM as depicted in appendix figure 23 assumes a constant rate of mean flow energy loss. This does not necessarily have to be the case. As the most extreme scenario, it can be assumed that the mean flow losses all of its energy (maximum possible head level change in appendix figure 21) the moment it reaches the end of the BFS. Using this assumption, the ATM uncertainty margin can be depicted as an area. It is assumed that due to the uncertainty in the head level input, the ATM output can fluctuate freely inside this area.
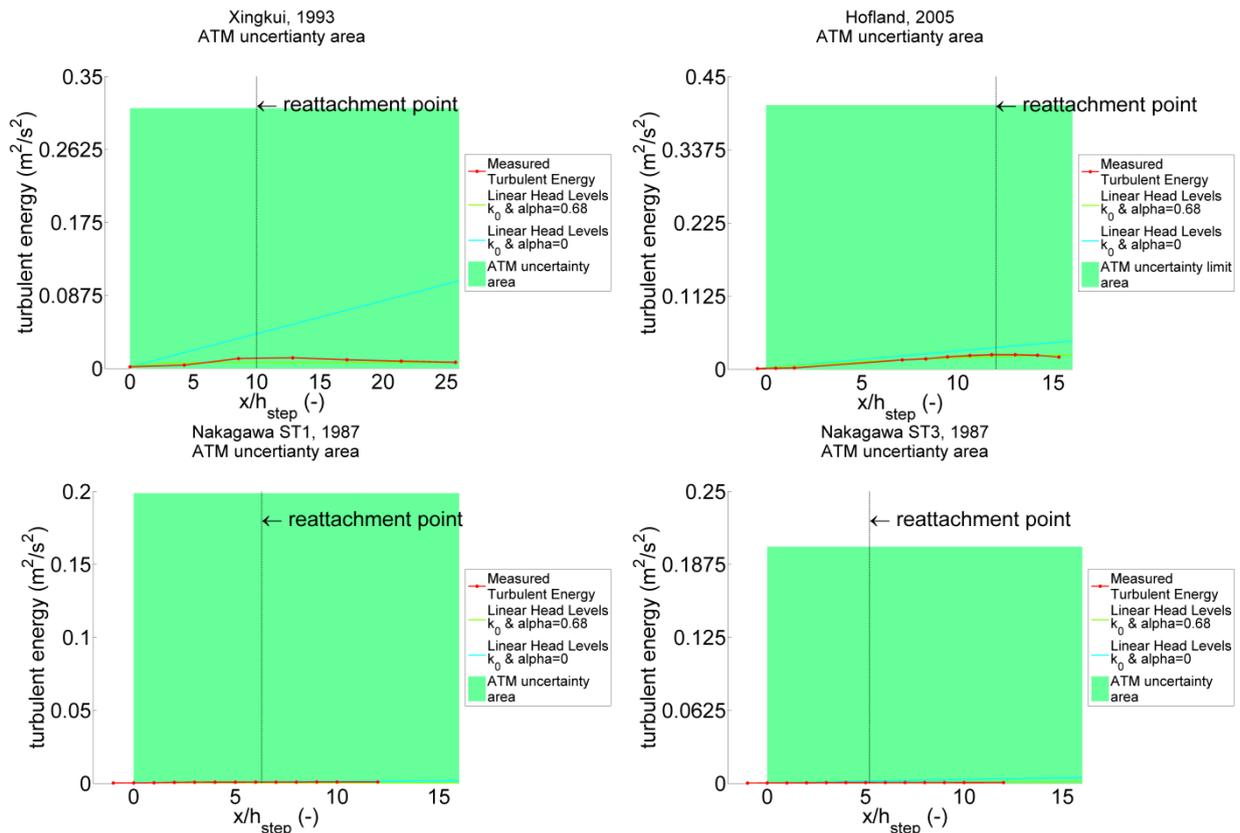
**Appendix figure 24** Uncertainty limits of the ATM as a result of uncertainty in the measured head level input assuming all turbulence is produced at $x/h_{step} = 0$

The shaded area in appendix figure 24 gives an indication of the ATM output uncertainty limits when the uncertainty margins of the measured head levels and the uncertainty of the head level shape are considered. The shaded area in appendix figure 24 is quite large in comparison to the measured turbulent energy levels used to validate the ATM. The reason for this is the large uncertainty margins of the head level input. Conclusions based on ATM results using the measured head levels (raw, linear or polynomial) as input should therefore be handled with some reserve. However, chapter 7 showed that the ATM using measured head levels as input found turbulent energy levels that were in the same order of magnitude as the experimentally measured turbulent energies. Thus the extreme uncertainty in the ATM output as depicted in appendix figure 24 is at least not reflected in the actual ATM output. The large uncertainty margins depicted in appendix figure 24 should therefore not be a reason to reject the ATM results altogether[30].

**The ATM uncertainty margins    due to momentum head level uncertainty**

The uncertainty in the ATM results due to the uncertainty in the momentum head level input are found in a different way.

The water depth and the flow velocity at the downstream edge of the study area are calculated using the conservation of momentum:

---

[30] As an one time reward for reading all the way up to this appendix, a Snickers is available for every member of the graduation commission that asks for it. When no remark is made about the Snickers reward by the graduation commission during my colloquium, sadly, they will not be distributed.

$$h_{downstream} = \frac{M_{upstream} - \frac{1}{2}\rho_w g(h_{downstream})^2}{\rho_w \frac{q^2}{h_{downstream}^2}} \qquad (2.7)$$

Where $M_{upstream}$ equals the momentum at an infinitesimal distance downstream of the step. $M_{upstream}$ is calculated using the following formula:

$$M_{upstream} = \frac{1}{2}\rho_w\left(h_{upstream} + h_{step}\right)^2 + \rho_w h_{upstream}\bar{\bar{u}}_{upstream}^{\;2} \qquad (2.6)$$

The only measurement data required to calculate $M_{upstream}$ is the water depth $h_{upstream}$ and the flow velocity $\bar{\bar{u}}_{upstream}$ at the end of the step. The uncertainty in calculated downstream waterdepth $h_{downstream}$ and flow velocity $\bar{\bar{u}}_{downstream}$ is therefore only dependent on the uncertainty in those measurements.

The uncertainty area of the ATM output as the result of the uncertainty in the momentum head level input is calculated in the following way: The mean flow energy loss, as the result of the BFS is calculated using the momentum water depths and flow velocities at the downstream location, as discussed in section 6.5. This process is repeated for a number of values for $h_{upstream}$ and $\bar{\bar{u}}_{upstream}$ (values for $h_{upstream}$ and $\bar{\bar{u}}_{upstream}$ chosen within their uncertainty margins). The combination of $h_{upstream}$ and $\bar{\bar{u}}_{upstream}$ that resulted in the largest mean flow energy loss was then choses as the momentum head level input into the ATM. The resulting turbulent energy level are depicted in the appendix figure below.
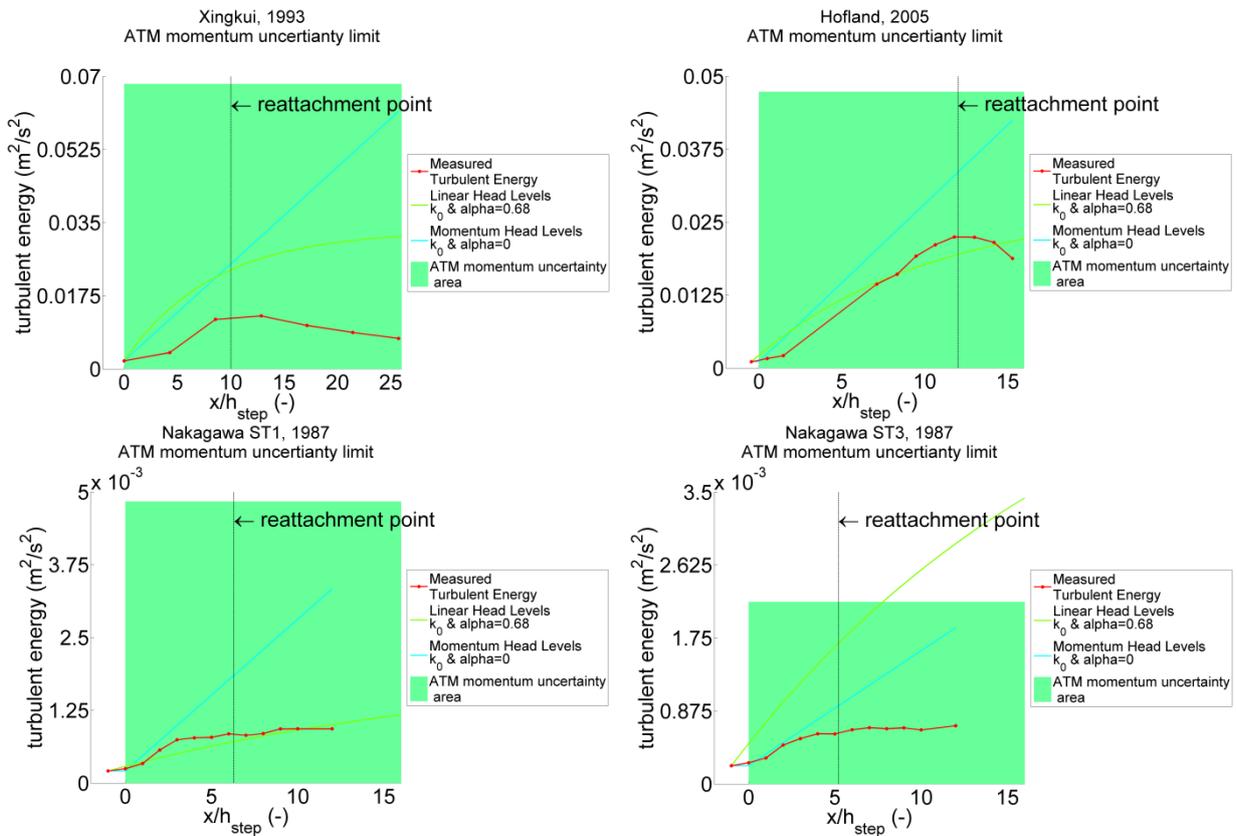


Appendix figure 25 Uncertainty limits of the ATM as a result of uncertainty in the momentum head level input assuming all turbulence is produced at $x/h_{step} = 0$

As can be seen, the uncertainty in the ATM output as the result of the uncertainty in the measured input is much smaller when momentum head levels are used. This gives a little bit

more confidence in the ATM results using the momentum head level input. However, keep in mind that that the conservation of momentum does not take into account the momentum loss due to bottom friction. Thus, some additional uncertainty in the ATM results using momentum head level input is expected.

Note in the both uncertainty analyses presented above, the uncertainties in the non-uniformity coefficients $\alpha_{Bern}$ and $\beta$ were not taken into account. Uncertainty in these coefficients will enlarge the uncertainty margins of the ATM output.